AD_____

Award Number: DAMD17-03-2-0021

TITLE: Molecular Genetic and Gene Therapy Studies of the Musculoskeletal System

PRINCIPAL INVESTIGATOR: David J. Baylink, M.D.
Subburaman Mohan, Ph.D.

CONTRACTING ORGANIZATION: Loma Linda Veterans Association for Research and Education
Loma Linda, California 92357

REPORT DATE: October 2004

TYPE OF REPORT: Annual

PREPARED FOR: U.S. Army Medical Research and Materiel Command
Fort Detrick, Maryland 21702-5012

REPORT DOCUMENTATION PAGE

Form Approved
OMB No. 074-0188

1. AGENCY USE ONLY (Leave blank)	2. REPORT DATE	3. REPORT TYPE AND DATES COVERED
	October 2004	Annual (9 Sep 2003 - 8 Sep 2004)

4. TITLE AND SUBTITLE
Molecular Genetic and Gene Therapy Studies of the Musculoskeletal System

5. FUNDING NUMBERS
DAMD17-03-2-0021

6. AUTHOR(S)
David J. Baylink, M.D.
Subburaman Mohan, Ph.D.

7. PERFORMING ORGANIZATION NAME(S) AND ADDRESS(ES)
Loma Linda Veterans Association for Research and Education
Loma Linda, California 92357

E-Mail: baylid@lom.med.va.gov; subburaman.mohan@med.va.gov;

8. PERFORMING ORGANIZATION REPORT NUMBER

9. SPONSORING / MONITORING AGENCY NAME(S) AND ADDRESS(ES)
U.S. Army Medical Research and Materiel Command
Fort Detrick, Maryland 21702-5012

10. SPONSORING / MONITORING AGENCY REPORT NUMBER

11. SUPPLEMENTARY NOTES
Original contains color plates: All DTIC reproductions will be in black and white.

12a. DISTRIBUTION / AVAILABILITY STATEMENT
Approved for Public Release; Distribution Unlimited

12b. DISTRIBUTION CODE

13. ABSTRACT (Maximum 200 Words)

The primary goal of the proposed work is to apply several state of the art molecular genetic and gene therapy technologies to address fundamental questions in bone biology with a particular emphasis on attempting: 1)to clarify gene functions of the those genes that are involved in the musculoskeletal system; and 2)to promote rapid healing and eventually regeneration of soft and hared tissues using appropriate animal models. To discover novel genes and evaluated functional genes relevant to the musculoskeletal system, we are performing a number of molecular genetics studies using appropriate mouse models. To develop therapeutic approaches for treating systemic and local lesions in the skeleton by means of gene therapy, we are developing technologies o target one or more growth factor genes to bone using experimental animal model systems. During the last funding period, we have successfully accomplished all of the specific objectives. Our work during this period has resulted in 2 manuscripts and 3 abstracts. We believe that successful accomplishment of the proposed studies will provide a better understanding of the molecular mechanics involved in soft and hard tissue regeneration and will provide a frame work for future development of therapies for soft and hard tissue injuries.

14. SUBJECT TERMS
No subject terms provided.

15. NUMBER OF PAGES
257

16. PRICE CODE

17. SECURITY CLASSIFICATION OF REPORT	18. SECURITY CLASSIFICATION OF THIS PAGE	19. SECURITY CLASSIFICATION OF ABSTRACT	20. LIMITATION OF ABSTRACT
Unclassified	Unclassified	Unclassified	Unlimited

Table of Contents

I. GENERAL INTRODUCTION

This proposal is divided into three sections: A) Molecular Genetic Projects, of which there are four projects. In our initial proposal, our final Molecular Genetic project was a fifth project involving a large human clinical trial, but work on this project has not been initiated at this time due to the Army suspension of human related activities and thus there is no progress to report; B) Gene Therapy Projects, of which there are three projects; and C) Support Service Facilities, of which there are four projects. Each of the above projects has an introduction .

Our goals for the first 12-months of this funding period for each of the technical objectives, as well as our progress for each of the technical objectives, are described below. The progress report for each project is organized according to the outline provided by the office of the U.S. Army Medical Research and Material Command.

A. MOLECULAR GENETICS PROJECTS

Project 1: Studies on Genetic Regulation of Digit Tip Regeneration

Introduction

Experiments with amphibian limbs, first undertaken in the 18th century, demonstrate that limb regeneration in vertebrates is possible [1, 2]. It is also known that higher mammals have only marginal ability to regenerate. One example of regeneration in mammals is the healing of ear holes in rabbits without scarring [3, 4]. Recently, we have also demonstrated that the MRL inbred mouse strain shows greater regeneration and scarless healing of ear-hole punches as opposed to several other inbred strains of mice. [5-7]. It has also recently been shown that the MRL mouse is capable of cardiac muscle regeneration [8]. Thus, the MRL mouse is a unique model to study the genetic mechanisms that regulate wound healing and tissue regeneration. However, to date, the MRL mouse has not been investigated extensively for its abilities to regenerate more complex biological structures such as digit tips. This project examined digit tip regeneration in inbred strains of mice in an attempt to identify good and poor digit tip regenerators. We also undertook global RNA expression profiling in those strains in order to identify the genes and genetic mechanisms responsible for wound healing and digit tip regeneration.

Body

Technical Objectives

We will utilize two approaches to identify the molecular pathways that contribute to limb regeneration. In approach 1, we will employ microarray technology to identify global gene expression changes between a good (MRL) and a poor (e.g. SJL) healer strain of mice. In approach 2, we will use linkage studies to identify the genetic loci responsible for limb regeneration. If, for any reason, we are unable to pursue QTL studies for digit tip regeneration, we will shift our focus to another key model of regeneration, namely neurological regeneration after nerve ablation, for example of either the peripheral nerves or the spinal chord.

Our Specific Objectives for the first twelve months of this grant were as follows:

a) To compare digit tip regeneration in four to six different inbred strains of mice (MRL, DBA, SJL, C57BL/6J, C3H and 129/Sv). This will be measured by digitizing faxitron x-rays or by micro-computerized tomography (9m resolution).

b). To evaluate whether or not a blastema is seen during digit tip regeneration in six different inbred strains of mice.

c). To initiate microarray to the digit tip healing tissue at one and four days post amputation in the MRL mouse and the SJL mouse. Control tissue will be obtained from both strains of mice at 0 time.

Progress for Specific Objectives

Technical Objective 1a:

Our goal was to compare digit regeneration in four to six inbred strains of mice (MRL, DBA, SJL, C57BL/6J, C3H and 129/Sv). We obtained four-week old MRL, SJL, C3H, 129, B6 and DBA mice from The Jackson Laboratories (Bar Harbor, ME). The mice were housed at the Animal Research Facility, JL Pettis VA Medical Center, Loma Linda, CA, under the standard conditions of 14 hours light, 10 hours darkness, ambient temperature of 20°C, and relative humidity of 30-60%. Three female and one male for each strain were housed in one cage. When female mice were found to be pregnant, they were caged separately. The day that mouse pups were born, surgery was conducted on each of the pup's digit tips. The neonatal mice were anesthetized with 5% Halothane mixed with O2 5L/min. The right front 3rd and 4th digit tips were amputated, with the left side used as uncut controls. The amputation level was set up at the bottom of nail level under the microscope. The amputated tissues were collected into RNA later (Ambion), and the tissues from the pups of one litter were pooled. Both left (uncut) and right (cut) paw X-ray images were taken at 0, 7, 14, 21, and 28 days post surgery with a Faxtron. In addition, mice were sacrificed at four days post surgery and regenerating digit tips were collected by surgery. The collected tissue was pooled in RNA later and stored at –80°C for later RNA extraction. One problem we experienced was with mother pups abandoning or cannibalizing pups following surgery. This was particularly a problem for the SJL mouse strain. No pups in the SJL strain survived more than 1-day following surgery. For this reason we compared the MRL to the DBA strain in the microarray expression studies rather than the SJL strain.

Growth Rate Measurements

Faxitron x-ray images were measured using the ruler feature of Photoshop (Adobe) (Figures 1, 2). Four growth amounts were determined. 1) the amount of dissected tissue; 2) the length of first phalanx of 3rd and 4th fingers of front two paws; 3) the length from the bottom of 2nd phlanx to the tissue edge; and 4) the length from the top of 2nd phalanx to the tissue edge. Measurements were made of both left uncut and right cut digits. The growth was determined for 7, 14, 21 and 28 days post surgery.

Figure 1. Measurement of Amounts of Dissected Tissues in Newborn Mouse Pups. The digit tip dissections were carried out on the 3rd and 4th tips of the right paw. The left paw digit tips were not dissected and used as uncut controls to correct for inbred mouse strain size differences. Mice were x-rayed before and after digit tip dissection. Amounts of tissue dissected were calculated by subtracting the after dissection values from the before dissection values of the top of the second phalanx to the digit tip edge (Table 1).

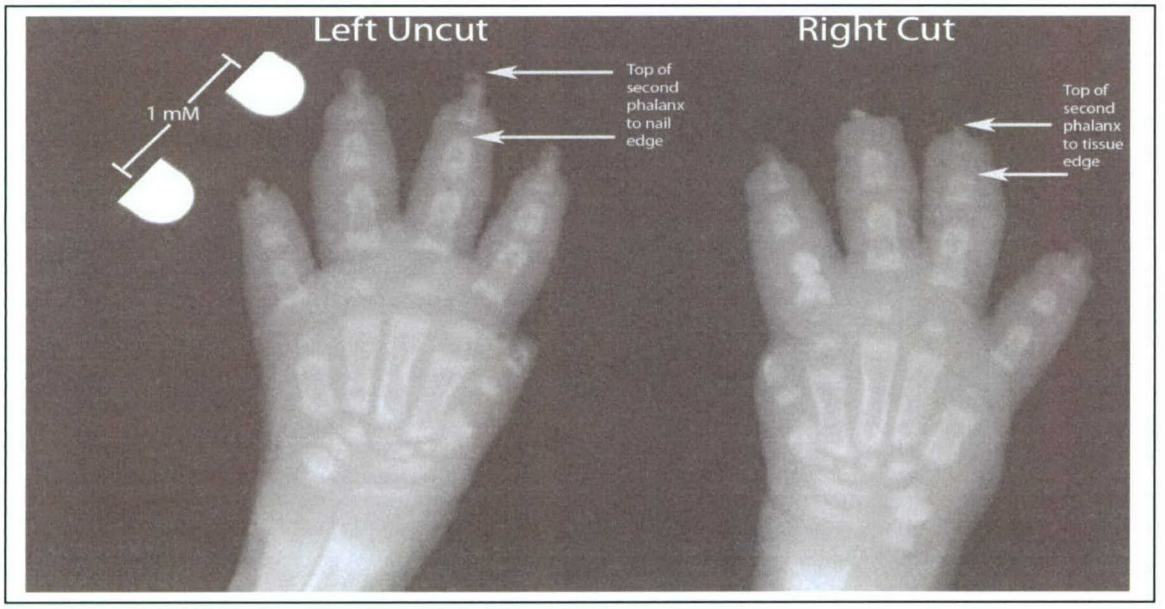

Table 1. Amount of digit tip tissue dissected in mice. The mean amount of tissue dissected in MRL mice was slightly greater (0.14 mM) than in other mouse strains.

Digit	Strain	N	Mean Tissue Dissected (mM)	SD
3rd Right Digit	MRL	20	0.14	0.04
	C3H	4	0.09	0.04
	DBA	24	0.12	0.05
	B6	26	0.12	0.05
	129	4	0.11	0.04
	Total	78	0.14	0.09
4th Right Digit	MRL	20	0.14	0.06
	C3H	4	0.16	0.07
	DBA	24	0.11	0.05
	B6	26	0.11	0.05
	129	4	0.12	0.05
	Total	78	0.13	0.11
Mean of 3rd and 4th Digits	MRL	20	0.14	0.04
	C3H	4	0.13	0.05
	DBA	24	0.12	0.05
	B6	26	0.11	0.05
	129	4	0.12	0.04
	Total	78	0.13	0.10

Figure 2. Measurement of Digit Tip Regrowth. Mice were x-rayed at days 7, 14, 21 and 28 post digit tip dissection. Growth was calculated as follows:

The length of first phalanx of 3rd and 4th fingers of both front paws (C to D below);
The length from the bottom of 2nd phlanx to the tissue edge (C to A below)
The length from the top of 2nd phalanx to the tissue edge (B to A below).

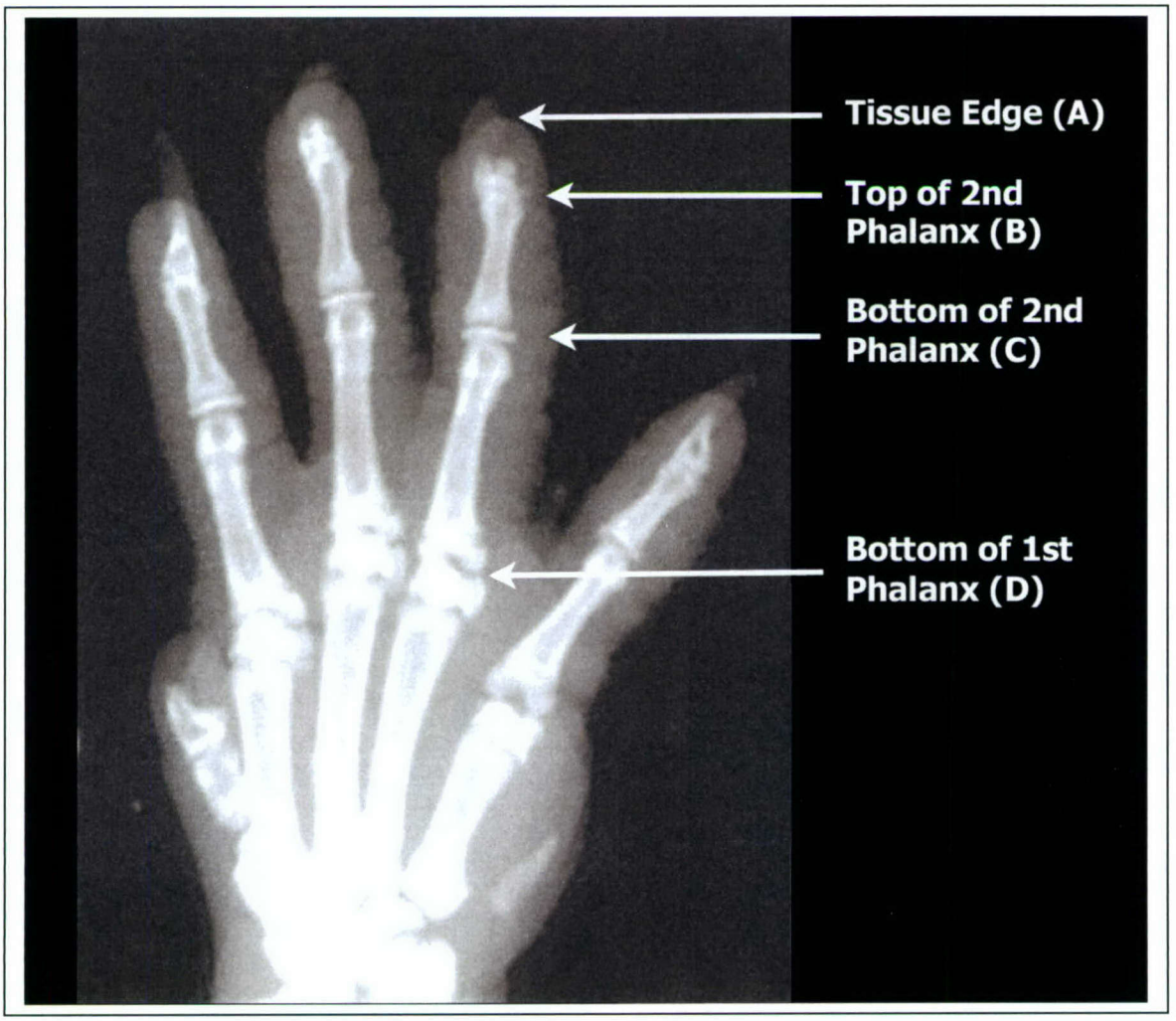

Regeneration Results

In order to insure that regeneration results were not influenced by differences in strain size, the data was normalized by dividing right cut growth measurements by left uncut growth measurements. We first tested the validity of this normalization by dividing the right first phalanx measurements by the left first phalanx measurements (Figure 3). As shown below, these ratios do not show significant differences among the mouse strains and the growth ratios all cluster around 1.00. Since the first phalanges were not dissected, this indicates that normalizing for strain size by calculating a growth ratio is a valid method of correcting for strain size.

Figure 3. Normalization for Strain Size. Division of first phalanx right measurements by left measurements gives expected ratios of ~1.00. Also, no significant difference between strains is seen in normalized data for the first phalange growth ratios.

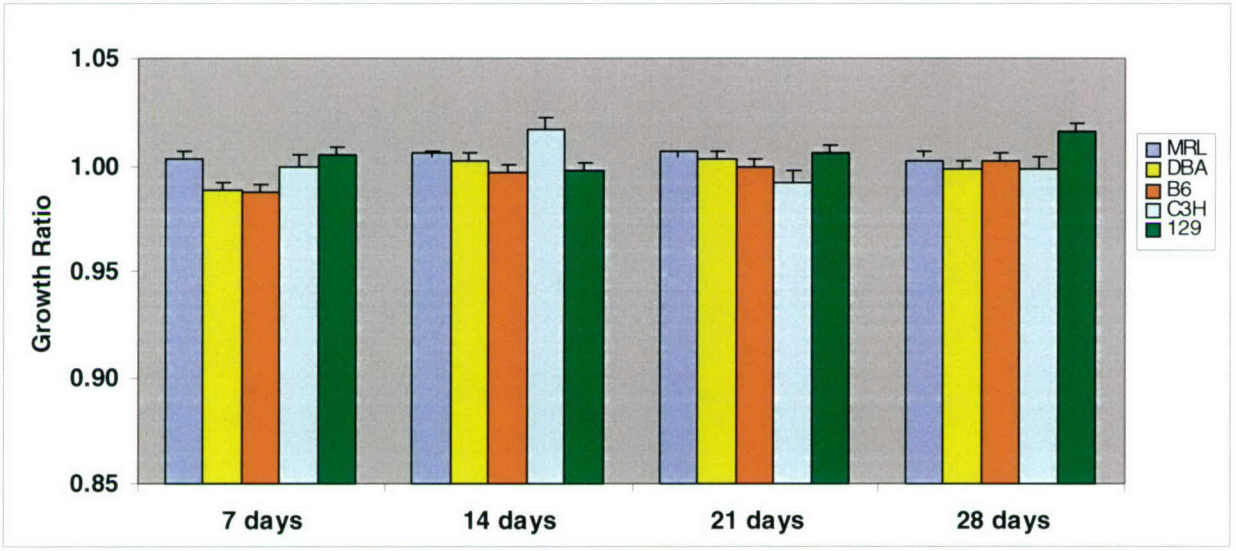

Next we examined the normalized regeneration ratios for dissected digit tips in the mice. As expected, the regeneration ratios are less than one, indicating growth of dissected digit tips is less than undissected digit tips (Figure 4). However, the MRL mouse regenerates digit tips significantly greater than the other mouse strains ($p < 0.05$). This is seen particularly at times when mice are in their primary growth phase (days 0 to 21).

Figure 4. Normalized Growth Ratio Regeneration of MRL, DBA, B6, C3H and 129 Digit Tips. Growth ratios measured from the bottom of 2nd phlanx to the tissue edge (C to A in Figure 2) for 14 and 21 days post dissection, show that MRL mice regenerate digit tips greater than other strains of mice ($p < 0.05$, marked by * in plot).

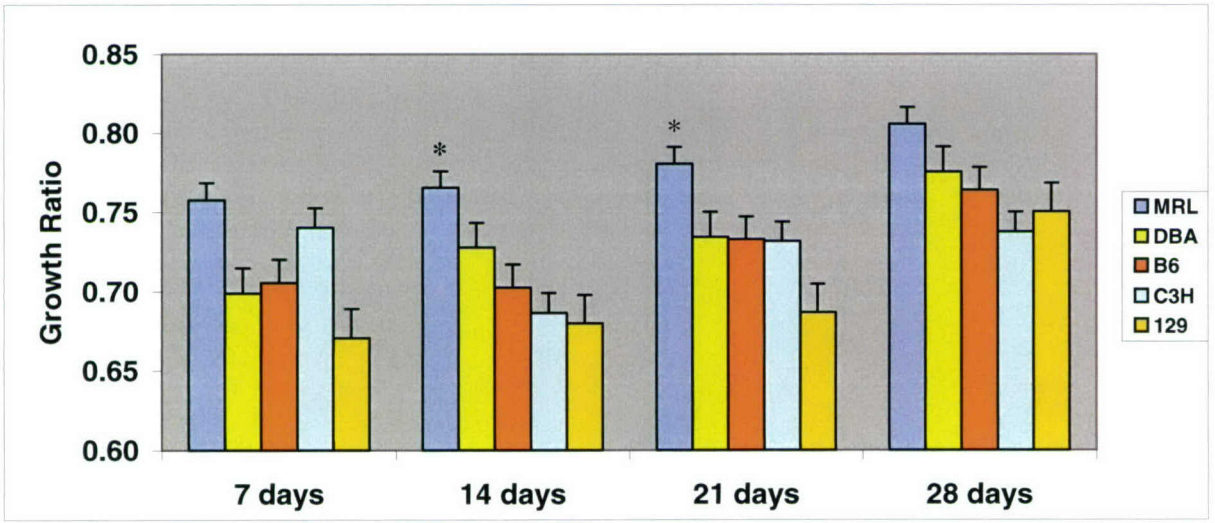

Table 2. Statistical Analysis for Growth among MRL, DBA, B6, C3H and 129 mice. Statistical analysis of the regeneration data was undertaken by 1-way ANOVA using SPSS software. Differences that are statistically significant ($p < 0.05$) are highlighted. Note that for normalized growth ratios of the first phalanges there is no significant difference between the strains. Since no surgery was done on the first phalanges this demonstrates that the growth ratio method of comparison is valid. However, in regenerating digit tips there are significant differences among the mouse strains, particularly when the mice are in their primary growth phase (days 0 to 21).

Time and Phalanx		SS	df	Mean Square	F	Sig.
7 days 1st phalanx	**Between Groups**	0.01	4.00	0.00	1.06	0.38
	Within Groups	0.20	73.00	0.00		
	Total	0.21	77.00			
14 days 1st phalanx	**Between Groups**	0.00	4.00	0.00	0.26	0.90
	Within Groups	0.13	73.00	0.00		
	Total	0.13	77.00			
21 days 1st phalanx	**Between Groups**	0.00	4.00	0.00	0.34	0.85
	Within Groups	0.06	73.00	0.00		
	Total	0.06	77.00			
28 days 1st phalanx	**Between Groups**	0.00	4.00	0.00	0.33	0.86
	Within Groups	0.06	73.00	0.00		
	Total	0.06	77.00			
7 days digit tip	**Between Groups**	0.06	4.00	0.01	2.37	0.06
	Within Groups	0.42	73.00	0.01		
	Total	0.48	77.00			
14 days digit tip	**Between Groups**	0.06	4.00	0.01	2.93	0.03
	Within Groups	0.37	73.00	0.01		
	Total	0.43	77.00			
21 days digit tip	**Between Groups**	0.05	4.00	0.01	2.73	0.04
	Within Groups	0.31	73.00	0.00		
	Total	0.35	77.00			
28 days digit tip	**Between Groups**	0.03	4.00	0.01	1.82	0.13
	Within Groups	0.30	73.00	0.00		
	Total	0.33	77.00			

We also examined the degree of nail regeneration seen in the mice. Mice were sacrificed at day 28 and examined to determine if digits had completely or partially regenerated nails, or if no nail regrowth was seen. As shown in Table 4, partial and full regeneration of nails in MRL mice approached but did not reach statistical significance. This may be due to slightly greater amounts of tissue being initially dissected from the MRL mice (Table 1).

Table 3. Nail Regrowth in 129, B6, C3H, DBA and MRL Mouse Strains.

Mouse Strain	No Regrowth	Partial Regrowth	Full Regrowth	Total
129	1	7	0	8
B6	18	28	8	54
C3H	2	5	1	8
DBA	13	25	10	48
MRL	4	29	7	40
Total	38	94	26	158

Chi-Square Tests

	Value	df	Asymp. Sig. (2-sided)		
Pearson Chi-Square	11.1	8	0.20		
Likelihood Ratio	13.0	8	0.11	N of Valid Cases	158

Similar to previous studies that have shown that MRL mice have increased capabilities of healing of ear punches, these results demonstrates that MRL mice also have increased digit regenerative capabilities in comparison to other mouse strains. This regeneration is more complex than simple wound healing since it involves the replacement of multiple cell types as well as patterning to direct the fate of undifferentiated cells. The determination of the fundamental molecular causes of the increased regenerative capabilities of MRL mice could eventually lead to treatments for regeneration of tissues in human diseases and trauma injuries.

Technical Objective 1b:

We examined DBA, B6, MRL, C3H and 129 in-bred strains for blastema formation by sacrificing the mice at 1-day post digit tip dissection. No SJL pups survived after surgery since all were abandoned or cannibalized by the SJL mother mice. For the five other strains at 1-day post surgery two pups were sacrificed and paws were dissected. The dissected tissues were stored in 10% formalin until processing. The MDC Phenotype Core facility fixed the tissues in paraffin and mounted and stained five micron tissue sections from each of the strains. Following hematoxylin and eosin (H&E) staining, the tissues were examined under a microscope.

In amphibians, the first stages prior to regeneration are initial wound healing by formation of an epidermal layer over the wound, followed by dedifferentiation (a loss of specialized cellular characteristics and a return to a less specialized cellular structure). These dedifferentiated cells cluster under the epidermal layer of the dissected tip and are termed a blastema. The blastema then rediffentiates into other cell types including bone, cartilage and epithelial cells. This involves pattern formation genes and pathways that are thought to direct the fate of the blastema cells. In the five mouse strains examined, we see the formation of an epidermal layer over the wound only in the MRL and DBA mouse strains at 1 day post dissection. No epidermal layer is seen at 1-day in the C3H, B6 and SJL strains (Figure 5).

Figure 5. Histology Images of Digit Tip Regeneration at Day 1 Post Surgery. In MRL and DBA mice an epidermal layer has formed after 1-day post surgery. In 129/Sv, B6 and C3H mice little or no epidermal growth has formed to close over the wound.

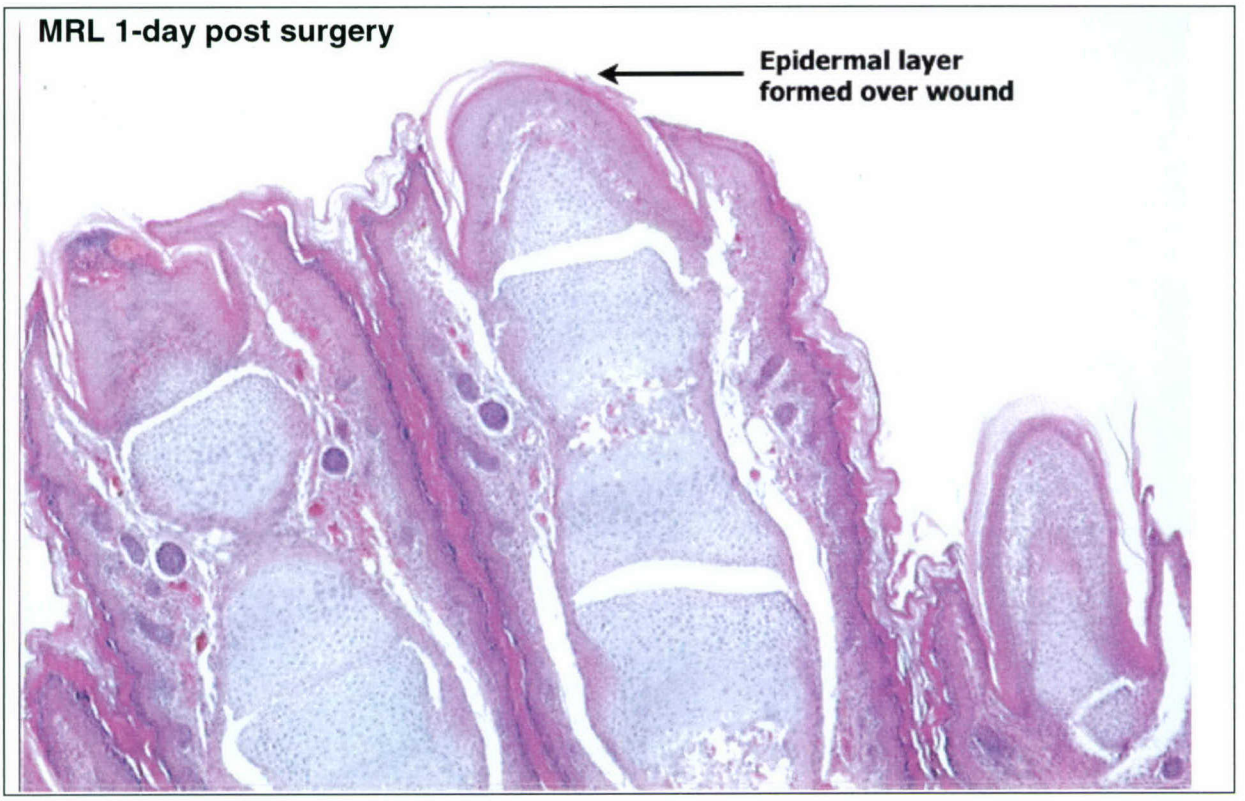

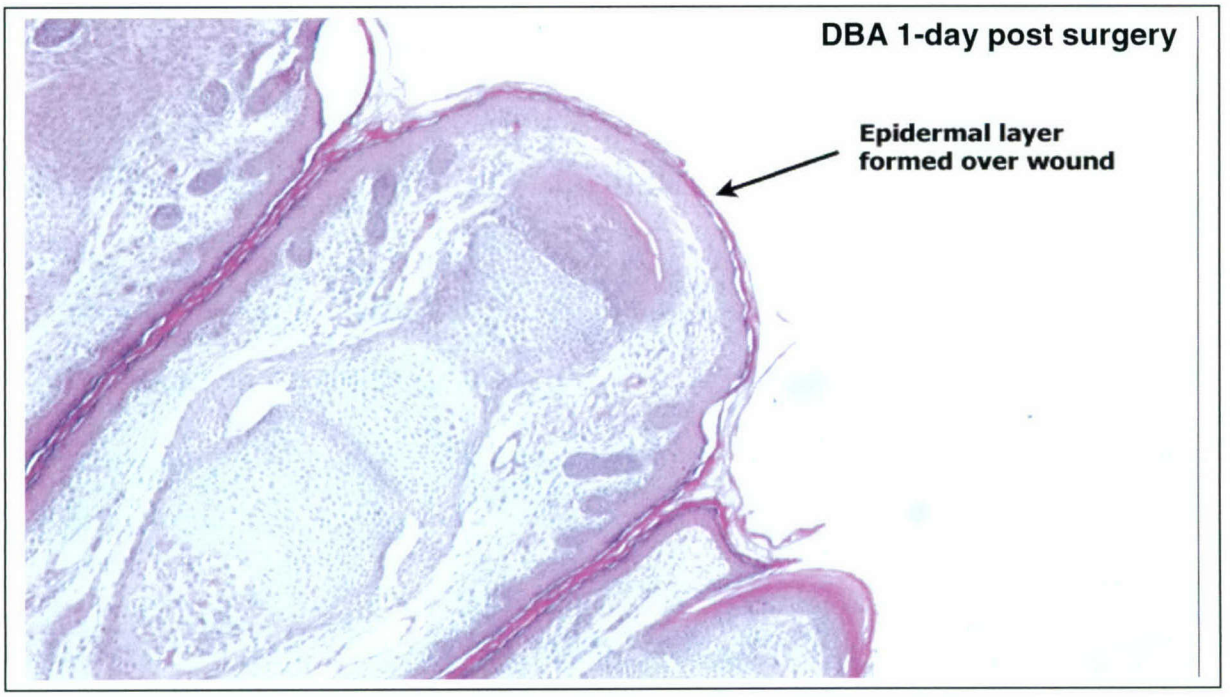

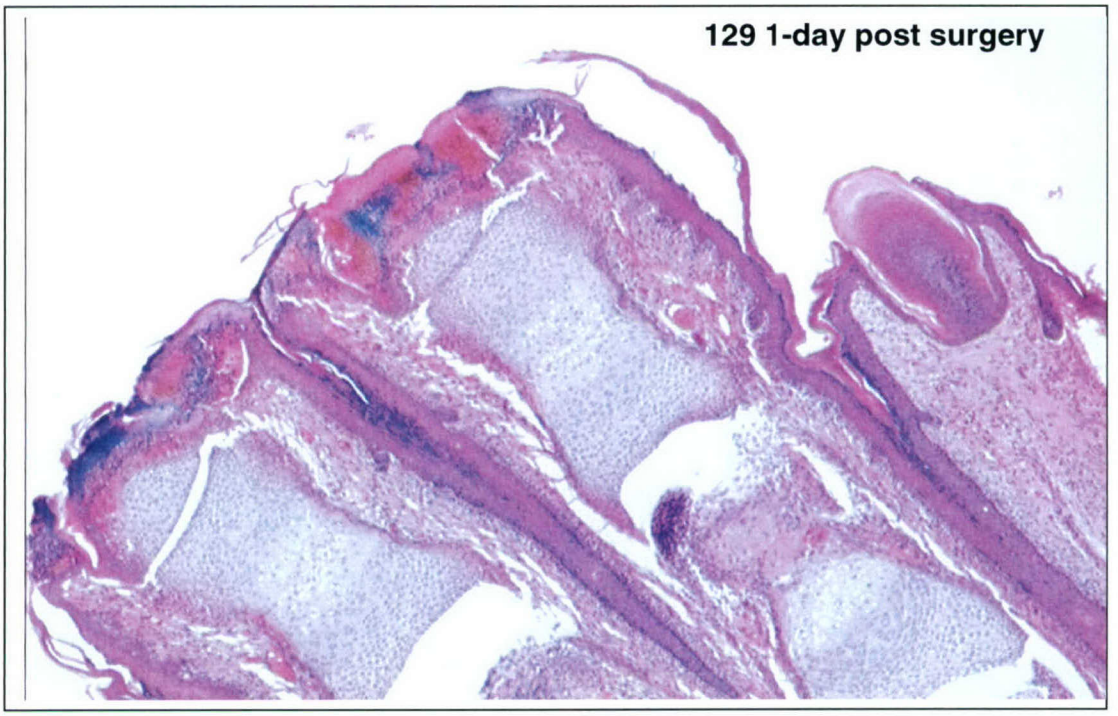
129 1-day post surgery

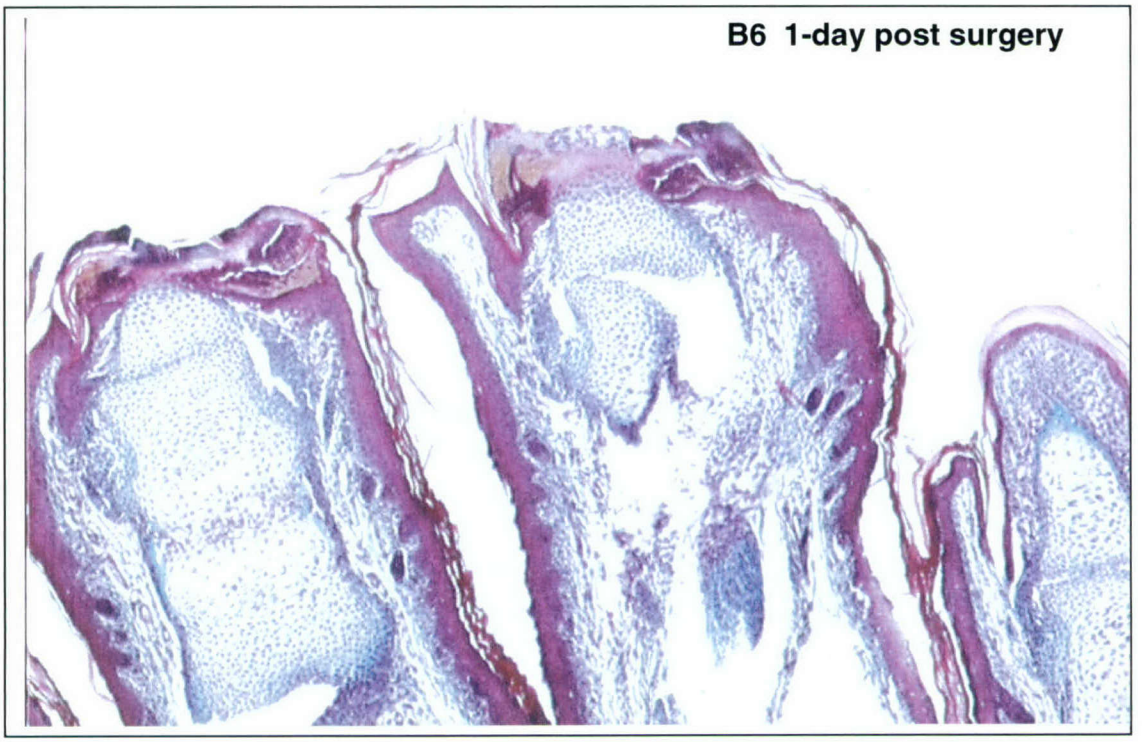
B6 1-day post surgery

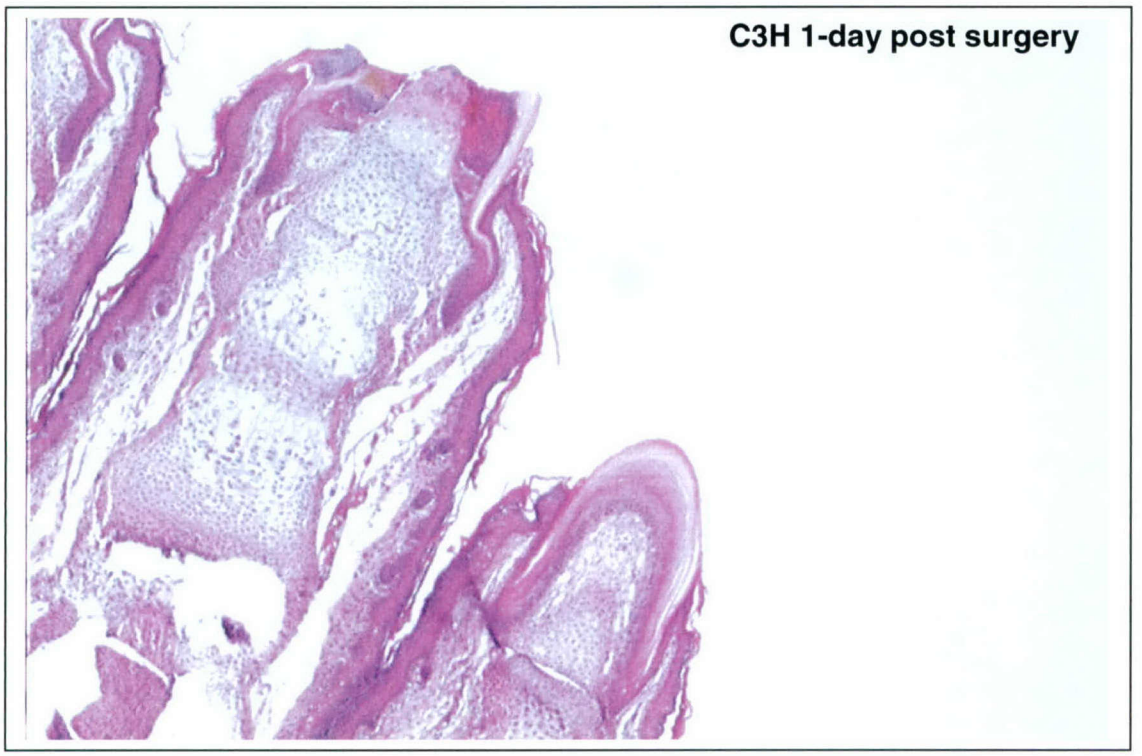

The histology results indicate that the 1-day time point is too early for a blastema to form since only an epidermal wound layer is seen in the MRL and DBA mice. Thus, we are currently examining later times points to determine when blastemas form in each of the different in-bred strains of mice.

Technical Objective 1c:

RNA Extraction for Expression Analysis

Total RNA was isolated from dissected tissues at day 0 and day 4 day using the Agilent Total RNA Isolation Kit (Agilent Technologies). Tissues were lysed using a Polytron Generator (Kinemalica AG, Switzerland), and then processed following the manufacturer's protocol (Agilent). The total RNA concentration was determined by NanoDrop spectrophotometer and RNA quality was determined by 18S/28S ribosomal peak intensity on an Agilent Bioanalyzer. For microarray expression profiling and real-time PCR, RNA samples were used only if they showed little to no degradation.

Microarray Hybridization

Custom cDNA slides were spotted in duplicate with ~15,000 cDNA clones obtained from the National Institute on Aging (NIA) [9]. A Q-Array2 robot (Genetix) was used for spotting. The arrays were also spotted with Amersham Lucidea Universal Scorecard controls to insure correct gene expression values were obtained from each array. These spotting and spike-in controls contain 10 calibration RNAs of increasing gene copy number with 1:1 Cy3:Cy5 ratios, 8 ratio controls of 1:3 low, 3:1 low, 1:3 high, 3:1 high, 1:10 low, 10:1 low, 1:10 high, 10:1 high Cy3:Cy5 ratios and two negative hybridization controls (Amersham). Controls were spotted in

duplicate in the first and last PCR plates to insure proper data tracking. A total 250 ng RNA was used to synthesize double stranded cDNA using the Low RNA Input Fluorescent Linear Application Kit (Agilent). First strand cDNA synthesis was primed with T7-(dT24) promoter primer. From the purified cDNA, cRNA was synthesized using transcription master mix and purified. 250 ng of purified cRNA was used to reverse transcribe to fluorescent cDNA. Cyanine-3-dCTP and cyanine-5-dCTP were used to label experimental samples (day 4) and control samples (day 0). Dye swaps were also conducted to eliminate potential dye bias effects. Samples were hybridized at 60°C for 17 hours. The slides were then washed with Solution I (6X SSC, 0.005% Triton X-102) for 10 min. in the dark and then with Solution II (0.1X SSC, 0.005% Triton X-102) for 5 min. in the dark. The slides were dried with pressurized nitrogen and immediately scanned using a GSI Lumonics ScanArray 4000 scanner. The signal intensity of all microarray images was determined using Imagene 5.6 software.

Normalization and Analysis of Microarray Data

Expression analysis of microarray experiments was performed with GeneSpring 6.1 (Silicon Genetics) using the raw intensity data generated by the ImaGene software. Local background-subtracted median signal intensities were used as intensity measures, and the data was normalized using per spot and per chip LOWESS normalization. The transcripts that passed with flag values present or marginal were targeted for further analyses. The transcripts were then further analyzed by utilizing a one-sample Student's t-test to test whether the mean normalized expression level for the gene is statistically different from 1.0. Genes greater than 1.5 fold up and downregulated at day 4 vs day 0 were determined for both the MRL and DBA strains.

Microarray Expression Results

Over 500 genes out of 15,000 on the microarrays were significantly differentially expressed ($p < 0.05$) in MRL and DBA mice at day four in comparison to control tissue at day zero. Of these, 170 genes were upregulated and 280 were downregulated in both mouse strains. About 50% of these genes represent ESTs and unknown genes. Pathway analysis of the known genes reveals that genes in the BMP/TGF pathway are differentially expressed in both mouse strains (BMP-1, Actr2, Smad 4, TGFb1i4, Fstl3, Twsg1, TSC22), thus implicating the BMP/TGF signaling pathway in regulation of digit tip regeneration ($p < 0.05$). Shown in Table 5, is a summary of genes with known functions that are differentially expressed in regenerating digits in both MRL and DBA strains at day 4 in comparison to control tissue at day 0.

Table 5. Genes Differentially Expressed in Both MRL and DBA at Day 4 Post Digit Tip Dissection. Over 500 genes out of 15,000 were significantly differentially expressed ($p < 0.05$) in MRL and DBA mice at day four in comparison to control tissue at day zero. Of these, 170 genes were upregulated and 280 were downregulated in both mouse strains. About 50% of these genes represent ESTs and unknown genes. Pathway analysis of the known genes reveals that genes in the BMP/TGF pathway are differentially expressed in both mouse strains (BMP-1, Actr2, Smad 4, TGFb1i4, Fstl3, Twsg1, TSC22), thus implicating the BMP/TGF signaling pathway in regulation of digit tip regeneration. In the following table, only genes whose functions are known are listed, not ESTs of unknown function. Genes involved in the BMP/TGF signaling pathway are in bold.

Clone Name	Gene Name	Gene Ontology Function
H3031B07	**Twsg1**	**GO:0001503 ossification**
H3005D09	**Fstl3**	**GO:0030514 negative regulation of BMP signalling pathway**
H3098E10	Mor1	GO:0006099 tricarboxylic acid cycle
H3052A04	Mor2	GO:0006099 tricarboxylic acid cycle
H3138A12	4632428N09Rik	GO:0006118 electron transport
H3156A07	Nme6	GO:0006228 UTP biosynthesis
H3031E10	Ahcy	GO:0006306 DNA methylation
H3051D06	2700078H01Rik	GO:0006350 transcription
H3004A11	Tceb3	GO:0006350 transcription
H3097C06	**TGFB1I4 (TSC-22)**	**GO:0006355 regulation of transcription**
H3087E04	Cnot7	GO:0006355 regulation of transcription
H3016G05	Ewsh	GO:0006355 regulation of transcription
H3113H06	Fem1b	GO:0006355 regulation of transcription
H3123B05	Hdac2	GO:0006355 regulation of transcription
H3055B11	Nrf1	GO:0006355 regulation of transcription
H3058C01	Rora	GO:0006355 regulation of transcription
H3016H10	Sp1	GO:0006355 regulation of transcription
H3017H05	Wbp4	GO:0006355 regulation of transcription
H3089B10	Zfp398	GO:0006355 regulation of transcription
H3076G09	9430065L19Rik	GO:0006397 mRNA processing
H3107B08	Upf2	GO:0006397 mRNA processing
H3045D06	Psmd7	GO:0006413 translational initiation
H3023F07	Cct5	GO:0006457 protein folding
H3023D07	D630041K24Rik	GO:0006464 protein modification
H3066E06	C430014H23Rik	GO:0006468 protein amino acid phosphorylation
H3057F01	Csnk1e	GO:0006468 protein amino acid phosphorylation
H3063A08	Lgmn	GO:0006508 proteolysis and peptidolysis
H3048C09	Fbxl12	GO:0006511 ubiquitin-dependent protein catabolism
H3113D07	Psma3	GO:0006511 ubiquitin-dependent protein catabolism
H3013F01	Alad	GO:0006779 porphyrin biosynthesis
H3089A11	Abcf2	GO:0006810 transport
H3054H04	Kcnn4	GO:0006811 ion transport
H3109D12	2210017A09Rik	GO:0006813 potassium ion transport
H3030E02	Gabarapl2	GO:0006886 intracellular protein transport
H3040F06	Mpv17	GO:0006886 intracellular protein transport
H3028C06	Sec13r	GO:0006886 intracellular protein transport
H3076G10	Tomm22	GO:0006886 intracellular protein transport
H3085H07	Vps26	GO:0006886 intracellular protein transport
H3153D07	Ngfrap1	GO:0006917 induction of apoptosis
H3002C02	Actr2	GO:0006928 cell motility
H3006C11	Rps18	GO:0007046 ribosome biogenesis
H3125H12	Rps6	GO:0007046 ribosome biogenesis

H3147D06	Cdk4	GO:0007049 cell cycle
H3054A03	D5Ertd249e	GO:0007049 cell cycle
H3098A09	Epdm2-pending	GO:0007160 cell-matrix adhesion
H3066H10	Mapk8	GO:0007165 signal transduction
H3007D07	Pwp2h	GO:0007165 signal transduction
H3133D05	Rock1	GO:0007165 signal transduction
H3002D10	**Madh4**	**GO:0007184 SMAD protein nuclear translocation**
H3091D08	Gna14	GO:0007186 G-PCR protein signaling pathway
H3018D02	Gnai2	GO:0007186 G-PCR protein signaling pathway
H3001E05	Homer2	GO:0007186 G-PCR protein signaling pathway
H3154B03	Frap1	GO:0007281 germ-cell development
H3065C08	Ppp3cb	GO:0007507 heart development
H3040F05	Smyd1	GO:0007507 heart development
H3022F08	Tpm3	GO:0007517 muscle development
H3054D06	Ovgp1	GO:0008152 metabolism
H3082B04	Pfkfb3	GO:0008152 metabolism
H3048G06	Srm	GO:0008295 spermidine biosynthesis
H3069G01	9930118K05Rik	GO:0008654 phospholipid biosynthesis
H3115C03	**Bmp1**	**GO:0009887 organogenesis**
H3029F09	Atp6v1e1	GO:0015986 ATP synthesis coupled proton transport
H3002B06	Ehd1	GO:0016197 endosome transport
H3001H10	Tmsb10	GO:0030036 actin cytoskeleton organization and biogenesis
H3043B04	**Strap**	**GO:0030512 regulation of TGFB receptor signaling pathway**
H3020F08	Was	GO:0042110 T-cell activation
H3114B04	Rdx	GO:0045176 apical protein localization

Table 6. Genes Differentially Expressed in Only MRL Mice at Day 4 Post Digit Tip Dissection. The NIA15K library was created from developing mouse embryos and represents 15,264 unique genes (78% novel and 22% known). Many of these genes are expressed primarily in development and the clones are a unique source for studies of regeneration. Genes that are differentially expressed only in MRL include multiple transcription factors suggesting increased cellular replication in regenerating digit tips. Additional genes are implicated in gastrulation and pattern formation (Mesp2, Shrm). Also, genes differentially expressed are highly expressed in nerve cells (Fmn2, Net1). These genes are particularly intriguing since previous studies have shown that signals from nerves are required to induce formation of blastemas [10]. These results suggest that many genes and unknown ESTs are involved in digit regeneration.

Clone ID	Gene ID	Expression Ratio	Description	Gene Ontology Biological Process
H3046D02B		6.3	UNKNOWN	
H3094C11	A630020C 16Rik	5.5	UNKNOWN	ubiquitin-dependent protein catabolism(GO:0006511)
H3069B02	1810037G0 4Rik	4.1	EST similar to Bola-like transcription factor	
H3072F08		3.8	UNKNOWN	
H3001G12		3.4	UNKNOWN	
H3139B07	Hnrpu	3.2	Mus musculus heterogeneous nuclear ribonucleoprotein U (Hnrpu), mRNA	
H3139F02	Tcea1	3.2	UNKNOWN: Similar to Mouse transcription factor S-II, clone PSII-2	regulation of transcription, DNA-dependent(GO:0006355)
H3118G08 A	G7e-pending	3.1	Mus musculus G7e protein (G7e-pending), mRNA	
H3139G05	EST Mm. 270291	3.0	UNKNOWN: Similar to Mus musculus similar to zinc finger protein 97 [Mus musculus] (LOC233168), mRNA	
H3043F11		2.9	UNKNOWN	
H3074G12	Mesp2	2.8	Mus musculus mesoderm posterior 2 (Mesp2), mRNA	gastrulation (GO:0048276)
H3133G07	Daf1	2.8	UNKNOWN	complement activation, classical pathway(GO:0006958)
H3076F01	Pdzk2	2.7	Mus musculus natrium-phosphate cotransporter IIa C-terminal-associated protein 2 (AF334612), mRNA	intracellular signaling cascade(GO:0007242)

H3138A06		2.6	UNKNOWN	
H3115F01	2610027O18Rik	2.6	Mus musculus RIKEN cDNA 2610027O18 gene (2610027O18Rik), mRNA	
H3137F08	G630041M05Rik	2.5	UNKNOWN: Similar to Homo sapiens chromosome 1 clone RP11-397P13, complete sequence	
H3072D07		2.2	UNKNOWN	
H3004A01	Gjb3	2.2	Mus musculus gap junction membrane channel protein beta 3 (Gjb3), mRNA	cell communication(GO:0007154);cell-cell signaling(GO:0007267)
H3138F07		2.2	UNKNOWN	
H3082B03	Mylk	2.2	Mus musculus myosin, light polypeptide kinase (Mylk), mRNA	cytoskeleton organization and biogenesis(GO:0007010)
H3155G11	1810024J12Rik	2.2	UNKNOWN: Similar to Mus musculus LOC244336 (LOC244336), mRNA	
H3098E07A	Calb1	2.2	Mus musculus calbindin-28K (Calb1), mRNA	
H3126F07		2.1	UNKNOWN	
H3024A05	Sparc	2.1	Mus musculus secreted acidic cysteine rich glycoprotein (Sparc), mRNA	
H3130D01	4933421G18Rik	2.1	UNKNOWN: Similar to Homo sapiens, Similar to IDN3 protein, clone IMAGE:5496103, mRNA	
H3028F04	Ctsl	2.0	Mus musculus cathepsin L (Ctsl), mRNA	proteolysis and peptidolysis(GO:0006508)
H3019H05		2.0	UNKNOWN	
H3029B05		2.0	Mus musculus brachyury (T), mRNA	regulation of transcription, DNA-dependent(GO:0006355);development(GO:0007275)
H3046F02A		2.0	UNKNOWN	
H3026H02	Nrd1	1.9	Mus musculus hypothetical protein MGC25477 (MGC25477), mRNA	proteolysis and peptidolysis(GO:0006508)

H3089C10	8430436C05Rik	1.9	Mus musculus 16 days embryo lung cDNA, RIKEN full-length enriched library, clone:8430436C05:unclassifiable transcript, full insert sequence	
H3077A05		1.9	UNKNOWN	
H3031F01	Uqcrc1	1.9	Mus musculus ubiquinol-cytochrome c reductase core protein 1 (Uqcrc1), mRNA	electron transport(GO:0006118);proteolysis and peptidolysis(GO:0006508)
H3048F06		1.9	UNKNOWN	
H3021A04		1.9	UNKNOWN	
H3078D11	shrm	1.9	Mus musculus, clone IMAGE:3484373, mRNA, partial cds	pattern specification(GO:0007389);intracellular signaling cascade(GO:0007242)
H3083B07		1.8	UNKNOWN	
H3099H03		1.8	UNKNOWN	
H3022C07		1.8	UNKNOWN	
H3101C02		1.8	UNKNOWN	
H3149D01	2810450M21Rik	1.8	Mus musculus similar to Rad50-interacting protein 1; hypothetical protein FLJ11785 [Homo sapiens] (LOC231040), mRNA	
H3043C06		1.8	UNKNOWN	
H3148C11		1.7	UNKNOWN	
H3015C11	Arcp-pending	1.7	Mus musculus, RIKEN cDNA 2310016N05 gene, clone MGC:29418 IMAGE:5043872, mRNA, complete cds	biological_process unknown(GO:0000004)
H3011B08	2310061B02Rik	1.7	Mus musculus, clone IMAGE:3584936, mRNA	
H3050B08		1.7	UNKNOWN	
H3062H03		1.7	UNKNOWN	
H3086H09	Net1	1.7	Mus musculus mRNA for Rho guanine nucleotide-exchange factor, splice variant NET1A	
H3083E03	Raly	1.7	Mus musculus hnRNP-associated with lethal yellow (Raly), mRNA	

H3080H11	Plat	1.7	Mus musculus plasminogen activator, tissue (Plat), mRNA	proteolysis and peptidolysis(GO:0006508)
H3119C09		1.7	UNKNOWN	
H3073G03		1.7	Mus musculus histone binding protein NASP (Nasp) gene, complete cds, alternatively spliced	
H3015F12	1110056N09Rik	0.47	UNKNOWN: Similar to Mus musculus RIKEN cDNA 1110056N09 gene (1110056N09Rik), mRNA	
H3094E02	A230106A15Rik	0.46	UNKNOWN	
H3001E07		0.45	UNKNOWN	
H3057F01	Csnk1e	0.44	Mus musculus casein kinase 1, epsilon (Csnk1e), mRNA	circadian rhythm(GO:0007623);protein amino acid phosphorylation(GO:0006468)
H3023G09	Ddx5	0.44	Mus musculus DEAD (aspartate-glutamate-alanine-aspartate) box polypeptide 5 (Ddx5), mRNA	
H3030D06	Dctn5	0.43	Mus musculus, dynactin 4, clone MGC:19347 IMAGE:4235312, mRNA, complete cds	
H3070F07	9430020K16Rik	0.42	UNKNOWN	
H3113H06	Fem1b	0.42	Mus musculus LOC213060 (LOC213060), mRNA	regulation of transcription, DNA-dependent(GO:0006355)
H3061A09C		0.41	UNKNOWN	
H3115D09	9630025B04Rik	0.38	UNKNOWN	
H3016H10	Sp1	0.35	Mus musculus trans-acting transcription factor 1 (Sp1), mRNA	regulation of transcription, DNA-dependent(GO:0006355)

H3156A07	Nme6	0.35	Mus musculus expressed in non-metastatic cells 6, protein (nucleoside diphosphate kinase) (Nme6), mRNA	GTP biosynthesis(GO:0006183);UTP biosynthesis(GO:0006228);CTP biosynthesis(GO:0006241)
H3109A10		0.33	UNKNOWN	
H3040F03		0.30	UNKNOWN	
H3059A01		0.28	UNKNOWN	
H3050D11	D2Ertd391e	0.27	Mus musculus similar to Hypothetical protein KIAA0652 (LOC228360), mRNA	
H3052A04	Mor2	0.26	Mus musculus malate dehydrogenase, soluble (Mor2), mRNA	tricarboxylic acid cycle(GO:0006099)
H3133H08	1110067M05Rik	0.16	Mus musculus 18 days embryo whole body cDNA, RIKEN full-length enriched library, clone:1110067M05:unclassifiable transcript, full insert sequence	
H3031E07	Myg1-pending	0.13	Mus musculus melanocyte prolifeating gene 1 (Myg1-pending), mRNA	
H3085D12		0.12	Mus musculus NIMA-related kinase Nek9 (Nek9), mRNA	
H3143D05C	4930562C03Rik	0.12	UNKNOWN: Similar to Mus musculus RIKEN cDNA 4930562C03 gene (4930562C03Rik), mRNA	
H3007D07	Pwp2h	0.12	Mus musculus RIKEN cDNA 6530411D08 gene (6530411D08Rik), mRNA	signal transduction(GO:0007165)
H3045D06	Psmd7	0.11	Mus musculus proteasome (prosome, macropain) 26S subunit, non-ATPase, 7 (Psmd7), mRNA	translational initiation(GO:0006413)
H3037A08		0.09	UNKNOWN	
H3089A11	Abcf2	0.07	Mus musculus similar to ATP-binding cassette, sub-family F, member 2 [Homo sapiens] (LOC214267), mRNA	transport(GO:0006810)

H3138A12	4632428N09Rik	0.07	Mus musculus RIKEN cDNA 1810019E15 gene (1810019E15Rik), mRNA	electron transport(GO:0006118)
H3094C04		0.05	UNKNOWN	
H3043F09	Grcc8	0.01	UNKNOWN: Similar to Mus musculus, gene rich cluster, C8 gene, clone MGC:5778 IMAGE:3592108, mRNA, complete cds	
H3055B11	Nrf1	0.01	UNKNOWN	regulation of transcription, DNA-dependent(GO:0006355);carbohydrate metabolism(GO:0005975);mitochondrion organization and biogenesis(GO:0007005)
H3040F05	Smyd1	0.01	Mus musculus t-BOP (Bop) mRNA, complete cds	heart development(GO:0007507);chromatin modeling(GO:0006338);negative regulation of transcription(GO:0016481)
H3114D02		0.01	UNKNOWN	
H3084G12	C630029K18Rik	0.01	UNKNOWN	
H3134E08		0.01	UNKNOWN	

Confirmation of Microarray Results by Real Time PCR

Reverse transcription of 200ng of total RNA (Day 4 and Day 0) was carried out in a final volume of 20ul using Invitrogen's reverse transcriptase kit according to the manufacturer's instructions. To prevent 3' bias of the real-time PCR reactions random decamers (Ambion) were used for priming rather than oligo-dT. Real-time PCR was done using the SYBR Green PCR Core Reagents Kit (Applied Biosystems). Five microliters of cDNA at a concentration of 10ng/ul, and 0.1 uM of each primer in a final volume of 25 ul was used. For statistical significance, each RT-PCR had six replicates. Once the master mix was made, the 25ul aliqots were transferred into a MicroAmp optical 96-well reaction plate (Applied Biosystems). vortexed, and sealed with an optical adhesive cover (Applied Biosystems). Cycling and signal detection was done using the ABI-7900HT Sequence Detection System with the following cycling conditions: initial activation at 95^0C for 10 minutes, then 40 cycles at 95^0C for 15 seconds and 60^0C for 1 minute. Product specificity was checked by including a dissociation stage according to the manufacture's instructions (Applied Biosystems). The gene expression level was normalized by housekeeping gene Beta-Actin expression level. A subset of all RT-PCRs were sequenced to insure gene specificity for the reactions.

Figure 6. Confirmation of MRL Microarray Results by Real-time PCR. Plotted below are the fold change values of RNA expression in MRL mice at day 4 in comparison to day 0 control RNA. Real-time PCR fold changes are normalized to beta-actin. Most genes determined to be differentially expressed by microarray also show differential expression by real-time PCR. Differences in Smad4, MMP9 and Maged are likely due to cross hybridization of genes with high sequence similarity or polymorphic sequence mismatches in real-time PCR primers.

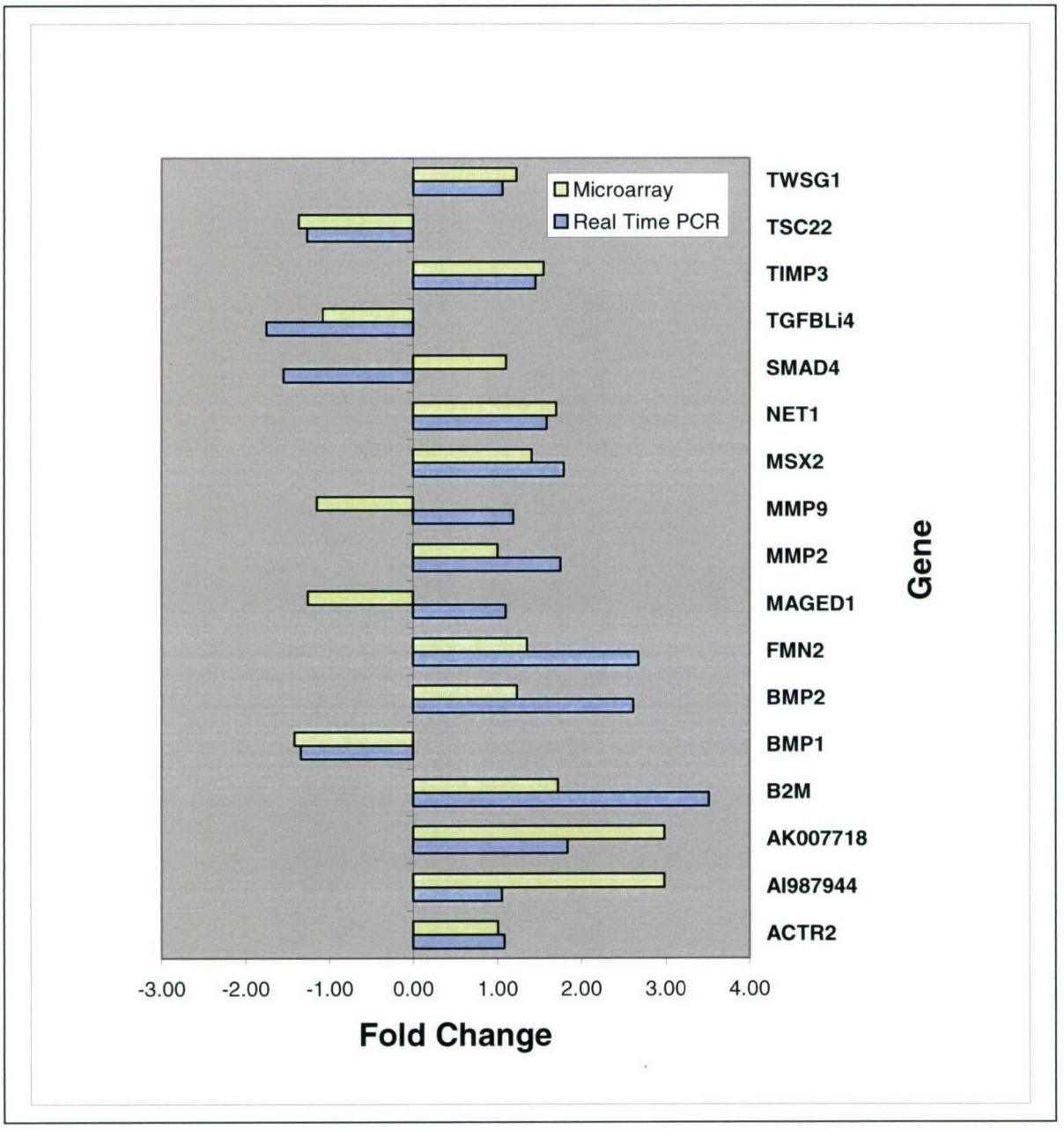

Figure 7. Confirmation of DBA Microarray Results by Real-time PCR. Plotted below are the fold change values of RNA expression of digit tips in DBA mice at day 4 in comparison to day 0 control RNA. Most genes determined to be differentially expressed by microarray also show differential expression by real-time PCR. Differences in BMP2 are likely due to cross hybridization of genes with high sequence similarity or polymorphic sequence mismatches in real-time PCR primers.

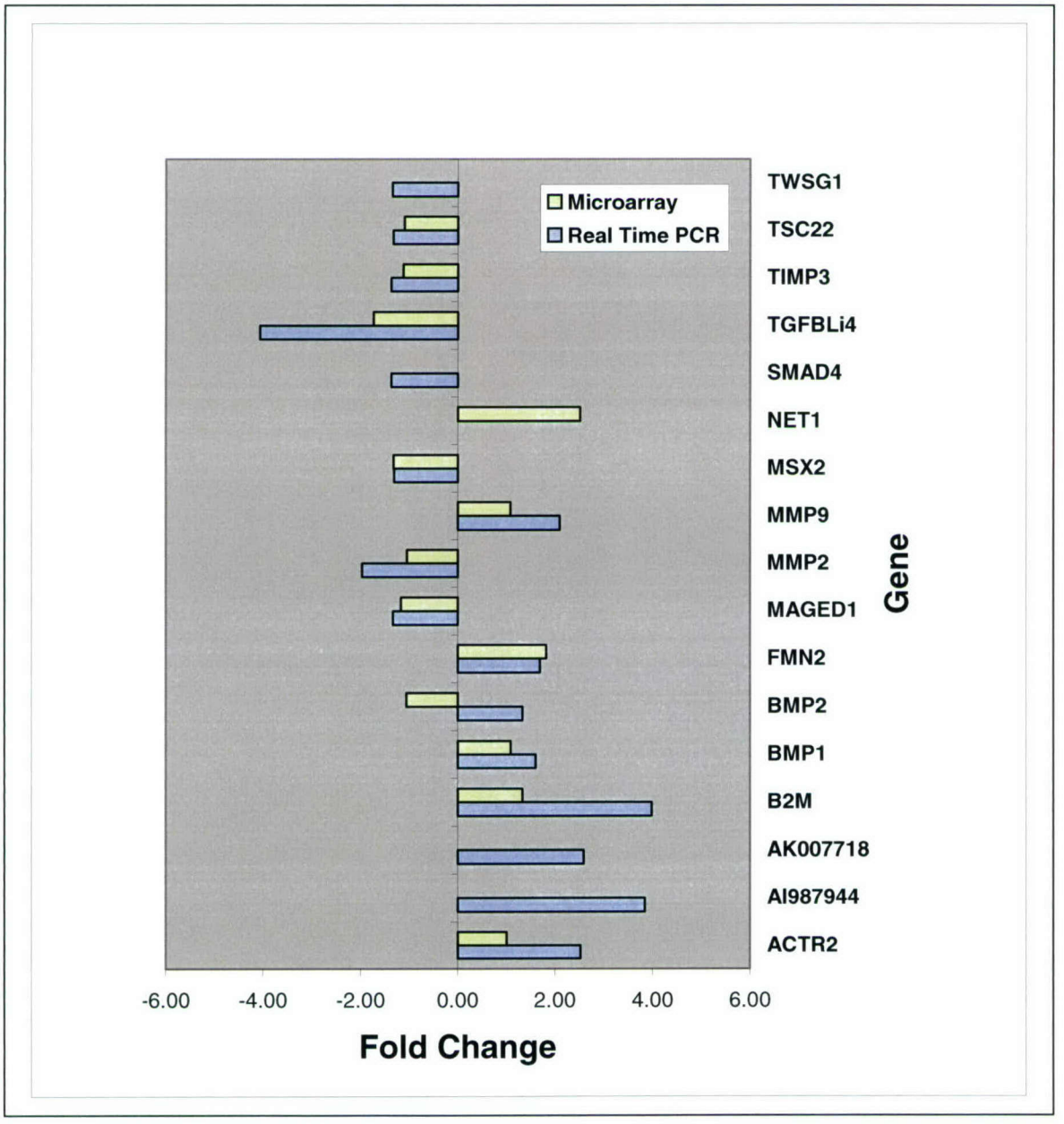

Additional Progress

Since blastemas were not seen to form at 1 day post digit tip dissection, we have begun examining other times points. We believe that we have seen the beginning of blastema formation by 4 days post dissection in B6 mice. As shown in Figure 8, a mass of dedifferentiated cells is seen below the epithelial layer in a B6 mouse pup at 4 days post surgery. We are in the process of confirming these results and extending the histology studies to additional times point and the other mouse strains.

Figure 8. Blastema Formation in B6 Regenerating Digit Tip at Four Days Post Surgery.

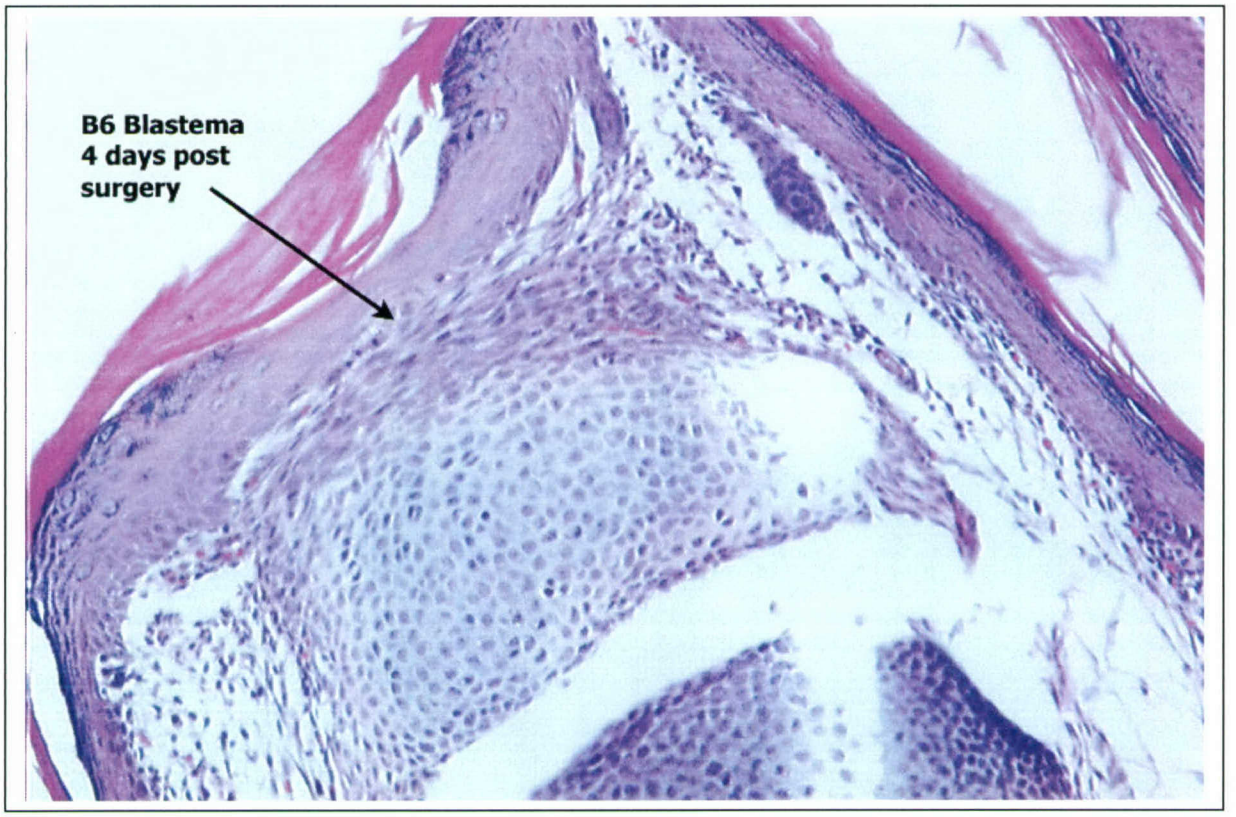

Key Research Accomplishments

- Determined that MRL mouse strains regenerate digit tips more quickly and to a greater extent than DBA, SJL, C57BL/6J, C3H and 129/Sv mouse strains.
- Found that at 1-day post surgery only the MRL and DBA strains have formed an epidermal layer over the dissected digit tip.
- Discovered evidence of blastema formation at day 4 post digit tip dissection in B6 mice.
- Undertook global microarray expression profiling in MRL and DBA regenerating digit tips in RNA isolated from day 4 regenerating digit tips in comparison to control RNA at day 0.
- Identified that the BMP/TGF-beta signaling pathway is likely involved in digit tip regeneration in the MRL and DBA mouse strains.

- Found several interesting candidate genes that are differentially expressed only in MRL regenerating digit tips (Shrm, Mesp2, Fmn2, Net1). These are known to function in embryogenesis and pattern formation and/or are highly expressed in neurons.

Reportable Outcomes

Presentations:

1. Chadwick R.B., Bu L.M., Yu H., Hu Y., Sachdev R., Tan Q.W., Wergedal J.E., Mohan S., and Baylink D.J. Digit Tip Regeneration and Global Gene Expression Profiling in the MRL Super-Healer Mouse. American Society for Bone and Mineral Research, Seattle, WA, October 2004.

Conclusions

1) MRL mice show greater regenerative capacity to heal digit tips compared to DBA mice. This increased regeneration is seen primarily during the times of greatest growth in young mice (days 0 to 14).

2) Expression results suggest indicate that the BMP/TGF signaling pathway is likely involved in digit tip regeneration in both MRL and DBA in-bred strains of mice.

3) Increased regenerative capacity of the MRL mouse may be due to strain specific increased expression of transcription factors that function in embryogenesis, pattern formation and development.

4) After surgery of newborn pups, mothers often reject or cannibalize the pups. This appears to be more of a problem in some strains (e.g. SJL, 129, C3H) than others (MRL, DBA, B6). However, the rejection and cannibalization of pups makes a QTL study of 300 F2 mice not feasible since the pups won't survive to phenotype (measure growth rates following dissection). Thus in the second year of the study we propose to:

a) Extend the histological studies to additional time points (days 4, 7, 14, 21) to further characterize cells involved in blastema formation and digit regeneration in four to six strains of mice.
b) Do additional microarray and real-time PCR expression studies at these times points to determine the genes and genetic pathways involved in the digit tip regeneration at each time point.
c) Use immunohistochemistry of a selected subset of differentially expressed genes to determine what cellular types express those genes involved in digit tip regeneration.
d) Develop in vitro models of determining gene function by establishing primary cultures of regenerating digit tip cells and using siRNA transfections to selectively block expression of candidate genes.
e) Examine knockout mice of differentially expressed genes (if they are available from Jackson Laboratories) to further characterize the function of genes involved in digit tip regeneration.

References

1. Muller, T.L., et al., Regeneration in higher vertebrates: limb buds and digit tips. Semin Cell Dev Biol, 1999. 10(4): p. 405-413.

2. Brockes, J.P., Amphibian limb regeneration: rebuilding a complex structure. Science, 1997. 276(5309): p. 81-87.
4. Goss, R.J., et al., Epidermal downgrowths in regenerating rabbit ear holes. J Morphol, 1975. 146(4): p. 533-542.
5. Joseph, J., et al., Effect of anabolic androgens on tissue replacement in the ear of the rabbit. Nature, 1966. 211(45): p. 193-194.
6. Li, X., et al., Genetic control of the rate of wound healing in mice. Heredity, 2001. 86(Pt 6): p. 668-674.
7. Clark, L.D., R.K., et al., A new murine model for mammalian wound repair and regeneration. Clin Immunol Immunopathol, 1998. 88(1): p. 35-45.
8. Leferovich, J.M., et al., Heart regeneration in adult MRL mice. Proc Natl Acad Sci U S A, 2001. 98(17): p. 9830-9835.
9. Tanaka T.S. et al., Genome-wide expression profiling of mid-gestation placenta and embryo using a 15,000 mouse developmental cDNA microarray. Proc Natl Acad Sci U S A, 2000. 97(16), p. 9127-9132.
10. Endo T. et al., Developmental Biology 2004. 270(1), p. 135-45.

Project 2: Sensitizer Screening to Enhance Detection of ENU-Induced Mutant Phenotypes

Introduction

In the present study, we propose to employ mouse models in which genes that have been previously implicated to play a critical role in the development and maintenance of musculoskeletal tissues have been knocked out. By using mice with mutation in a gene known to affect musculoskeletal phenotypes, we propose to sensitize a classical ENU mutagenesis screening system (1), and thereby increase the recovery of mutants by discovering genes that have subtle effects on musculoskeletal phenotype. The principle for increased sensitivity of recognition is synergism between the unknown ENU mutation and the known knock out gene (2-4). One of the important requirements for the success of our approach involving sensitizer screen to identify novel mouse mutants for musculoskeletal phenotypes relates to which knockout mouse models are selected for ENU mutagenesis screens. In this regard, it is now widely accepted that IGF-I (5) and TGF β (6) are two critical regulatory molecules that regulate growth and development of musculoskeletal tissues and that deficiencies in these two growth factors contribute to impaired growth and maintenance. Furthermore, IGF-I and TGF β have been implicated in mediating the effects of many systemic and local factors that regulate musculoskeletal system. We therefore propose to employ growth hormone knockout *lit/lit* (IGF-I deficient) and Smad2 (a key signaling molecule for TGF β signaling pathway) knockout mouse models to screen for ENU-induced mutant phenotypes based on the hypothesis that mutant genes will exhibit greater effect on the musculoskeletal phenotype under reduced dosage of IGF-I and TGF-β.

Body

Technical Objectives

To identify the mouse mutants with musculoskeletal phenotypes in the F1 progeny of ENU treated male mice mated with IGF-I deficient *lit/lit* and TGF β deficient Smad2 knockout female mice compared to their respective wild type female mice.

To achieve the above technical objective, we have undertaken the following specific objectives during the first 12 months of this study.

a) Establish breeding colonies for *lit/lit* and Smad 2 knockout mice (We currently have *lit/lit* mice. Breeding pairs of Smad2 knockout mice will be obtained from our academic collaborator). Generate homozygous and heterozygous mutant mice for production of normal data for our screens for musculoskeletal phenotypes

b) Breed knockout females with wild type ENU treated males to generate 50 F1 progeny for each *lit/lit* and Smad2 mutant. Breed wild type females with ENU treated males to produce 50 F1 control progeny.

c) Perform musculoskeletal screens at 10 weeks of age in the F1 progeny to measure bone mineral content, bone density, bone size, muscle size and fat content using PIXImus and pQCT instruments. Perform biochemical measurements of bone turnover in the serum samples.

Progress on Specific Objectives

Technical Objective 1a:

Establish breeding colony of *lit/lit* and Smad2 knockout mice.

We obtained two breeding pairs of *lit/lit* mice from our ongoing studies and purchased four heterozygous male (*lit*/+) and four homozygous females (*lit/lit*) from The Jackson Lab, Main. We bred heterozygous (*lit*/+) male mice with either homozygous (*lit/lit*) or heterozygous (*lit*/+) females to produce approximately 40 *lit/lit* or *lit*/+ male and female progeny. To establish our Smad2 breeding colony, we obtained two breeding pairs (both male and female heterozygous) from our collaborator Dr. Michael Weinstein, Molecular Genetics Division, Ohio State University. The original heterozygous Smad2/+ (the homozygous Smad2/Smad2 mice are not viable, in this report our reference to the 'Smad2' sign indicates disabled a 'Smad2' gene while the '+' sign indicates the presence of a normal Smad2 gene) mice were bred with WT B6 male and females for two generations to produce approximately 18 Smad2/+ male and female mice. These heterozygous mice were bred to produce 15 Smad2/+ second generation progeny for breeding with ENU injected males. We used only second-generation Smad2/+ females for generating pups for sensitized screening. Both *lit*/+ and Smad2/+ progeny were identified by PCR based genotyping assays described below.

Development of a SNP assay for genotyping of sensitized screen progeny generated from ENU injected B6 males and lit/lit females

The little (*lit/lit*) mouse is a dwarf strain with an autosomal recessive mutation in the growth hormone-releasing hormone receptor (GHRHR) gene. The mutation affects only one nucleotide, an A to G mutation, at base number 112 in the GHRHR gene. Since a genotype assay for this mouse has not been reported, we developed a single nucleotide polymorphism (SNP) assay to identify the '*lit*' allele especially for identifying heterozygote (*lit*/+) mice that have only one mutated copy of the gene and are difficult to identify by phenotype screen. The Jackson Laboratory, Maine, from where we procured these mice, relies on phenotype to identify the *lit/lit* mice.

The assay used for SNP genotyping of the *lit* gene is the 5' nuclease assay. This assay uses primers that amplify the *lit* gene region and probes that are specific to the target region containing the SNP (A to G) to determine which alleles are present in each sample of DNA. Each probe has a reporter dye and a quencher attached to opposite ends of the 20 base pair sequence. The wild type probe has a different reporter dye than the probe used for *lit/lit* mice. These fluorescent dyes cannot be detected when the probe is intact because when the quencher is in close proximity, it quenches the dye by fluorescence resonance energy transfer (FRET). To identify *lit* alleles, the 5' nuclease activity of Taq Polymerase is utilized to cleave the probe and allow the reporter dye to fluoresce (see Figure 1).

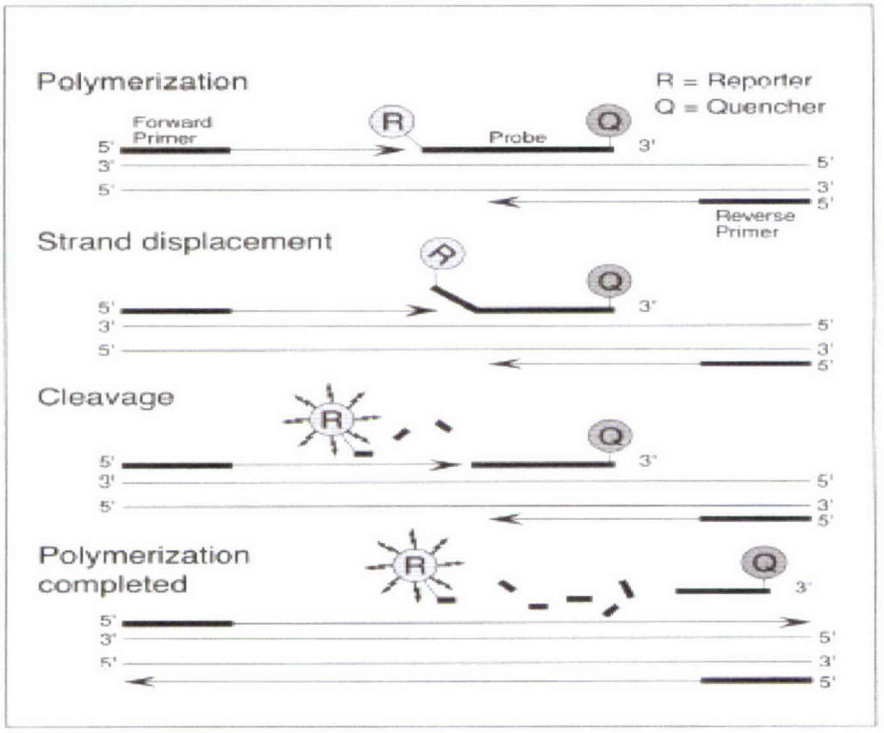

Figure 1: PCR amplification and detection with fluorogenic probes in the 5' nuclease assay.

In a sample with only the normal gene, the probe for the mutant gene will not bind to the DNA, so the Taq Polymerase will not get a chance to cleave it, thus the only signal will be from the wild type reporter dye. For the genotyping assay, the DNA was extracted from mouse tails (clips <1 cm in 2 pieces) using the DNeasy 96 kit and SNP specific region of GHRHR gene was amplified using primer pair- 5'-CCT TCA GCA CTG CCA TTC AG-3'and 5'-CAG GGG AGA GAG ACC CAC TG-3.' To identify wild type alleles we used "ACC TGG GAT GGG CTG CTG TG—BHQ" probe and "ACC TGG GGT GGG CTG CTG T—BHQ" probe was used for the *lit/lit* allele. After PCR amplification of the gene, the ABI Prism 7900 Sequence Detection System (SDS) was used to detect how much of each dye is reporting in each sample and results (mutant dye vs. wild-type dye) were presented in a graph form. Three distinct groups (see Figure 2) could be identified. One group of points represents those that are +/+; a second represents those that are *lit*/+, and the third, those that are *lit/lit*. We used three controls; a wild-type B6 mouse, the *lit/lit* pair of mice obtained from The Jackson Lab and a non-template control (NTC).

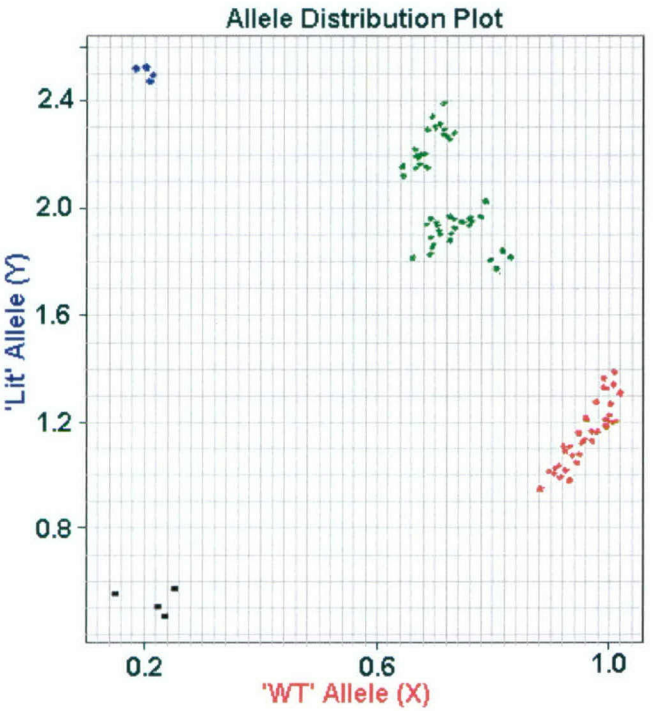

Figure 2: Allele X is the wild type allele (shown in red), and Allele Y is the Mutant allele (*lit*) (shown in blue). The wild type probe has a different reporter dye than the mutant probe. The heterozygotes (green) have both reactions taking place in the well. Black dots indicate non-template controls.

Development of a PCR based genotype assay for screening progeny generated from ENU injected B6 males and Smad2/+ *females*

Smad2 is an intracellular mediator of TGF-β signaling pathway. The homozygous (Smad2/Smad2) KO mice die during embryonic development, whereas, heterozygous (Smad2/+) mice survive and live normally. Our sensitized screen is designed to screen ENU mutations in a Smad2/+ background. Therefore, in order to determine which mice have the 'Smad2' allele, it is necessary to genotype them. We took advantage of the fact that in Smad2 KO mice, the Smad2 gene is replaced with a neomycin reporter gene. Our assay is based on detection of the PCR product corresponding to the neomycin sequence. Primers listed in Table –1 and specific to the Smad2 gene and the neo gene were used to distinguish which mice are Smad2 heterozygous. For the genotyping assay, DNA was extracted using the DNeasy 96 kit and the Smad2 sequence was amplified using a primer pair described in Table – 1. The PCR products were separated on 6% polyacrylamide gel, stained with ethidium bromide and visualized by Chemilmager 4400 Low Light Imaging system. Primer pair 1 amplifies a region, about 150 base pairs (BP) long, of the Smad2 gene and thus a band indicates a wild type allele. Primer pair 2 amplifies a larger region of the same gene, about 300 BP. Primers 3, 4, and 5 are all from the neo gene. Using primer pairs 1,3 and 6, we have genotyped each mouse generated from smda2/+ and ENU injected B6 mice. All mice will have a wild type band and mice that have a band with primer pair 6 were identified as Smad2/+ (Figure-3).

Table 1. Primers and PCR products used for genotype assay for screening Smad2 allele.

Primer Pair No	Sequence Information	Size of band (Base Pair)	Allele
1	5'—CAT GAA TAC TAC GAC GGA GG—3' 5'—GGA CCA GAC TCA CTA GTT CA—3'	150	WT
2	5'—CAT GAA TAC TAC GAC GGA GG—3' 5'—CTC CTT GAT GGA TGA ACT TC—3'	300	WT
3	5'—TGA ATG AAC TGC AGG ACG AG—3' 5'—ATA CTT TCT CGG CAG GAG CA—3'	171	Smad2
4	5'—AGA CAA TCG GCT GCT CTG AT—3' 5'—AGT GAC AAC GTC GAG CAC AG—3'	176	Smad2
5	5'— AGA CAA TCG GCT GCT CTG AT —3' 5'—CAA TAG CAG CCA GTC CCT TC—3'	203	Smad2

Normative data on musculoskeletal phenotypes in lit/lit and Smad2 *knockout mice.* To obtain normative data we bred homozygous (*lit/lit*) and heterozygous (*lit*/+ or Smad2/+) mice with wild type B6 males and females to generate approximately 50 F1 progeny each from *lit*/+ and Smad2/+ strain (see details in Table-2). These mice were genotyped at 10-week age when blood collection, DEXA, and pQCT measurements were performed as described below in section-B (age varied by ±2days). The phenotype measurements were repeated at 16-weeks age to establish reference values for the 16-week old mice. The availability of normative data is essential for identification of outlier mice based on quantitative differences.

Technical Objective 1b:

Production of ENU mutagenized male.

I) We injected two batches of 8-10 week old C57BL/6J mice with 3x100 mg/kg of ENU. Previous studies by our group have shown that B6 mice can tolerate this dose and regain fertility within 12-20 weeks post ENU injection. Two batches of ENU injected males were spaced at a 3-month period to allow us a continuous supply of ENU mutagenized B6 males for breeding with *lit/lit* or Smad2/+ mice.

II) 12-Weeks after the last ENU injections, each ENU injected B6 male was bred with two 8-20 week old *lit/lit* or Smad2/+ females. The B6 ENU injected male

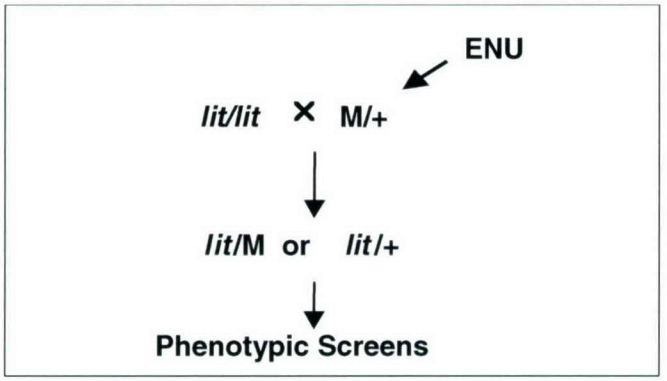

Figure 3 . Breeding strategies for sensitized screening using *lit/lit* mouse as an example.

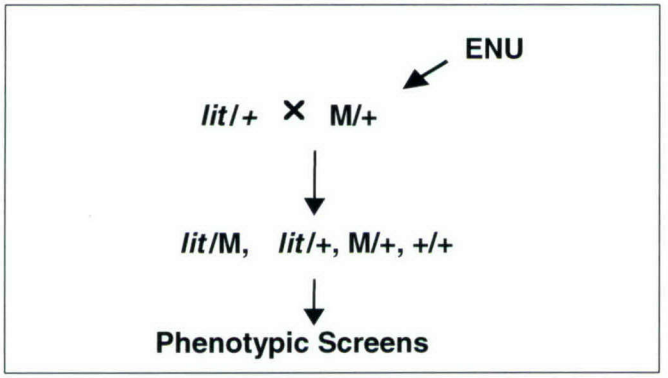

Figure 4. Alternative breeding strategy employed for sensitized screening using *lit*/+ mice.

mice typically recovered in 14-15 weeks and produced litters with 2-6 pups/litter. However, the fertile period was brief and lasted between 10-14 weeks. About 50% males were fertile and 20% males died before recovery of fertility. Females are checked routinely for pregnancy, and the pregnant mice are removed from mating cages and replaced by fresh females.

III) The generation and screenings of B6 mice were initially attempted as proposed in Figure-3. However, we observed that *lit/lit* female mice (which have 30-40% lower body weight) were difficult to breed and took a longer period to produce fewer litters. The breeding with ENU injected males was especially slow because of small period of time (fertility window) during which ENU injected males are fertile. To overcome this difficulty, we changed our strategy to breed *lit*/+ female mice, which have normal body weight and produce litters more frequently with ENU injected males (this new breeding scheme is described in Figure-4).

Due to the change in breeding strategy, we generated additional animals that have the +/+ genotype, which are not useful for our sensitized screen. However, this strategy eliminates the need for additional breeding of wild type B6

with ENU injected males to produce about 50 pups for calculating and comparing mutation frequency rate between sensitized and non-sensitized ENU screen as proposed in Specific Objective-2. We can use all mice that have been generated from breeding *lit*/+ with ENU injected males and have +/+ genotype for non-sensitized screen. During this reporting period, we have screened a total of 109 mice for dominant mutations in *lit*/+ or Smad2/+ background. Out of these, 49 mice had the +/+ genotype.

Technical Objective 1c:

Musculoskeletal screening of 10 week old F1 progeny from *lit*/+ or Smad2/+

- All sensitized screen mice and control mice were first screened for visible phenotypes at weaning when their body weights were also recorded. After weaning, mice were kept in groups of 2-3 males/cage and 3-4 females/cage until 10-week old. At 10-week, mice were screened for: a) visible abnormalities, b) body weight; c) total body bone density determined by DEXA instrument PIXImus (excluding skull area); d) total body bone mineral content by DEXA; e) total body bone area by DEXA; f) total body fat mass; g) lean mass; h) volumetric bone density at tibia determined by peripheral quantitative computed tomography; i) IGF-I levels in *lit*/+ mice; j) skeletal alkaline phosphatase; k) serum calcium; l) lipid profile; and m) blood creatinine kinase levels. An abnormality is usually recognized if a phenotype differs by 2.5-3 standard deviations (SD) units (since some mutations could have subtle effects, we considered 2 SD units as an acceptable criteria if consistent differences are observed in repeat testing at 16-weeks) as compared to values obtained from age and sex matched non-mutagenized control mice. Measurements that are found to be outside the cutoff range are repeated at 16-weeks to confirm the phenotype. For this purpose, we have obtained additional baseline values for age and sex matched *lit*/+ and Smad2/+ mice at 16-week of age. Some phenotype measurements, such as BMC, bone area, femur BMD, and endosteal and periosteal circumference are size-dependent and show strong correlation with body weight, thus, they were normalized with body weight for identifying phenodeviants or mutant mice. Those phenodeviants that are confirmed after repeat testing are introduced to inheritance-test (IT) or backcross with wild type *lit/lit* or Smad2/+ mice. Because of the significant efforts involved in progeny testing, we have focused on those phenodeviants that had highest differences in phenotypes. A mutation is considered inheritable if the phenotype is recovered in backcross progeny.

- Since the TGF-β pathway has been implicated in the tissue regeneration, we added additional screening of 'soft-tissue regeneration' (STR) in the 'Smad2' sensitized screen. To screen mice, we punched a 2 mm hole in both ears and tissue regeneration was monitored by measuring hole size after 14-day and 21-day period using a magnifying glass (4x)

with an embedded measuring scale (reading capabi*lity* of ±0.1 mm). We observed that healing is normally slow in Smad2/+ background with mean hole size after 3-weeks of 1.7±0.2. Therefore, we anticipate hypomorphic mutation could be easier to identify.

Screening of Control Mice: We have generated 111 mice from breeding of *lit/lit* or *lit*/+ mice (n=52) or Smad2/+ mice (n=59) with wild type B6 mice. About 60% mice carried *lit*/+ alleles when *lit*/+ mice are bred with WT B6 males, which was close to expected 50% ratio. However, this ratio was less efficient than breeding *lit/lit* mice with WT B6 males, which could result in 100% pups with *lit*/+ background, as proposed in our Specific Objective-2 (as explained earlier, we have to use an altered breeding strategy due to difficulty in breeding *lit/lit* females). Similarly, about 60% of control mice carried Smad2/+ genotype. Representative phenotype data on *lit*/+ is shown in Table – 3. Similar data was obtained from Smad2/+ male and female mice.

Phenodeviants Identified in Sensitized ENU Screening: We have screened 109 F1 progeny (Table –2) for all phenotypes listed above in Item-CI. We observed 19 phenodeviants in our primary screening performed at 10-weeks and confirmed 13 quantitative phenodeviants in 16-weeks repeat testing. Table – 4 and Figures 5-7 show several outlier mice that were confirmed in our repeat testing of phenotype. These are classified in two main categories: 1) phenodeviants with high body weight, high bone density and high bone mineral content; and 2) phenodeviants with low body weight, low bone density and low bone mineral content. Both these categories were anticipated because mutations in GHRHR and Smad2 genes are involved in developmental type phenotypes.

Results of our previous ENU screen employing the B6 mouse strain reveal a frequency of 2-3% outliers per 100 mice screened from ENU injected males (with a dose of 100 mg/kg). If we compare the frequency of a non-sensitized ENU mutation rate with results obtained in our current sensitized screen where we observed 13 quantitative phenodeviants, we see approximately 4-5 fold higher rate of phenodeviants. However, our estimate of mutation rate for the current sensitized screen is only based on about 100 mice, which could be misleading. We will be able to compare the mutation frequency better after completion of second year of the grant period when we would complete screening of about 300 sensitized mice.

In the control ENU screen, we observed a few interesting phenotypes in +/+ background; one such phenodeviant was with high bone mineral content (Z-score=3.0) and high total body bone area (Z-score=2.9) at 10- and 16-week screens. We will breed these phenodeviants with WT B6 mice for further follow-up.

Table 2. Number of mice generated, mice screened for various phenotypes, and number of mice introduced to inheritance testing.

Procedure	**Number of *lit*/+ Mice**	**Number of Smad2/+ Mice**
Control Mice Screened for Dominant Mode of Inheritance (F1)	52	59
Sensitized ENU Mice Screened for Dominant Mode of Inheritance (F1)	58	51
Abnormal Phenotypes Identified in Primary Screen (in *lit*/+ or Smad2/+ background and excluding +/+ background)	14	5
Abnormal Phenotypes Confirmed in Secondary Screen (in *lit*/+ or Smad2/+ background and excluding +/+ background)	9	4
Phenotypes Introduced to Progeny Testing	5	2

Table 3. Representative data on reference values of bone density and other parameters on 10-week and 16-week old non-mutagenized control mice (n=15-20).

Phenotype	Sex	10-Week Old Mice		16-Week Old Mice	
		Mean±SD	Population Variance (CV)	Mean±SD	Population Variance (CV)
Total body BMD (g/cm^2)	F	0.0491±0.0021	4.4	0.0523±0.0027	5.1
	M	0.0483±0.0016	3.2	0.0533±0.0018	3.5
Total body BMC (g)	F	0.427±0.024	5.7	0.492±0.031	6.3
	M*	0.464±0.035	7.6	0.506±0.048	9.4
Total body Bone Area (cm^2)	F	8.8±0.34	3.9	9.2±0.49	5.3
	M*	9.5±0.45	4.8	9.7±0.68	7.1
Body Weight	F	21.5±1.2	5.6	23.8±1.6	6.9
	M*	26.0±2.2	8.4	28.6±2.8	9.7
Bone Density at Midshaft Tibia (mg/cm^3)	F	720±20	5.6	750±21	2.9
	M*	720±20	2.8	750±28	3.7
Periosteal Circumference at Tibia Midshaft (mm)	F	4.1±0.1	4.3	4.1±0.11	4.4
	M*	4.3±0.2	4.6	4.4±0.2	4.5

*Male significantly ($p<0.05$) different from female.

Table 4. Representative data on reference values of bone density and other parameters on 10-week and 16-week old non-mutagenized smad2 control mice (n=20-30).

Phenotype	Sex	10-Week Old Mice	
		Mean±SD	Population Variance (CV)
Total body BMD (g/cm^2)	F	0.0509±0.0018	3.6
	M	0.0566±0.0051	8.9
Total body BMC (g)	F	0.518±0.031	5.9
	M*	0.531±0.043	8.1
Total body Bone Area (cm^2)	F	10.0±0.5	5.4
	M*	10.7±0.4	3.7
Body Weight	F	23.8±1.8	7.6
	M*	30.6±2.9	9.5
Bone Density at Midshaft Tibia (mg/cm^3)	F	682±20	3.0
	M*	719±29	4.0
Periosteal Circumference at Tibia Midshaft (mm)	F	4.5±0.2	3.7
	M*	4.7±0.2	4.3

*Male significantly ($p<0.05$) different from female.

Table 5. List of interesting phenodeviants identified in sensitized ENU screen.

Phenotype (Mice ID)	Description of 10-Week Phenotype	Description of 16-Week Repeat Phenotype	Sensitizer Screen
14.9.8.EM	BMD Z-Score=3.1 BMC Z-Score=2.1	BMD Z-Score=3.0 BMC Z-Score=3.3 (Body weight adjusted BMC 20% High)	Lit/+
14.10.8.BM	BMD Z-Score=2.0 BMC Z-Score=1.7	BMD Z-Score=2.3 BMC Z-Score=1.9 (Body weight adjusted BMC 18% High)	Lit/+
15.2.3.BM	Body Weight Z-Score=3.2 BMD Z-Score=3.6 BMC Z-Score=3.8	Body Weight Z-Score=3.2 BMD Z-Score=3.6 BMC Z-Score=3.8	Lit/+
15.12.7.FF	Mouse too small to screen	Body Weight Z-Score=-5.7 BMD Z-Score=-6.1 BMC Z-Score=-5.5	Lit/+
14.10.6.AF	Body Weight Z-Score=-3.3 BMD Z-Score=-4.8 BMC Z-Score=-4.8	Body Weight Z-Score=-2.3 BMD Z-Score=-2.6 BMC Z-Score=-2.6	Lit/+
14.10.6.FF	BMD Z-Score=-4.1 BMC Z-Score=-3.9	BMD Z-Score=-2.3 BMC Z-Score=-2.8	Lit/+
16.1.7.EF	STR Z-Score=3.1		Smad2/+
16.6.5.CM	Body Weight Z-Score=2.8 BMD Z-Score=2.9 BMC Z-Score=3.5	Body Weight Z-Score=2.2 BMD Z-Score=3.8 BMC Z-Score=3.7	Smad2/+
16.6.5.DF	Body Weight Z-Score=2.7 BMD Z-Score=2.5 BMC Z-Score=3.5	Body Weight Z-Score=2.4 BMD Z-Score=4.9 BMC Z-Score=4.1	Smad2/+
16.16.8.CM	Body Weight Z-Score=4.0 Lean Mass Z-Score=3.3 BMC Z-Score=2.6	Body Weight Z-Score=4.4 Lean Mass Z-Score=1.5 BMD Z-Score=3.3 BMC Z-Score=2.1	Smad2/+

BMD= Bone Mineral Density, BMC= Bone Mineral Content, STR= Soft tissue regeneration
Z-Score indicates differences in a particular phenotype in terms of SD units from non-mutagenized control mice.

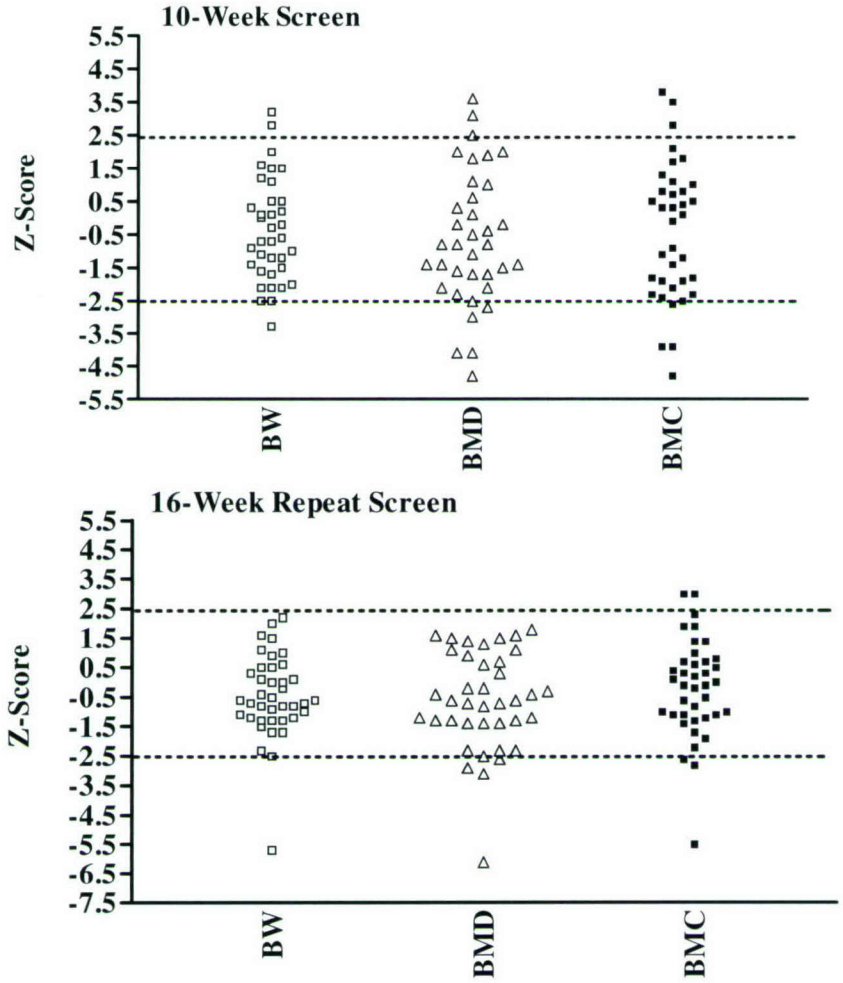

Figure 5. Sensitized ENU mutation screen in lit/+ background. Three main phenotypes, body weight, total body bone density and total body bone mineral content as shown as Z-Score, which indicates differences in a particular phenotype in terms of SD units from non-mutagenized control mice (in this case lit/+ mice generated from breeding lit/lit mice with wild type B6). The horizontal lines indicate our cutoff levels for identifying outlier mice. Data points out side 2.5 SD units represents phenodeviants. BW=Body weight, BMD=Total body bone mineral density, BMC=Total body bone mineral content

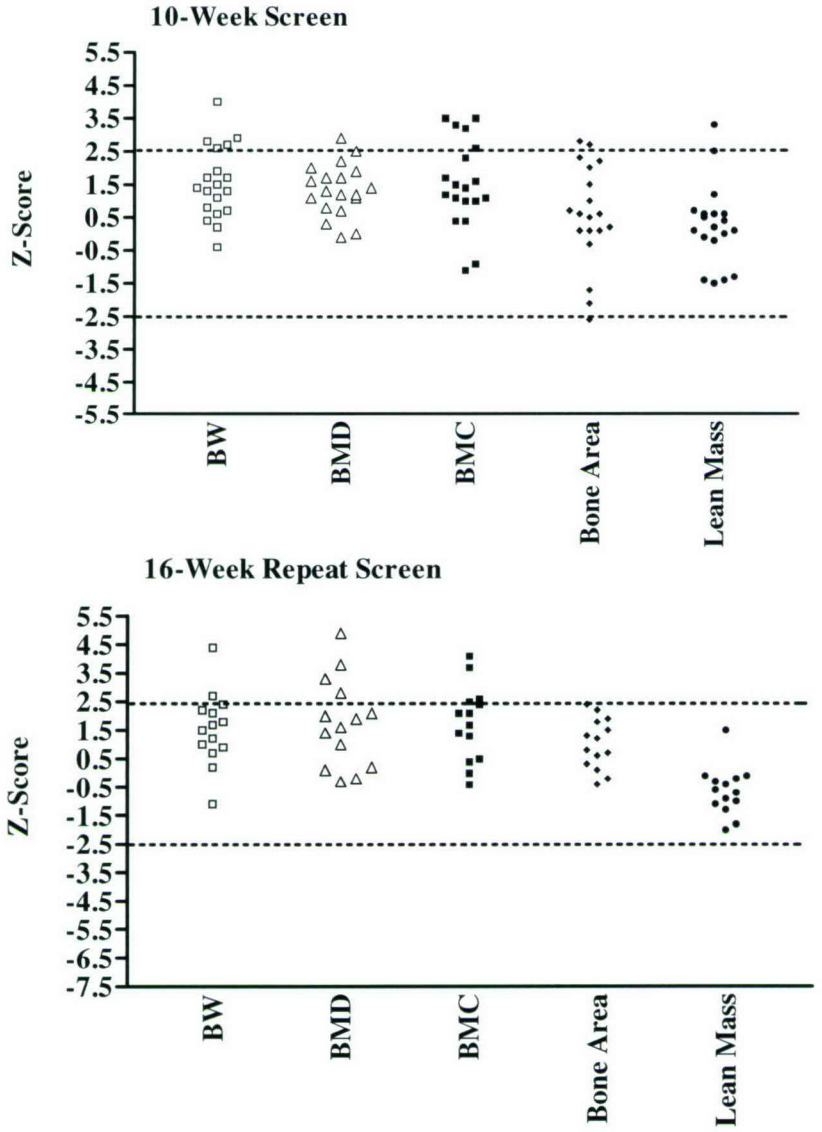

Figure 6. Sensitized ENU mutation screen in Smad2/+ background. Five main phenotypes, body weight, total body bone density, total body bone mineral content, total body bone area, and lean body weight are shown as Z-Score, which indicates differences in a particular phenotype in terms of SD units from non-mutagenized control mice (in this case Smad2/+ mice generated from breeding Smad2/+ mice with Smad2/+ or wild type B6 mice). The horizontal lines indicate our cutoff levels for identifying outlier mice. Data points out side 2.5 SD units represents phenodeviants. BW=Body weight, BMD=Total body bone mineral density, BMC=Total body bone mineral content

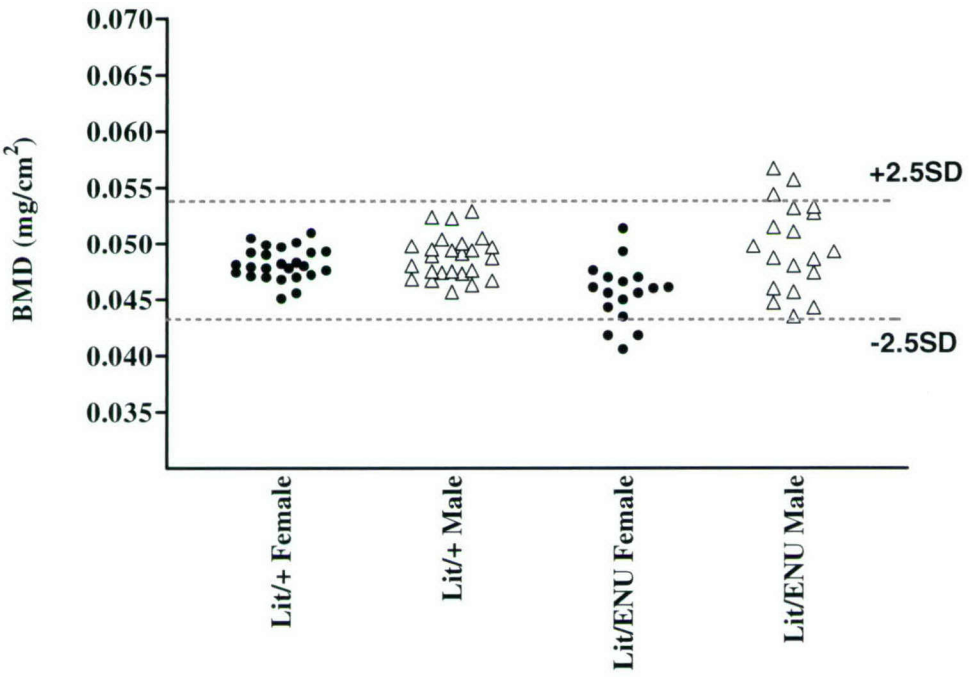

Figure 7. Representative data for total body bone mineral density for sensitized screen in *lit*/+ background. This figure shows the comparison between sensitized screen and wild type control mice and criteria used for identification of outliers. The *Lit*/+ mice were generated by breeding *lit/lit* or *lit*/+ females with WT B6 males, and *lit*/ENU mice were generated by breeding *lit/lit* or *lit*/+ females with ENU injected B6 males.

Key Research Accomplishments

- We have established a breeding colony of *lit/lit* mice and Smad2/+ mice. We currently maintain enough breeders to have a continuous supply of *lit*/+ and Smad2/+ mice for breeding with ENU injected B6 males.
- We injected two batches of B6 males with a 3 X 100 mg/kg dose of ENU and bred them with *lit/lit*, *lit*/+, and Smad2/+ mice.
- To obtain control data, we bred wild type B6 mice with *lit/lit*, *lit*/+, and Smad2/+ mice.
- We have screened 111 F1 control mice generated from breeding wild type B6 mice with *lit*/+ or Smad2/+ mice.
- We have screened 109 F1 sensitized screen mice generated from breeding ENU injected B6 males mice with *lit*/+ or Smad2/+ mice.
- We have identified 19 phenodeviants in sensitized screens.
- We have confirmed 13 phenodeviants in repeat testing.
- We have introduced 7 phenodeviant mice for inheritance testing.

Reportable Outcomes

None at the present time

Conclusions

1) We have acquired breeding pairs of *lit/lit* mice and Smad2 knockout mice and established a breeding colony of *lit/lit* mice and Smad2/+ mice.

2) We have developed assays to identify genotype of breeding pairs.

3) We currently maintain enough breeders to have continuous supply of *lit*/+ and Smad2/+ mice for breeding with ENU injected B6 males, therefore, we have achieved our goals for 'Specific Objective-1.'

4) We have injected two batches of C57BL/6J males with ENU dose of 3 X 100 mg/kg to generate ENU founder males. We bred the ENU injected males in a breeding scheme to generate about 102 F1 mice for dominant screening, therefore, we have succeeded our main goal of the 'Specific Objective-2.'

5) Due to difficulty in breeding *lit/lit* mice, we have used our resources in processing alternative breeding strategies, which was slightly less efficient but required much lower time, a crucial factor in breeding ENU injected males. This breeding strategy generated 49 mice that had +/+ genotype. Therefore, we felt there was no need to generate additional non-sensitized ENU mice as proposed in the later part of the Specific Objective-2. We can use the +/+ mice thus generated and our historical data on non-sensitized ENU screen to calculate mutation frequency. Thus we have met our goals set in Specific Objective-2.

6) We have screened 111 F1 control mice generated from breeding wild type B6 mice with *lit*/+ or Smad2/+ mice and 102 F1 sensitized screen mice generated from breeding ENU injected B6 male mice with *lit*/+ or Smad2/+ mice.

7) We identified 19 phenodeviants in sensitized screens, confirmed 13 phenodeviants in repeat testing, and introduced 7 phenodeviant mice for inheritance testing, therefore, we exceeded our goals for final objective 'Specific Objective-3.'

References

1. Srivastava AK, Mohan, S, Wergedal JE, Baylink DJ. A Genome-wide Screening of N-Ethyl-N-nitrosourea Mutagenized Mice for Musculoskeletal Phenotypes. Bone, 33, 179-191, 2003.
2. Go MJ and Tsakonas SA. A genetic screen for novel components of the Notch signaling pathway during Drosophila bristle development. Genetics 150:211-220, 1998.
3. Carrera P, Abrell S, Kerber B, Walldorf U, Preiss A, Hoch M, Jackle H. A modifier screen in the eye reveals control genes for Kuüppel activity in the Drosophila embryo. Proc. Natl. Acad. Sci. 95:10779-10784, 1998.
4. Satterthwaite AB, Willis F, Kanchanastit P, Fruman D, Cantley LC, Helgason, Humphries RK, Lowell CA, Simon M, Leitges M, Tarakhovsky A, Tedder TF, Lesche R, Wu H, and Witte ON. A sensitized genetic system for the analysis of murine B lymphocyte signal transduction pathways dependent on Bruton's tyrosine kinase. Proc. Natl. Acad. Sci. 97: 6687-6692, 2000
5. Attisano, L. and J.L. Wrana, Signal transduction by the TGF-beta superfamily. Science, 296(5573): 1646-7, 2002.
6. Donahue, L.R. and W.G. Beamer, Growth hormone deficiency in 'little' mice results in aberrant body composition, reduced insulin-like growth factor-I and insulin-like growth factor-binding protein-3 (IGFBP-3), but does not affect IGFBP-2, -1 or -4. J Endocrinol, 136(1): 91-104,1993.

Project 3: Development of Transgenic Approaches Using BAC Clones to identify Candidate Genes for Musculoskeletal Phenotypes

Introduction

The primary goal of our studies is to localize chromosomal regions and subsequently identify genes responsible for various musculoskeletal phenotypes including bone density, fracture repair and soft tissue regeneration, and evaluate the molecular function of these genes. We have been using two main strategies to identify these genes for the musculoskeletal system: 1) Ethylnitrosourea (ENU) chemical mutagenesis to induce mutant mice with significant musculoskeletal alteration; and 2) Genetic linkage analysis to discover genetic components of quantitaive trait loci (QTL) that contribute to phenotypic changes. In our previous studies, we have made significant progress with both ENU and QTL approaches, and identified several mutant mouse strains and genetic loci that are associated with phenotypes of small bone size, high bone density and soft tissue regeneration. However, these regions contain dozens of intact genes with a large piece of genomic DNA in several overlapping bacterial artificial chromosomes (BACs) and need to be further tested for their functions. The aim of this project is to develop a gene transfer system of BAC to deliver a genomic locus as large as 150-kb into bone cells to "rule out" or "rule in" a genetic component contributing to the phenotype of interest.

Body

Technical Objectives

Our specific objectives during the first 12 months of this grant period were as follows:

1. To develop an optimal protocol for efficient transfer of BAC clones into mouse bone cells *in vitro* for functional evaluation using a known test gene, we will:
    i) Screen BAC clone library using appropriate markers to identify BAC clones containing a known gene (e.g. BMP-2).
    ii) Retrofit selected BAC clone with selection marker for transfer using chemical transfection agent.
    iii) Retrofit selected BAC clone with herpes simplex virus type I (HSV-1) amplicons and prepare infectious amplicon for viral transfer.
    iv) Transfect osteoblast (e.g. mouse bone marrow stromal cells, calvarial bone cells, fibroblasts) cell models with retrofitted BAC clone using chemical or viral transfer.
    v) Identify efficiency of transfection in transiently transfected cells by BMP-2 immunostaining.
    vi) Incubate cells in the presence of appropriate antibiotic selection marker to select table BAC clone containing cells.
    vii) Compare short term (transient) and long-term (stable) expression level of candidate gene in cells transfected with BAC clone using chemical and viral methods.

2. To construct a BAC contig for the chromosomal region containing ENU mutant locus that contributes decreased bone size, we will:
    i) Perform genome wide screening of F2 mice (generated by breeding ENU mutant C57BL/6J with C3H/Hej) using appropriate microsatellite and SNP markers.
    ii) Begin to construct a BAC contig using physical location of markers and SNPs (CELERA).

Our progress in each of the specific objectives is given below.

To achieve our objective of developing an optimal protocol for efficient transfer of BAC clones into mouse cells *in vitro* for functional evaluation, we proposed to use an improved infectious BAC (iBAC) technology mediated by the herpes simplex virus type 1 (HSV-1) amplicon to deliver a genomic locus containing intact BMP-2 gene into MC3T3-E1 cells (4). We modified our retrofitting strategies to make a construct more useful by utilizing a vector containing multiple marker genes. We believe that the iBAC offers a rapid and simple method of BAC DNA transfer for functional genomic studies.

Progress for Specific Objectives

Specific Objective 1:

In order to identify the BMP-2 gene, we modified our strategy by searching databases instead of screening a BAC clone library that we originally proposed. This is because BAC and P1 artificial chromosomes (PAC) libraries have been generated for sequencing the human and mouse genomes, and are commercially available for most genes. In addition, the commercial BAC or PAC clones contain one wild type loxp site built-in in the library vectors (e.g. pbeloBAC11, PBACe3.6, PCYPAC2, PPAC4), which allow us to retrofit any DNA sequence without further DNA manipulations. We searched the GenBank database and identified a mouse BAC library clone (clone, RP23-302H4) containing a complete 8.7-kb BMP-2 genomic DNA locus driven by a 20.5-kb native promoter within a 128.5-kb insert. We chose this clone because it contains a single BMP-2 gene with most, if not all, of the regulatory elements in the promoter, introns and 3' non-coding regions that may regulate a physiological gene expression (1, 2). The length of the BAC clone is also within the size limits that the HSV-1 vector can efficiently package into an iBAC (3).

We chose pEHHG that consists of HSV-1 amplicon elements, enhanced green fluorescent protein (GFP), hygromycin resistance gene, Epstein-Barr virus (EBV) episome retention cassette, R6K bacterial replication origin, and a *loxP* site as a retrofitting vector for several reasons: 1) the GFP marker facilitates evaluation of the transfection or transduction efficiency in living cells, and GFP-positive cell sorting by Flow cytometry, if necessary, without drug-selection; 2) the hygromycin resistance gene allows us to select antibiotic resistant cells (e.g. stable cell line containing BAC transgenes) when chemical transfection is applied; 3) the EBNA-1 episomal cassette from the Epstein Barr virus allows long-term retention and high level of position-independent expression of BAC transgenes as mini-chromosomes in the host cells (3, 5).

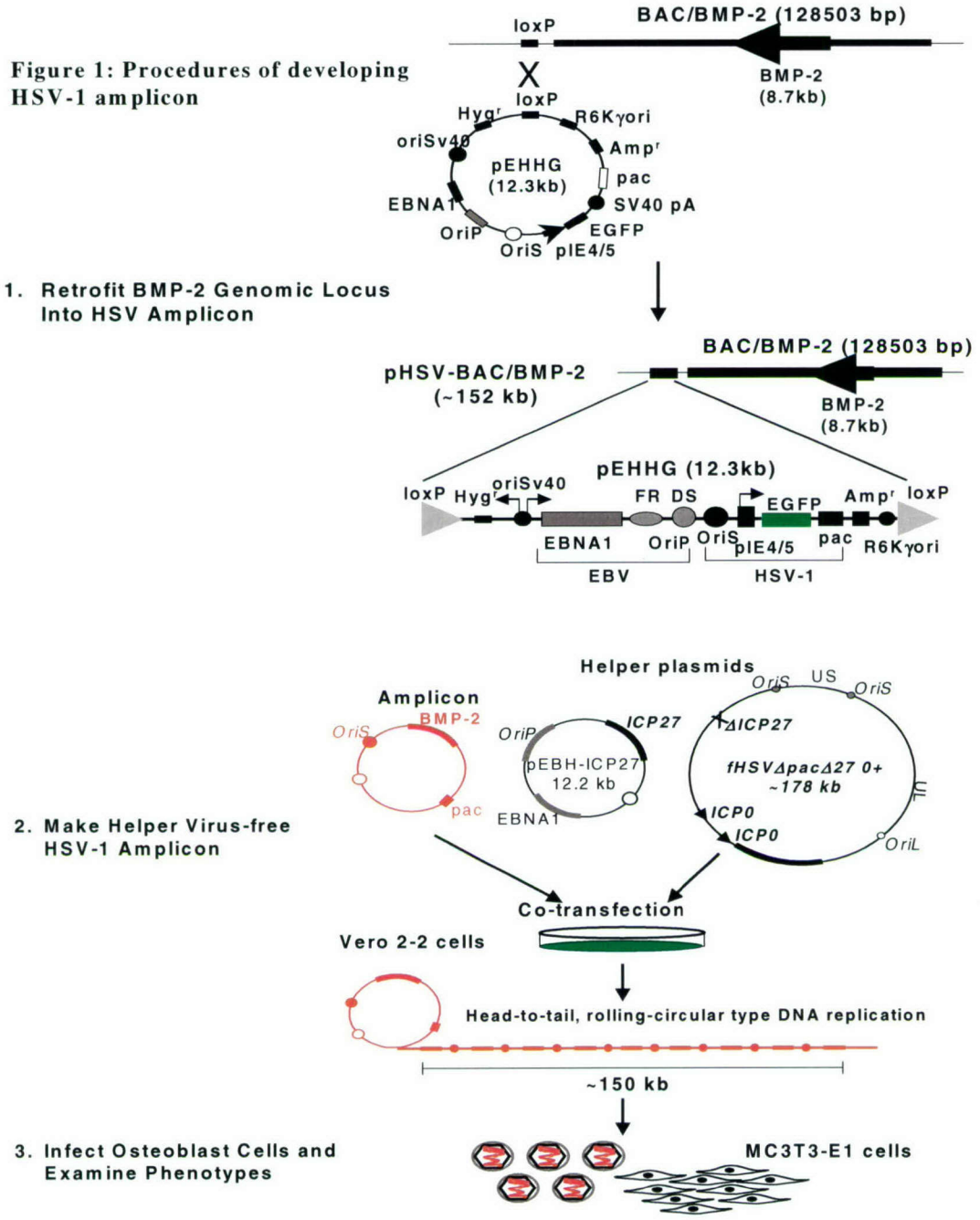

Figure 1: Procedures of developing HSV-1 amplicon

A detailed protocol of our study is illustrated in Figure 1. Briefly, an aliquot of 35 µl electro-competent cells containing BAC/BMP-2 (RP23-302H4) was mixed with 10 ng each of pEHHG and pCTP-T plasmid DNA, and the mixture was transferred into 0.1-cm gap width electroporation cuvette. After 5 minutes incubation on ice, the cells were electroporated with 25 µF at 1800 V using a Gene Pulser, and then transferred into a 15-ml conical tube containing 500 µl SOC with 20 µg chlortetracycline, and incubated at 30

°C with rigorous shaking for 1 hour. An aliquot of 100 µl of the bacterial culture was transferred into a new 15-ml tube containing 20 µg/ml chlortetracycline, 100 µg/ml ampicillin, and 20 µg/ml chloramphenicol in 900 µl SOC, and incubated at 30 °C with shaking for another 3 hours. Subsequently, 50-100 µl of the bacterial culture was plated on LB plates containing 100 µg/ml ampicillin and 20 µg/ml chloramphenicol, and incubated overnight at 43 °C. We used a Cre/loxP-based retrofitting method to convert the BAC/BMP-2 with the pEHHG to generate a 152-kb construct of pHSV-BAC/BMP-2 (Fig 2A) (3, 5). DNA of individual clones was purified, and verified by PCR using specific primers to BMP-2 and GFP to confirm the presence of two genes within a single pHSV-BAC/BMP-2 construct (Fig 2B). Thus, the retrofitted BAC can be either transfected into osteoblast cells or packed into iBAC for functional testing.

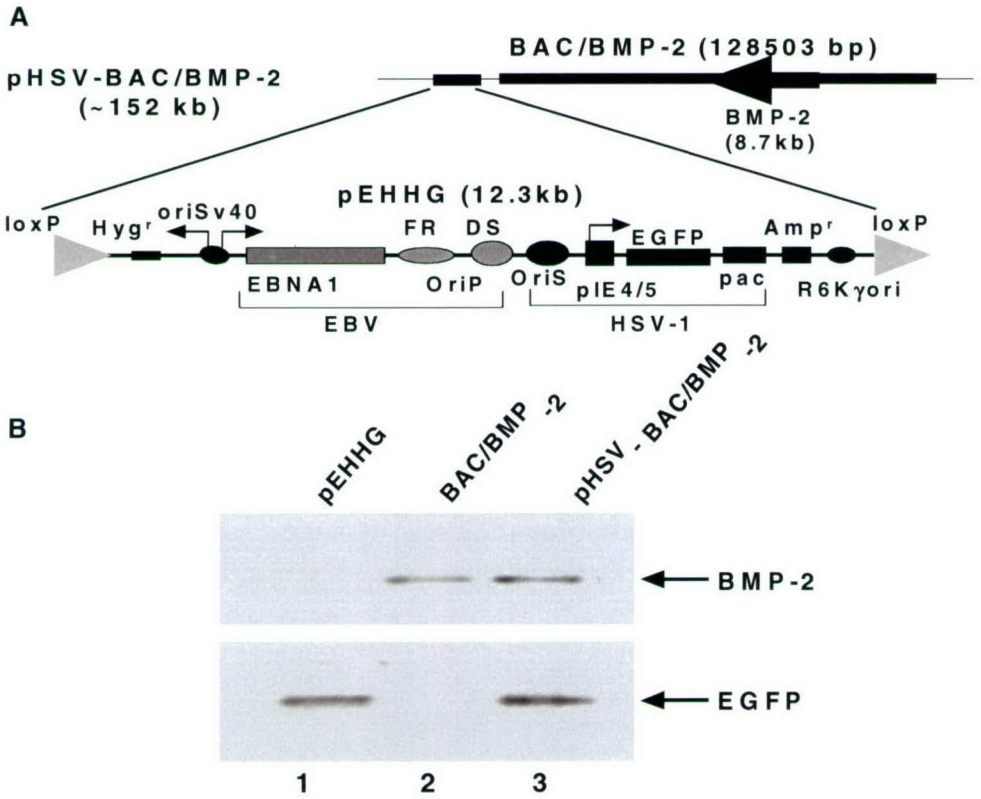

Figure 2. Schematic diagram of infectious HSV-1/BAC/BMP-2 construct. **A**: The retrofitted BAC contains both GFP reporter and BMP-2 genes **B**: Verification of pHSV-BAC/BMP-2 construct by polymerase chain reaction (PCR). Lane 1: pEHHG control; Lane 2: BAC/BMP-2 control; Lane 3: pHSV-BAC/BMP-2 containing both GFP and BMP-2 genes.

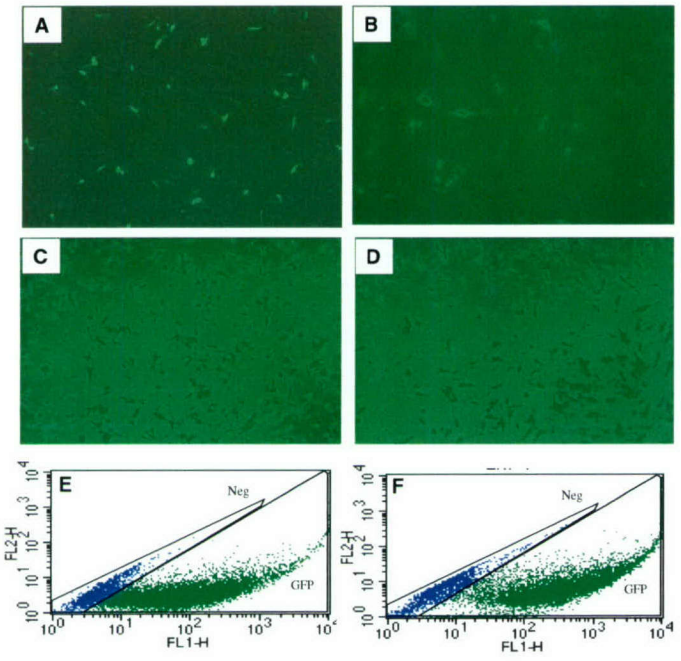

Figure 3. GFP expression in MC3T3-E1 cells transfected and transduced with HSV-1 amplicon for 24 hours **A & B**: the cells transfected with pEHHG and pHSV-BAC/BMP-2, respectively using optimized lipofectamine; **C**: the cells transduced with infectious HSV-1 mock amplicon; **D**: the cells transduced with infectious HSV-1 amplicon containing a BMP-2; **E**: Representive data of flow cytometric analysis in the cells infected with HSV-1 mock amplicon; **F**: Representive data of flow cytometric analysis in the cells infected with HSV-1 amplicon containing a BMP-2 gene.

We then packaged HSV amplicon into infectious virion as described in the diagram (Figure 1). We plated Vero 2-2 cells (10^6) in a 60-mm dish. After 18 hours, the cells were co-transfected with 2.0 μg pHSV-BAC/BMP-2 or pEHHG, 0.2 μg pEBHICP27, and 2 μg fHSVΔ-pac, Δ-27, 0+ using LipofectAMINE Plus for 4 hours. The cells were scraped into the supernatant 60 hours post infection, frozen and thawed once, sonicated for 1 minute and centrifuged at 3,500 r.p.m. for 15 minutes. The supernatant was then concentrated through a 25% sucrose by ultracentrifuging, and the amplicon pellet was resuspended in Hank's buffered salt solution. The purified HSV-1 amplicon was tittered in Vero 2-2 cells by counting the number of GFP positive cells after 24 hours infection. Typically, the titration of HSV-1 amplicon stocks was around 5 x 10^6 to 10^7 GFP transducing units/ml. After 24 hours, the cells were infected at a multiplicity of infection (MOI) of 5 with HSV-1 amplicon. After 6 hours infection, the medium was removed, and fresh medium was added to the cells. Twenty-four hours after infection, the GFP reporter gene was expressed in most of MC3T3-E1 cells transduced with either an HSV-1 mock (Fig 3C) or an HSV-BAC/BMP-2 amplicon (Fig 3D). Flow cytometry analyses revealed that 84% of the osteoblast cells transduced with HSV-1 mock amplicon expressed GFP (Fig 3E) and 77% of the cells infected with HSV-BAC/BMP-2 virion showed GFP-positive (Fig 3F). To compare the efficiencies of transduction and transfection, we also transfected MC3T3-E1 cells with pEHHG and pHSV-BAC/BMP-2 (Fig 2A) using Lipofectamine-Plus. Only less than 5% of MC3T3-E1 cells transfected with pHSV-BAC/BMP-2 expressed GFP (Fig 3A) whereas approximately 10% of the cells transfected with pEHHG control vector turned green (Fig 3A). Obviously, the efficiency of transduction of BAC-based amplicon was at least 15-fold higher than that of lipid-based transfection (Fig 3).

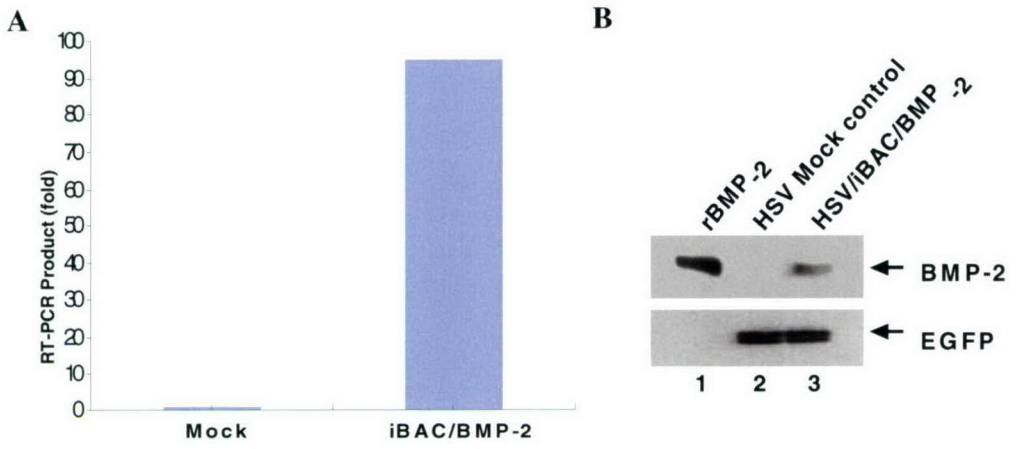

Figure 4. BMP-2 transgene expression in MC3T3-E1 cells. **A**: Real-time PCR data. **B**: Western blot analysis. Lane 1: positive control of recombinant BMP-2 (100 ng); Lane 2: the cells infected with HSV-1 mock amplicon containing GFP only; Lane 3: the cells infected with HSV-1 amplicon containing GFP and a BMP-2 locus.

The expression of the transgene was examined by utilizing Western blot with specific antibodies against BMP-2 and GFP, and by real-time PCR with specific primers to BMP-2 and GFP genes (Fig 4). The cells infected by iBAC containing BMP-2 gene trasncripted approximately 99-fold higher of BMP-2 mRNA than the cells transduced control BAC only containing GFP gene. The amount of BMP-2 protein was estimated to be 10 ng per 10^6 cells based on Western blot analysis (Fig 4). However, we failed to detect BMP-2 expression in the same number of either native MC3T3-E1 cells or the cells transfected with pHSV-BAC/BMP-2 (Fig 4).

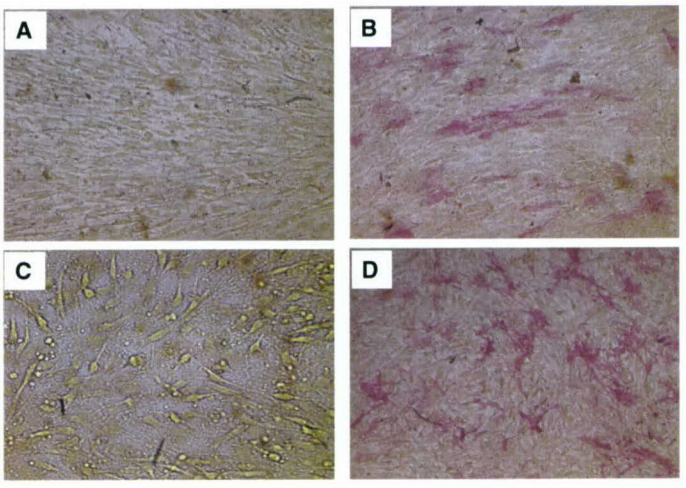

Figure 5: Alkaline phosphatase (ALP) staining of differentiated MC3T3-E1 cells (x 40 images). The cells are differentiated for 9 days and subjected for ALP staining. **A**: the cells infected with HSV-1 mock amplicon; **B**: the cells infected with HSV-1 amplicon containing a BMP-2 locus; **C**: The cells treated with vehicle; **D**: The cells treated with recombinant BMP-2 (200 ng/ml).

To assess osteoblast phenotype in the cells expressing BMP-2 transgene, we carried out an ALP staining 9 days after transduction (Fig 5). Like the cells treated with 200 ng/ml recombinant human BMP-2, about 20% of the osteoblast cells were differentiated and exhibited positive ALP-staining (Fig 5B and 5D). No ALP-

positive cells were seen in the control cells infected with HSV-1 mock amplicon without BMP-2 genomic locus (Fig 3A) or the cells treated with vehicle alone (Fig 5C).

We have observed that the HSV-1 amplicon can efficiently transfer a large piece of genomic locus, and retain it as episomes in proliferating cells. The GFP gene is consistently active and visible for at least 2 weeks, although the intensity becomes weaker. The functional BMP-2 protein in the infected cells was detectable 72 hours and even longer after infection, and mediated cell differentiation. In addition, viral infection yields more than 75% efficiency without antibiotics selection. Therefore, we believe that making a stable cell line is not necessary. In the proposal for the first 12 months, specific objective 1, we developed a simple protocol described above for efficient transfer of BAC clones into osteoblast cells *in vitro* for functional evaluation. We have demonstrated that the retrofitting of the BAC clone and packaging of the HSV-1 amplicon into infectious virion can be accomplished within 1-2 weeks of work. By utilizing this approach, a candidate gene search in a QTL region is feasible once an appropriate cell model and end points for candidate gene function are determined.

Specific Objective 2:

In a previous study funded by the Department of Defense (DAMD17-99-1-9571), we identified a bone size mutant mouse strain, the B6. This B6 mouse mutant displayed a total body bone area that was 10-13% lower and periosteal circumference 5-8% lower at the femur and tibia midshaft compared to wild type B6 mice. Interval mapping in B6C3H F2 males (n=69) indicated two major loci affecting bone size on Chr 1 at 45 cM (LOD 4.9) and Chr 4 at 10.5 cM (LOD 7.9, genome wide $p<0.01$). Interval mapping using body weight as covariate revealed only one significant interval at Chr 4 (LOD 6.8). Alleles of the Chr 4 interval inherited from the B6 mutant strain contribute to a significantly lower bone size than those inherited from C3H.

Interval mapping using additional markers for Chromosome 4 revealed an ENU mutant locus located between 7.5-36 cM. Thus, we developed a BAC contig for this region using RP23 clones. This contig is shown in Table 1 below.

Table 1.

id	name	acc	start	stop	length	weight	orient_end1	orient_end2	overlap
1	RP23-115F19		9832065	10039368	207303	Highest	+	-	#VALUE!
2	RP23-444O1		10000160	10163727	163567	Highest	+	-	39208
3	RP23-455B8	AL805930	10116748	10291395	174647	Medium	+	-	46979
5	RP23-429I15		10215570	10427388	211818	Highest	+	-	75825
8	RP23-438A13		10395367	10536785	141418	Highest	+	-	32021
10	RP23-240F1		10437823	10614357	176534	Highest	+	-	98962
11	RP23-354G12		10531758	10719885	188127	Highest	+	-	82599
12	RP23-144K18	AL671880	10614403	10806382	191979	Highest	+	-	105482
16	RP23-480O3		10773401	10961298	187897	Highest	+	-	32981
18	RP23-464D11		10910403	11087548	177145	Highest	+	-	50895
23	RP23-25E12		11058315	11266413	208098	Highest	+	-	29233
26	RP23-322G9	AL772170	11219514	11442995	223481	Highest	+	-	46899
27	RP23-295B7		11282889	11503029	220140	Highest	+	-	160106
28	RP23-244J11		11489317	11707550	218233	Highest	+	-	13712

30	RP23-417N13		11590964	11828972	238008	Highest	+	-	116586
33	RP23-295L9		11796064	11976935	180871	Highest	+	-	32908
35	RP23-203A12	AL772167	11821926	12026956	205030	Highest	+	-	155009
36	RP23-301C4		11969851	12122812	152961	Highest	+	-	57105
37	RP23-107F24		12185639	12382896	197257	Highest	+	-	-62827
38	RP23-271J14		12210164	12418212	208048	Highest	+	-	172732
39	RP23-119J18		12441690	12627439	185749	Highest	+	-	-23478
40	RP23-59O21		12581371	12767705	186334	Highest	+	-	46068
41	RP23-219E6		12630106	12831827	201721	Highest	+	-	137599
42	RP23-122G12		12814760	12994496	179736	Highest	+	-	17067
45	RP23-56F9		12869355	13125165	255810	Highest	+	-	125141
48	RP23-34L17		13071447	13290840	219393	Highest	+	-	53718
54	RP23-456G17		13270110	13432510	162400	Highest	+	-	20730
59	RP23-306G24		13407005	13642549	235544	Medium	+	-	25505
62	RP23-291L14		13619670	13773556	153886	Medium	+	-	22879
65	RP23-472I19		13691231	13883435	192204	Highest	+	-	82325
67	RP23-134H12	AL807804	13769980	13976684	206704	Medium	+	-	113455
69	RP23-287O8	AL808118	13946512	14138756	192244	Highest	+	-	30172
71	RP23-384E7		14097032	14270979	173947	Highest	+	-	41724
72	RP23-458M15		14132437	14302944	170507	Highest	+	-	138542
73	RP23-194M5		14285852	14492095	206243	Highest	+	-	17092
77	RP23-138B7		14448706	14676988	228282	Highest	+	-	43389
80	RP23-129D22		14550220	14776118	225898	Highest	+	-	126768
82	RP23-379L17	AL831792	14726182	14895882	169700	Highest	+	-	49936
87	RP23-153A15		14841308	15028457	187149	Highest	+	-	54574
89	RP23-356M11		14955220	15139976	184756	Highest	+	-	73237
90	RP23-113G17		15027414	15213099	185685	Highest	+	-	112562
91	RP23-193N22		15208207	15413927	205720	Highest	+	-	4892
94	RP23-396L22		15363948	15563390	199442	Medium	+	-	49979
95	RP23-233N14		15486676	15721025	234349	Highest	+	-	76714
97	RP23-298B17		15670284	15846237	175953	Highest	+	-	50741
99	RP23-384F21		15822641	16030052	207411	Highest	+	-	23596
103	RP23-267K10		15962449	16132815	170366	Highest	+	-	67603
104	RP23-300F16		16328336	16512721	184385	Highest	+	-	-195521
105	RP23-360O17	AL929447	16566011	16751208	185197	Highest	+	-	-53290
106	RP23-358M21	AL772196	16644062	16882025	237963	Highest	+	-	107146
107	RP23-227B13		16928466	17116541	188075	Highest	+	-	-46441
109	RP23-222P6		16999309	17226274	226965	Highest	+	-	117232
111	RP23-477N19		17200316	17393629	193313	Highest	+	-	25958
112	RP23-297F22		17350546	17536575	186029	Medium	+	-	43083
113	RP23-290G13		17551730	17751307	199577	Highest	+	-	-15155
114	RP23-293O10		17678222	17868125	189903	Highest	+	-	73085
116	RP23-259P7	AL805957	17839699	18072289	232590	Highest	+	-	28426
117	RP23-191I13		17903818	18111672	207854	Highest	+	-	168471
118	RP23-99G22		18070478	18268431	197953	Highest	+	-	41194
120	RP23-276F7	AL732623	18159272	18338972	179700	Highest	+	-	109159
121	RP23-382A14		18390689	18592081	201392	Highest	+	-	-51717
124	RP23-421D17	AL929519	18556811	18762392	205581	Highest	+	-	35270
125	RP23-377M4		18678056	18844880	166824	Highest	+	-	84336

126	RP23-13I21		18763159	18995336	232177	Medium	+	-	81721
127	RP23-309E23		19047584	19228869	181285	Highest	+	-	-52248
128	RP23-199B9	BX001053	19133772	19345874	212102	Medium	+	-	95097
131	RP23-138O20	AL772281	19288747	19504225	215478	Highest	+	-	57127
134	RP23-106F23		19437061	19651682	214621	Highest	+	-	67164
135	RP23-408P4		19537851	19744683	206832	Highest	+	-	113831
138	RP23-334P1		19708115	19926937	218822	Highest	+	-	36568
141	RP23-89A4		19812399	20062499	250100	Highest	+	-	114538
142	RP23-311D6		19991668	20186163	194495	Highest	+	-	70831
146	RP23-305O17		20142441	20319129	176688	Highest	+	-	43722
147	RP23-319K20		20181514	20369784	188270	Highest	+	-	137615
150	RP23-382D19		20345282	20534268	188986	Highest	+	-	24502
152	RP23-393P6		20501299	20697883	196584	Highest	+	-	32969
154	RP23-137M6		20624964	20823185	198221	Highest	+	-	72919
155	RP23-234B18		20693535	20884688	191153	Highest	+	-	129650
157	RP23-437K10		20854327	21035838	181511	Medium	+	-	30361
160	RP23-431N12		20969446	21126427	156981	Highest	+	-	66392
161	RP23-55D6		21590786	21840569	249783	Highest	+	-	-464359
163	RP23-365O14		21724003	21934485	210482	Highest	+	-	116566
166	RP23-433G4		21875138	22094897	219759	Highest	+	-	59347
170	RP23-237K13	AL683854	22071102	22305715	234613	Medium	+	-	23795
173	RP23-402G3		22238022	22416760	178738	Highest	+	-	67693
175	RP23-28C12		22345389	22570432	225043	Highest	+	-	71371
176	RP23-456B13		22650776	22826521	175745	Highest	+	-	-80344
177	RP23-447O9		22729576	22893250	163674	Highest	+	-	96945
178	RP23-242O10		23003571	23180326	176755	Highest	+	-	-110321
179	RP23-310N9		23200512	23428113	227601	Highest	+	-	-20186
182	RP23-210D12		23384254	23612212	227958	Highest	+	-	43859
183	RP23-338P7		23479510	23655179	175669	Highest	+	-	132702
184	RP23-370B12		23665380	23842338	176958	Highest	+	-	-10201
185	RP23-140J12	AL671868	23665394	23851178	185784	Highest	+	-	176944
186	RP23-239J20		23917008	24135881	218873	Highest	+	-	-65830
187	RP23-202E18		23956913	24141953	185040	Highest	+	-	178968
188	RP23-26N2		24336305	24564681	228376	Highest	+	-	-194352
192	RP23-367L15		24542438	24704925	162487	Highest	+	-	22243
194	RP23-24I19		24589598	24809622	220024	Highest	+	-	115327
195	RP23-434I23		24687651	24889841	202190	Highest	+	-	121971
196	RP23-19M3		24789836	24965497	175661	Highest	+	-	100005
197	RP23-333P3		24952684	25152670	199986	Highest	+	-	12813
200	RP23-111M14		25070275	25291808	221533	Highest	+	-	82395
202	RP23-145B24		25233506	25449652	216146	Highest	+	-	58302
207	RP23-299E10		25419408	25596627	177219	Medium	+	-	30244
208	RP23-389G9		25882666	26077969	195303	Medium	+	-	-286039
210	RP23-69N21		25952322	26160118	207796	Highest	+	-	125647
211	RP23-117E19	AC101374	26137965	26358054	220089	Highest	+	-	22153
212	RP23-476K17		26343507	26512139	168632	Highest	+	-	14547
214	RP23-336M1		26362829	26577759	214930	Highest	+	-	149310
215	RP23-177K20		26537554	26741391	203837	Highest	+	-	40205
219	RP23-274H7		26681842	26900864	219022	Highest	+	-	59549

220	RP23-313C1		26908311	27120120	211809	Highest	+	-	-7447
221	RP23-402O20		27138118	27337835	199717	Highest	+	-	-17998
222	RP23-205F9		27276337	27481451	205114	Highest	+	-	61498
223	RP23-203B4		27458396	27670845	212449	Highest	+	-	23055
224	RP23-24H13		27569105	27739866	170761	Highest	+	-	101740
225	RP23-353L18		27654752	27869296	214544	Highest	+	-	85114
227	RP23-94C13		27811937	28054445	242508	Highest	+	-	57359
231	RP23-151N17	AL671872	27944773	28133102	188329	Highest	+	-	109672
233	RP23-408N9		28110865	28417496	306631	Highest	+	-	22237
236	RP23-87N9	AL929397	28389920	28571993	182073	Highest	+	-	27576
237	RP23-59L20		28440521	28698812	258291	Highest	+	-	131472
238	RP23-223D8		28615364	28794277	178913	Highest	+	-	83448
240	RP23-105F14		28755808	28958098	202290	Medium	+	-	38469
241	RP23-358I18	BX323546	28900904	29108984	208080	Highest	+	-	57194
243	RP23-134E11		29047944	29255584	207640	Highest	+	-	61040
245	RP23-425N3		29190830	29382804	191974	Highest	+	-	64754
247	RP23-451B19		29339048	29511833	172785	Highest	+	-	43756
250	RP23-439A9		29400053	29607504	207451	Highest	+	-	111780
251	RP23-440K16		29550507	29765460	214953	Medium	+	-	56997
252	RP23-334M6	BX530076	29625830	29828304	202474	Highest	+	-	139630
253	RP23-215H7		29828360	30038027	209667	Highest	+	-	-56
255	RP23-192D22	AC101535	29923607	30149686	226079	Highest	+	-	114420
256	RP23-446K23		30054226	30235797	181571	Highest	+	-	95460
257	RP23-325J14		30149726	30334334	184608	Highest	+	-	86071
258	RP23-145H16		30316201	30492178	175977	Highest	+	-	18133
261	RP23-192E7		30451258	30631164	179906	Highest	+	-	40920
263	RP23-296F5	BX255966	30606622	30795237	188615	Highest	+	-	24542
265	RP23-456B2	AL929408	30715673	30912535	196862	Highest	+	-	79564
266	RP23-165G10	AC073702	30794337	30986486	192149	Highest	+	-	118198
267	RP23-77O12	AC100998	30912584	31153806	241222	Highest	+	-	73902
269	RP23-221I2		31133464	31350304	216840	Highest	+	-	20342
274	RP23-76B2		31280927	31522928	242001	Highest	+	-	69377
276	RP23-351L1		31493636	31718430	224794	Highest	+	-	29292
280	RP23-84I16	AC101029	31694096	31900515	206419	Highest	+	-	24334
283	RP23-31M8		31743192	31947761	204569	Highest	+	-	157323
284	RP23-120K20		31898012	32114942	216930	Highest	+	-	49749
288	RP23-142K3		32078095	32287725	209630	Highest	+	-	36847
292	RP23-358N13	BX323545	32254690	32433770	179080	Highest	+	-	33035
294	RP23-24E11	AL732547	32399866	32606572	206706	Highest	+	-	33904
304	RP23-308C15		32580304	32800453	220149	Highest	+	-	26268
312	RP23-117E21		32763885	32973196	209311	Highest	+	-	36568
318	RP23-248A9		32939929	33184079	244150	Highest	+	-	33267
320	RP23-360H6	AL772288	33147084	33352181	205097	Medium	+	-	36995
321	RP23-122L3		33230371	33473325	242954	Highest	+	-	121810
324	RP23-369I8	AL772272	33354189	33608475	254286	Highest	+	-	119136
325	RP23-225I6		33629777	33834477	204700	Highest	+	-	-21302
329	RP23-224K19		33731735	33966913	235178	Highest	+	-	102742
331	RP23-437A5		33923544	34143144	219600	Highest	+	-	43369
334	RP23-16I2		34056626	34223923	167297	Medium	+	-	86518

335	RP23-286P4		34505704	34671808	166104	Highest	+	-	-281781
336	RP23-209A17		34613329	34795928	182599	Highest	+	-	58479
339	RP23-29M7		34718098	34951116	233018	Medium	+	-	77830
341	RP23-320J8		34903072	35144150	241078	Highest	+	-	48044
342	RP23-232A6		34961509	35174689	213180	Medium	+	-	182641
343	RP23-434N2		35195819	35396676	200857	Highest	+	-	-21130
346	RP23-192E23		35302782	35465120	162338	Highest	+	-	93894
347	RP23-140F12		35394632	35583670	189038	Highest	+	-	70488
348	RP23-12K18		35641708	35857978	216270	Highest	+	-	-58038
350	RP23-429H11		35741492	35952060	210568	Highest	+	-	116486
352	RP23-39F22	AL844199	35888045	36093575	205530	Highest	+	-	64015
354	RP23-415O10		36012374	36213105	200731	Highest	+	-	81201
355	RP23-118A20	AL831712	36096748	36307595	210847	Highest	+	-	116357
356	RP23-293H21		36307690	36506338	198648	Highest	+	-	-95
360	RP23-19I8		36475537	36670011	194474	Highest	+	-	30801
363	RP23-287B11	AL833783	36647227	36876019	228792	Highest	+	-	22784
366	RP23-34B14		36835176	37086325	251149	Highest	+	-	40843
368	RP23-341A3		37026179	37229381	203202	Highest	+	-	60146
369	RP23-15N22		37203732	37414430	210698	Highest	+	-	25649
376	RP23-30J14		37387965	37617485	229520	Highest	+	-	26465
377	RP23-65A23		37606191	37747717	141526	Highest	+	-	11294
380	RP23-211C18		37674193	37878686	204493	Highest	+	-	73524
381	RP23-323B18		37857355	38069363	212008	Highest	+	-	21331
386	RP23-336H21		38000593	38208014	207421	Highest	+	-	68770
388	RP23-86I14		38163074	38375993	212919	Highest	+	-	44940
389	RP23-63K11		38562343	38772354	210011	Highest	+	-	-186350
390	RP23-202J15		38718728	38912474	193746	Highest	+	-	53626
394	RP23-330D5		38862393	39103890	241497	Highest	+	-	50081
396	RP23-90G18		39033975	39253238	219263	Highest	+	-	69915
397	RP23-290N7		39166443	39370973	204530	Medium	+	-	86795
398	RP23-138K24		39258295	39457676	199381	Highest	+	-	112678
401	RP23-296O13		39437174	39595457	158283	Highest	+	-	20502
402	RP23-374J24		39499874	39707613	207739	Medium	+	-	95583
403	RP23-101C9		39609108	39804310	195202	Highest	+	-	98505
406	RP23-263N5		39754170	39967831	213661	Highest	+	-	50140
408	RP23-403C16		39927626	40126248	198622	Highest	+	-	40205
410	RP23-259I21		40100354	40267760	167406	Highest	+	-	25894
411	RP23-9F23	AL831793	40224573	40460999	236426	Highest	+	-	43187
417	RP23-102N20		40402937	40616929	213992	Highest	+	-	58062
418	RP23-284I1		40569227	40773814	204587	Highest	+	-	47702
421	RP23-218M7		40702111	40931461	229350	Highest	+	-	71703
425	RP23-236N23		40901357	41090246	188889	Highest	+	-	30104
428	RP23-404A21		41043467	41251856	208389	Highest	+	-	46779
432	RP23-65E3		41212067	41470453	258386	Highest	+	-	39789
436	RP23-368G11		41411067	41596920	185853	Highest	+	-	59386
439	RP23-100C7	AL831723	41565407	41796051	230644	Highest	+	-	31513
441	RP23-311O23		41704592	41903060	198468	Highest	+	-	91459
442	RP23-80L18		41890078	42095507	205429	Highest	+	-	12982
446	RP23-111G9		42073923	42286654	212731	Highest	+	-	21584

452	RP23-77L9		42241273	42491944	250671	Highest	+	-	45381
458	RP23-173O17		42459169	42683683	224514	Highest	+	-	32775
464	RP23-207P5		42632959	42870507	237548	Highest	+	-	50724
470	RP23-86E14		42794041	42988555	194514	Highest	+	-	76466
471	RP23-321C13		42906622	43113645	207023	Highest	+	-	81933
472	RP23-9F18	AL773539	42988635	43170791	182156	Highest	+	-	125010
473	RP23-107K17		43139726	43345065	205339	Highest	+	-	31065
480	RP23-140C14		43287091	43501348	214257	Highest	+	-	57974
484	RP23-140K8		43456332	43675550	219218	Highest	+	-	45016
489	RP23-46K20		43613859	43836653	222794	Highest	+	-	61691
494	RP23-125D9		43796363	44021380	225017	Highest	+	-	40290
496	RP23-159N16	AL805914	43877463	44055236	177773	Highest	+	-	143917
498	RP23-346F11		44028258	44241108	212850	Highest	+	-	26978
504	RP23-405L15		44133053	44328987	195934	Highest	+	-	108055
507	RP23-238D21		44292056	44462804	170748	Highest	+	-	36931
510	RP23-348H14		44428069	44643717	215648	Highest	+	-	34735
514	RP23-30F6	AL772376	44599936	44837186	237250	Highest	+	-	43781
518	RP23-12C18		44703454	44947686	244232	Highest	+	-	133732
520	RP23-139E24		44916535	45143642	227107	Medium	+	-	31151
528	RP23-421O11		45062725	45275851	213126	Highest	+	-	80917
529	RP23-102E20		45184060	45438063	254003	Highest	+	-	91791
533	RP23-91P12		45408725	45623429	214704	Highest	+	-	29338
535	RP23-97L12		45593269	45843711	250442	Highest	+	-	30160
540	RP23-161K7	AL772350	45785434	45998179	212745	Highest	+	-	58277
542	RP23-339F2		45833973	46033037	199064	Highest	+	-	164206
543	RP23-246L2		46137134	46374964	237830	Highest	+	-	-104097
545	RP23-350C18		46228496	46477456	248960	Highest	+	-	146468
548	RP23-206K1		46380555	46590964	210409	Highest	+	-	96901
551	RP23-351M21		46522259	46723947	201688	Highest	+	-	68705
553	RP23-217M8		46608104	46792158	184054	Highest	+	-	115843
558	RP23-22N16		46758120	46993352	235232	Highest	+	-	34038
560	RP23-311J14		46948048	47103489	155441	Highest	+	-	45304
562	RP23-144L20	AL732553	47072595	47273481	200886	Highest	+	-	30894
568	RP23-22D16		47250356	47486727	236371	Highest	+	-	23125
574	RP23-383M4		47441938	47657650	215712	Highest	+	-	44789
577	RP23-302J16		47596320	47770389	174069	Highest	+	-	61330
580	RP23-298H2		47733929	47920374	186445	Highest	+	-	36460
583	RP23-141C15	AL807771	47873771	48106817	233046	Highest	+	-	46603
589	RP23-357A7		48083637	48310354	226717	Highest	+	-	23180
592	RP23-187F9		48287386	48491862	204476	Highest	+	-	22968
595	RP23-135G14		48454555	48659621	205066	Highest	+	-	37307
596	RP23-34B24	AL772310	48657081	48868928	211847	Highest	+	-	2540
603	RP23-111F13		48806068	49024179	218111	Highest	+	-	62860
607	RP23-193M14		48999110	49214549	215439	Highest	+	-	25069
609	RP23-325E1		49166355	49390361	224006	Highest	+	-	48194
610	RP23-332L19	AL928574	49301702	49498899	197197	Highest	+	-	88659
611	RP23-361M6		49703801	49847911	144110	Highest	+	-	-204902
613	RP23-408J1		49791206	49992745	201539	Highest	+	-	56705
614	RP23-67K2		49925519	50114187	188668	Medium	+	-	67226

617	RP23-368A8		50058554	50247450	188896	Highest	+	-	55633
618	RP23-208P1		50331804	50513622	181818	Highest	+	-	-84354
619	RP23-215O19	AL732569	50486275	50663530	177255	Highest	+	-	27347
620	RP23-37H21		50694375	50881242	186867	Highest	+	-	-30845
623	RP23-32J7		50809393	51016890	207497	Highest	+	-	71849
625	RP23-123E1	AL732520	50974368	51182095	207727	Medium	+	-	42522
629	RP23-73L2		51161652	51385712	224060	Medium	+	-	20443
630	RP23-82G13		51323256	51457573	134317	Highest	+	-	62456
631	RP23-343C10		51486182	51690120	203938	Highest	+	-	-28609
634	RP23-187K5		51592274	51822435	230161	Highest	+	-	97846
636	RP23-113N2		51767148	51959992	192844	Highest	+	-	55287
640	RP23-148K17		51857184	52061970	204786	Highest	+	-	102808
641	RP23-115G24		52099283	52306878	207595	Medium	+	-	-37313
646	RP23-25D17	AL807243	52244978	52440813	195835	Highest	+	-	61900
648	RP23-300B24		52338512	52531242	192730	Highest	+	-	102301
650	RP23-204P1	AL773567	52492665	52682574	189909	Highest	+	-	38577
655	RP23-399G23		52562649	52782525	219876	Highest	+	-	119925
656	RP23-324N5		52670061	52905255	235194	Highest	+	-	112464
659	RP23-46H3		52879888	53042813	162925	Highest	+	-	25367
660	RP23-356K15		52888111	53079637	191526	Highest	+	-	154702
661	RP23-92G18		53053003	53257216	204213	Highest	+	-	26634
666	RP23-436E9		53204887	53402600	197713	Highest	+	-	52329
670	RP23-125G19		53312069	53543866	231797	Medium	+	-	90531
672	RP23-265E5		53410662	53592287	181625	Highest	+	-	133204
673	RP23-351I4		53579263	53789951	210688	Highest	+	-	13024
675	RP23-466A17	AL772349	53625815	53822051	196236	Highest	+	-	164136
676	RP23-390I8	AL772353	53817819	54006164	188345	Highest	+	-	4232
682	RP23-115N23		53932903	54149508	216605	Highest	+	-	73261
687	RP23-68C16		54104555	54295369	190814	Highest	+	-	44953
692	RP23-331C13		54272257	54490073	217816	Highest	+	-	23112
698	RP23-86N13		54426634	54638162	211528	Highest	+	-	63439
702	RP23-111D19		54615839	54841457	225618	Highest	+	-	22323
706	RP23-308I5		54783200	55036177	252977	Highest	+	-	58257
709	RP23-142K12		54956167	55183932	227765	Highest	+	-	80010
710	RP23-434J11		55123124	55309454	186330	Highest	+	-	60808
714	RP23-82K8	AL929491	55251304	55450933	199629	Highest	+	-	58150
715	RP23-160J6		55524154	55740356	216202	Highest	+	-	-73221
718	RP23-37N10		55615842	55797129	181287	Highest	+	-	124514
721	RP23-148O2		55769983	55982546	212563	Highest	+	-	27146
726	RP23-155E17		55932774	56150984	218210	Highest	+	-	49772
728	RP23-303I1		56047142	56229919	182777	Highest	+	-	103842
729	RP23-337I1		56151055	56392018	240963	Highest	+	-	78864
732	RP23-11H12		56286285	56495043	208758	Highest	+	-	105733
734	RP23-424G21		56461870	56638395	176525	Highest	+	-	33173
737	RP23-434P11		56489604	56709398	219794	Highest	+	-	148791
739	RP23-178E9		56638475	56860792	222317	Highest	+	-	70923
743	RP23-301E13		56787106	57007247	220141	Highest	+	-	73686
744	RP23-85M8		56990023	57216682	226659	Highest	+	-	17224
746	RP23-448N14		57158401	57341365	182964	Highest	+	-	58281

750	RP23-284I12		57297237	57534183	236946	Highest	+	-	44128
752	RP23-181I22		57509495	57718850	209355	Highest	+	-	24688
757	RP23-317N18		57693285	57911784	218499	Highest	+	-	25565
762	RP23-228M22		57882790	58047953	165163	Highest	+	-	28994
764	RP23-57J9		57964737	58165878	201141	Highest	+	-	83216
769	RP23-67A22		58140096	58421829	281733	Highest	+	-	25782
773	RP23-57N22	AL808112	58383829	58619927	236098	Highest	+	-	38000
775	RP23-351O5		58588398	58795271	206873	Highest	+	-	31529
780	RP23-6E12	BX005031	58737676	58953140	215464	Highest	+	-	57595
789	RP23-443B13		58922558	59130769	208211	Highest	+	-	30582
791	RP23-235L20		59105133	59257642	152509	Highest	+	-	25636
794	RP23-452J18		59112150	59296107	183957	Highest	+	-	145492
795	RP23-67O19		59799125	60123861	324736	Medium	+	-	-503018
796	RP23-61I16		59936348	60174849	238501	Medium	+	-	187513
797	RP23-57A6		60414343	60638749	224406	Medium	+	-	-239494
802	RP23-107D12		60567103	60757537	190434	Medium	+	-	71646
805	RP23-429G9		60692732	60898779	206047	Medium	+	-	64805
808	RP23-39D14		60851886	61108846	256960	Highest	+	-	46893
812	RP23-103G7		60992900	61213298	220398	Highest	+	-	115946
815	RP23-139I19		61162879	61380834	217955	Highest	+	-	50419
817	RP23-24J18	AL928565	61307378	61513589	206211	Highest	+	-	73456
819	RP23-324B9		61490683	61719836	229153	Highest	+	-	22906
825	RP23-341G1		61613928	61828236	214308	Highest	+	-	105908
826	RP23-454E10	AL928624	61744755	61920212	175457	Highest	+	-	83481
829	RP23-101D6		61869262	62062865	193603	Highest	+	-	50950
832	RP23-345F15		62021866	62236689	214823	Highest	+	-	40999
838	RP23-456C2		62200467	62398759	198292	Highest	+	-	36222
840	RP23-344I2		62295715	62511272	215557	Highest	+	-	103044
841	RP23-76N22		62427953	62653074	225121	Highest	+	-	83319
842	RP23-396A15		62532140	62745664	213524	Highest	+	-	120934
844	RP23-381O16		62724135	62929698	205563	Highest	+	-	21529
847	RP23-132F4	BX649255	62904300	63098916	194616	Highest	+	-	25398
849	RP23-4E22		62984839	63222739	237900	Highest	+	-	114077
853	RP23-173C3	AL691481	63173943	63404018	230075	Highest	+	-	48796
856	RP23-452N7		63242552	63431485	188933	Highest	+	-	161466
857	RP23-206A1		63426630	63613965	187335	Highest	+	-	4855
862	RP23-142L5		63585413	63791477	206064	Highest	+	-	28552
866	RP23-357C7		63755339	63949482	194143	Highest	+	-	36138
869	RP23-74M12		63884985	64122791	237806	Highest	+	-	64497
873	RP23-36A3		64085961	64294558	208597	Highest	+	-	36830
879	RP23-291O18		64271609	64466397	194788	Highest	+	-	22949
883	RP23-240I15		64425121	64639814	214693	Highest	+	-	41276
887	RP23-321H19		64615184	64811219	196035	Medium	+	-	24630
892	RP23-323E15		64782893	64982482	199589	Highest	+	-	28326
894	RP23-153P14	BX571882	64851844	65044106	192262	Highest	+	-	130638
895	RP23-15K21		64978652	65189770	211118	Highest	+	-	65454
898	RP23-348N14		65150003	65331989	181986	Highest	+	-	39767
901	RP23-27M9		65253677	65476329	222652	Highest	+	-	78312
904	RP23-30E14		65425388	65594375	168987	Highest	+	-	50941

905	RP23-87K16		65476130	65679905	203775	Highest	+	-	118245
906	RP23-206P23	BX322649	65627979	65825370	197391	Highest	+	-	51926
907	RP23-195E16	BX571887	65825447	66029840	204393	Highest	+	-	-77
910	RP23-118N17		65999067	66205006	205939	Highest	+	-	30773
911	RP23-94O16	BX936372	66205043	66383927	178884	Highest	+	-	-37
912	RP23-402A22		66723550	66920315	196765	Highest	+	-	-339623
913	RP23-61I15		66864062	67115743	251681	Highest	+	-	56253
917	RP23-399C17		67081840	67280191	198351	Highest	+	-	33903
920	RP23-333J24		67223351	67436826	213475	Highest	+	-	56840
924	RP23-164F9		67388341	67589047	200706	Highest	+	-	48485
925	RP23-294N12		67632247	67808324	176077	Highest	+	-	-43200
926	RP23-284H21		67750284	67983192	232908	Highest	+	-	58040
927	RP23-380M15		67920070	68087259	167189	Highest	+	-	63122
928	RP23-356I15		68087505	68288965	201460	Highest	+	-	-246
929	RP23-432L24		68109485	68317318	207833	Highest	+	-	179480
930	RP23-233I19		68335067	68526095	191028	Highest	+	-	-17749
934	RP23-159F17		68439028	68644485	205457	Highest	+	-	87067
939	RP23-435J11		68599625	68810278	210653	Highest	+	-	44860
941	RP23-38N8	AL845171	68774027	69003527	229500	Highest	+	-	36251
943	RP23-432P15		68957947	69172090	214143	Highest	+	-	45580
945	RP23-95M20	AL929442	69101339	69311758	210419	Highest	+	-	70751
946	RP23-380I15		69317645	69499131	181486	Highest	+	-	-5887
949	RP23-458G19		69343723	69515289	171566	Highest	+	-	155408
950	RP23-420C7		69515436	69709344	193908	Highest	+	-	-147
951	RP23-358A23		69545558	69728433	182875	Highest	+	-	163786
952	RP23-29G22		70017793	70270141	252348	Highest	+	-	-289360
955	RP23-161B14		70195530	70395928	200398	Highest	+	-	74611
958	RP23-420G13		70356077	70559607	203530	Highest	+	-	39851
959	RP23-347D6		70410010	70579554	169544	Highest	+	-	149597
960	RP23-309C6		70547278	70699596	152318	Highest	+	-	32276
961	RP23-439M13		70573929	70757382	183453	Highest	+	-	125667
962	RP23-379O23	BX640496	70955452	71127752	172300	Medium	+	-	-198070
964	RP23-222P16		71084834	71303436	218602	Highest	+	-	42918
966	RP23-342C12		71270077	71506148	236071	Highest	+	-	33359
967	RP23-180O12		71385786	71599301	213515	Medium	+	-	120362
968	RP23-313M22		71678040	71875731	197691	Medium	+	-	-78739
969	RP23-357O16		71859807	72026378	166571	Highest	+	-	15924
970	RP23-32H24		72026461	72217073	190612	Highest	+	-	-83
971	RP23-438B17		72286282	72453868	167586	Highest	+	-	-69209
972	RP23-476C7		72395139	72587746	192607	Highest	+	-	58729
974	RP23-115P24		72475717	72677349	201632	Highest	+	-	112029
976	RP23-268I2		72648058	72844666	196608	Highest	+	-	29291
979	RP23-101H20		72781739	72984142	202403	Highest	+	-	62927
980	RP23-92G15		73131844	73281564	149720	Highest	+	-	-147702
982	RP23-302J8		73176066	73412450	236384	Highest	+	-	105498
985	RP23-141O2	CR396588	73365424	73558131	192707	Highest	+	-	47026
989	RP23-147F16		73537874	73725026	187152	Highest	+	-	20257
991	RP23-87H14		73696384	73919630	223246	Highest	+	-	28642
996	RP23-431G10		73859033	74057005	197972	Highest	+	-	60597

998	RP23-290N18		73976029	74135358	159329	Highest	+	-	80976
999	RP23-451G1		74127733	74292762	165029	Medium	+	-	7625
1001	RP23-325D14		74151599	74339799	188200	Medium	+	-	141163
1002	RP23-42K13		74273912	74533139	259227	Medium	+	-	65887
1011	RP23-247N5	AL844848	74462714	74664550	201836	Highest	+	-	70425
1012	RP23-310L11	BX296523	74610670	74841754	231084	Highest	+	-	53880
1017	RP23-467N14		74787304	74977155	189851	Highest	+	-	54450
1021	RP23-15P19		74948199	75178164	229965	Highest	+	-	28956
1023	RP23-180H11		75049598	75244731	195133	Highest	+	-	128566
1024	RP23-391A4		75161880	75348597	186717	Highest	+	-	82851
1025	RP23-14G7		75349227	75553228	204001	Highest	+	-	-630
1026	RP23-245E19	AL845333	75434470	75620603	186133	Highest	+	-	118758
1028	RP23-303H3		75566191	75766219	200028	Highest	+	-	54412
1033	RP23-342O7		75716202	75949676	233474	Highest	+	-	50017
1036	RP23-416J19		75838768	76031604	192836	Highest	+	-	110908
1040	RP23-415E9		76007998	76229284	221286	Highest	+	-	23606
1045	RP23-232K22		76178165	76368591	190426	Highest	+	-	51119
1046	RP23-405M24	AL954189	76327020	76544942	217922	Medium	+	-	41571
1047	RP23-117O5		76479718	76655408	175690	Highest	+	-	65224
1048	RP23-147D24		76585946	76800250	214304	Medium	+	-	69462
1049	RP23-426O2		76970319	77151403	181084	Highest	+	-	-170069
1050	RP23-101C7		77139405	77362207	222802	Medium	+	-	11998
1052	RP23-79D4		77265388	77476558	211170	Highest	+	-	96819
1053	RP23-128L7		77617526	77808655	191129	Highest	+	-	-140968
1054	RP23-183M11		77795700	77984914	189214	Highest	+	-	12955
1055	RP23-444K7		77811412	77997705	186293	Highest	+	-	173502
1056	RP23-34E12		78014156	78246085	231929	Highest	+	-	-16451
1059	RP23-120A3		78141881	78351641	209760	Highest	+	-	104204
1063	RP23-235B22		78293459	78480525	187066	Highest	+	-	58182
1064	RP23-149B22		78453914	78637585	183671	Highest	+	-	26611
1065	RP23-419H18	BX640502	78542802	78754537	211735	Medium	+	-	94783
1066	RP23-416O14		78750536	78916089	165553	Medium	+	-	4001
1068	RP23-205K24		78872174	79087361	215187	Highest	+	-	43915
1074	RP23-212J5		79042646	79258811	216165	Highest	+	-	44715
1078	RP23-325F19		79210496	79401074	190578	Highest	+	-	48315
1079	RP23-338C16		79358158	79562037	203879	Highest	+	-	42916
1081	RP23-233O19		79483226	79665146	181920	Highest	+	-	78811
1083	RP23-390K8		79590541	79788603	198062	Highest	+	-	74605
1086	RP23-125N5	BX682542	79750484	79957669	207185	Highest	+	-	38119
1087	RP23-475N10		79773937	79966759	192822	Highest	+	-	183732
1088	RP23-293L20		80102236	80297982	195746	Highest	+	-	-135477
1093	RP23-454C1		80277637	80475958	198321	Highest	+	-	20345
1095	RP23-458C21		80424659	80598877	174218	Highest	+	-	51299
1097	RP23-181G21		80546632	80760188	213556	Medium	+	-	52245
1102	RP23-56D19		80684936	80958115	273179	Highest	+	-	75252
1104	RP23-117M16		80916458	81131980	215522	Highest	+	-	41657
1110	RP23-109N19		81099549	81323059	223510	Highest	+	-	32431
1112	RP23-152G9		81288850	81498577	209727	Highest	+	-	34209
1117	RP23-354A4		81460078	81660380	200302	Medium	+	-	38499

1122	RP23-138G14		81608565	81791763	183198	Highest	+	-	51815
1129	RP23-228O1		81769935	81963942	194007	Highest	+	-	21828
1134	RP23-22O4		81934131	82141082	206951	Highest	+	-	29811
1136	RP23-381B20		82105700	82293773	188073	Highest	+	-	35382
1142	RP23-471O23	AL807790	82250232	82429805	179573	Highest	+	-	43541
1146	RP23-78O19		82364226	82619636	255410	Highest	+	-	65579
1150	RP23-292P23		82541931	82750906	208975	Highest	+	-	77705
1155	RP23-395M3	AL805919	82727249	82926267	199018	Medium	+	-	23657
1162	RP23-148E3		82852383	83075683	223300	Highest	+	-	73884
1166	RP23-146L3		83020700	83236502	215802	Highest	+	-	54983
1167	RP23-79O16		83166991	83410055	243064	Highest	+	-	69511
1172	RP23-203M7		83374319	83595928	221609	Medium	+	-	35736
1174	RP23-459J19	AL929430	83497008	83697592	200584	Highest	+	-	98920
1177	RP23-9G18		83643134	83869752	226618	Highest	+	-	54458
1181	RP23-15H18		83809822	84004283	194461	Highest	+	-	59930
1182	RP23-433E8		83937670	84147428	209758	Highest	+	-	66613
1187	RP23-313G2	AL929448	84097770	84301884	204114	Highest	+	-	49658
1188	RP23-26E20		84190175	84402249	212074	Highest	+	-	111709
1192	RP23-152G19	AL807242	84370394	84584033	213639	Medium	+	-	31855
1200	RP23-190E17		84563912	84762092	198180	Highest	+	-	20121
1204	RP23-95O1	AL824707	84724583	84949479	224896	Medium	+	-	37509
1207	RP23-85A2		84860314	85104771	244457	Highest	+	-	89165
1210	RP23-110F8	AL773553	85081655	85304723	223068	Highest	+	-	23116
1213	RP23-367C18		85276168	85471942	195774	Highest	+	-	28555
1215	RP23-222F14		85356041	85579188	223147	Highest	+	-	115901
1216	RP23-325L22	AL953839	85463601	85654762	191161	Medium	+	-	115587
1217	RP23-298K4		85654771	85842305	187534	Highest	+	-	-9
1221	RP23-212O24	BX284642	85806126	86006582	200456	Highest	+	-	36179
1227	RP23-263N20		85959042	86148944	189902	Highest	+	-	47540
1230	RP23-222G21		86112676	86317952	205276	Highest	+	-	36268
1236	RP23-402B13		86264324	86473699	209375	Medium	+	-	53628
1240	RP23-83N3		86419634	86625190	205556	Highest	+	-	54065
1242	RP23-11A16		86587657	86795373	207716	Highest	+	-	37533
1244	RP23-64G11		86674327	86871124	196797	Highest	+	-	121046
1245	RP23-67C1	AL772394	86777925	86916608	138683	Highest	+	-	93199
1246	RP23-213G4		86987500	87239681	252181	Highest	+	-	-70892
1250	RP23-357D3		87199228	87419867	220639	Highest	+	-	40453
1254	RP23-139P5		87388260	87584747	196487	Highest	+	-	31607
1255	RP23-95P16		87412520	87613876	201356	Highest	+	-	172227
1256	RP23-445E3	BX649611	87695879	87877749	181870	Highest	+	-	-82003
1262	RP23-357N14		87787908	87980897	192989	Highest	+	-	89841
1263	RP23-12N4		87860970	88101732	240762	Highest	+	-	119927
1264	RP23-266G24		88084755	88282686	197931	Highest	+	-	16977
1266	RP23-359B13		88239390	88424184	184794	Highest	+	-	43296
1267	RP23-21I15		88333674	88571603	237929	Highest	+	-	90510
1268	RP23-462D2		88499893	88679888	179995	Medium	+	-	71710
1269	RP23-236O21	AL671925	88702697	88921064	218367	Medium	+	-	-22809
1270	RP23-183P20		88775544	88966654	191110	Highest	+	-	145520
1271	RP23-118I21		88909335	89128079	218744	Highest	+	-	57319

1273	RP23-326H20		89085282	89274074	188792	Highest	+	-	42797
1274	RP23-137B11		89327668	89535374	207706	Medium	+	-	-53594
1279	RP23-173M22		89450949	89678246	227297	Highest	+	-	84425
1285	RP23-240F2		89637929	89815335	177406	Highest	+	-	40317
1287	RP23-190K9	BX537306	89740758	89925194	184436	Highest	+	-	74577
1289	RP23-2O10	AC099413	89888398	90096939	208541	Highest	+	-	36796
1291	RP23-256D21		90075496	90220319	144823	Highest	+	-	21443
1294	RP23-282K2		90153849	90321451	167602	Highest	+	-	66470
1296	RP23-129H4		90236370	90419080	182710	Highest	+	-	85081
1297	RP23-24G6		90384214	90533741	149527	Highest	+	-	34866
1298	RP23-132L3		90499853	90693444	193591	Highest	+	-	33888
1300	RP23-127K21		90554929	90768757	213828	Highest	+	-	138515
1302	RP23-145B12		90716064	90927887	211823	Highest	+	-	52693
1303	RP23-288P14		90920592	91132922	212330	Highest	+	-	7295
1305	RP23-12K12		91074255	91275743	201488	Highest	+	-	58667
1308	RP23-322F24		91211628	91425841	214213	Medium	+	-	64115
1311	RP23-328I9		91381855	91569779	187924	Medium	+	-	43986
1315	RP23-442C1		91541902	91731622	189720	Highest	+	-	27877
1317	RP23-103J13		91694849	91896838	201989	Highest	+	-	36773
1319	RP23-301A10		91727542	91935523	207981	Highest	+	-	169296
1320	RP23-138N13	BX664632	91934344	92175787	241443	Highest	+	-	1179
1323	RP23-337H15		92136269	92366716	230447	Highest	+	-	39518
1326	RP23-356F18		92343111	92533626	190515	Highest	+	-	23605
1330	RP23-432K21		92485473	92698369	212896	Highest	+	-	48153
1333	RP23-82L24		92621775	92826407	204632	Highest	+	-	76594
1336	RP23-173G7		92796792	93001533	204741	Highest	+	-	29615
1337	RP23-82J4		92891589	93138388	246799	Highest	+	-	109944
1339	RP23-225D6		93067908	93308115	240207	Highest	+	-	70480

Key Research Accomplishments:

- Have successfully developed an approach using an HSV-1 amplicon system for efficient transfer of BAC genomic locus into bone cells, and established that the candidate gene is expressed at high level and is functional.
- We developed a BAC contig for an ENU mutant locus located between 7.5-36 cM on Chromosome 4 of the B6 mouse mutant.

Reportable Outcomes:

Papers:

1. Xing W, Baylink D, Kesavan C and Mohan S. HSV-1 Amplicon-Mediated Transfer of 128-kb BMP-2 Genomic Locus Stimulates Osteoblast Differentiation *in vitro* Biochem Biophys Res Commun 319(3): 781-6, 2004

2. Xing W, Baylink D, Kesavan C and Mohan S Transfer of 128-kb BMP-2 Genomic Locus by HSV-Based Infectious BAC Stimulates Osteoblast Differentiation: A Platform for Functional Genomic Studies. *ASBMR-2004, in press*

Conclusions

1) We have successfully transferred 128-kb 1.BMP-2 genomic locus into osteoblast cells with high efficiency by utilizing HSV amplicon system.

2) The transgene was retained in osteoblast cells as minichromosomes for a long period of time.

3) The infected cells with transgene express functional protein, and induced cell differentiation.

4) The BAC gene transfer provides a rapid and efficient approach for functional testing of candidate genes within the QTL region *in vitro.*

5) A BAC contig has been developed for environmental region containing bone size mutant gene.

References

1. Abrams, K. L., Xu, J., Nativelle-Serpentini, C., Dabirshahsahebi, S., and Rogers, M. B. An evolutionary and molecular analysis of BMP2 expression. J Biol Chem; 2004.
2. Helvering, L. M., Sharp, R. L., Ou, X., and Geiser, A. G. Regulation of the promoters for the human bone morphogenetic protein 2 and 4 genes. Gene 256:123-38; 2000.
3. Saeki, Y., Breakefield, X. O., and Chiocca, E. A. Improved HSV-1 amplicon packaging system using ICP27-deleted, oversized HSV-1 BAC DNA. Methods Mol Med 76:51-60; 2003.
4. Wade-Martins, R., Saeki, Y., and Antonio Chiocca, E. Infectious delivery of a 135-kb LDLR genomic locus leads to regulated complementation of low-density lipoprotein receptor deficiency in human cells. Mol Ther 7:604-12; 2003.
5. Wade-Martins, R., Smith, E. R., Tyminski, E., Chiocca, E. A., and Saeki, Y. An infectious transfer and expression system for genomic DNA loci in human and mouse cells. Nat Biotechnol 19:1067-70; 2001.

Project 4: The Application Of Transgenic Mice To Assess Gene Function In Mechanical Loading And In Bone Fracture Healing Models

Introduction

Bone formation in response to exercise or injury requires the coordinated interactions of a number of molecular pathways of gene expression. However, a more complete understanding of gene expression in bone formation and fracture repair requires definitive proof of the functional significance of the genes participating in the pathways. In this regard the analysis of mice engineered to be deficient in the expression of a particular gene-of-interest (i.e., knockout mice) is especially valuable. The study of knockout mice provides conclusive evidence of the functional significance of particular genes in the development and repair of bone. These studies will eventually help to elucidate the regulation of gene expression in bone formation and repair and suggest therapeutic strategies to augment or accelerate bone formation and repair.

We have utilized commercially available knockout mice to determine what effect the absence of expression a particular gene has on bone formation in response to mechanical loading and in fracture repair. Not only will the examination of bone formation and repair characterize the effects of the knockout gene in each case, but subsequent examination of the expression of other genes in knockout mouse tissues will help to define the regulatory networks that modulate the observed knockout phenotype. Ultimately, this approach will suggest additional gene candidates for additional therapeutic alternatives in bone formation and healing.

Body

Technical Objectives

Our Technical Objectives were as follows:

Technical Objective 1: The functional significance of a gene of interest on bone formation will be identified by characterizing the skeletal phenotype in mice deficient in that gene (i.e., knockout mice) in response to mechanical loading of the bone by exercise.

Our specific objectives during the first 12 months of this grant period were as follows:

1. adapt a mechanical loading model for mouse bones that approximates an exercise routine.
2. acquire breeder pairs of three strains of knockout mice (Longjohn, Leptin and Bax), establish a breeding colony and generate sufficient numbers of knockout mice to test for the bone response to mechanical loading.
3. identify differences in bone formation between knockout and wild-type mice, through measurements of mechanically loaded bone by peripheral quantitative computed tomography (pQCT) and conventional molecular markers of bone formation.

Technical Objective 2: The functional significance of a gene of interest on bone formation in response to injury will be identified by characterizing the skeletal phenotype in mice deficient in that gene (i.e., knockout mice) during fracture healing.

Our specific objectives for fracture repair during the first 12 months of this grant period were as follows:

1. develop a model for femur fracture in mice.
2. acquire breeder pairs of three strains of knockout mice (Longjohn, Leptin and Bax), establish a breeding colony and generate sufficient numbers of knockout mice to test the Technical Objective.

3. establish the phenotypic differences between knockout mice and wild-type control mice by X-ray examination, pQCT measurements, histological examination of the fracture callus and molecular bone marker analysis of the fracture tissues.

Progress on Technical Objectives

Technical Objective 1:

Mechanical loading determines both the mechanical density and the architecture of bone. Previous studies have established changes in bone mineral content and bone mineral density in response to exercise among boys (1), and our own studies have demonstrated that mechanical loading by exercise increased bone formation in mice (2). In this study, we used knockout mice to identify and characterize the functional effects of exercise-induced bone formation in mice deficient for a gene-of-interest previously implicated in bone growth or development (Table 1, "Longjohn", "Leptin" and "Bax" mice). The phenotypic response to mechanical loading in the particular strain of knockout mouse was correlated to X-ray and molecular measurements of bone formation.

Table 1. Knockout Mice with Phenotypes for Exercise and Fracture Studies.

Gene	Stock #	Strain Description	Knockouts Used	Phenotype Description
Longjohn	3507	B2;B6-Npr3 $^{lgj\text{-}2J}$	4 (loading) 23(fracture)	skeletal overgrowth
Leptin	0632	B6-*Lep* ^{ob}	7(loading) 15(fracture)	NIDDM, obese delayed wound healing
Bax	2994	B6.129X1-*bax* ^{tm1Sjk}	0(loading) 10(fracture)	delayed apoptosis organ defects (gonads)

The wild-type control genotype is DBA (for "Longjohn") or C57BL/6 (B6, for "Leptin' and "Bax").

Specific Objective 1: Adapt a mechanical loading model for mouse bones that approximates an exercise routine.

We have developed a mechanical loading procedure that approximates exercise. Briefly, it consisted of a 12-day four-point bending routine of a 9 Newton (N) force applied at 2 Hertz (Hz) and 36 cycles to the right tibia of the mouse. This routine was developed from a load response trial that tested bone formation in C57BL/6J (B6) mice in response to loads of 6N through 9N. The loaded and unloaded contra-lateral tibiae were analyzed for bone formation by pQCT following the final loading after the 12-day four-point bending regimen. The bone parameters examined in knockout and B6 wild-type control mice were total bone mineral content, total bone area, periosteal circumference, endosteal circumference, total bone mineral density, cortical bone mineral content, and cortical bone mineral density. The pQCT analysis and the expression of molecular markers of bone formation revealed that the 9N load produced the optimal bone formation response in adult B6 mice (data not shown).

Specific Objective 2: Breed and genotype the knockout mice, and identify homozygotes that lack expression of a knockout gene-of-interest that might regulate the bone formation or influence wound healing.

We had selected three prospective knockout mice (Table 1), which have good viability and fertility, and are commercially available from the Jackson Labs: the Leptin knockout, Bax knockout and natriuretic peptide receptor 3 ("Longjohn") knockout mice.

a) Leptin Knockout (Obese) Mice. Leptin is a 16 kDa protein, expressed predominantly in adipose tissue and functions as a hormone that keeps the brain appraised of the amount of body fat and regulates carbohydrate metabolism. This mouse line is also a model for non-insulin dependent (NIDDM, Type 2) diabetes (Table 1). Other functions of this protein related to bone formation include: a) it stimulates osteoblastic differentiation and mineralization of bone matrix (3); b) it stimulates the development of the periosteal envelope in growing bone; and c) peripheral Leptin administration increases bone formation increases and infusion of leptin to the third ventricle in *ob/ob* mice reduces bone formation (4). However, the systemic vs local effects of leptin on the fat and bone cell lineages have not been well characterized.

The heterozygous Leptin knockout (*op/op*) breeder mice were purchased from the Jackson Labs and were bred in our animal research facility. Because of the character of recessive inheritance, only ~¼ of the pups were homozygous. The homozygous mice were readily recognized by the obese phenotype and were confirmed by genotyping. However, we initially faced a problem of high litter mortality due to neglect or cannibalization of the pups by the mother. We have subsequently used more experienced surrogate mothers for the nursing of pulps, which led to a great increase in litter survival. Consequently, we have now established a colony of Leptin knockout mice in our animal research facility within the Jerry L. Pettis Memorial VA Medical Center. These knockout mice and their wild-type littermates will be used for these studies.

b) Bax Knockout Mice. Bax, Bcl-2-associated X protein, is a member of the Bcl-2 protein family. Bax forms hetero-dimer with Bcl-2, which prevents Bcl-2 from being functional. Accordingly, Bax functions to oppose Bcl-2 and to promote apoptosis (7). The cellular Bax/Bcl-2 ratio determines the cell fate (apoptosis or cell survival). Both genes are expressed in cartilage and bone cells in the rat (8). Apoptosis has a major impact on skeletal development and remodeling. Accordingly, apoptosis is the major mechanism for the elimination of osteoblasts during skeletal development. The frequency of osteoblast apoptosis determines osteoblast lifespan and subsequently bone formation rate during the postnatal life. We have obtained heterozygous breeder pairs of mice from the Jackson Labs and were bred in our animal facility. Approximately one-fourth of the pups were homozygous mice, which were not readily identified due to the lack of an obvious phenotype. As a result, homozygous Bax knockout mice were identified by genotyping. The breeding of homozygous Bax knockout mice has been slow, primarily because the high rate of litter mortality due to neglect and/or cannibalization of the pups by the mothers. Thus, there have been so far only a limited number of homozygous mice available for use in this study. We are working to improve our breeding protocol to reduce litter mortality.

c) Longjohn Mice. The natriuretic peptide receptor C gene (*Npr3*) in these mice had a point mutation, rendering the Npr3 nonfunctional. This results in a defect in the clearance of natriuretic

peptides and causes a delayed endochondral ossification, leading to an extended proliferative zone of the cartilage and skeletal overgrowth syndrome (5, 6). Thus, the natriuretic peptide receptor C deficient mice are commonly referred to Longjohn mice. We had purchased homozygous breeders from the Jackson Labs. These mice were bred well and we had a colony of these mice in our animal research facility. Initially, we were surprised that the mice did not show the skeletal overgrowth ("longjohn") phenotype. We contacted the Jackson Labs about the lack of phenotype. We were told that, because of the difficulties associated with the breeding of these mice in their original background, the mice were bred into a different background (DBA). This has led to a reduction in the "longjohn" phenotype. We trusted the Jackson Labs, who ensured us that these mice were indeed the Longjohn mice. Consequently, we have performed preliminary studies with our colony of Longjohn mice and consistently obtained negative results (i.e., there were no difference in any measured parameters between the Longjohn mice and their corresponding DBA wild-type mice). We then began to question the genotype identity of these mice and decided to confirm their genotype identity by DNA sequencing. The sequencing analyses revealed that, contrary to the claim of the Jackson Labs, the *Npr3* gene of these mice did not contain the point mutation or any mutations. It appeared that what we had obtained from the Jackson Labs was the wild-type DBA mice and not the Longjohn mice. When we confronted the Jackson Labs with our genotyping data, they acknowledged the error of the mis-identification. They also told us that they do not have the original Longjohn mouse strain and therefore have lost the Longjohn mutant mice from their stocks. Consequently, we have now learned our mistake and are no longer so willingly to trust the suppliers. We have subsequently confirmed the genotype of the Leptin and Bax knockout mice. We are no longer working on the "Longjohn" mice and are currently looking for another suitable knockout mouse strain to replace "Longjohn" mice for the proposed work.

Specific Objective 3: Determine and compare the bone formation response to mechanical loading in knockout mice and their respective wild-type control mice.

As indicated above, we have established a mechanical loading protocol (i.e., the "four-point bending" regimen using a 9 N load) to evaluate the bone formation response to mechanical loading in the knockout mice. Accordingly, to assess the potential role of the Leptin gene on the bone formation response to mechanical loading, we applied a 9 N load at 2 Hertz (Hz) for 36 cycles for 12 consecutive days on the right tibia of 4 female Leptin mice at 10 weeks of age. The same loading regimen was also applied on the right tibia of 4 female corresponding wild type mice at 10 weeks of age for comparison. Bone formation was measured on both tibiae by pQCT after the final loading and the results of the loaded, right tibia and those of the unloaded, left tibia were compared to determine the bone formation response.

The responses to the 9N load in various bone parameters determined by pQCT of the Leptin knockout mice and the age-matched wild-type mice are shown in Table 1 and Table 2, respectively. It appears that the 9N load produced bigger bone responses in the wild-type mice than in the Leptin knockout mice. However, it is noteworthy to note that the bone in the Leptin knockout mice was much bigger than that in the corresponding wild type mice. The actual mechanical strain sensed by the bigger bone of a given load would be significantly less than that sensed by the smaller bone, since the amount of mechanical strain on a bone depends on its size and geometry. Because the bone response depends on mechanical strain rather than mechanical loading, the direct comparison of the bone response to the same load (9N) between the larger

bone of Leptin knockout mice and the smaller bone of the wild-type mice is not appropriate. Consequently, we next determined and compared the amount of strains produced by the 9N load on the Leptin knockout tibia and that on wild-type B6 tibia using a microstrain gauge. It was confirmed that the 9N load produced a much smaller strain [2,129 microstrains (με)] on the tibia of the Leptin knockout mice as opposed to that on the tibia of wild-type mice [3,600 με]. Therefore, the apparently smaller response in the Leptin knockout mice compared to the wild-type B6 mice could be due to the fact the Leptin knockout mice experienced a much smaller mechanical strain than the wild-type mice. Consequently, in order to have a valid comparison, we decided to compare the bone response to the same or similar mechanical strain in the Leptin knockout mice with that in the wild-type mice.

Table 2. Mechanical loading results on 10-week female Leptin knockout (KO) mice for a 9N load (strain = 2,129 με). (n=4).

Parameter	10-week female Leptin KO mice **Mean ± SD**		**Loaded vs. Unloaded**	
Bone parameters	**Unloaded**	**Loaded**	**% Increase**	**P-value**
Total content (mg/mm)	**1.24 ± 0.07**	**1.41 ± 0.02**	**13.7**	**0.01**
Total Area (mm^2)	**2.43 ± 0.24**	**2.71 ± 0.16**	**11.5**	**0.11**
Periosteal circumference (mm)	**5.51 ± 0.26**	**5.81 ± 0.16**	**5.4**	**0.1**
Endosteal circumference (mm)	**4.54 ± 0.28**	**4.76 ± 0.18**	**4.8**	**0.23**
Total Density (mg/ccm)	**585.26 ± 25.67**	**631.81 ± 25.35**	**8.0**	**0.04**
Cortical Density (mg/ccm)	**1004.06 ± 18.21**	**1026.55 ± 10.06**	**2.2**	**0.07**

Table 3. Mechanical loading results on 10-week female C57BL/6 (B6) control mice for a 9N load (strain = 3,600 με). (n=4)

Parameter	10-week female B6 **Mean ± SD**		**Loaded vs. Unloaded**	
Bone parameters	**Unloaded**	**Loaded**	**% increase**	**P-value**
Total content (mg/mm)	**0.89 ± 0.02**	**1.08 ± 0.02**	**21.3**	**0.00004**
Total Area (mm^2)	**1.48 ± 0.04**	**1.74 ± 0.04**	**17.6**	**0.0001**
Periosteal circumference (mm)	**4.31 ± 0.06**	**4.67 ± 0.05**	**8.4**	**0.0002**
Endosteal circumference (mm)	**3.26 ± 0.06**	**3.45 ± 0.08**	**5.8**	**0.01**
Total Density (mg/ccm)	**635.26 ± 19.81**	**673.17 ± 16.58**	**6.0**	**0.02**
Cortical Density (mg/ccm)	**1078.1 ± 39.50**	**1115.40 ± 34.70**	**3.5**	**0.005**

Using the microstrain gauge, we determined the mechanical strain imparted on the wild-type mice with a 6N load was 2,500 με, which is in the same range that is exerted by a 9N load on the Leptin knockout mice. Accordingly, we next determined the bone response to a 6N loading regimen in the tibia of wild-type B6 mice (Table 4) and compared to the bone response to a 9N loading regimen in the tibia of Leptin knockout mice (Table 2).

Table 4. Mechanical loading results on 10-week female C57BL/6 (B6) control mice for a 6N load (strain = 2,500 με). (n=6).

Parameter	10-week female B6 mice **Mean ± SD**		Loaded vs. Unloaded	
Bone parameters	**Unloaded**	**Loaded**	**% increase**	**P-value**
Total content (mg/mm)	**0.88 ± 0.09**	**0.92 ± 0.10**	**4.5**	**0.42**
Total Area (mm^2)	**1.40 ± 0.35**	**1.51 ± 0.42**	**7.8**	**0.59**
Periosteal circumference (mm)	**4.18 ± 0.53**	**4.32 ± 0.61**	**3.3**	**0.63**
Endosteal circumference (mm)	**3.1 ± 0.54**	**3.19 ± 0.63**	**2.9**	**0.76**
Total Density (mg/ccm)	**701.75 ± 111**	**689.25 ± 121**	**-1.8**	**0.83**

Table 4 shows that the application of 2,500 με to wild-type B6 mice had no significant effect on any measured parameters; whereas the application of 2,129 με markedly enhanced the bone formation response in the age-matched Leptin knockout mice (in B6 background) (Table 2). These findings strongly suggested that knocking out the Leptin gene in B6 mice resulted in a highly significant enhanced bone formation response to the mechanical loading, in that a mechanical strain that would normally be not sufficient to induce a bone formation response in the wild-type mice is sufficient to induce a highly significant bone response. This would suggest that the Leptin gene has a negative role in the bone response to mechanical strain. These findings are exciting and indicate that the role of the Leptin in the bone formation response to mechanical loading deserves further investigations.

Molecular analysis of the expression of bone formation marker genes in response to the mechanical loading in these mice will begin soon and is one of the focuses of the next year funding of this project. In preparation of this work, we have designed and validated various PCR primers for bone marker genes (mouse collagen 1 and osteocalcin) and housekeeping control genes (mouse beta-actin and cyclophilin). These primers have been tested and validated in preliminary real-time PCR assays. Therefore, they will be ready for use in the proposed real-time PCR assays scheduled for the second year of this project.

As indicated earlier, we have only been able to obtain a limited number of homozygous Bax knockout mice. These mice have all been used in the fracture healing portion of this project (see Tachnical objective 2 below). Consequently, we have not yet determined the bone response to mechanical loading in the Bax knockout mice. This work will be initiated as soon as we have obtained sufficient numbers of Bax knockout mice.

In summary, we have encountered some difficulties in the breeding of the knockout mice. Thus, we chose to limit our focus on the fracture healing portion of the proposed work (Tachnical Objective 2). Accordingly, our progress toward Technical Objective 1 has been somewhat impeded. As a result, we were only able to partially complete this Technical Objective. However, we have now improved our breeding program of the knockout mice and significantly more Leptin and Bax knockout mice are becoming available for use. Consequently, we anticipate that our progress in this Technical Objective will be much increased from now on.

Technical Objective 2:

During the first twelve months of the study, the functional significance of a knockout gene of interest in bone formation induced by fracture repair will be established by a comparison of the skeletal phenotypes in knockout mice deficient in that gene with wild-type control mice. Our original plan was to use the tibial fracture model which we have established in the rat. Unfortunately, we have had significantly difficulties in transferring this tibial fracture model to the mouse due to problems associated with consistent fracture stabilization. Accordingly, unless the rat tibia, the mouse tibia showed high degrees in curvature. Moreover, the length of mouse tibia is substantially shorter than that of the rat tibia. Any means to increase the stabilization of the tibial fracture greatly affect the fracture healing. We subsequently developed a femoral fracture model in the mouse and found that, because the mouse femur showed significantly less curvature than mouse tibia, the mouse femoral fracture model showed a much lower variations with respect to the pin stabilization. As a result, although the femoral fracture model is more difficult surgically than the tibial fracture, we decided to use the femoral fracture model rather than the tibial fracture model for this work.

The same three knockout mouse strains used in Technical Objective 1 (Table 1) were used in the studies of Technical Objective 2. Bone formation parameters at each healing interval corresponding to characteristic landmarks of fracture callus maturation were measured by pQCT, X-ray, histology, and/or expression of bone formation genes.

Specific Objective 1: Develop femoral fracture model of bone repair in mice.

Preliminary experiments indicated that the tibia fracture model was inadequate for this fracture healing study. The tibia fracture and subsequent healing were inconsistent and produced unacceptable statistical variations due to variations in the tibial dimensions and curvature. Although its size and proximity to the torso made the femur fracture surgery more difficult, we successfully developed the femur fracture model in wild-type mice. Briefly, an intramedullary pin is surgically implanted in the femur prior to fracture and the incisions closed. The mechanical testing device used in Technical Objective 1 was used to produce a complete fracture by the three-point bending technique. The procedure produced fractures that were consistently transverse and at the midshaft (Figure 1). These would allow good and reliable comparison of fracture healing between knockout mice and their corresponding wild-type mice.

Figure 1. The mouse femoral fracture model. An X-ray photograph was obtained immediately after femoral fracture surgery in a C57BL/6 mouse. The arrow indicates the fracture site. The stabilizing pin is easily visible.

Fractures were produced in several C57BL/6 mice (wild-type control) mice. The progression of fracture healing was assessed by X-rays of individual fractured femurs at days 7, 14, 21 and 28 after facture were (Figure 2). The expected progression of callus development was easily visible by X-ray. An apparently complete fracture union occurred on day 28. Therefore, this mouse femoral fracture model is suitable for use in the proposed work.

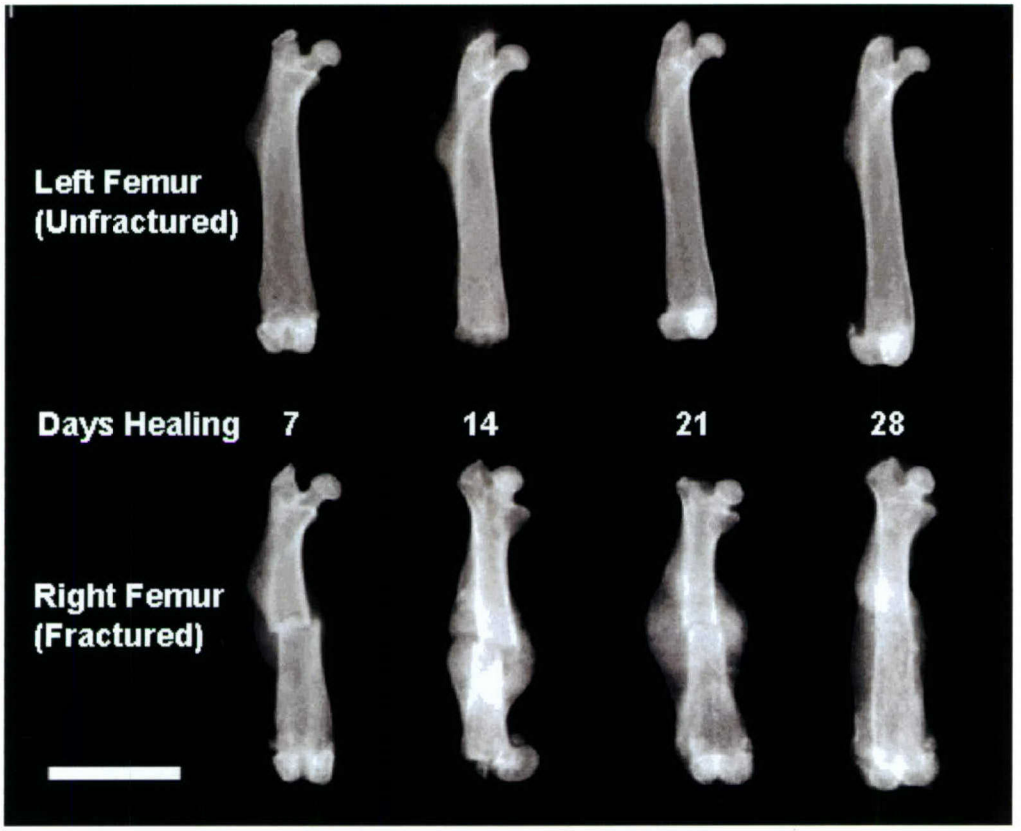

Figure 2. X-ray photograph of healing mouse fractured right femurs compared with unfractured left femurs at 7, 14, 21 and 28 days post-fracture. The development of the mineralized (hard) callus can be monitored from its early stages, at 7 days, through its maximum, at 14 to 21 days, and into remodeling to cortical bone, at 28 days. Each stage has characteristic features for comparison to impaired fracture repair. Healing is defined as that point when the bony tissue of the hard callus bridges the fracture gap, usually after 28 days in the mouse; remodeling to cortical bone continues after this time, eventually resolving the fracture callus. Scale bar = 5 mm.

pQCT measurements of bone mineral content (BMC) were done at 4 time points of fracture healing times in C57BL/6 mice (Figure 3). For analysis of callus development during healing, it was necessary to adapt the pQCT analysis to quantify soft and hard tissues of the maturing fracture callus. We therefore adjusted the thresholds of the pQCT analysis and measured the bone mineral content at 1-mm intervals along the length of the fracture callus so that only the lower density (noncortical) bone was detected. The values at each interval were added together to quantify the bone mineral content of the entire fracture callus. As expected, the bone mineral content of this low-density callus bone peaked at 14 and 21 days, and then declined upon remodeling later in healing (Figure 3). An additional analysis further adjusted the pQCT thresholds and measured the cross-sectional area at 1-mm intervals along the length of the fracture callus, detecting all soft callus tissues and lower density (noncortical) bone of the hard callus. The cross-sectional area values at each 1-mm interval were added together to quantify the cross-sectional area of all callus tissues of the entire fracture callus (data not shown). These cross-sectional areas therefore represent a measure of the size of the fracture callus that can be compared with the bone mineral content measurements to determine the amount of bone in the

callus relative to the cross-sectional area of the callus. In this way, we used pQCT data to analyze the development of the soft and hard callus and identify differences between wild-type (normal) and knockout (impaired) healing in mice.

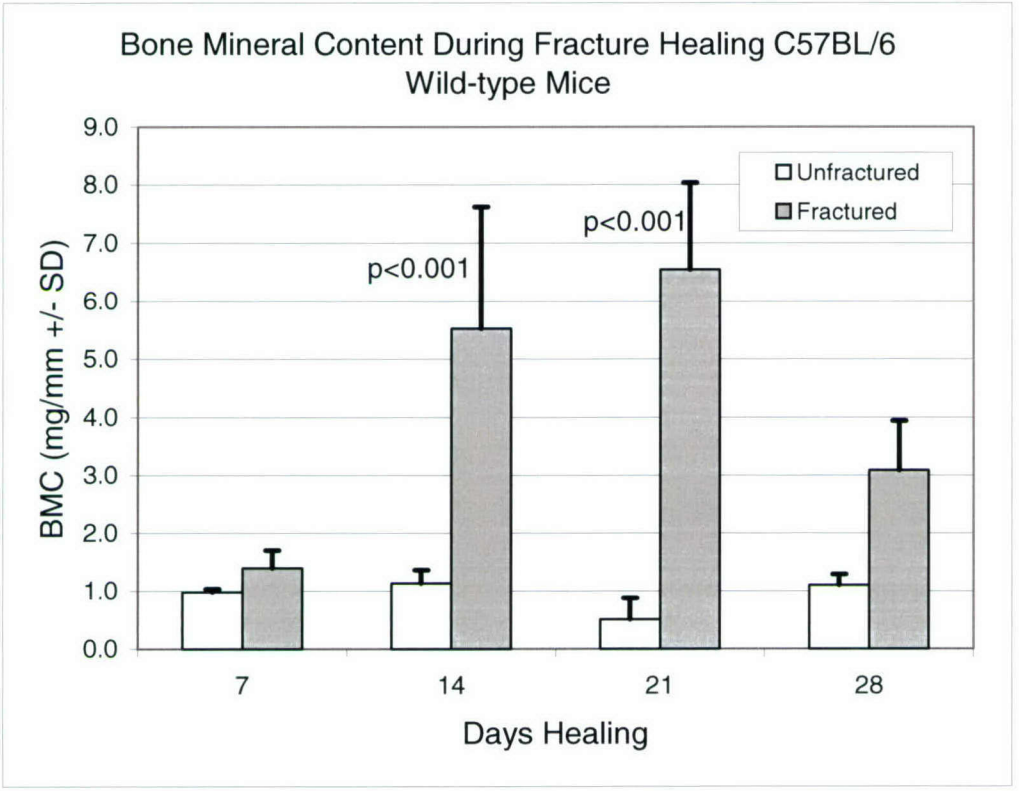

Figure 3. Bone mineral content after femoral fracture in C57BL/6J wildtype control mice. Results represent fractures produced in the (right) femurs of 4 mice at each healing time as compared to the unfractured (left) contralateral bone in each mouse. pQCT parameters are adjusted to exclude the bone mineral content of the cortical bone and measure only the lower density bone of the hard callus or the intramedullary trabecular bone (the values observed in the unfractured left bones, above). This profile of the bone mineral content during healing is typical; it quantifies the visual interpretation of the X-rays (previous figure) and serves as a basis of comparison for the knockout mouse fracture analysis at different stages of healing.

Histological analysis of the C57BL/6J wild-type control mice fractures throughout healing confirmed that fracture repair was progressing normally. The histology at the 7, 14, 21 and 28 day post-fracture time points was highly characteristic of the usual development of the fracture callus (Figure 4). The histology of the knockout mouse fractures are currently being examined at these times to identify any tissues affected by the lack of expression of the knockout gene, and thereby gain mechanistic insights to the functions of that gene in fracture repair.

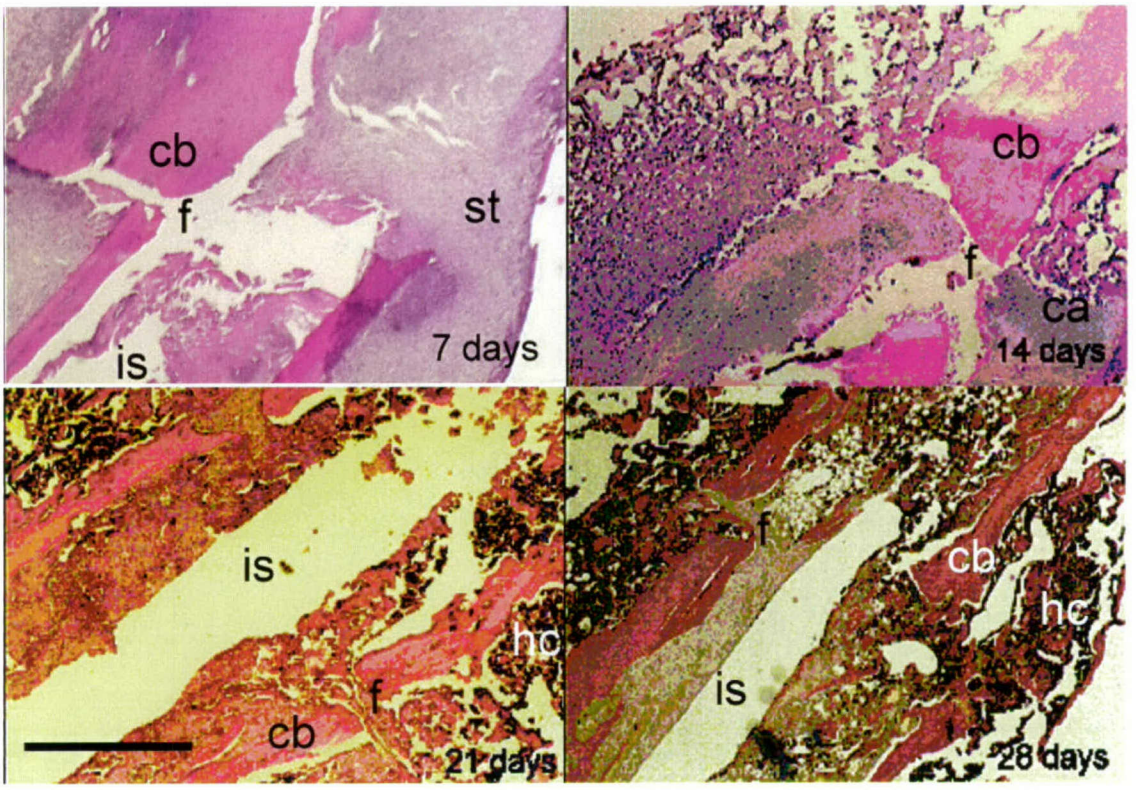

Figure 4. Hematoxylin and eosin stains of histological sections for each post-fracture healing time point show fracture healing at 7 days (upper left), 14 days (upper right), 21 days (lower left) and 28 days (lower right). The cortical bone (cb) and fracture (f) are visible in each panel, and the intramedullary space (is) where the marrow has been ablated by the stabilizing pin is visible in three pictures. The soft tissue (st) at 7 days healing matures to cartilage (ca) the noncortical bone that comprises the hard callus (hc) at 14 days, which eventually bridges the fracture at approximately 28 days healing. The hard callus that is measured for bone mineral content by pQCT under our parameters that exclude the cortical bone, and all tissues except the cortical bone are measured in the cross-sectional area. Scale bar = 0.50 mm.

In summary, the mouse femoral fracture model has been developed and validated. Accordingly, we have successfully completed the proposed work of this Specific Objective.

Specific Objective 2: Breed and genotype the knockout mice, and identify homozygotes that lack expression of a knockout gene-of-interest that might regulate the bone formation or influence wound healing.

As indicated earlier, we had selected three prospective knockout mice (Table 1), which have good viability and fertility, and are commercially available from the Jackson Labs: the Leptin knockout, Bax knockout and natriuretic peptide receptor 3 ("Longjohn") knockout mice. A description of each knockout mouse, the relevance of the phenotype to bone formation in mechanical loading and fracture repair and the results of our breeding program are described in Technical Objective 1, Specific Objective 2 (above). As summarized in Specific Objecitve 2 of Technical Objective 1, we have made significant progress towards this aim.

Specific Objective 3: Establish the phenotypic differences between knockout mice and wild-type control mice by X-ray examination, pQCT measurements, histological examination of the fracture callus and analysis of molecular bone markers.

A total of 15 homozygous mice at 12 weeks of age were used for the fracture repair study. Breeding sufficient numbers of this mouse proved to be difficult due to litter mortality. The mothers have often ignored or cannibalized the pups, especially if they were the first litter. Surprisingly, the yield of homozygote knockouts, expected to be approximately 25% of the litter, was found by genotyping to be very low, which may suggest possible embryonic lethality. Unfortunately, there was also a higher than expected mortality after surgery, and more than 50% died due to difficulties following surgical anesthesia. We are modifying the anesthesia by incorporating an isofluorane intubation procedure and will perform more fracture surgery to confirm the differences observed to date

Although this study initially progressed slowly, pQCT results have been obtained (Figure 5). On days 14 and 28 after surgery, total callus area in Leptin knockout mice was comparable to control total callus area, but knockout bone formation appeared to lag behind control bone formation. Although we cannot conclude statistically significant differences at some post-fracture times, the X-rays taken of the healing fractures at 7, 14 and 28 days offer visual support for a delayed bone formation in the knockout callus as compared to the control callus (Figure 6). At this time, because of the limited numbers of mice in this study, statistical analysis of the results is not possible. More animals will be analyzed at all time points, but especially at 7 days and 21 days, when mice are only now becoming available for analysis.

Figure 5 (below). Analysis of fracture healing in Leptin knockout mice by pQCT. Fractures were allowed to heal for 7, 14, 21 or 28 days and analyzed using parameters adjusted to detect the sum of the cross-sectional area of all hard and soft noncortical callus tissues (upper panel) or the bone mineral content of the noncortical callus tissues (lower panel). This approach allows a measurement of the relative contributions of soft and hard (bony) callus tissues during healing.
Upper Panel. Although data at 21 days is lacking at this time, soft callus area in the Leptin knockout mice examined to date appears to be similar at 14 and 28 days, suggesting that the larger fracture callus size persists, either consisting of soft tissues with a lack of bone formation earlier in healing, or hard tissues and a lack of remodeling later in healing.
Lower Panel. The Leptin knockout fractures display less bone mineral content than the control fractures at 14 days ($p<0.05$ by Least Significant Difference Test), but similar bone mineral content at 7 and 28 days. This profile of low early bone formation suggests that Leptin knockout fracture healing might be increasing in a bone formation phase at 28 days; control fractures display the expected control mouse healing profile (Figure 3) that suggests that bone formation has peaked at 14 and 21 days, remodeling is underway and the callus bone mineral content is declining at 28 days. When evaluated with the persistence of the soft tissues in Leptin knockout mice (upper panel) the lower born mineral content suggests impaired bone formation in Leptin knockout mice.

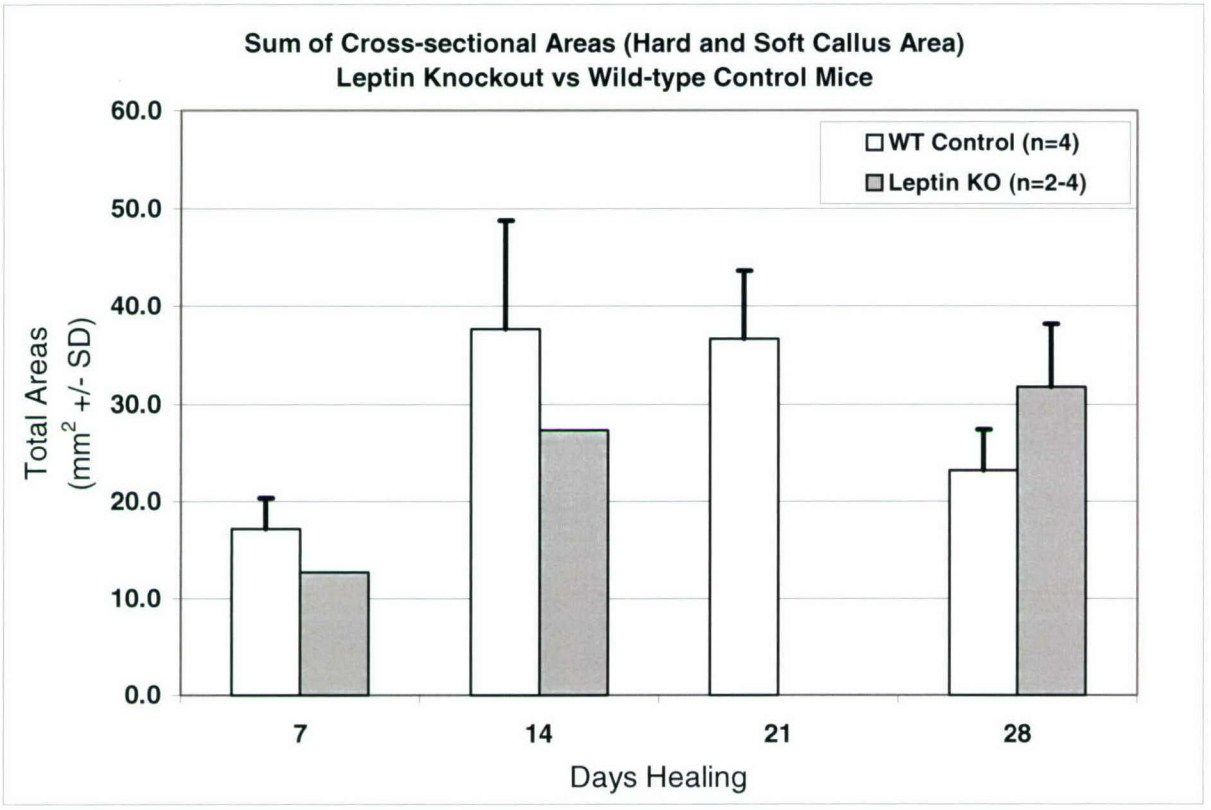
Sum of Cross-sectional Areas (Hard and Soft Callus Area)
Leptin Knockout vs Wild-type Control Mice
WT Control (n=4)
Leptin KO (n=2-4)
Total Areas
(mm2 +/- SD)
60.0
50.0
40.0
30.0
20.0
10.0
0.0
7
14
21
28
Days Healing

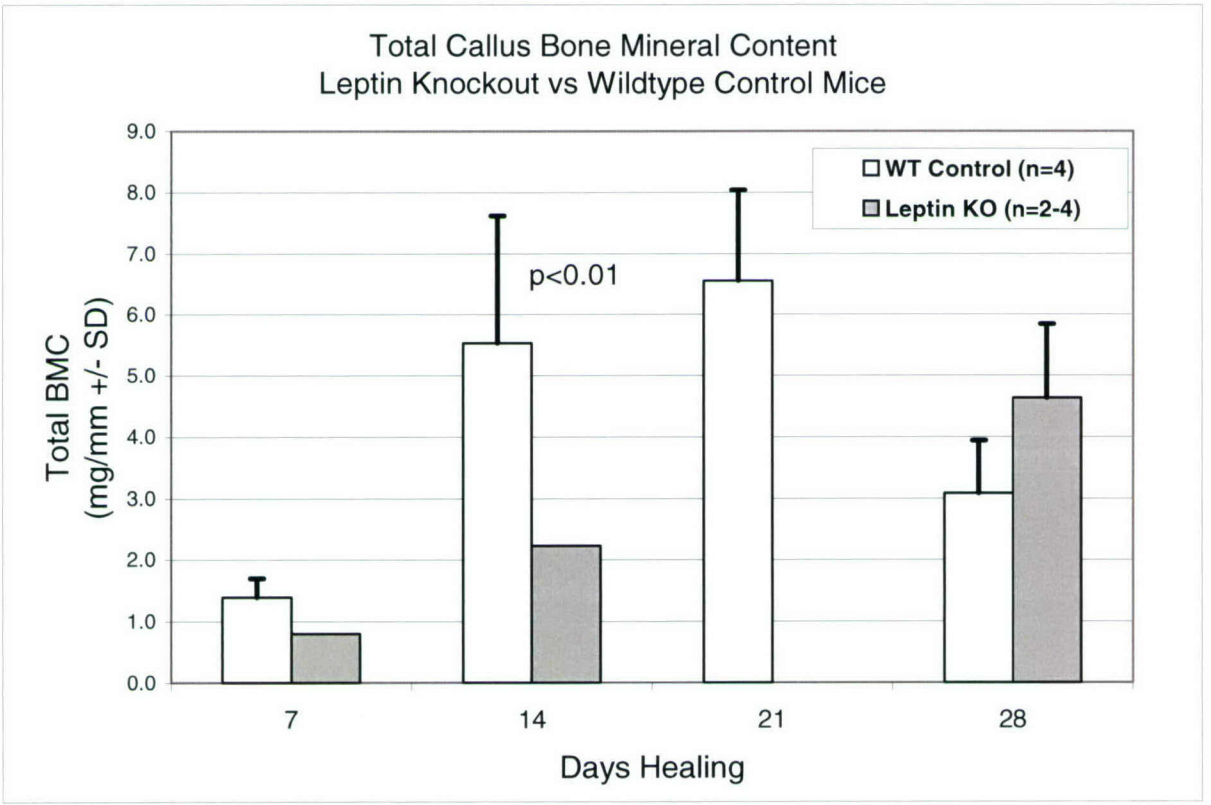
Total Callus Bone Mineral Content
Leptin Knockout vs Wildtype Control Mice
WT Control (n=4)
Leptin KO (n=2-4)
p<0.01
Total BMC
(mg/mm +/- SD)
9.0
8.0
7.0
6.0
5.0
4.0
3.0
2.0
1.0
0.0
7
14
21
28
Days Healing

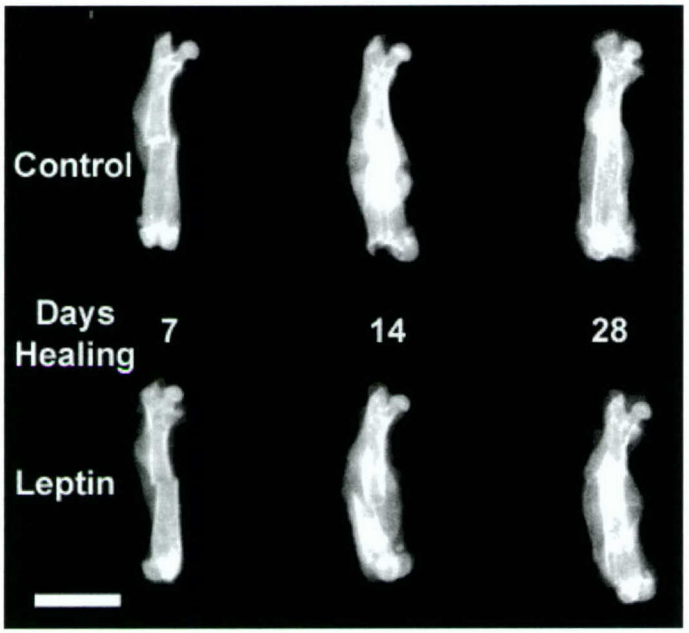

Figure 6. X-ray photograph comparing healing in the Leptin knockout with C57BL/6 control at 7, 14 and 28 days post-fracture. The mineralized callus appears similar in both cases, but pQCT data indicates that the Leptin fracture callus is characteristic of early fracture repair and delayed relative to the C57BL/6 control fracture callus, which is characteristic of remodeling in late healing. A lack of Leptin expression probably affects the bone formation phases of early fracture healing. Scale bar = 5 mm.

As with the mechanical loading studies, the Bax mouse fracture project is improving as breeding improves and more Bax knockout mice become available. Initially, this knockout strain displayed a litter mortality similar to the Leptin knockout mouse, with a high proportion of pups either neglected or cannibalized. However, at this time the problem has improved, probably because the mothers have become more experienced with additional litters. To date, 9 homozygous mice at the age of 12 weeks have been used for fracture repair study and analyzed by X-ray and pQCT (Figure 7). From the pQCT results, Bax knockout mice have callus areas similar to wildtype control mice throughout fracture healing (Upper Panel), but bone mineral content that is increased at both 14 and 28 days of healing (Lower Panel). This observation suggests normal soft callus formation, but reduced apoptosis in early healing (14 days) that prolongs osteoblast function and increases bone formation, and slower remodeling later in healing (28 days) that reduces the removal of hard callus bone. This observation is visible in the X-ray of the slightly more mineralized Bax knockout callus at 14 and 28 days post-fracture (Figure 8). The interpretation is, however, based upon relatively few knockout animals at 7 and 21 days. As of now, this conclusion is consistent with our hypothesis that the absence of Bax gene expression might reduce osteoblast apoptosis and both increase bone formatuion and reduce bone remodeling. More knockout mice need to be analyzed, especially at 7 and 21 days, to confirm whether the bone mineral content is observed throughout fracture healing, and might be explained by an inhibition of Bax-mediated apoptosis.

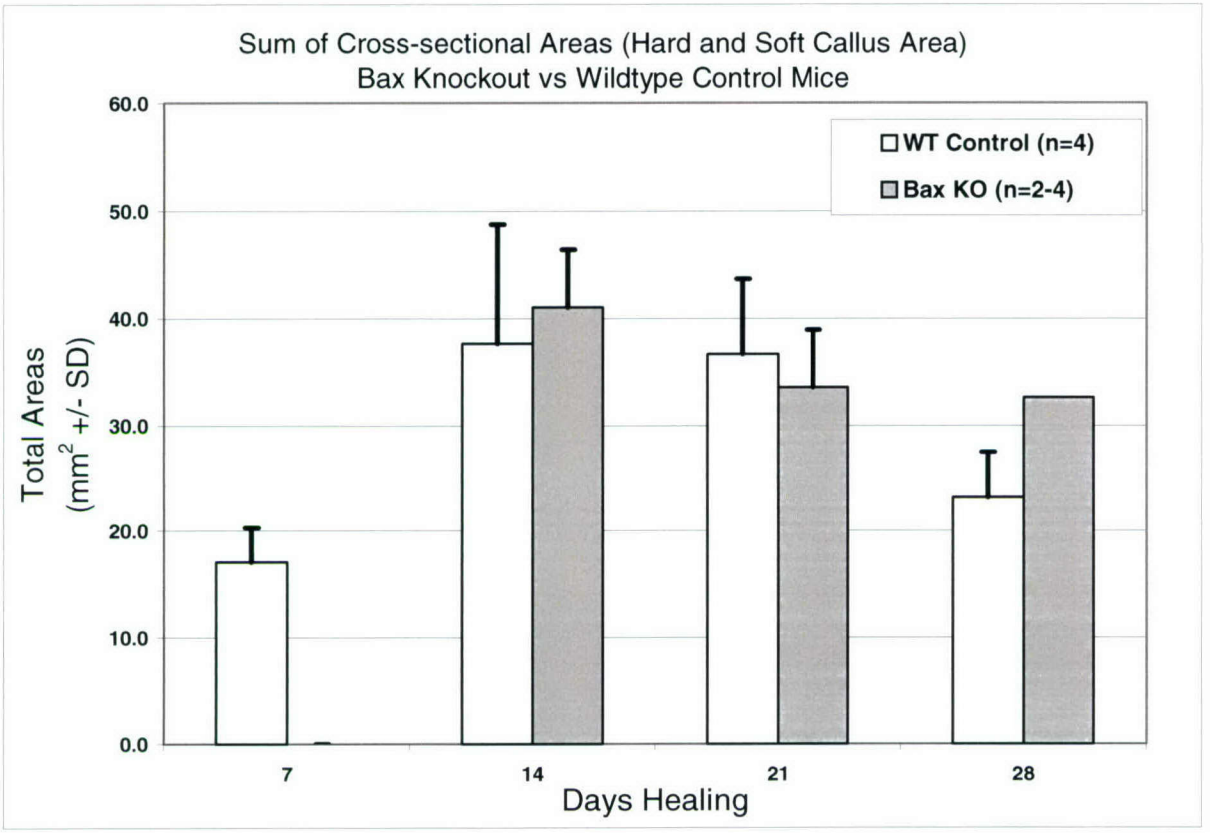
Sum of Cross-sectional Areas (Hard and Soft Callus Area)
Bax Knockout vs Wildtype Control Mice
WT Control (n=4)
Bax KO (n=2-4)
Total Areas
(mm2 +/- SD)
60.0
50.0
40.0
30.0
20.0
10.0
0.0
7
14
21
28
Days Healing

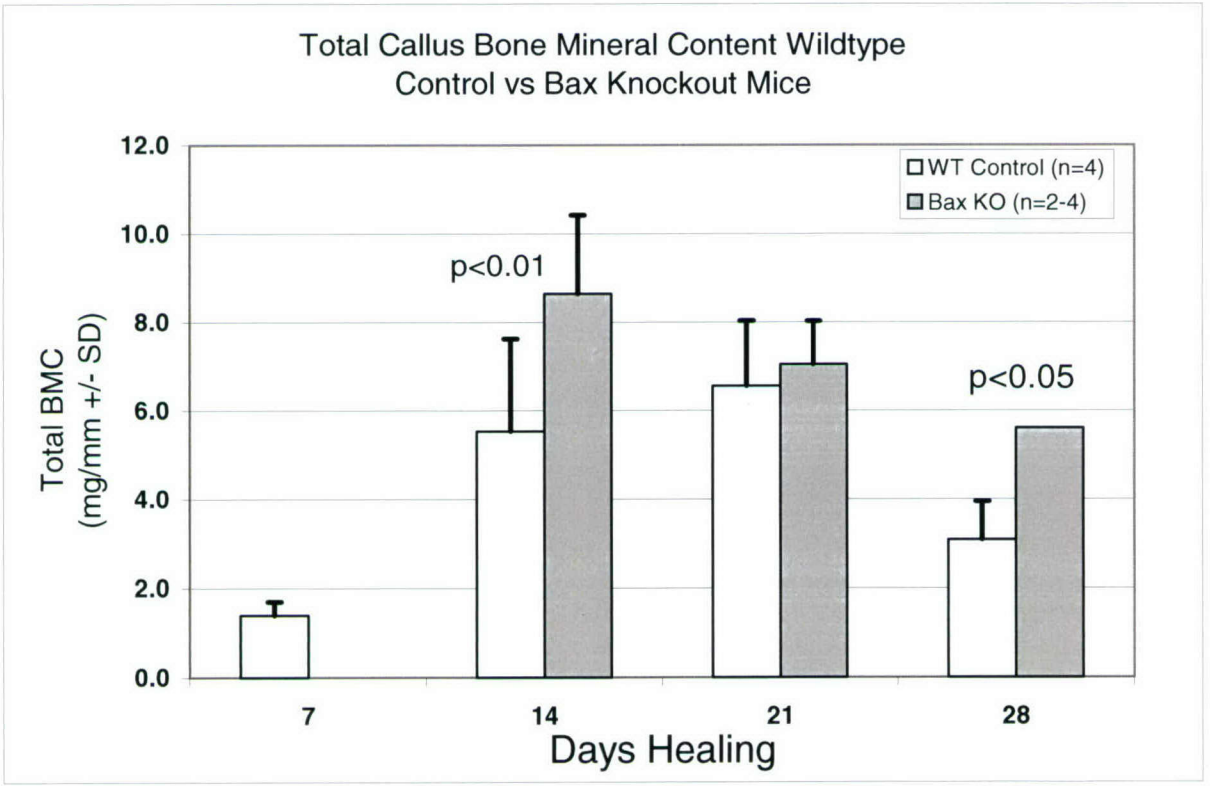
Total Callus Bone Mineral Content Wildtype
Control vs Bax Knockout Mice
WT Control (n=4)
Bax KO (n=2-4)
p<0.01
p<0.05
Total BMC
(mg/mm +/- SD)
12.0
10.0
8.0
6.0
4.0
2.0
0.0
7
14
21
28
Days Healing

Figure 7. Analysis of fracture healing in Bax knockout mice by pQCT. Fractures were allowed to heal for 7, 14, 21 or 28 days and analyzed using parameters adjusted to detect the total cross-sectional area of all hard and soft noncortical callus tissues (upper panel) or the bone mineral content of the noncortical callus tissues (lower panel). This approach allows a measurement of the relative contributions of soft and hard (bony) callus tissues during healing.
Upper Panel. Although data at 7 days is lacking at this time, total callus area in the Bax knockout mice examined to date appears to be similar at 14 and 21 days, but slightly higher at 28 days. This pattern is consistent with either soft tissue persistence or with a delay in hard callus remodeling.
Lower Panel. The Bax knockout fractures display a higher bone mineral content than the control fractures at 14 and 28 days ($p<0.05$, Least Significant Dfference Test). This profile suggests that Bax knockout fracture healing might exhibits higher bone formation in early fracture healing due to osteoblast persistence, and more bone later in fracture healing due to reduced remodeling of the hard callus; control fractures again display the expected profile (Figure 3) that suggests that bone formation has peaked at 14 and 21 days and that remodeling is well underway at 28 days. Thus, the more mineralized callus in Bax knockout mice probably results from both increased bone formation and reduced remodeling. This observation requires additional confirmation, especially at 7 and 21 days healing.

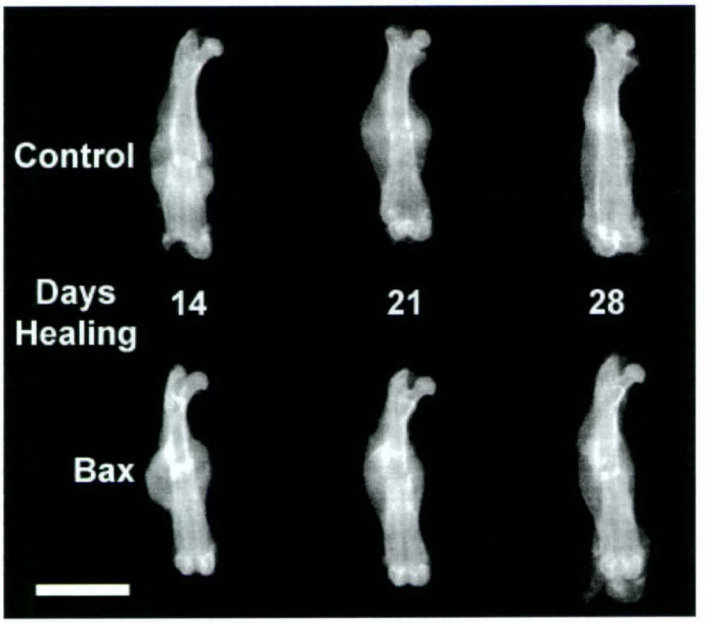

Figure 8. X-ray photograph comparing healing in the Bax knockout with C57BL/6 control at 14, 21 and 28 days post-fracture. The slightly more mineralized callus at 28 days healing supports pQCT data and suggests that a lack of Bax expression delays remodeling of the callus to cortical bone in the later stages of fracture healing. Scale bar = 5 mm.

Because the Longjohn mice breeders were guaranteed by the supplier to be homozygous, and the pups were assumed to be homozygous, surgery and fracture were performed as soon as they became available and the bones were collected for X-ray, pQCT and RNA extraction. A total of 23 mice were fractured at 12 weeks of age (maturity). However, at this time, when the phenotype should have been apparent, there was no significant difference in phenotype observed between these knockout mice and wild-type DBA mice by gross examination, X-ray and pQCT examination. As described above, after cDNA sequencing confirmed that the Longjohn mutation

was not present the supplier (Jackson Labs) was notified, initiated an investigation and admitted that the genotype was not in fact Longjohn. We will replace this knockout mouse with a different strain to complete the study.

Key Research Accomplishments:

- The mechanical loading model and the femoral fracture model have been developed and adapted to knockout mouse studies.
- Two of three knockout mice strains are now successfully breeding and being characterized for genotype and inclusion in both the mechanical loading and fracture study.
- X-ray and pQCT data suggest that Leptin influences bone formation in mechanical loading and fracture repair; based upon the numbers of animals analyzed to date, Leptin influences bone formation in fracture healing that is delayed in the absence of its expression.
- X-ray and pQCT data suggest that Bax influences callus remodeling in fracture healing that is delayed in the absence of its expression.

Reportable Outcomes:

There are no reportable results at the present time.

Conclusions:

Mechanical Loading:

1) Leptin Knockout Mice:

The basal value for the total mineral content, perisoteal and endosteal expansion in unloaded Leptin knockout tibia was greater when compared to the unloaded tibia, suggesting that bone responses to mechanical loading are affected by Leptin gene expression. Additional mice need to be tested to confirm these results.

2) Bax Knockout Mice

Since there were not many bred homozygous Bax mice available for this test, we have not started the mechanical loading on this strain.

3) Longjohn Knockout Mice:

The homozygous Npr3 breeders that were purchased from the Jackson Labs and bred in our animal facility did not show the described phenotype, and we suspected that the genotype was misidentified. Sequence analysis failed to identify the Npr3 point mutation and confirmed that the genotype of the mice which the Jackson Labs provided was in fact wild-type DBA, and not the knockout Longjohn mice. We will have to acquire another knockout mouse to complete the mechanical loading study.

Fracture Repair:

4) Leptin Knockout Mice:

Leptin expression regulates the bone formation phase of fracture repair, both reducing and delaying callus bone formation in the fracture callus. This observation requires confirmation with additional knockout animals.

5) Bax Knockout Mice:

Bax expression regulates apoptosis during the bone formation and remodeling phases of fracture repair. During the bone formation phase, the absence of its expression might prolong osteoblast function in the callus. During the remodeling phase, the absence of its expression

might inhibit the removal of the hard callus bone. This observation also requires confirmation with additional knockout animals at both early and late healing times.

6) Longjohn Knockout Mice:

As described above, the Longjohn genotype was misidentified and we will have to acquire another knockout mouse to complete the fracture study.

References:

1. Mackelvie KJ. McKay HA., Petit MA., et al. (2002). Bone mineral response to a 7-month randomized controlled, school-based jumping intervention in 121 pre-pubertal boys: Associations with ethnicity and body mass index. J. Bone Miner. Res 17:834-844.
2. Kodama Y., Dimai HP., Wergedal J., et al. (2000). Exercise and mechanical loading increase periosteal bone formation and whole bone strength in C57BL/6J mice but not in C3H/Hej mice. Calcif. Tissue Int. 66:298-306.
3. Steppan CM., Crawford DT., Chidsey-Frink KL., et al. (2002). Leptin is a potent stimulator of bone growth in ob/ob mice. Regulatory Peptides 92:73-78.
4. Takeda S., Elefteriou F., Levasseur R. et al. (2002). Leptin Regulates Bone Formation via the Sympathetic Nervous System. Cell 111:305-317.
5. Suda, M., Ogawa Y, Tanaka K., et. al. (1998). Skeletal overgrowth in transgenic mice that overexpress brain natriuretic peptide. Proc. Natl. Acad. Sci USA 95:2337-2342.
6. Yasoda A., Ogawa Y., Suda M et al. (1998). Natriuretic Peptide Regulation of Endochondral Ossification. J. Biol. Chem. 273, 11695-11700.
7. Knudson CM., Tung KSK., Tourtellotte WG., et al. (1995). Bax-Deficient Mice with Lymphoid Hyperplasia and Male Germ Cell Death. Science 270:96-98.
8. Mocetti P., Silvestrini G., Ballanti P., et al. (2001). Bcl-2 and Bax expression in cartilage and bone cells after high-dose corticosterone treatment in rats. Tissue & Cell 33:1-7.

B. GENE THERAPY PROJECTS
Project 6: Systemic Gene Therapy For The Skeleton

Introduction:

For this project, we propose to develop and test the efficacy of a mouse model for systemic gene therapy for massive skeletal tissue damage by means of hematopoietic stem cell (HSC) transplant. For this model, we will determine the skeletal marrow tissue[1] and non-skeletal sites of engraftment, the quantity of short-term and long-term bone formation achieved, and the effect of the age of the recipient mice on the bone formation response. To our knowledge, our studies will be the first to use transplantation of transduced HSCs to deliver gene therapy to induce bone formation. These studies will focus on the induction of bone formation for massive skeletal injury. However, there is evidence that HSCs have the plasticity to regenerate other tissue types. Therefore, a successful HSCs-delivered gene therapy strategy for bone injury could be adapted to treat other damaged tissues, such as skin and muscle that are likely to be sustained along with massive skeletal injury, by the insertion of tissue-specific promoters to drive the therapeutic gene.

Body:

Technical Objectives:

To develop and test the efficacy of a mouse model for systemic gene therapy for massive skeletal tissue damage by means of hematopoietic stem cell (HSC) transplant. For this model, we will determine the skeletal marrow tissue and non-skeletal sites of engraftment, the quantity of short-term and long-term bone formation achieved, and the effect of the age of the recipient mice on the bone formation response.

Our specific objectives for the first 12 months are:

Specific Objective 1: To initiate studies to determine the skeletal marrow and non-skeletal sites of engraftment in recipient mice after transplant with donor HSCs.

a. Transplant GFP-expressing HSCs derived from transgenic mice into myelosuppressed recipient mice and assess the short-term (8 weeks), mid-term (6 months) and long-term (1 year) engraftment in the skeletal marrow and non-skeletal sites. Engraftment efficiencies will be quantitated by measuring the percentage of GFP-expressing cells in the peripheral blood and bone marrow of the recipient mice using flow cytometry.

b. Assess the pluripotent ability of the engrafted donor cells to produce mature hematopoietic lineages (T-cell, B-cell, neutophil/granulocyte/monocyte and erythroid) by using lineage-specific immunostaining and FACs analysis of the recipients' peripheral blood.

c. Detection of donor cells in non-skeletal tissues will be accomplished by frozen sectioning of the heart, lungs, liver and spleen of the recipients and fluorescent microscopic observation.

---

[1] For purposes of this proposal the term "skeletal marrow tissue" will be used to designate the endosteal surface of trabecular bone.

Specific Objective 2: To initiate studies to assess and quantitate the short-term and long-term bone formation achieved in mice following transplantation with HSCs transduced to express a growth factor gene.

a. Transduce HSC-enriched cells with an HIV-based vector expressing the BMP 2/4 gene under the control of the CMV promoter. Transgene expression will be assessed using immunohistochemical staining of the transduced cell cultures and Western blot analysis of the conditioned media

b. Transplant transduced donor cells via tail vein into myelosuppressed recipient mice and evaluate bone formation after 8 weeks, 6 months and 1 year. Bone formation will be evaluated by measuring serum osteocalcin and alkaline phosphatase. Bone density and cortical thickness in the host animals will also be assessed by faxitron X-ray and pQCT analysis.

Specific Objective 3: To initiate studies to determine the effect of recipient age on engraftment and the bone formation response in mice transplanted with HSCs transduced to express a growth factor gene.

a. Transplant transduced donor cells expressing the BMP-2/4 gene into myelosuppressed recipient mice of 2 ages (8 weeks old vs. greater than 1 year old).

b. Compare the engraftment and bone formation response in young vs. old recipient mice by measuring serum osteocalcin and ALP, 12 weeks and 6 months post-transplant. We will also perform faxitron X-ray and pQCT analysis to evaluate the effects of transgene expression on bone density and cortical thickness in the recipient animal.

Our progress in each of the specific objectives is given below.

Progress for Specific Objectives

Specific Objective 1a:

The Sca-1 molecule has been implicated as a marker for hematopoietic stem cell (HSCs). Sca-1^+ cells isolated from TgN-GFP donor mice were transplanted into recipient mice, and skeletal marrow and non-skeletal sites were analyzed for engraftment at various time points post-transplant. The donor TgN mouse is a transgenic strain transduced to produce the eGFP marker gene. Use of this donor strain allows for the tracking of donor cells *in vivo* after transplantation. For these studies, whole bone marrow cells were harvested by flushing tibiae and femur with PBS using a 26g needle and syringe. Erythrocytes were removed by osmotic lysis using a solution of 155 mM NH_4Cl, 10mM $KHCO_3$ and 110μM Na_2EDTA, followed by rinsing with PBS. The cell preparation was then incubated with Sca-1 specific antibody-magnetic microbead conjugates and applied to an automated magnetic separation column (AutoMacs™) according to manufacturer instructions. Viable cell yields at each stage of enrichment were determined by manual cell count using a hemocytometer and trypan blue dye exclusion assay. To assess enrichment efficiency at each stage of preparation, aliquots were incubated with either PE conjugated Sca-1 specific or rat isotype control antibody and assessed by FACs analysis. Figure 1 shows the FACs analysis of cell preparations after each preparation step for the Sca-1^+ specific antibody. Table 1 is a summary of enrichment data from several experiments and includes total % Sca-1^+ cells (derived by adding the upper right FACs quadrant (Sca-1^+/GFP$^-$) plus the upper left FACs quadrant (Sca-1^+/GFP$^+$)). Comparison of the % total Sca-1^+ cells in the WBM (5.8%) and the final Sca-1^+-enriched preparations (74.3%) indicates that the average increase in Sca-1^+ cells achieved with our enrichment method is approximately 12-fold.

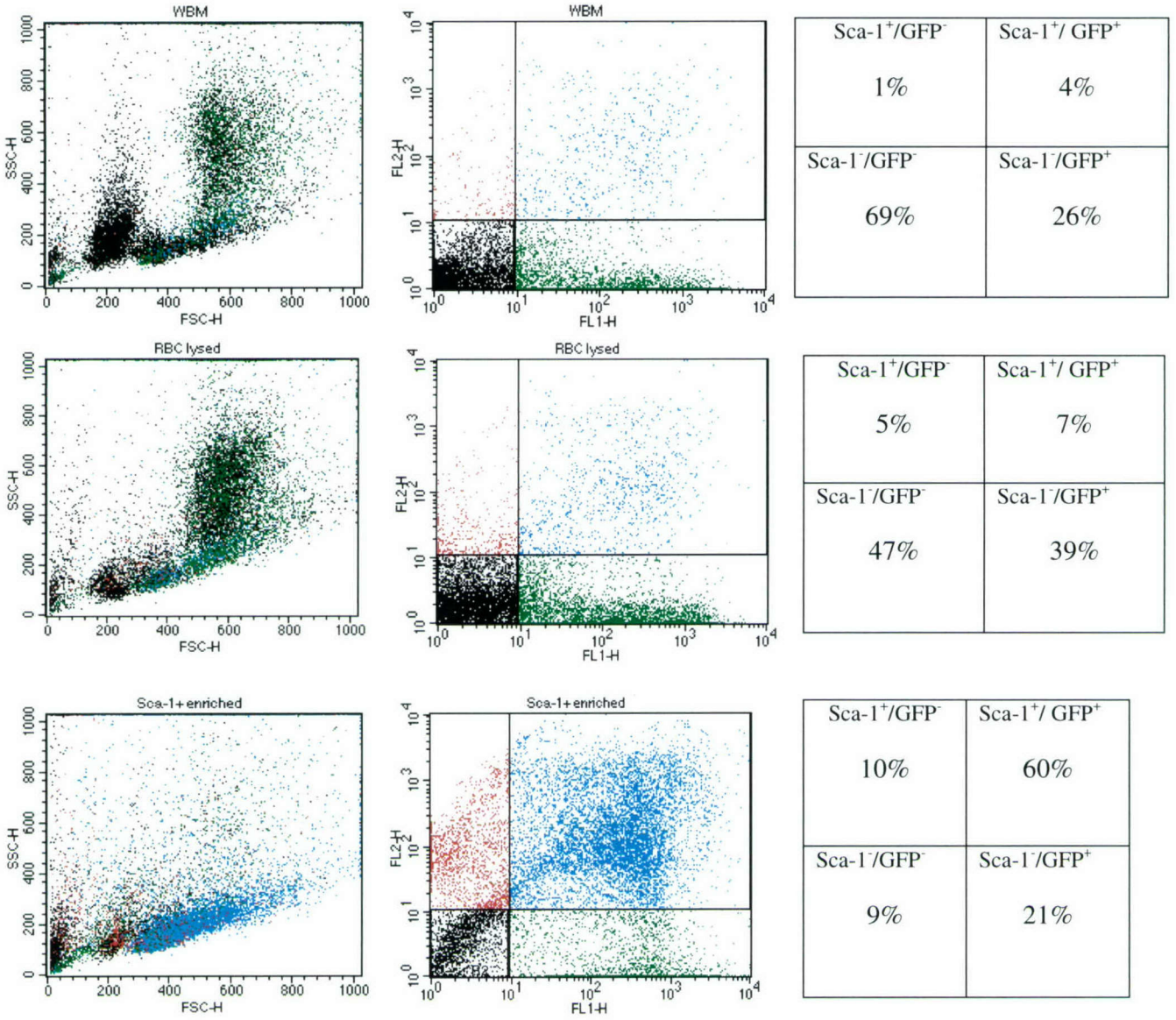

Figure 1: Flow cytometeric analysis of cell preparations at each step of the enrichment process. Cell preparations were incubated with PE-conjugated antibodies specific for Sca-1. Upper 3 panels show data for whole bone marrow (WBM), middle 3 panels for cells after osmotic lysis of erythrocytes and lower 3 panels for Sca-1$^+$-enriched cells after magnetic microbead selection.

Cell counts	Total cells per donor mouse Mean (st. dev.) X 10^6	% Sca-1^+ and GFP^-	% Sca-1^+ and GFP^+	% Total Sca-1^+
Whole bone marrow	116.0 (15.5)	1.2 (0.4)	4.7 (0.5)	5.8 (0.7)
RBC-lysed	43.9 (8.5)	2.8 (0.8)	8.0 (1.7)	10.7 (0.9)
Sca-1-enriched	3.0 (0.7)	16.6 (5.1)	57.7 (9.9)	74.3 (5.3)

Table 1: Cell yields and % Sca-$1^+$and/or GFP^+ cells at each step of the enrichment process. Values in Parentheses represent S.D. of 10 experiments.

Next, the donor cells were transplanted into 12 preconditioned $W^{41}W^{41}$ recipient mice. This mouse stain has a c-kit mutation that results in a deficiency in hematopoietic stem cells. Use of this strain as recipients in our model has allowed us to achieve high engraftment efficiencies with a sub lethal preconditioning regimen. For preconditioning, the mice were irradiated with a single 500cGy dose of irradiation. The mice were then transplanted via retro-orbital injection with 1 million of the Sca-1^+ enriched cells. To assess engraftment in the skeletal marrow, peripheral blood was collected at 12, 24, and 36 weeks post-transplant and assayed by FACs for the presence of GFP^+ donor cells. At the site of hematopoietic regeneration, peripheral blood was used to assess donor cell engraftment in the skeletal marrow. Results of this experiment are displayed in Figure 2. All 12 mice were engrafted (100% success) at a high level of chimerism (range 88.8 – 98.5% donor cells at 12 weeks). This high level of engraftment was also observed at the later time points. These data show that with our transplant model, we are able to achieve high, stable engraftment for up to 36 weeks. A parallel group of 6 mice is currently being maintained and will be analyzed for the presence of donor cells at 12 month after transplant.

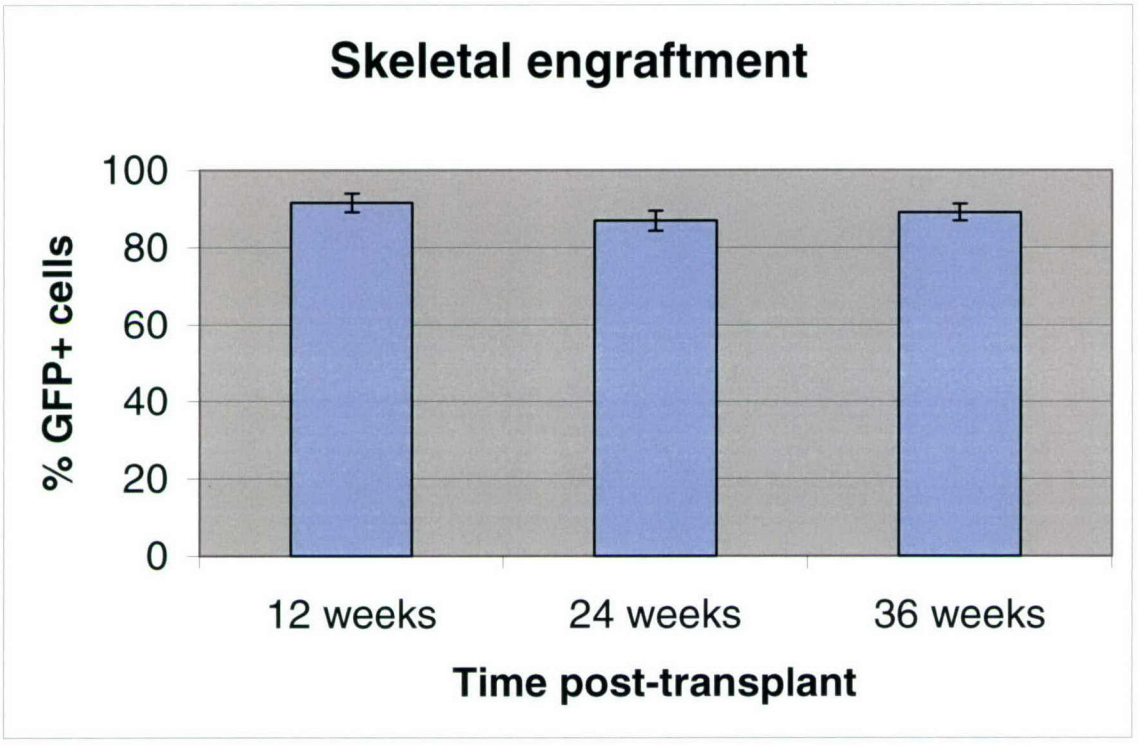

Figure 2: Mean ± S.D. % GFP-positive cells in host mice peripheral blood. 12 Recipient mice were preconditioned by sub lethal irradiation prior to transplantation with 1 x 10^6 Sca-1^+ cells from TgN-GFP donors. At the indicated time points, peripheral blood was collected and assayed for % GFP cells by flow cytometry.

Specific Objective 1b:

To assess the pluripotent ability of the engrafted Sca-1^+ donor cells to produce mature hematopoietic lineages, we measured the percentage of four hematopoietic lineages (T-cell, B-cell, neutophil/granulocyte/monocyte and erythroid) in the recipient bone marrow cells of mice transplanted with Sca-1^+ cells. For this analysis, mononuclear blood samples from recipient mice were incubated with PE-conjugated antibodies specific for mature hematopoietic lineages. For T-lymphocytes (T-cells) lineage, a mixture of CD3-, CD4e-, and CD8a-specific antibodies was used. For monocytes/macrophages/neutrophils lineage, a mixture of Mac-1- and Gr-1-specific antibodies was use. For B-lymphocytes (B-cells), a B220-specific antibody was use and for erythroid lineage cells, a Ter-119-specific antibody was used. Table 2 shows the mean and standard deviation for each cell lineage type in mice transplanted with Sca-1 cells at 5 months. The column labeled "Total % PE^+" includes all cells which stained for the specific antibody and therefore, represents cells contributed by both the host animal, whereas the columns labeled "% PE^+ & GFP^-" and "% PE^+ & GFP^+" represent cells contributed by the host animal and donor animal, respectively. No significant difference in contribution of T-cell lineage was observed between host (14.7%) and donor animals (11.8%). In contrast, donor cells, compared to host cells, contributed a larger percentage than host cells to the macrophage-monocyte-neutrophils lineage (22.9 vs. 6.9%, respectively, $p < 0.001$) and B-cell (22.9 vs. 6.9%, $p<0.01$). Furthermore,

the erythroid hematopoietic compartment was made up exclusively of cells of donor origin (not detectable vs. 5.4%). We plan on repeating this experiment to confirm these results.

Table 2: Peripheral blood cells were immunostained with PE-conjugated antibodies of hematopoietic lineages.

	Total % PE^+ mean (st.dev.)	% PE^+ & GFP^- mean (st. dev.)	% PE^+ & GFP^+ mean (st.dev.)
T-cells	19.4 (5.8)	14.7 (3.0)	11.8 (4.4) ^{ns}
Mac/Mono/Gr	32.2 (25.7)	6.9 (3.5)	22.9 (5.8) **
B-cells	21.4 (6.7)	11.6 (5.2)	22.9 (7.2) *
Erythroid	4.8 (3.8)	Non-detectable	5.4 (2.8)

Independent t-test comparisons of % PE^+ & GFP^- (host) vs. % PE^+ & GFP^+ (donor): NS = non-significant, * $p< 0.01$, ** $p<0.001$
St. Dev. = Standard Deviation of Mean

Specific Objective 1c:

The engraftment of donor Sca-1^+ cells in the skeletal marrow and in non-skeletal tissues was assessed by histological examination of tissues in control mice and mice transplanted with GFP-expressing Sca-1^+ cells. Six months after transplantation, 6 mice were euthanized and their femora, spleens, hearts, livers and lungs were removed. Several 8-μm thick longitudinal frozen sections of each organ were prepared by cryostat and visualized by fluorescent microscopy. Figures 3-7 show representative frozen sections under bright field (left panels) and fluorescent (right panels) microscopy. Under the fluorescent filter in the marrow space of the femora of mice transplanted with the GFP-expressing cells, numerous small, bright, GFP-expressing cells were observed (figure 3, lower right panel). No such cells were observed in the femora of control mice (figure 3, upper right panel). In the non-skeletal tissues, few or no GFP-expressing cells were observed. In the rare cases that GFP-expressing cells were observed in the non-skeletal tissues of GFP-transplanted mice (such as the heart tissue seen in figure 5, lower right panel), the green donor cells were observed to be part of the hematological tissue compartment rather than the parenchymal cardiac tissue. These data suggest that Sca-1^+ cells engraft primarily in the skeletal bone marrow but not in the non-skeletal sites such as the spleen, heart, liver and lungs. Similar observations were observed in tissues collected from mice from this experiment euthanized at 6 months post-transplant (data not shown). Six additional mice from this experiment will be euthanized and analyzed at the 12 month post-transplant time point in December, 2004.

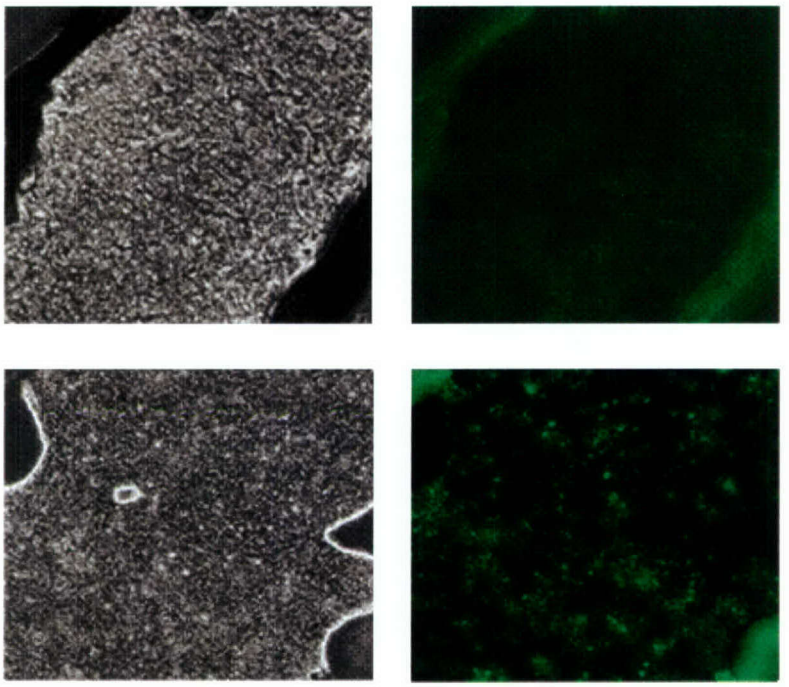

Figure 3: Longitudinal frozen sections of femurs, six months after transplantation.
Upper panels are from a representative control mouse, bright field (left) and fluorescent (right.)
Lower panels are from a representative mouse transplanted with TgN-eGFP derived Sca-1$^+$ cells

Magnification = 4X

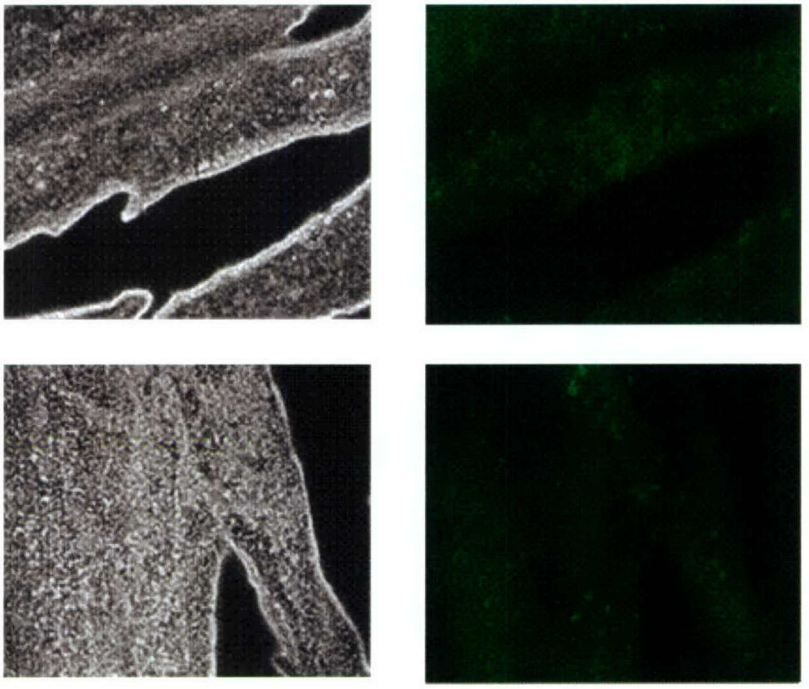

Figure 4: Frozen sections of dissected splenic tissue, six months after transplantation.
Upper panels are from a representative control mouse, bright field (left) and fluorescent (right.)

Lower panels are from a representative mouse transplanted with TgN-eGFP derived Sca-1$^+$ cells

Magnification = 4X

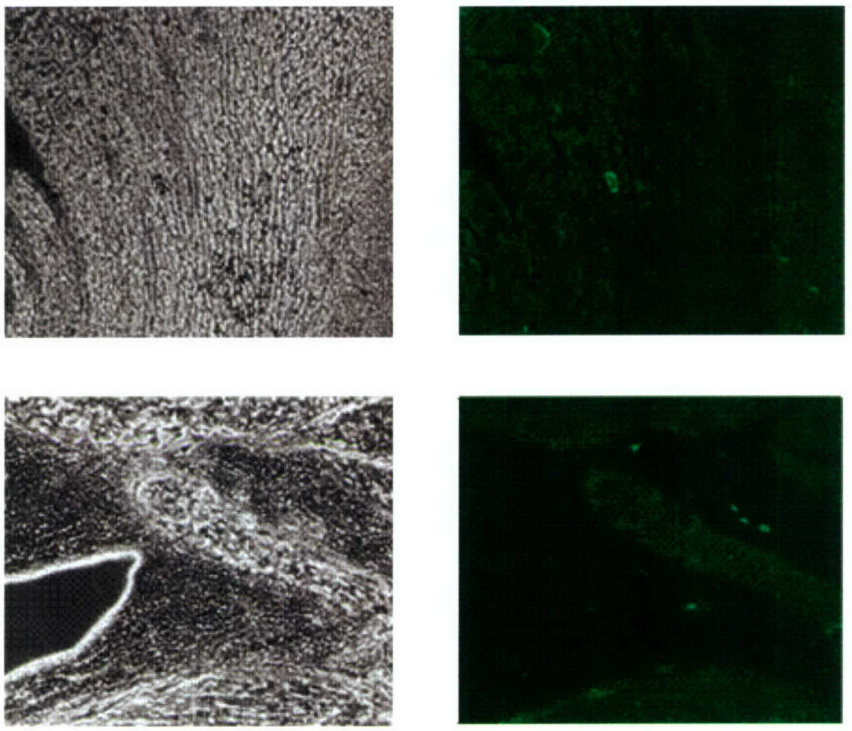

Figure 5: Frozen sections of dissected cardiac tissue, six months after transplantation.
Upper panels are from a representative control mouse, bright field (left) and fluorescent (right.)

Lower panels are from a representative mouse transplanted with TgN-eGFP derived Sca-1$^+$ cells

Magnification = 4X

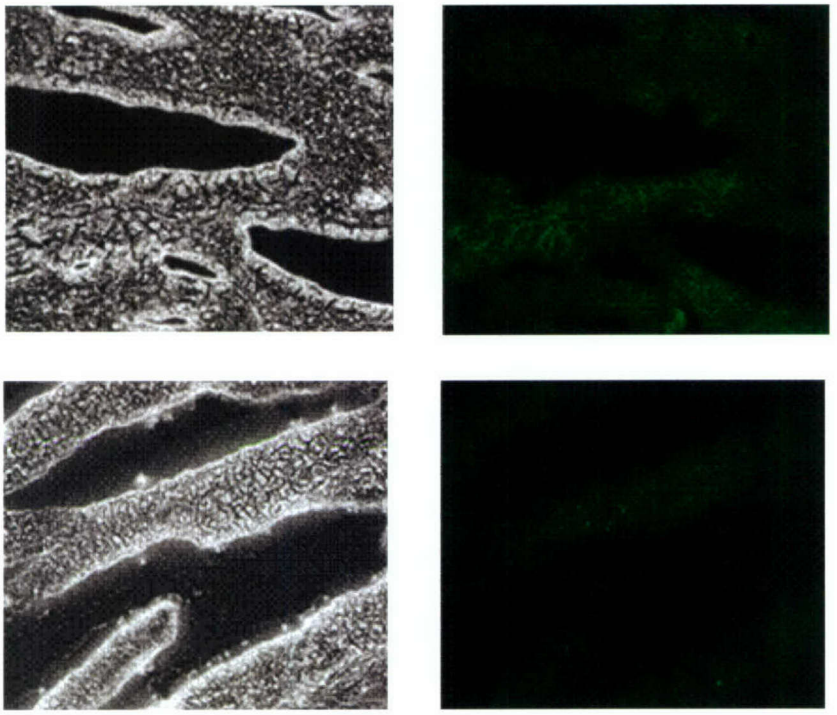

Figure 6: Frozen sections of dissected liver tissue, six months after transplantation.
Upper panels are from a representative control mouse, bright field (left) and fluorescent (right.)

Lower panels are from a representative mouse transplanted with TgN-eGFP derived Sca-1$^+$ cells

Magnification = 4X

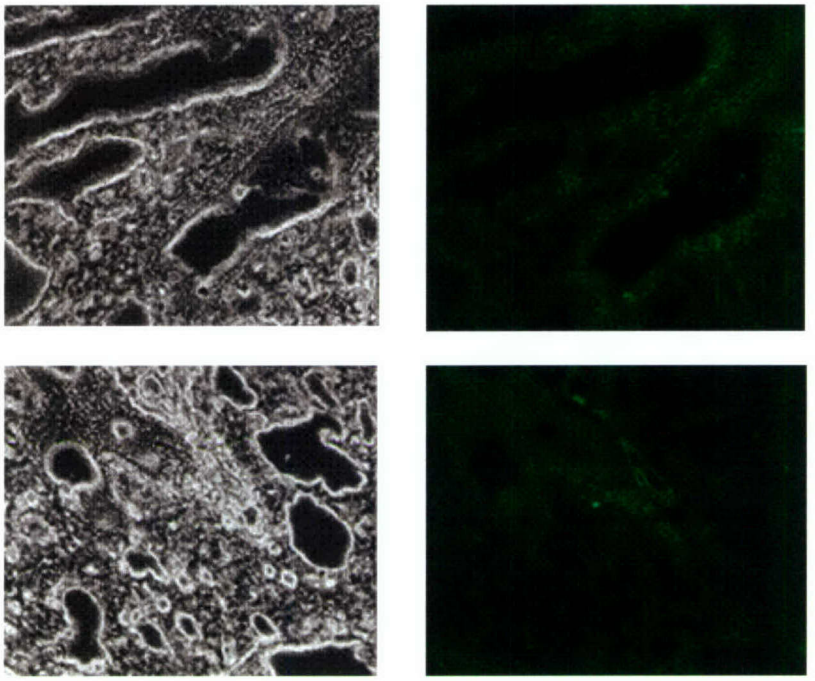

Figure 7: Frozen sections of dissected lung tissue, six months after transplantation.
Upper panels are from a representative control mouse, bright field (left) and fluorescent (right.)

Lower panels are from a representative mouse transplanted with TgN-eGFP derived Sca-1$^+$ cells

Magnification = 4X

Specific Objective 2a:

Whole bone marrow cells were harvested from wild type C57BL/6 mice and enriched for HSCs by selection of Sca-1$^+$ cells. The cells were transduced with an HIV-based viral vector expressing either the GFP marker gene or a modified human BMP4 therapeutic gene. The modified BMP vector (BMP2/4) was created by replacing the propeptide of the BMP4 gene with the BMP2 propeptide. As a result of this substitution, high expression levels of BMP4 (0.5 to 1μg/10^6cells/24 hours) are obtained. For the transduction procedure, the cells were cultured in 6-well retronectin-coated plates at a density of 4 x 10^6 cells/well in IMDM media containing fetal bovine serum, human Flt-3 ligand, murine stem cell factor, murine IL-6, murine IL-1α and murine IL-3 and 100μM additional dNTPs. After 24 hours, unconcentrated viral stocks (MOI = 15) were applied to the cells. After 8 hours and 16 hours, fresh media, cytokines and viral stocks were reapplied. Five days after transduction, aliquots of 500,000 cells were extracted and assayed for BMP4 by SDS-PAGE and Western blot analysis. Blots were probed using a primary

anti-BMP4: monoclonal antibody (host mouse) at a 1:1000 dilution and a secondary anti-Mouse IgG-HRP antibody (host goat) at a 1:10,000 dilution. Figures 8 and 9 are photographs of the blots of the GFP-transduced and BMP2/4-transduced cell preparations, respectively. In Figure 9 (right panel), a distinct band corresponding to BMP4 (24kD) is evident in Lane 1 (BMP-transduced cells), while no such band is observed in the GFP-transduced control cells (Figure 8, Lane 3) (left panel).

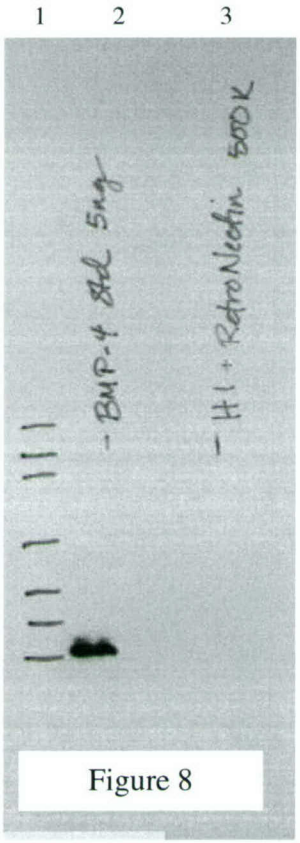

Figure 8

Figure 8. (Left) Western blot for BMP4 protein in extracts of control (GFP-transduced) cells. Sca-1$^+$ cells were transduced with an HIV-based viral vector expressing GFP. Blots were probed using a primary anti-BMP-4: monoclonal antibody and a secondary anti-Mouse IgG-HRP antibody.
Lane 1: Molecular weight standards,
Lane 2: BMP4 protein standard (5ng)
Lane 3: 500,000 Sca-1$^+$ cells transduced with the GFP-expression HIV-based vector

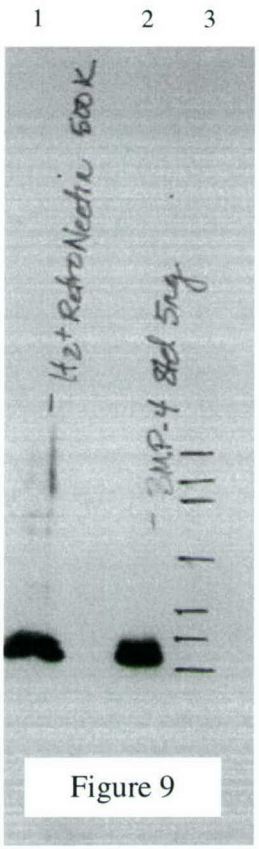

Figure 9

Figure 9. Western blot for BMP4 protein in extracts of BMP4-transduced) cells. Sca-1$^+$ cells were transduced with an HIV-based viral vector expressing BMP4. Blots were probed using a primary anti-BMP-4: monoclonal antibody and a secondary anti-Mouse IgG-HRP antibody
Lane 1: BMP4 protein standard (5ng)
Lane 3: 500,000 Sca-1-positive cells transduced with the BMP-expression HIV-based vector.
Lane 1: Molecular weight standards.

To further examine BMP2/4 transgene expression, we attempted to develop a BMP2/4 immunohistochemical staining method using a two-antibody system. Bone marrow cells were collected from a mouse transplanted with Sca-1 cells transduced with the HIV-based BMP2/4 viral vector and from a control (non-transplanted) mouse. The bone marrow samples were fixed with formalin, rinsed 3 times with PBS and then smeared on microscope slides. The slides were baked for 45 minutes in a dry oven and stored overnight at 4°C. The cells were then incubated with a primary anti-BMP-4 antibody (Chemicon™, monoclonal, 1:200 dilution) for 45 minutes. After washing, the slides were incubated with a biotinylated anti-mouse IgG antibody (1:100 dilution) for 30 minutes. After additional washing, the slides were incubated with Strept-avidin-HRP (Vector Lab™, 1:200 dilution) for 15 minutes, washed and incubated with DAB-H_2O_2 for 5 minutes. The slides were counterstained with hematoxylin for 1 minute, dehydrated with ethanol and cleared with 3 changes of xylene. Microscopic visualization of the control mouse and the transplanted mouse showed similar results (data not shown). Numerous brown stained cells were

visible on both slides indicating an unacceptable degree of background staining. This background staining is likely due to endogenous production of BMP4 and cross-reactivity with the human BMP4 antibody. From these data we concluded that immunohistochemical staining would not be an appropriate means to assess expression of the BMP2/4 transgene.

As a result of the difficulty we experienced in developing an immunohistochemical assay for BMP4 detection, we adapted an immunostaining protocol developed in a related project as an alternative method. Preliminary studies were performed using D1 cells. The D1 cell line is a bone marrow-derived mesenchymal stem cell line that has been shown to localize to bone marrow after intravenous injections. These cells have been generously provided to us by Dr. Gary Balian's laboratory and are relatively easy to maintain in culture. D1 cells were transduced with the hybrid BMP2/4 vector. Cells were cultured in the standard media and plated in 6-well dishes at a density of 4 million cells per well. The cells were transduced by 2 exposures to the viral preparation at a multiplicity of infection (MOI) of 20. Intracellular staining for BMP4 was performed using reagents and antibodies purchased from Santa Cruz Biotechnologies, Inc. BMP2/4 transduced and non-transduced (control) D1 cells were fixed and then rendered permeable. The cells were then blocked with 2% normal donkeys serum and incubated for 30 minutes in either a 1:400 or 1:800 dilution of the primary antibody (anti-BMP4 goat polyclonal IgG). After washing, the cells were incubated for 30 minutes in one of two concentrations (1:800 or 1:1600) of the PE-conjugated secondary antibody (donkey anti-goat IgG $F(ab')_2$). Table 3 shows the results of flow cytometry for PE-positive cells. These results suggest that the best results occurred using either dilution of primary antibody dilution followed by incubation with the secondary antibody of 1:1600 dilution. In the future, we plan on using immunostaining and FACs analysis, rather than immunohistochemistry for assessment of transgene expression.

Table 3 – FACs analysis of PE positive BMP4 transduced D1 cells after immunostaining using a 2 antibody system (PE-conjugated).

[primary ab]	[secondary ab]	control cells	BMP4 transduced
1:400	1:800	8	40
1:800	1:800	4	30
1:400	1:1600	5	58
1:800	1:1600	5	54

Specific Objective 2b:

Sca-1^+ cells were isolated and transduced with either the GFP or BMP2/4 transgene vectors using the protocols described above. Forty eight hours after transduction, aliquots of 500,000 cells of the cell preparations were injected via tail vein into 24 sub lethally irradiated W^{41}/W^{41} recipient mice (N =12 per group). Additional aliquots of the cells were stained with propridium iodide for measurement of cell survival and GFP expression. Both HIV-virus-transduced cells preparations showed a large % of cell death (81% and 80% for GFP- and BMP4-transduced cells, respectively). Parallel cultures of GFP-transduced cells were assayed by FACs for transduction efficiency two and five days after transduction. Approximately half [51% at 2 days and 49% at 5 days (Figure 10) post-transduction] were expressing the GFP transgene.

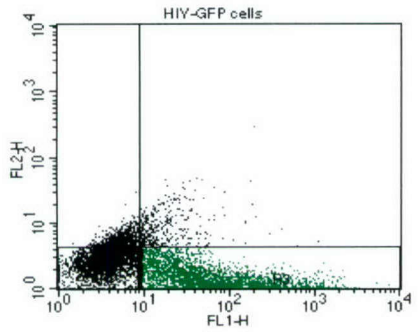

Figure 10 – %GFP-expressing donor cells. Sca-1 positive cells from C57BL mice were transduced with an HIV-based vector expressing the GFP marker. Five days post-tranduction, the cells were assayed by FACs analysis for %GFP-expressing cells.

At 9 weeks post-transplant, peripheral blood was collected from the two groups (GFP-transduced transplants and BMP2/4-transduced transplants) of recipient mice and assayed for RNA expression of the transgenes by real time RT-PCR and for % GFP positive cells by FACs analysis. The real time RT-PCR studies were performed using primers specific for the two transgenes (GFP and BMP2/4). In addition, GAPDH expression was measured as a reference gene. Quantitation was made using standardization with external reference DNA. In the recipient mice receiving GPF-transduced cells, 5 of the 12 mice showed detectable GFP expression (mean GFP:GAPDH ratio 91.9 ± 54.3). Engraftment was confirmed in the same 5 mice by FACs analysis for GFP^+ mononuclear blood samples. No GFP^+ cells were observed in the other GFP-treated mice or in the BMP2/4-treated mice. Results for BMP2/4 expression showed 5 of the 12 mice transplanted with the BMP2/4-transduced cells showed significant BMP expression (mean BM2/4:GAPDH ratio 11.5 ± 9.4). These results show an 8-fold difference in transgene expression between the GFP-positive and BMP-positive results. However, this data should be interpreted with caution due to the large variation that was observed. We plan on repeating these studies to confirm these results.

Figure 11 shows the % GFP^+ cells determined by flow cytometry in the 5 GFP-positive recipient mice at 5, 9 and 22 weeks post transplant. A slow decline in % GFP positive cells was observed in the mean % GFP^+ cells. Individual analysis of the engrafted mice revealed that this observed declined occurred in all mice except for mouse 7 which showed relatively consistent 80% engraftment at all three time points (data not shown). This decline is likely the result of transplanting Sca-1^+ cells, a relatively heterogeneous stem cell population. At early engraftment time points, progeny cells from GFP-positive hematopoietic progenitor cells and from GFP-positive hematopoietic stem cells are present. However, at later time points, as donor progenitor cells differentiate, only the progeny from donor stem cells are evident. Alternatively, this decline could be due to changes in transgene expression over time.

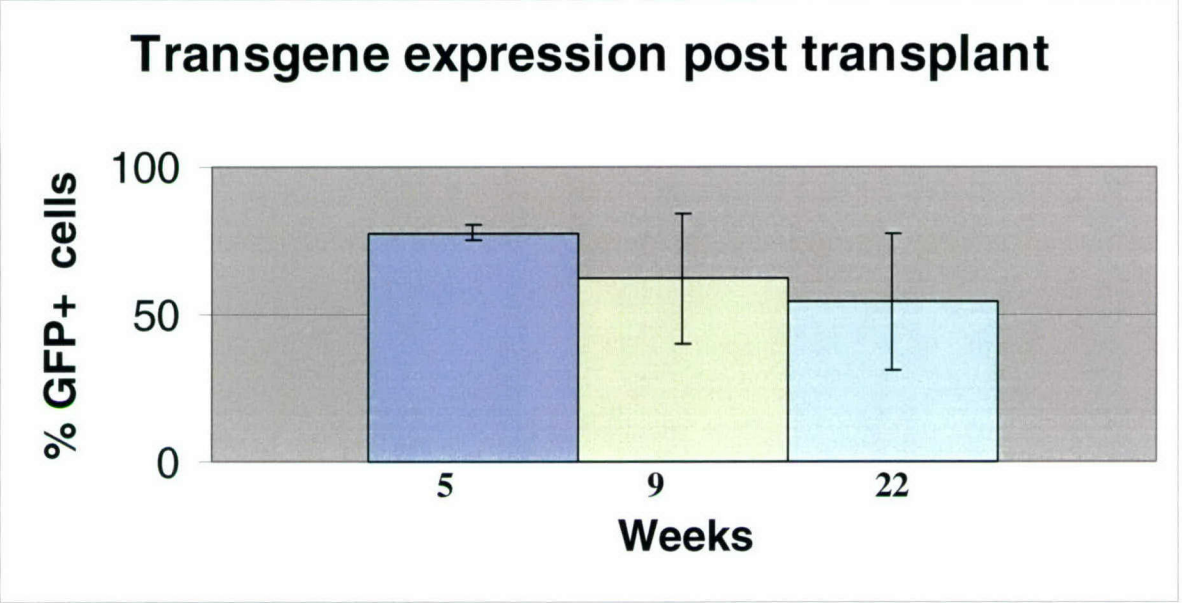

Figure 11: Mean ± S.D. % GFP positive cells determined by flow cytometry at 5, 9 and 22 weeks post transplant in the 5 recipient mice that were successfully transplanted with HIV-GFP transduced Sca-1$^+$ donor cells.

At 5, 9, 17 and 22 weeks, serum was prepared from tail vein bleedings and assayed for alkaline phosphatase (AP). AP activities were determined in 0.15M CO_3 buffer (pH 9.3) containing 1mM $MgCl_2$, 10mM p-nitrophenylphosphate (PNPP) and 10mM L-phenylalanine in 96-well microtiter plates and were calculated from the time-dependent increase in absorbance at 410 nm measured with an automatic recording microtiter plate spectrophotometer. Comparisons using Students t-test for independent variables were made between the 5 successfully GFP-engrafted mice (as determined by real time RT-PCR and FACs) and the 5 successfully BMP2/4 engrafted mice (as determined by real time RT-PCR). As seen in Table 4, no significant differences in AP activity were observed at any of the time points. Serum osteocalcin was also measured in the 17-week serum samples using a modified mouse osteocalcin ELISA assay. No significant difference in osteocalcin was observed (data not shown).

Table 4 Serum alkaline phosphatase (AP) U/L. Values reported are means ± standard deviation of the 5 successfully engrafted mice from each treatment group (mice transplanted with GFP-tranduced donor cells vs. mice transplanted with BMP2/4 transduced donor cells).

Treatment	Mean AP (st. dev) 5 weeks	Mean AP (st. dev) 9 weeks	Mean AP (st. dev) 17 weeks
GFP-tranduced donor cells	77.1 (12.9)	73.4 (29.6)	65.9 (6.0)
BMP2/4 transduced donor cells	76.5 (8.2)	85.5 (14.8)	72.7 (16.7)

At 22 weeks post transplant, the mice were euthanized and femurs and tibiae were dissected out. The femurs were assayed for total bone density (BMD) and cortical BMD by pQCT. BMD was calculated by averaging the two femurs of each mouse from the 5 successfully transplanted mice from each treatment group. No significant differences were detected in mean total BMD between mice engrafted with GFP-transduced donor cells vs. mice engrafted with BMP2/4-transduced donor cells (766.5 ± 31.3 vs. 786.8 ± 44.1, respectively). Similarly, no significant difference in cortical thickness was observed between the two groups (0.330 ± 0.013 vs. .341 ± 0.022, respectively). Faxitron analysis of the bones was not attempted. No differences were detected using pQCT (a sensitive quantitative analysis); therefore, it is unlikely that differences would be observed using the less sensitive, non-qualitative Faxitron analysis.

Skeletal AP was extracted from the dissected tibiae by incubation in a solution of 0.1% triton x-100 (250μL). AP activity was determined as described above and normalized to total protein using a bicinchonicinic acid colorimetric assay (BCA Protein Assay™, Pierce, Rockford, IL). No significant differences in AP activity/mg protein were observed between the two treatment groups (data not shown). These results suggest that transplantation with BMP2/4-transduced Sca-1^+ cells did not result in significant bone formation.

One possible explanation for the lack of bone formation in treated mice is that engraftment in the BMP2/4-transplanted group may have been low. To examine this possibility, we conducted a similar experiment using donor cells from a transgenically marked mouse. For this experiment, Sca-1^+ cells were isolated from the bone marrow of TgN donor mice. The TgN mouse strain is a transgenic strain that expresses the GFP marker gene. Use of this strain provided an endogenous marker by which we could track engraftment. The GFP-expressing Sca-1^+ cells were transduced with our HIV-based BMP2/4 viral vector as described above. Half of the cells were mock transduced (cultured in parallel but not exposed to viral vector) to serve as controls. Two days after transduction, the two cell preparations were injected via tail vein into 36 sub-lethally irradiated W^{41}/W^{41} recipients (N=18 per treatment group). Engraftment was assessed by FACs analysis for GFP-positive cells at 8, 24, 33, 37 and 40 weeks. As in the previous experiment, not all mice were successfully engrafted. At 8 weeks, only 8 of 18 mice transplanted with mock-transduced cells had evidence of engraftment. Of these 8 mice, 1 mouse showed moderate engraftment (37.4% GFP^+ cells), whereas the remaining 7 showed high engraftment (range 71.9 – 90.7% GFP^+ cells). One of the highly engrafted mice from this group unexpectedly died at 9 weeks of unknown causes. At the same time point, in the group transplanted with BMP2/4-transduced cells, only 9 of 18 mice were engrafted with donor cells. Two of these mice showed low engraftment (17.7, 15.6% GFP^+ cells) while the remaining 7

were highly engrafted (63.5 – 90.4% GFP^+ cells). Only the 13 highly engrafted mice (6 from the mock group and 7 from the BMP2/4 group) are included in the subsequent analysis for this report. As seen in Figure 12, stable engraftment was achieved for up to 40 weeks after transplantation. No significant difference was noted between the mock-transduced and BMP2/4-transduced groups at any time point.

FACs analyses from this experiment and the previous experiment suggest that we are able to achieve good engraftment efficiencies (60-90%) with our transplant methodology. However, results from both experiments, indicate sub-optimal transplant success (40-50%). We believe this low engraftment success is due to the use of the tail vein method. In a related project, we have improved our method by employing retro-orbital injection as a means of delivering donor cells. With this new protocol, we now consistently achieve nearly 100% transplant success, with engraftment levels at 70-90%. Future transplants for this project will be performed using the retro-orbital injection method. An example of results from a transplant experiment performed using the retro-orbital injection method is described above in Objective 1a, Figure 2.

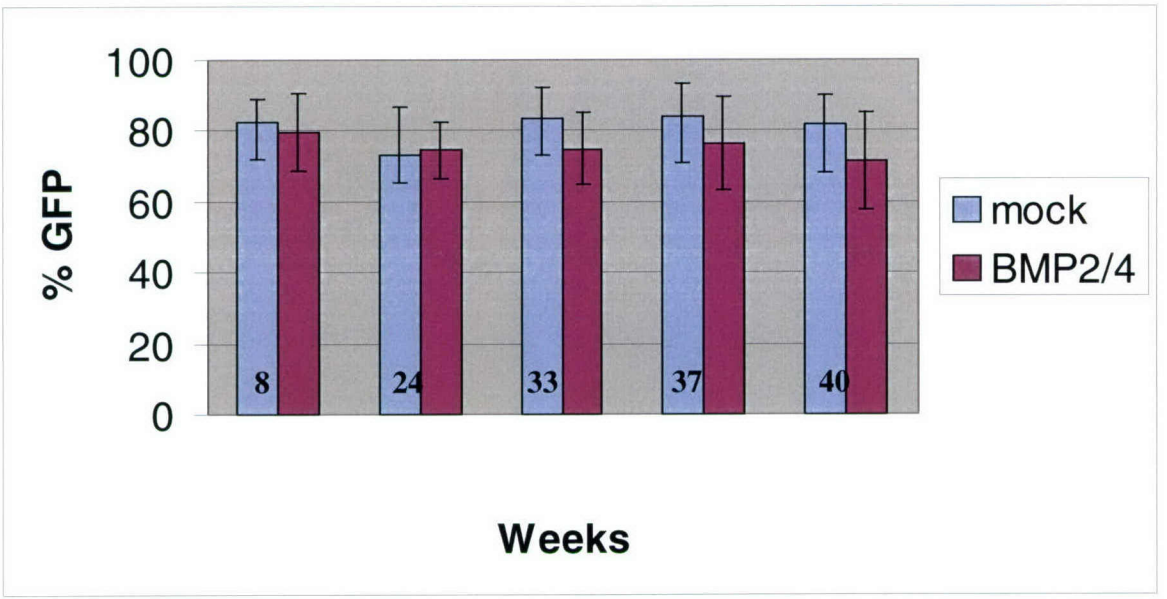

Figure 12: Mean ± S.D. % GFP positive cells as determined by flow cytometry at 8, 24, 33, 37 and 40 weeks post transplant in 6 recipient mice that were transplanted with GFP-expressing Sca-1^+ cells that were either mock –transduced or BMP2/4 transduced.

The 13 successfully engrafted mice (6 mock-transduced and 7 BMP2/4-transduced) were analyzed for bone formation by measurement of serum AP at 10 weeks, 26 weeks and 40 weeks post transplant. AP activities were assayed as described above and the results are listed in Table 5. As in the previous experiment, no significant difference was observed in serum AP activities between mice transplanted with mock-transduced cells and and mice transplanted with BMP2/4-transduced cells.

Table 5: Serum alkaline phosphatase (AP) U/L. Values reported are means ± standard deviation of the successfully engrafted mice from each treatment group (mice transplanted with mock-tranduced cells vs. mice transplanted with BMP2/4 transduced cells).

Treatment	Mean AP (st. dev) 10 weeks	Mean AP (st. dev) 26 weeks
Mock-tranduced donor cells	92.7 (22.0)	69.3 (30.7)
BMP2/4 transduced donor cells	73.3 (30.7)	55.7 (8.7)

At 40 weeks post transplant, the mice were euthanized and femurs and tibiae were dissected out. The right femurs were assayed for total, trabecular and cortical BMD by pQCT. BMD was calculated by averaging values from the successfully transplanted mice from each treatment group. As before, no significant difference was observed in mean total BMD between control mice and mice transplanted with BMP2/4-transduced (770.3 ± 33.8 vs. 783.4 ± 47.0 respectively). Similarly, no significant difference in cortical BMD was observed between the two groups (0.323 ± 0.022 vs. 0.337 ± 0.024, respectively). AP activity in triton extracts of the left tibiae and 2 tibiae was assayed as described above. No significant difference in AP activity/mg bone weight was observed between the two treatment groups (data not shown). These results, and those of the previous transplant experiment indicate that transplantation with BMP2/4-transduced Sca-1^+ cells does not result in significant bone formation.

Due to the negative results observed, we are examining a second therapeutic gene, human growth hormone (hGH). To this end, a new transplant experiment is presently in progress. For this experiment, Sca-1^+ cells from TgN donor mice were tranduced with either the β-galactosidase marker gene, the BMP2/4 gene or the hGH. At week 11 post transplant, the mean engraftment (%GFP^+ donor cells in peripheral mononuclear blood cells) was 77.9 ± 7.4 in the β-gal group, 77.7 ± 9.03 in the hGH group and 75.2 ± 11.0 in the BMP2/4 group. No significant difference by ANOVA was observed. Blood samples at various time points will be collected and analyzed for serum bone formation markers. These mice are scheduled for euthanasia and analysis of bone formation parameters in April 2005 (12 months post transplant).

There are several potential explanations for why cells transduced with BMP2/4 did not elicit the expected bone formation response. It is possible that silencing of the transgene occurred over time after engraftment. This is supported by the data presented in Figure 11, where a decrease in cells expressing the transgene GFP marker was observed. It is also possible that the transgene product (BMP4) is exerting an autocrine effect on HSC biology. For example, BMP4 may cause HSCs to undergo differentiation and release into the blood, resulting in a reduction in the number of high expressing transduced cells in the marrow cavity. Alternatively, BMP4 may be toxic to HSCs, causing a reduction in cell number of the high BMP4-expressing cells. In the future, we are planning in vitro and in vivo experiments to explore these possibilities.

Specific Objectives 3a & 3b:

These objectives require young (8 weeks) and old (1 year) W^{41}/W^{41} recipient mice. Since this mouse strain is not commercially available, over the past year, we have initiated and maintained

a breeding colony. At present, 22 recipient mice have been produced that will be used as old age recipients. These recipient mice are presently 8 months old. In four months, these mice and 8-week old recipients will be transplanted with Sca-1^+ cells that have been transduced to express a growth factor gene.

Key Research Accomplishments

- Achieved consistently high enrichment (74%) and good cell yields (3 x 10^6 cells/donor mouse) of Sca-1^+ cell
- Demonstrated consistently high, stable engraftment of Sca-1^+ cells (70-90%) in the skeletal tissues of recipient mice for up to 40 weeks
- Demonstrated that transplanted Sca-1^+ cells are able to reconstitute all four hematopoietic lineages (T-lymphocyte, macrophage/monocyte/neutrophils, B-lymphocyte and erythroid).
- Demonstrated that there is insignificant engraftment of Sca-1^+ cells in the non –skeletal tissues of recipient mice
- Successfully transduced Sca-1^+ cells using a retroviral-based vector, achieving up to 50% transduction efficiency
- Achieved relatively stable chimeras with transplanted retrovirally transduced Sca-1 cells. Initially (5 weeks post transplant), 77% of mononuclear peripheral blood cells from recipient mice expressed the transgene. Although this expression slowly declined over time, after 22 weeks 54% mononuclear peripheral blood cells from recipient mice were still expressing the transgene
- Demonstrated that Sca-1^+ cells retrovirally transduced to express BMP4 did not increase bone formation in recipient mice
- Successfully initiated and maintained a breeding colony of c-kit mutation mice (not commercially available) to produce progeny to serve as recipients in our transplantation experiments

Reportable Outcomes

None at the Present Time

Conclusions

1) In our systemic gene therapy subproject, we have consistently achieved high yields of highly enriched hematopoietic progenitor cells from donor mice. Transplantation of these cells into preconditioned recipient mice results in consistently high, stable engraftment in the skeletal tissues for up to 40 weeks. Minimal or no engraftment is observed in non-skeletal tissues of the recipient animal.

2) We have successfully transduced the hematopoietic progenitor cells using a retroviral-based vector, achieving up to 50% transduction efficiency. Transplantation with donor cells retrovirally transduced to express BMP4 did not increase bone formation in recipient mice as expected. Therefore, we plan on exploring other therapeutic genes, such as human growth hormone, in our gene therapy strategy.

Project 7: Study Of Synergistic Growth Factors In Skeletal Gene Therapy

Introduction:

Our preliminary studies have strongly suggested that gene therapy with a single bone growth factor gene can be a means by which healing of skeletal injuries can be considerably accelerated [1]. Although skeletal gene therapy utilizing a single osteogenic growth factor has shown promising results in our laboratory and others, a strong rationale has emerged for the development of combination therapies that employ two or more therapeutic genes that act synergistically to promote more rapid and complete healing of skeletal injuries. The long-term goal of this project is to develop safe and effective combination therapies for skeletal injuries that involve *ex vivo* gene transfer of two or more osteogenic genes to primary bone marrow stromal cell cultures, followed by transplantation of transduced cells expressing high levels of these therapeutic genes to the skeletal injury. Specifically, we have chosen to evaluate the therapeutic potential of primary bone marrow-derived stromal cells overexpressing the osteogenic genes Cox-2 and VEGF in a mouse calvarial critical defect model.

Body:

Technical Objective:

To evaluate the efficacy of *ex vivo* delivery of two sets of combinations of osteogenic genes (Cox-2 + VEGF) on bone regeneration in a mouse calvarial bone defect model.

The following specific objectives were proposed for the first year of the project:

1) To prepare MLV-based retroviral vectors expressing the Cox-1 and VEGF genes, and to characterize transgene expression levels following transduction of primary bone marrow derived stromal cell cultures (BMDSCs) *in vitro*.
2) To evaluate the impact of transplantation of BMDSCs expressing Cox-1 and VEGF on the rate and quality of healing of critical-sized mouse calvarial defects *in vivo*.

Significant progress has been made in each of these specific objectives. The results support the notion that this novel therapeutic approach is technically feasible and can significantly improve bone regeneration in a mouse calvarial model. However, the results also raise important questions relating to the mechanism of Cox-2 action *in vivo*.

Progress in Specific Objects

***Specific Objective 1*:**

1. Optimization of cell culture conditions for mouse bone marrow derived stromal cells.

Of the three cell types (skin fibroblasts, skeletal muscle-derived myoblasts, and bone marrow-derived stromal cells) that have been used successfully as donor cells in *ex vivo* skeletal gene therapy applications, we chose to utilize bone marrow-derived stromal cells (BMDSCs) in these experiments because of our previous success in healing critical sized bone defects in a rat calvarial model using an *ex vivo* gene therapy strategy that employed BMDSCs. However, we found that mouse BMDSCs do not grow well (long doubling time; limited number of passages) under cell culture conditions that support rat BMDC growth (DMEM + 10% FBS). We therefore needed to first optimize the growth conditions for mouse BMDSCs. We found that mouse BMDSCs grow best in

alpha-MEM containing 15% fetal bovine serum. Under these cell culture conditions, mouse BMDSCs exhibit a doubling time of 24 to 48 h, and can be continuously passaged for 8 –12 weeks without a significant loss in their proliferative capacity (Figure1). This is sufficient to produce enough cells for *ex vivo* gene therapy applications.

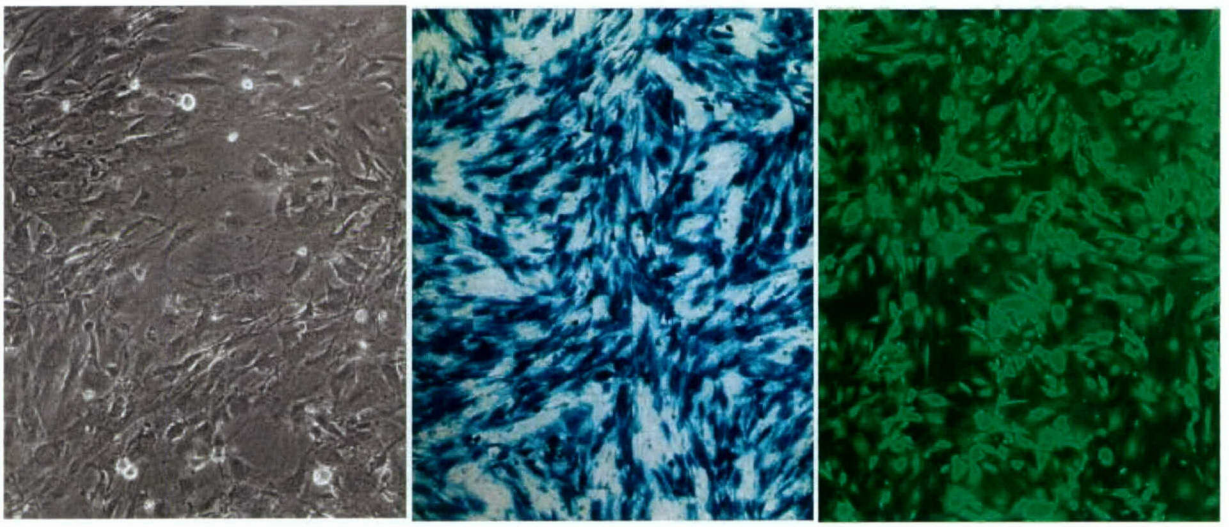

Figure 1. Culture of Mouse Bone Marrow-Derived Stromal Cells (BMDSC) and transduction with reporter genes. Stromal cell cultures were prepared by flushing out the marrow of tibiae and femurs, rinsing the cells 3x in PBS, and placing them in standard plastic culture dishes in alpha-modified Eagle's medium, containing 15% fetal bovine serum and antibiotics. Half the medium was changed on days 2, 3, and 4. Cells had attached and started to divide by then, and the medium was changed every 3-4 days until cells reached confluency, usually after 8 – 12 days. Cultures were then passaged weekly. The left panel shows a phase contrast image of a confluent MSC culture. MLV reporter gene preparations(βGal, EGFP) were used to transduce cells as described in the text. The center panel shows cells stained for βGal after transduction with MLV-βGal. The right panel shows a fluorescent image of cells transduced with MLV-EGFP.

2. Construction of MLV-based retroviral vectors expressing the VEGF and Cox-2 genes.

A plasmid containing the 165 amino acid form of human vascular endothelial growth factor (VEGF-A_{165}) [2] was kindly provided by Dr. D. Losordo, Tuft's University, Boston MA [3]. The VEGF gene was excised from this plasmid and inserted downstream of a constitutively active CMV promoter in an MLV-based retroviral expression plasmid. Similarly, an MLV-based retroviral expression plasmid containing the human Cox-2 (Cyclooxygenase 2; Prostaglandin H synthase 2) gene was prepared by Dr. D. Strong at the MDC. The 72 kDa Cox-2 gene product [5] catalyzes the first step in the biosynthesis of prostaglandins: the conversion of arachidonic acid to prostaglandin H_2. The biological activity of recombinant Cox-2 has been verified in the rat femoral fracture model [Dr. C. Rundle, personal communication]. An MLV retroviral vector expressing human bone morphogenetic protein 4 (BMP-4) was also prepared as a positive control to which the therapeutic efficacy of VEGF and Cox-2, either alone or

in combination, can be compared. In this construct (designated BMP2/4), the signal sequence of the BMP-4 gene is replaced by a signal sequence from the BMP-2 gene. The MLV retroviral vector expressing BMP2/4 has been described previously [4] and has been shown to completely heal critical-sized calvarial defects in a rat model [1]. All MLV (MFG-based) retroviral vectors used in this study were grown and titred by the Vector Support Service at the MDC as described previously [4].

3. Characterization of recombinant growth factor expression in transduced primary mouse BMDSCs *in vitro.*

Mouse BMDSCs were transduced with MLV-based retroviral vectors according to a 3-hit protocol established by the MDC Vector Support Service Facility. Briefly, cells are plated in 6-well dishes to 50-70% confluency, and then incubated 3 times over 36 h with a recombinant MLV vector at a dose of 10 – 20 infectious retroviral particles per cell. Transduced cells are allowed to recover for two days in normal growth medium (alpha MEM + 15% FBS) before being passaged. This protocol ensures that cells are actively proliferating and undergo at least one cell division in the presence of the retroviral vector, which is necessary for stable integration of the retroviral genome (carrying the growth factor transgene) into cellular DNA. Preliminary experiments performed with MLV vectors expressing the reporter genes beta-galactosidase (βGal) or enhanced green fluorescent protein (EGFP) demonstrated that transduction efficiencies exceed 90% of the BMDSC target cell population under these conditions (Fig. 1).

Expression levels of recombinant Cox-2 and BMP2/4 protein in transduced BMDSCs were examined by Western blot analysis (Figures 2 and 3). Densitometric analysis of band intensities on Western blots from several experiments that contained multiple sample and standard concentrations demonstrated that recombinant Cox-2 levels reach 600 – 1200 ng/10^6 cells, whereas recombinant BMP2/4 is expressed at levels of 100 – 200 ng/10^6 cells 7 days after transduction. Recombinant VEGF expression levels were measured by ELISA (R&D Systems) in conditioned medium collected from transduced BMDSC cultures. Recombinant VEGF was found to be secreted at a rate of 250 to 500 ng/10^6 cells in 24 h 7 days after transduction.

Although recombinant growth factor expression was maintained for several weeks after retroviral transduction, growth factor production levels were found to decrease at different rates for each of the three recombinant proteins. Over a 4-week period, Cox-2 and BMP2/4 levels declined to 10% of their initial values, whereas VEGF production decreased by only 40%. Interestingly, βGal and EGFP expression was reduced by only 20% over this period of time. It remains to be determined whether this decline is caused by gene silencing or by a decrease in the proportion of BMDSCs carrying the retroviral genome (e.g. due to growth arrest or apoptosis of cells expressing high levels of the recombinant protein).

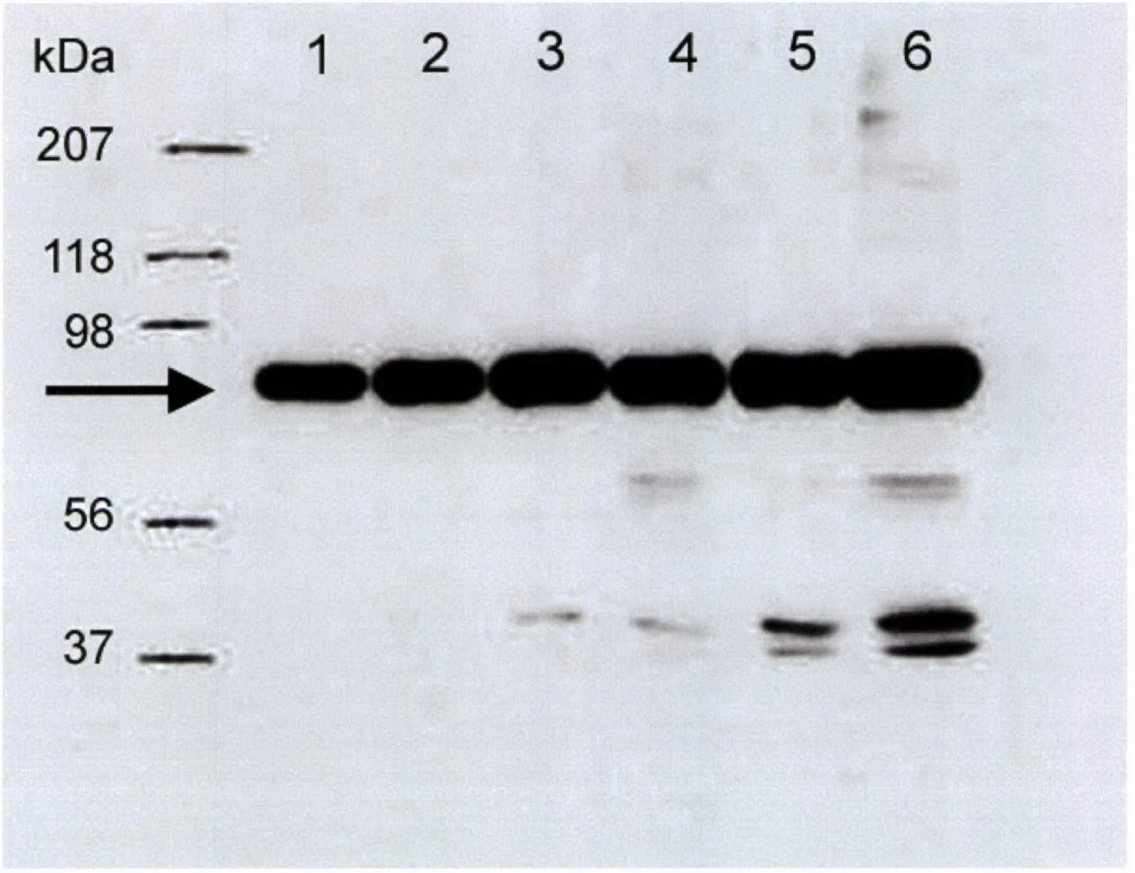

Figure 2: Western Immunoblot of Cox-2-Transduced Bone Marrow-Derived Stromal Cells (BMDC). Mouse BMDCs were harvested 10 days after transduction with MLV containing the gene for human Cox-2. After lysis in gel treatment buffer containing SDS and 2-mercaptoethanol, the equivalent of $2.5x10^4$, $5x10^4$, and $1x10^5$ cells were loaded in lanes 4, 5, and 6, respectively. Ovine Cox-2 standard (Cayman Chemical) was loaded in lanes 1 (25ng), 2 (50ng), and 3 (100ng). After separation on an 8% polyacrylamide gel, the proteins were transferred to a nylon membrane and then incubated with monoclonal Cox-2 (raised against a 19-amino acid peptide homologous to human Cox-2, Cayman Chemical). The membrane was incubated with HRP-conjugated secondary antibody and reacted proteins visualized using a chemiluminescence kit (Super Signal West Pico, Pierce). The position of marker proteins is indicated on the left. Transduced cells display a strong band at 72 kDa (arrow), comigrating with the standard.

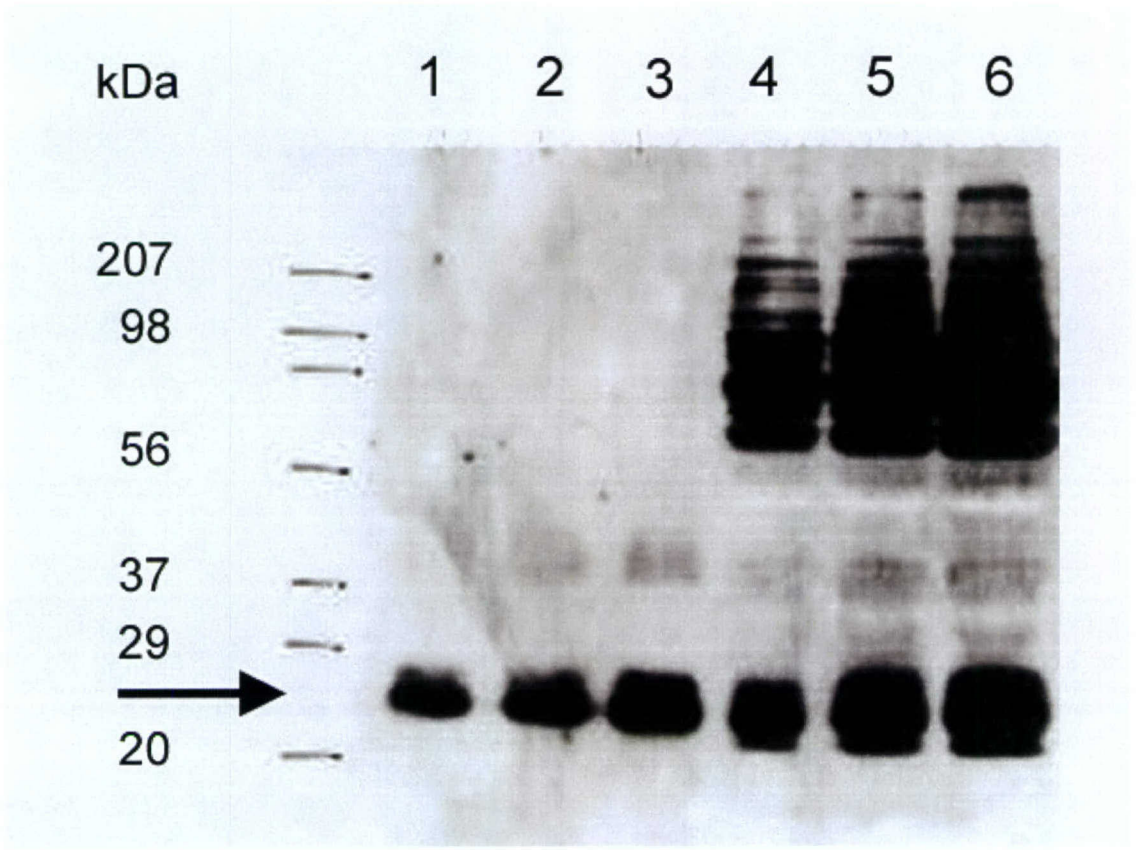

Figure 3: Western Immunoblot of BMP-producing BMDSC. Mouse bone marrow-derived stromal cells were harvested 2 weeks after transduction with MLV containing the gene for human BMP-2/4. The lysed cells were loaded in lane 1 ($5x10^4$), lane 2 ($1x10^5$), and lane 3 ($1.5x10^5$ cells). Lanes 1, 2, and 3 contain 1.5ng, 2.5ng, and 5ng of recombinant human BMP-4 standard, respectively. Electrophoresis separation was performed on a on a 10% polyacrylamide gel. After blotting to a nylon membrane, the separated proteins were incubated with monoclonal anti-human BMP-4 antibody (R&D Systems). and visualized as in Figure 2. The position of marker proteins (Bio Rad) is indicated on the left. Transduced cells display a strong band at 24 kDa (arrow), comigrating with the standard.

***Specific Objective 2*:**

1. Establishing a mouse calvarial model for *ex vivo* skeletal gene therapy.

A bone defect is defined to be of critical size if healing does not occur spontaneously over an extended period of time. Such defects are ideal for testing the growth promoting activity of novel therapeutic modalities such as growth factor gene therapy. A widely used model in bone biology is the rodent calvarial defect, which involves the creation of a circular defect in the center of the parietal bone. Without treatment, calvarial defects do not heal over a period of up to 12 weeks [6]. However, treatment with an appropriate growth promoting modality can effect complete healing within 3-4 weeks [1]. A main attraction of this model is the easy management of the surgical site. Unlike defects involving limbs or the spinal column, no stabilization is required because this site does not bear any load. Test substances can easily be inserted into the defect and are held tightly in place after suturing of the skin.

During the initial phase of healing of calvarial defects, osteoblasts at the margin of the defect proliferate rapidly, migrate a short distance towards the center of the wound and establish mineralization of the matrix along the wound periphery. This activity is stimulated by growth and differentiation factors that are released locally. Failure to close the critical size defect is thought to result from a deficiency in the level or persistence of local growth factor production [6]. Calvarial defects therefore provide an ideal model in which to test the effectiveness of gene therapy strategies aimed at increasing local growth factor production through transplantation of cells transduced *ex vivo* with recombinant retroviral vectors.

An important initial goal in this study was to successfully establish a mouse calvarial defect model. The move from a rat model, which has already been successfully established in our laboratory, to a mouse model will allow us to take advantage of the availability of a large number of transgenic and knockout mouse strains in which the impact of growth factor gene therapy on molecular mechanisms governing bone regeneration can be studied. In the last year, we have successfully established the methodologies needed to create a 5 mm diameter critical-sized defect in mouse calvariae using a diamond-based dental burr. Careful handling of the instrument is required to avoid damaging the highly vascularized dura mater, which can cause excessive blood loss and death of the animal.

2. Analysis of the impact of *ex vivo* gene therapy strategies on the rate and quality of healing of critical-sized mouse calvarial defects.

In our initial experiments, bone formation was assessed 14 d post-transplantation of 1 x 10^6 transduced mouse BMDSCs cultured overnight on a gelatin matrix scaffold designed to fit the size of the critical defect. Primary BMDSCs were transduced with recombinant MLV vectors expressing either Cox-2, VEGF, BMP2/4 (positive control), or EGFP (negative control) and expanded in culture for 14 to 21 days before being applied to the gelatin matrix scaffold. Bone formation was assessed 14 d post-transplantation using X-ray densitometry and histology.

As expected, no increase in bone density was observed in the defects transplanted with cells expressing EGFP, whereas significant increases in bone density were evident in all defects treated with BMP2/4 expressing BMDSCs. Surprisingly, transplantation of Cox-2 expressing cells produced no increase in bone density relative to EGFP treated controls. In addition, no increase in bone formation was evident in defects treated with VEGF-expressing cells. However, evidence of increased blood vessel formation in this group of animals indicated that recombinant VEGF was being expressed over the course of these experiments. No increase in angiogenesis was evident in animals treated with Cox-2 expressing cells.

Histological analysis confirmed the results of our bone density analysis. Staining for the bone formation marker alkaline phosphatase was strong throughout the entire defect in animals treated with recombinant BMP2/4 expressing cells, whereas all other experimental groups displayed only weak alkaline phosphatase staining along the old bone and at the edge of the defects. Consistent with alkaline phosphatase staining, von Kossa staining for calcium deposits showed increased mineralization in BMP2/4 treated animals. No mineralization was evident in any of the other experimental groups. Interestingly, in addition to increased blood vessel formation, critical defects treated with VEGF expressing cells also contained more soft tissue in the area of the defect. This was not observed in defects treated with Cox-2 or EGFP expressing cells. The absence of a bone formation response with VEGF was not unexpected as it had been shown that VEGF, while able to enhance the bone formation potential of BMP-4, was actually inhibiting bone formation when administered alone (7). While there are many reports showing osteogenic activity of VEGF, it may only be active in conjunction with other factors regulating skeletal healing.

The absence of an increase in bone formation in Cox-2 treated defects was somewhat surprising in view of the many reports that have demonstrated the osteogenic action of Cox-2 and its essential role in bone fracture healing (8). However, experiments utilizing Cox-2 as a therapeutic gene in a femur fracture model have shown that significant increases in bone formation do not occur until 14 to 21 days post-treatment (C. Rundle, personal communication).

To determine if calvarial healing is also delayed following Cox-2 treatment, a second experiment was performed in which bone formation was evaluated 4 weeks post-transplantation with MLV vector transduced BMDSCs expressing:

1. BMP2/4 alone (positive control);
2. βGal alone (negative control);
3. BMP2/4 + VEGF (4:1 mixture);
4. BMP2/4 + Cox-2 (4:1 mixture); and
5. Cox-2 + VEGF (4:1 mixture).

Each of these experimental groups consisted of 5 animals, each implanted with 1 x 10^6 MLV-transduced BMDSCs on a gelatin matrix as described above. Animals were sacrificed 4 weeks post-transplantation and calvariae were analyzed for bone formation by X-ray densitometry and histology.

Similar to the results seen after 2 weeks of treatment, substantial bone formation was seen in defects treated with BMDSCs expressing BMP2/4 alone. The extent of bone formation was much more pronounced at this later time point, as evidenced by the calvarial cross sections shown in Figure 4. Defects implanted with BMP2/4 expressing cells (panels B and D) exceeded the thickness of the original bone several fold. Soft X-ray imaging (Figure 5, panels A, B, and C) indicated that all defects treated with cells expressing BMP2/4 had completely healed by 4 weeks post-transplantation. On the other hand, no significant increase in bone formation was evident in defects treated with cells expressing Cox-2 and VEGF cells (4:1 ratio) (Figure 4, panel C and Figure 5, panel D) relative to negative control animals treated with cells expressing βGal (Figure 4, panel A and Figure 5, panel E).

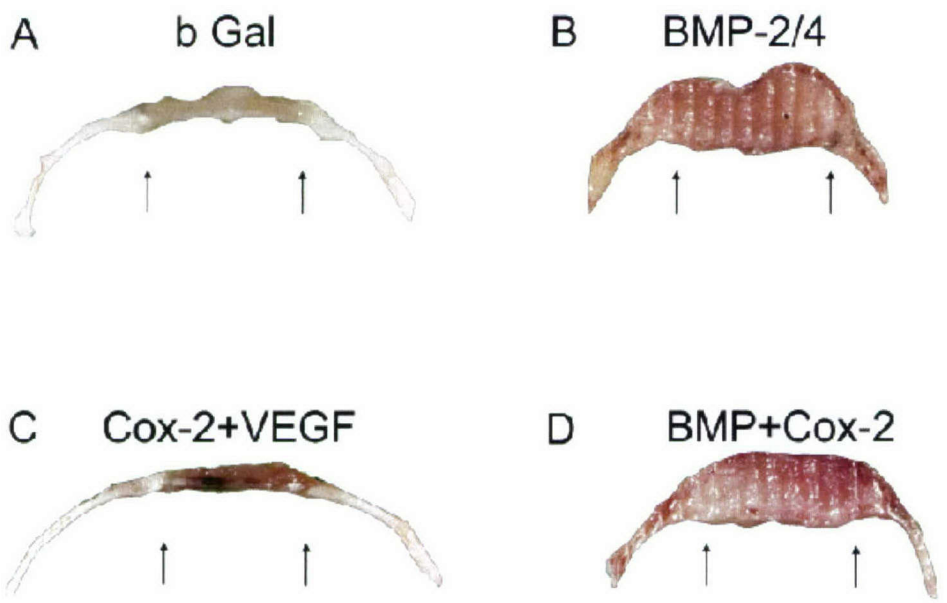

Figure 4: Cross-Section of Calvarial Defect 4 weeks after Implant. Calvariae were dissected after 4 weeks and photographed after coronal sectioning. Arrows mark the edges of the 5-mm defects that were implanted with 1 x 10^6 cells. Shown are representative examples of implant groups that obtained βGal control cells (A) and BMP-4 producing cells (B). Implants containing 4:1 mixture of Cox-2 and VEGF transduced cells (C) and 4:1 mixture of BMP and Cox-2 cells (D) are also shown.

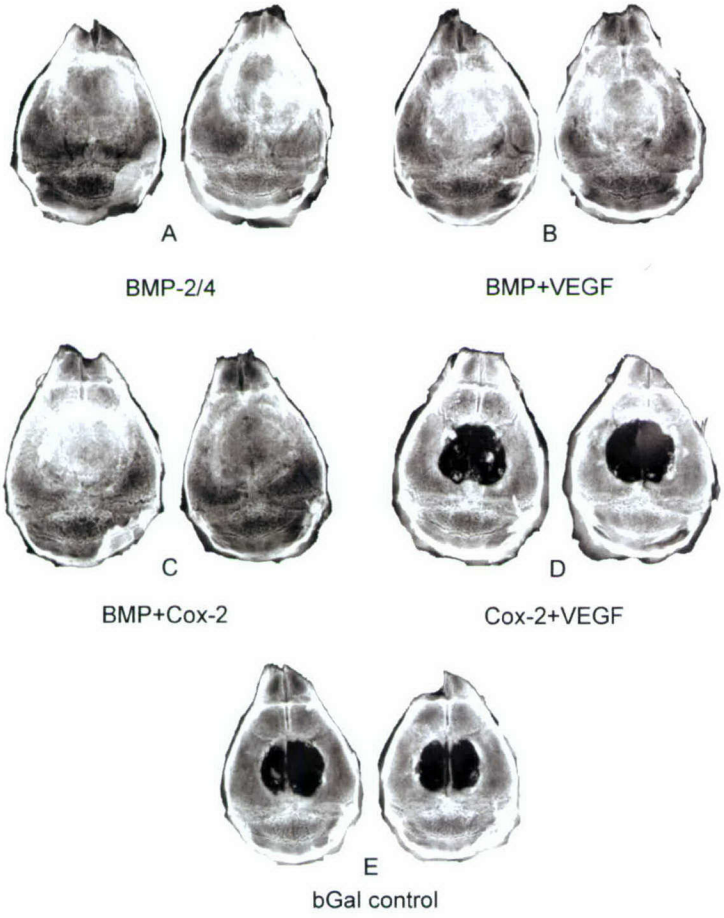

Figure 5: Digital X-Ray Images of Calvarial Defect Model. Shown are 2 representative examples from implant groups that obtained a total of 1 x 10^6 gene-modified mouse bone marrow stromal cells. Group A was implanted with BMP-cells only, and group E with βGal control cells only. Mixtures in a 4:1 ratio were implanted in groups B-D, namely BMP (8 x 10^5) plus VEGF (2 x 10^5) in B, BMP (8 x 10^5) plus Cox-2 (2 x 10^5) in C, and Cox-2 (8 x 10^5) plus VEGF (2 x 10^5) in D.

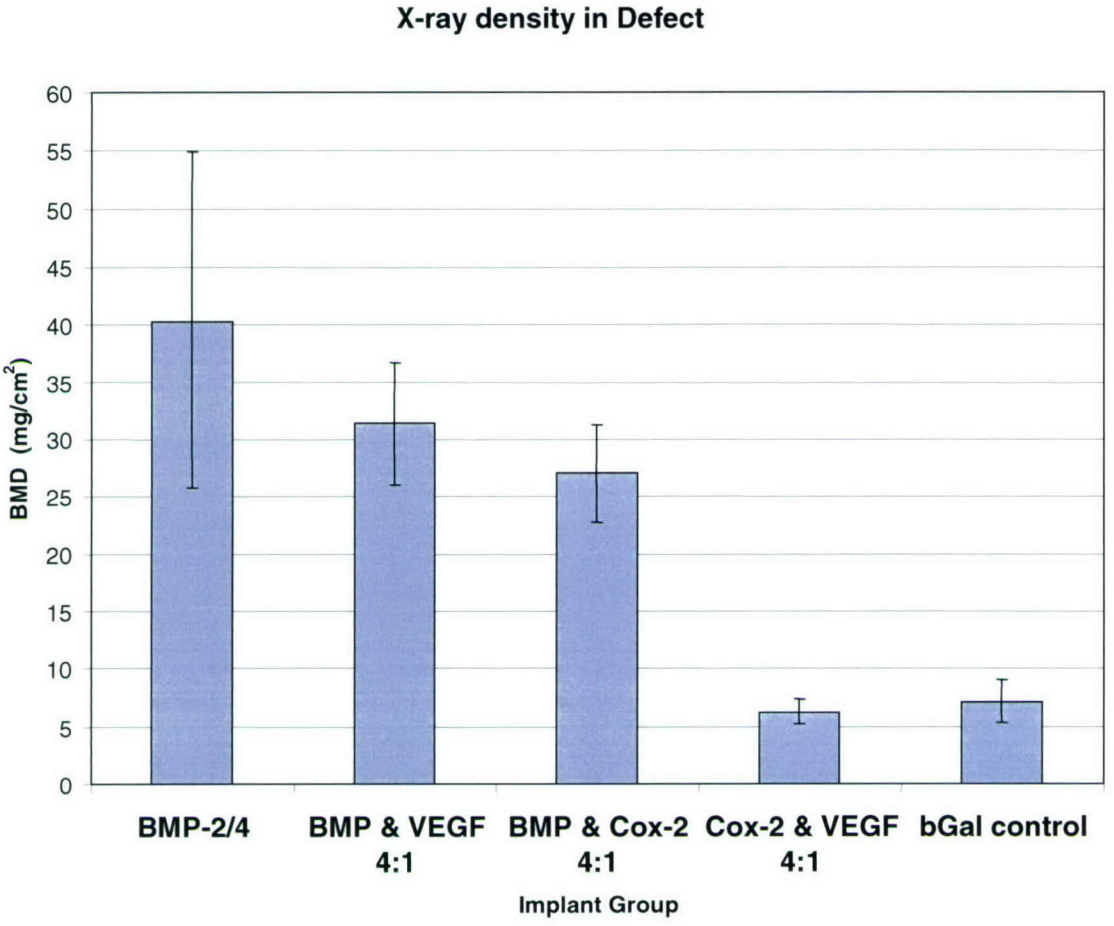

Figure 6: Bone Density in Calvarial Defects after Implanting with Marrow Stromal Cells. Calvariae were dissected 4 weeks after implant of cells as described in the text. Implant groups contained the modified stromal cells that were described in Figure 4. Bone mineral density (BMD) was measured by dual-energy X-ray absorptiometry (DEXA) using a PIXImus soft-X-ray densitometer (Lunar, Madison WI) and analysis software version 1.46 provided by the manufacturer. Values are average (+/- SD) from 4 animals for each group.

As shown in Figure 6, quantitative densitometry indicated that the highest bone mineral density (BMD) in the group with BMP-4 cells alone, reaching 159% (+/- 57%) of control values. Implants with mixtures of BMP +VEGF (123 +/- 57%) or BMP + Cox-2 (107 +/- 17%) were slightly lower. Implants with mixtures of BMDSCs expressing BMP2/4 and VEGF (123 +/- 57%) or Cox-2 (107 +/- 17%) produced slightly lower BMDs, in line with the 20% decrease in the number of cells expressing BMP2/4 in these mixed groups. Aside from increased bone formation in BMP2/4 treated defects, the only other consistent change seen in this study was an increase in vascular tissue mass in animals treated with cells expressing VEGF (data not shown). However, the presence of VEGF producing cells did not increase bone formation relative to BMP2/4 alone, and the presence of Cox-2 expressing cells had no significant impact on calvarial bone formation when combined with either BMP2/4 or VEGF.

Cyclooxygenase-2 (Cox-2) is an inducible enzyme that converts arachidonic acid to prostaglandin E2 (PGE2). Prostaglandins such as PGE2 are known to participate in inflammatory responses, increase osteoblast activity and new bone formation, and also increase osteoclast activity and subsequent bone resorption. In a recent study, PGE2 was shown to increase BMP-2 expression in osteoblasts [8]. In view of evidence that BMP-2 increases Cox-2 gene expression [9], BMP-2, Cox-2, and PGE2 may form a positive feedback loop that promotes osteoblast proliferation and differentiation. Observations such as these, along with studies of Cox-2 deficient mice, provide strong evidence that Cox-2 and PGE2 are important mediators of both endochondral and intramembranous bone formation. In fact, in Cox-2 deficient mice, intramembranous bone formation on calvaria was seen to be reduced by up to 60% compared to wild type mice [10].

The absence of a significant increase in bone formation in our mouse calvarial model following transplantation of Cox-2 expressing cells may be due to a number of factors, including:

1. Insufficient Cox-2 expression and PGE2 production in transplanted BMDSCs due to silencing of recombinant Cox-2 expression or cytotoxic effects on BMDSCs expressing high levels of recombinant Cox-2.
2. The inability of PGE2 synthesized by transplanted BMDSCs to influence bone formation due to physical barriers or distance from target cells in the wound site.
3. PGE2 can only function in an autocrine manner, requiring target cells to be directly transduced with the MLV vector expressing Cox-2.
4. Induction of Cox-2 expression and PGE2 synthesis by BMP-4 in cells involved in bone formation, thereby negating any added or synergistic effects by the presence of BMDSCs expressing recombinant Cox-2.

Vascular endothelial growth factor (VEGF) is also known to play an important role in bone repair by promoting angiogenesis as well as the recruitment and survival of chondrocytes, osteoblasts, and osteoclasts at the site of injury. VEGF is particularly important for hypertrophic cartilage remodeling and ossification. during endochondral bone formation. More recently, VEGF has been shown to be an early mediator of intramembranous bone formation in response to mechanical force (distraction

osteogenesis) [11]. The absence of a significant increase in bone formation following transplantation with BMDSCs expressing recombinant VEGF is consistent with the observation by Peng et al. [7] that VEGF alone does not improve bone regeneration in a mouse calvarial model. The absence of a significant increase in bone formation in the presence of both BMP2/4 and VEGF is likely due to the fact that the ratio of BMP2/4 and VEGF expression has not been optimized in our mouse calvarial model.

3) Consideration for Future Studies

1. Evidence from studies of Cox-2 effects in a femur fracture model indicate that little or no response is evident over the first 14 d post treatment with Cox-2, but that a significant bone regenerative response is evident after 21 d post-treatment. These results suggest that Cox-2 may need to be expressed continuously over a prolonged time period in order to be able to influence bone formation. On the other hand, BMP may only be required for a much briefer period, during which time the proliferation and differentiation signal has been transmitted to a sufficient number of osteoprogenitor cells in order to assure continued bone formation and closing of the defect.

2. In order to address this question, we will assess the transgene expression levels within the calvarial defect by real-time PCR. Expression levels at 14 and 28 day post-transplantation will be compared to expression in transplanted cells at time 0 and 2 days. This will provide a profile of growth factor expression levels over the course of 28 day post-transplantation that can be related to therapeutic outcomes. Real-time PCR analysis of the persistence of MLV genomic sequences over the course of the experiment will provide a measure of transplanted cell survival and will discriminate between the contribution of gene silencing and cell death to any reduction in growth factor expression. For this purpose, we have designed gene-specific primers and established conditions to measure the presence of transgenes by real time PCR (Figure 7). Experiments are currently in progress aimed at determining the fate of the transplanted cells in the implants by real time PCR and the level and duration of growth factor gene expression by real time RT-PCR. This will be crucial in order to find growth factor combinations that can successfully heal large bone defects.

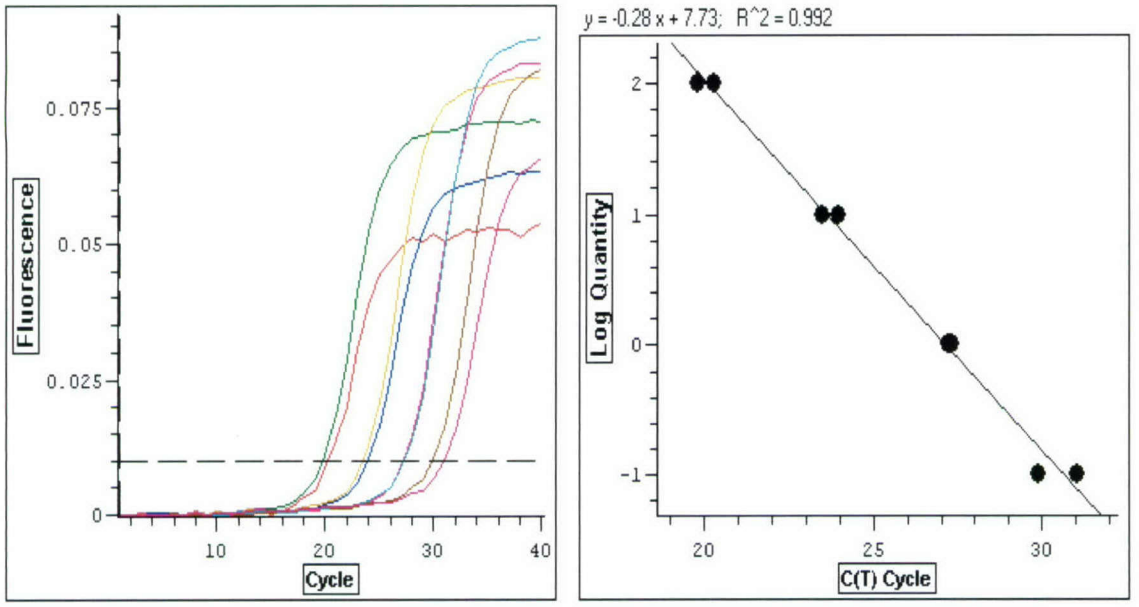

Figure 7: Standardization of real time PCR reaction with genomic DNA from transduced MSC. Cox-2-specific PCR reactions were set up in a final volume of 25 µl with 12.5 µl of 2x Brilliant SYBR Green Master Mix (Invitrogen), 0.75 µl each of 20 nM forward and reverse primers specific for human Cox-2, and DNA template in 2 µl. Nuclease free water (Ambion) was used to adjust to final volume and to solubilize primers and DNA preparations. DNA was prepared from mouse bone marrow stromal cells that had been transduced with MLV-based vector containing the Cox-2 gene. The reaction was performed in a DNA engine Opticon system (MJ Research) with an initial denaturation step of 15 min at 95°C, followed by 40 cycles consisting of 1 min at 95°C, 1 min at 56.4°C, and 1 min at 72°C. The left panel shows fluorescence from PCR product formation in duplicate reactions containing 100ng, 10ng, 1ng, and 0.1 ng of DNA. The right panel shows the standardization generated with the Opticon analysis software.

3. If our experiments indicate that expression of Cox-2 and/or VEGF are not sufficiently high or that expression in the implants declines too fast in order to sustain bone formation, we will explore alternatives that may result in higher activity in implanted cells. Specifically, new implant scaffolds have been described that promote adhesion, growth, and osteodifferentiation of BMDSCs (12). We will evaluate these newly developed carriers for implantation of our gene-modified cells. Otherwise, if we find that Cox-2 and VEGF, expressed at sufficiently high levels for 2 – 4 weeks in the defect, are not effective in promoting bone healing in combination with each other or with BMP-4, we will explore other osteogenic growth factors such as activin for synergistic effects in the healing response.

Key Research Accomplishments

- Cell culture conditions for the growth of mouse bone marrow derived stromal cells (BMDSCs) have been optimized.

- MLV-based retroviral vectors expressing recombinant Cox-2 and VEGF have been constructed.
- BMDSCs have been shown to be efficiently transduced by MLV-based retroviral vectors, and recombinant Cox-2 and VEGF expression has been verified and quantitated *in vitro* over a 4 week period.
- Surgical techniques needed to establish the mouse calvarial critical defect model have been developed.
- Transplantation of BMDSCs expressing recombinant BMP2/4 alone was shown to result in complete healing of critical sized mouse calvarial defects by 4 weeks post-treatment.
- Transplantation of BMDSCs expressing recombinant Cox-2 alone did not promote regeneration of critical sized mouse calvarial defects at either 2 or 4 weeks post-treatment.
- Transplantation of BMDSCs expressing recombinant VEGF alone was shown to increase blood vessel formation at 2 and 4 weeks post-treatment, but did not promote bone formation at either time point.
- Transplantation of mixtures of BMDSCs expressing recombinant BMP2/4 and VEGF, BMP2/4 and Cox-2, and Cox-2 and VEGF did not produce a significant increase in bone formation at 4 weeks post-treatment relative to the impact that each of these growth factors had alone.

Reportable Outcomes

None at the present time.

Conclusions

1) The results of these studies to date provide good evidence that this novel therapeutic approach is technically feasible and can significantly improve bone regeneration in a mouse calvarial model. Bone marrow derived stromal cells (BMDSCs) can be grown to sufficient numbers *in vitro* and are efficiently transduced by MLV-based retroviral vectors resulting in sustained expression of the therapeutic transgene.

2) Most importantly, transplantation of BMDSCs expressing recombinant BMP2/4 was shown to promote complete healing of a critical sized calvarial defect by 4 weeks post-treatment. This result establishes the feasibility of this novel therapeutic approach and demonstrates that all of the critical components of this experimental mouse model for bone regeneration have been successfully established in our laboratory.

3) The absence of a significant increase in bone formation in defects treated with BMDSCs expressing recombinant Cox-2 was unexpected but raises important questions relating to the mechanism of Cox-2 action *in vivo*. This experimental model will be used to systematically investigate ways to optimize the therapeutic impact of Cox-2 (and VEGF) on critical sized calvarial bone defects.

References

1. Gysin R, Wergedal JE, Sheng MH-C, Kasukawa Y, Miyakoshi N, Chen S-T, Peng H, Lau K-HW, Mohan S, Baylink DJ. (2002) *Ex vivo* gene therapy with stromal cells transduced with a retroviral vector containing the BMP4 gene completely heals critical size calvarial defect in rats. Gene Therapy 9:991-999.
2. Tischer E, Mitchell R, Hartman T, Silva M, Gospodarowicz D, Fiddes JC, Abraham JA (1991) The human gene for vascular endothelial growth factor: Multiple protein forms are encoded through alternative exon splicing. J. Biol. Chem. 266:11947-11954.
3. Simovic D, Isner JM, Ropper AH, Pieczek A, Weinberg DH (2001) Improvement in chronic ischemic neuropathy after intramuscular phVEGF165 gene transfer in patients with critical limb ischemia. Arch. Neurol. 58:761-768.
4. Peng H, Chen ST, Wergedal JE, Polo JM, Yee JK, Lau K-HW, Baylink DJ. (2001) Development of an MFG-based retroviral vector system for secretion of high levels of functionally active human BMP4. Mol.Ther. 4:95-104.
5. Hla T, Neilson K (1992) Human cyclooxygenase-2 cDNA. Proc. Natl. Acad. Sci. USA 89:7384-7388.
6. Krebsbach PH, Mankani MH, Satomura K, Kuznetsov SA, Gehron Robey P (1998) Repair of craniotomy defects using bone marrow stromal cells. Transplantation 66:1272-1278.
7. Peng H, Wright V, Usas A, Gearhart B, Shen H-C, Cummins J, Huard J (2002) Synergistic enhancement of bone formation and healing by stem cell-expressed VEGF and bone morphogenetic protein-4. J. Clin. Inv. 110:751-759.
8. Arikawa T, Omura K, Morita I (2004) Regulation of bone morphogenetic protein – 2 expression by endogenous prostaglandin E2 in human mesenchymal stem cells. J. Cell Physiol. 200:400-406.
9. Chikazu D, Li X, Kawaguchi H, Sakuma Y, Voznesensky OS, Adams DJM, Hoshio K, Katavic V, Herschman HR, Raisz LG, Pilbeam CC (2002) Bone morphogenetic protein 2 induces cyclo-oxygenase 2 in osteoblasts via a Cbfa1 binding site: Role in effexts of bone morphogenetic protein 2 *in vitro* and *in vivo*. J. Bone Min. Res. 17:1430-1440.
10. Zhang X, Schwarz EM, Young DA, Puzas JE, Rosier RN, O'Keefe RJ (2002) J. Clin. Invest. 110:1405-1415. Cyclooxygenase-2 regualtes mesenchymal stem cell differentiation into the osteoblast lineage and is critically involved in bone repair.
11. Carvalho RS, Einhorn TA, Lehmann W, Edgar C, Al-Yamani A, Apazidis A, Pacicca D, Clemens TL, Gerstenfeld, LC. (2004) The role of angiogenesis in a murine tibial model of distraction osteogenesis. Bone 34:849-861.
12. Blum JS, Barry MA, Mikos AG, Jansen JA (2003) *In vivo* evaluation of gene therapy vectors in *ex vivo*-derived marrow stromal cells for bone regeneration in a rat critical-size calvarial defect model. Human Gene Therapy 14:1689-1701.

Project 8: Nuclear Targeting Of Transposon-Based Plasmid Vectors For Gene Therapy

Introduction

Our primary research objective is to develop improved nonviral plasmid vectors for *in vivo* applications in hard and soft tissues by incorporating into a single vector both a nuclear entry sequence to increase transfection efficiency and a transposase to increase long term transgene expression. Plasmid vectors will provide a safer, less expensive and more easily manufactured reagent for gene delivery compared to viral vectors, but have not been widely used for *in vivo* applications because of several cellular barriers to *in vivo* transfection and transgene expression. These barriers include plasmid entry into the cell, subsequent entry into the nucleus and, for long term expression, stable transgene integration into transfected cell genomic DNA. After entering cells, traditional plasmids enter the nucleus during mitosis, so transfection efficiency is dependent on active cell proliferation. We and others have identified nuclear entry DNA sequences such as the SV40 DTS that enhance nuclear entry of plasmid DNA and increase *in vivo* transfection efficiency and transgene expression levels even in non-proliferating cells (1-7). Traditional plasmid DNA integrates into genomic DNA randomly and inefficiently. To improve efficiency of integration, we have also developed a plasmid vector that expresses a mammalian transposase, *Sleeping Beauty* (SBT), in addition to the transgene of interest. The transposase facilitates transgene integration into AT-rich regions of genomic DNA, resulting in high levels of long term expression (8). No plasmid vector has been developed that incorporates both a nuclear entry sequence and transposase expression. We propose that our enhanced plasmid expression vectors will significantly increase transfection efficiency and transgene integration, resulting in higher levels of long term therapeutic gene expression *in vivo* than are possible with existing nonviral gene therapy vectors. Our studies are designed to prepare new plasmid vectors with nuclear entry activity, a transposon/transposase and either a marker gene or the BMP-2/4 gene as a therapeutic.

Body

Technical Objectives

Develop and test a novel nonviral protein expression vector for use in gene therapy. The plasmid will contain DNA sequences to: a) increase movement of the plasmid DNA into the nucleus and thus increase immediate transfection efficiency and expression levels; and b) produce a transposase to increase stable vector DNA integration into genomic DNA, thus increasing long term maintenance of transgene expression.

Our specific objectives during the first 12 months of this grant period were to:

1. optimize the design of the new vector (SV40 DTS/SBT) which is based on the structure of the Prince Charming (pPC) vector for maximum transfection efficiency and long term expression in cultured cells.
2. insert the Nuclear Entry Sequence from the SV40 DNA virus (SV40 DTS) into different positions of an optimized plasmid vector that can express the sleeping beauty transposase (SBT) and a marker gene, Red Fluorescent Protein (RFP).

3. compare expression levels and longevity of marker genes *in vitro* in rat bone marrow stromal cells (MSCs), and osteoblasts transfected with the SBT/SV40DTS plasmid vectors or transduced with a MLV retroviral reporter gene vector for comparison.
4. prepare SBT/SV40DTS plasmid and MLV retroviral vectors to express human BMP-4, and test BMP-4 short term expression levels in transfected/ transduced rat MSC cultures.

Progress toward each specific objective described below reflects the work of only one technician because a suitable post doctoral fellow was not found. While significant progress was made, completion of the remaining work on the objectives above and completion of the second year objectives will require the work of two technicians. We have trained technical personnel to facilitate vector construction and *in vivo* studies for year two.

Progress on Specific Objectives

Specific Objective 1:

To optimize the design of the new vector with a SV40 DTS and Sleeping Beauty Transposase (SBT) which is based on the structure of the Prince Charming (pPC) vector for maximum transfection efficiency and long term expression in cultured cells.

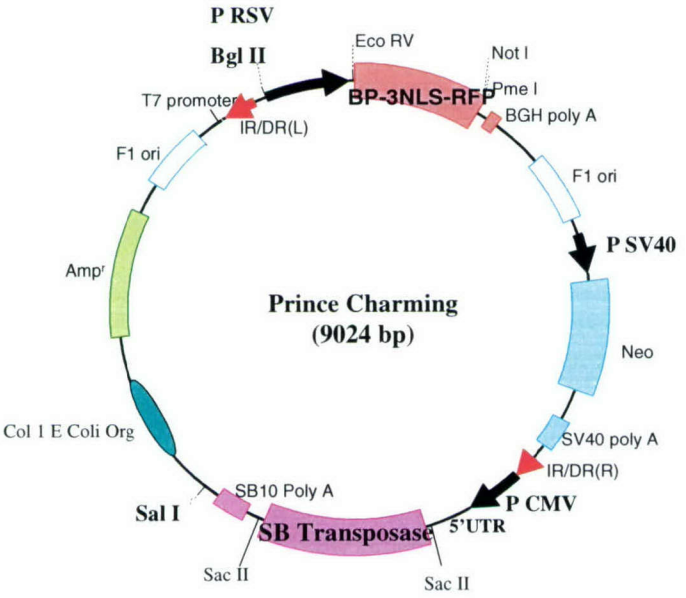

Figure 1. Structure of the Prince Charming (pPC) plasmid vector. The pPC plasmid vector contains three eukaryotic promoters: a gene for selection, a Sleeping Beauty (SB) transposon with a transgene and a SB transposase expression cassette. In the pPC vector, the Sleeping Beauty transposase (SBT) and (IR/DR) repeats flanking the transgene are required for chromosomal integration of the marker gene. A nuclear localization signal (NLS) peptide from the Insulin-like growth factor Binding Protein (BP)-3 gene was fused to the amino terminus of red fluorescent protein (RFP) to concentrate the fluorescent fusion protein in the nucleus. The marker transgene was driven by the Rous Sarcoma Virus promoter (P RSV). The Neomycin expression cassette driven by the SV40 promoter (P SV40) was intregrated with the BP3-NLS-RFP gene because of its positioning between the inverted transposon repeats. Neomycin resistance was used to select expressing cells with G418 because of the low transfection efficiency demonstrated by this vector. The Col1E. *Coli* origin and Amp resistance (Amp^r) gene are required for expression and selection in bacteria.

i) Reduction in size of the Prince Charming (pPC) expression vector. The 9 kb "pPC" vector contains a Transposon with inverted repeats flanking a reporter protein expression cassette and a SB transposase outside the inverted repeats driven by the CMV promoter (Figure 1). The reporter protein is a fusion protein consisting of Red Fluorescent protein (RFP) fused to a nuclear localization signal (NLS) from IGF binding protein-3 (BP-3NLS-RFP). The RFP fluorescence is confined to the nucleus, which reduces the toxicity of the RFP and increases the number of cells expressing this transgene. The inverted repeat sequences on both sides of the BP-3NLS-RFP sequence allow for efficient genomic integration of the transgene when SBT is expressed. The vector also contains a Neomycin resistance gene (driven by an SV40 promoter) to allow for selection of cells expressing the protein.

Because large plasmids (>7 kb) are difficult to transfect into cells without antibiotic selection, the first step in creating a better plasmid vector that would not require selection after *in vivo* gene delivery would be to reduce its size. In addition, nuclear entry and transposon technology can be used to increase transfection efficiency (>50% of cells) even more, making antibiotic selection of cells expressing the transgene unnecessary.

The (2 kb) Neomycin resistance gene expression cassette and second F1 origin was removed by PCR using the primers aggcaatgctaccaaatactaat and tcccggggttctttccgcctcagaagc (a unique Sma I site was introduced into the vector with this primer set). A 7 kb plasmid was obtained (Figure 2). The Bgl II, Sma I and Sal I sites are unique.

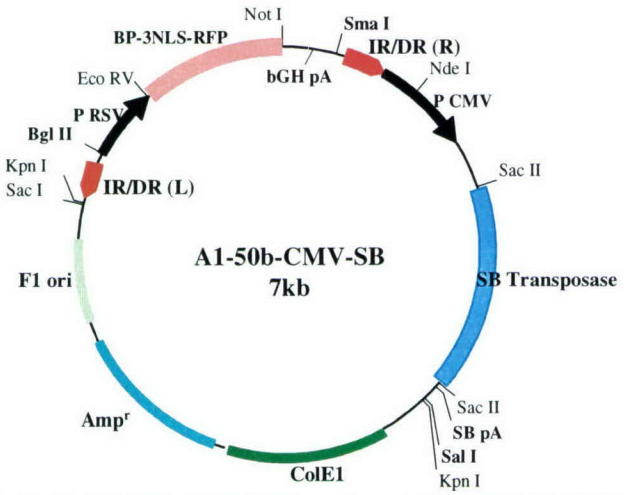

Figure 2. Structure of the 7 kb A1-50b-CMV-SB vector with BP3 NLS-RFP marker gene. The 9 kb pPC vector containing the BP-6- NLS-RFP fusion protein (Figure 1) was modified to remove the Neo cassette and the second F1 ori by PCR. The resulting 7 kb vector contains the transgene (BP-3NLS-RFP) located between the transposon repeats, IR/DRs (red pointed box). The SB transposase is located outside the IR/DR repeats so that the transposase is not integrated into the host cell genome. This increases the safety of the vector for gene therapy applications. This vector is ready to receive the 87 bp SV40 DTS (Figure 5) in the Bgl II, Sma I or Sal I unique restriction sites.

ii) Effect of size reduction on transfection efficiency. It was anticipated that the reduction in size from 9 to 7 kb would increase transfection efficiency. To test this, rat ROS 17/2.8 and human SaOS-2 cells were transfected with 1-3 ug of DNA and Effectene (Qiagen) in 6 well plates as suggested by the manufacturer. The cell contents of two wells were trypsinized, combined and 10,000 cells were counted. The number of fluorescent cells within the 10,000

counted is illustrated in Figure 3. In ROS cells, the transfection efficiency with the pPC vector was 7-15% of cells transfected at 48 hr and from 6-10% at 120 hours after transfection. Importantly, the transfection efficiency with the A1-50b vector was 26-28% at 48 h and 22-26% after 120 h. This preliminary experiment indicates that this method can be used to determine the effect of each plasmid manipulation on transfection efficiency and that efficiency increased after reducing plasmid size.

When the SV40 dts is inserted in the A1-50b vectors, this assay will be performed with 6 replicate wells with ~2 ug of plasmid DNA. Equivalent amounts of the pPC, A1-50b, and A1-50b-SV40 dts will be compared. The number of fluorescent cells in each well will be determined and the significance of the vector change on transfection efficiency will be determined.

In the more difficult to transfect SaOS-2 cells, the transfection efficiency with the pPC vector ranged from 5-7% at 48 hr and 3-4% at 120 hr. The transfection efficiencies with the A1-50b vector were 15-17% at 48 hr and 9-11 % at 120 h. The preliminary results of these experiments suggest that plasmid size reduction increases transfection efficiency.

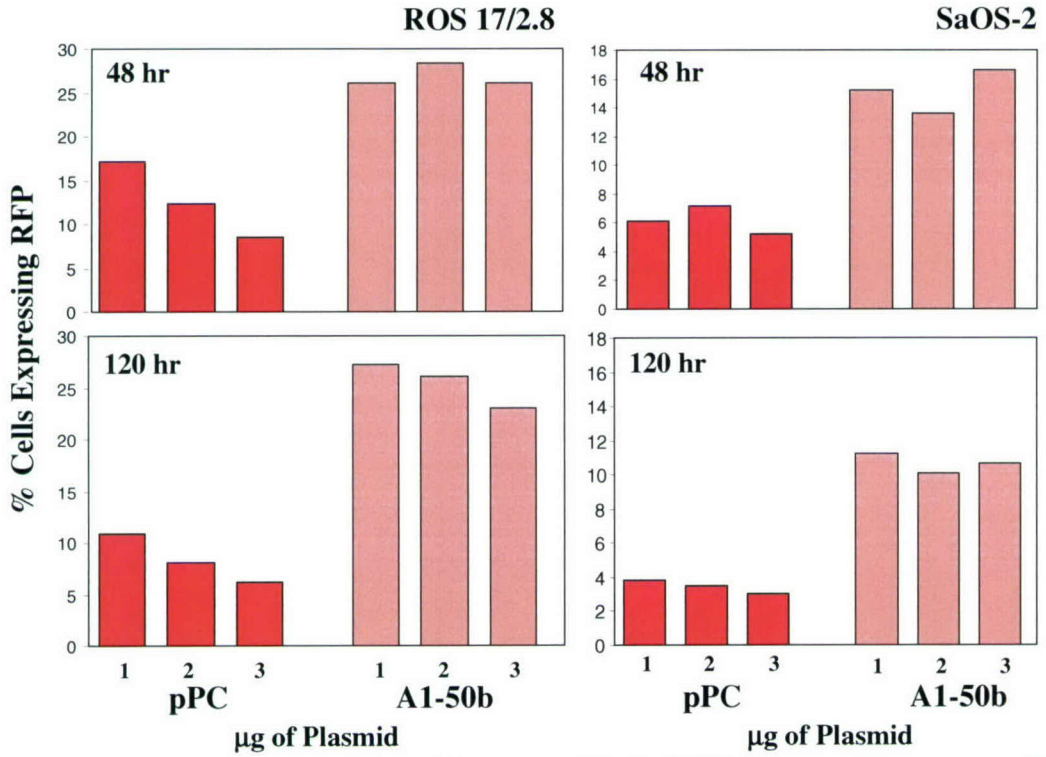

Figure 3. Transfection efficiency of plasmid vectors with the SB Transposon/Transposase. The transfection efficiency in ROS 17/2.8 rat and SaOS-2 human osteoblasts for two plasmid vectors with the SB Transposon/Transposase was compared. The pPC is a 9 kb vector with the Neomycin resistance expression cassette and the A1-50b vector is a modified pPC vector with the Neomycin resistance cassette and second F1 origin removed. Based on work in our laboratories and others, it was proposed that reducing the size of the pPC vector would increase transfection efficiency. Transfection efficiency was measured at 48 and 120 hrs after transfection by FACS analysis. Red Bars (black) represent the percentage of fluorescent cells after transfection with the pPC vector and the pink bars (grey) represent the percentage of fluorescent cells after transfection with the A1-50b vector. From 1-3 ug of plasmid DNA was transfected with Effectene in 6 well plates as described by the manufacturer.

iii) Modification of the SB Transposase expression cassette. A recent publication (9) indicated that some promoters used to drive SB transposase expression do not function well to provide long term transgene expression in liver tissue. It was found that the relative strength of different promoters expressed in mouse liver did not correlate with the amount of stable transgene expression. Peak levels of long term gene expression were obtained with promoters 30-40 fold less active than the CMV promoter. By correlating the relative strength of the promoter driving transposase production with levels of short term and stable transgene expression, a narrow window of optimal transposase expression could be defined. The investigators concluded that successful *in vivo* transposition may depend primarily on a narrow window of SB transposase concentration obtained shortly after plasmid injection, and that overproduction of transposase can cause inhibition of long term transgene expression (9). Different promoters driving SB transposase expression supported transposition and establishment of stable long term gene expression (7 to 122 days after high pressure injection of plasmid DNA) based on the following hierarchy: Phosphoglycerate kinase > inducible metallothionein> elongation factor 1 alpha > transthyretin > albumin >dihydrofolate reductase, promoterless cassette> CMV. All plasmid vectors that had both the SB transposon with the transgene and the SB transposase expression cassette on the same vector, except those with CMV-directed transposase production or without a promoter, induced levels of persistent expression of the transgene in liver cells.

The pPC vector has been constructed with the CMV promoter to drive SB transposase activity and thus might not be optimal for gene delivery in liver and other tissues. Our original grant was written without this information and we proposed to use the CMV promoter and the EF1α promoter to drive transposase activity. On the strength of our research since that time, we have modified this aim to use a promoter that is not expressed as strongly as the CMV promoter so that inhibitory levels of the SB Transposase are not produced in cells after plasmid vector delivery. We wanted to choose a promoter system that we could easily manipulate to alter SB transposase expression levels to be optimum in each cell type and provide for cell specific transgene production. We anticipated that by developing the weakly expressed minimal Thymidine Kinase (TK) promoter together with viral or tissue specific enhancers, we could both modulate the level of transposase expression and also provide for tissue specific expression by using different tissue specific enhancers. Tissue specific expression would also increase the safety of the plasmid vectors developed for clinical use. Thus, we have modified our vector design to include the TK promoter in the SB transposase expression cassette together with the CMV-SB transposase expression cassette that we had already prepared.

To prepare this TK promoter-based SB transposase expression cassette, we obtained the pTAL-Luc vector from Clontech/BD. In this vector, the minimal TK promoter is flanked on the 5' end by a multiple cloning site (Kpn I, MluI, NheI, XhoI, and Bgl II) to accept viral or tissue specific enhancers. The Nhe I site will be unique to the A1-50b vector and the Bgl II enzyme will also be unique to the A1-50b vector if the SV40 DTS is inserted into the existing Bgl II site as proposed. We inserted an optimized Kosak sequence (GCCGCCATG) into the SB transposase coding region to optimize protein expression. The insert was made by PCR with the forward primer gactagtgccgccatgggaaaatcaaaagaaatcagcc and reverse primer gatcgatgaatgcaattgttgttgttaact containing a Cla I site after the SB polyadenylation signal, using the pPC vector as a template. The PCR product was cloned into the PCR4Blunt Topo vector from Invitrogen. The optimized SB Transposase was removed from the vector with Eco RI, blunted with Klenow and inserted in the pTAL-Luc vector at the Hind III site by blunt-end

ligation. This positioned the SB Transposase cDNA downstream of the TK promoter and start of transcription. A fragment containing the multiple cloning site for introduction of enhancers, the TK promoter, SB Transposase coding region and the poly A signal were removed as a single 1.2 kb fragment with Cla I. The SB transposase expression cassette (CMV promoter, natural SB transposase Kosak sequence, coding region and pA (polyadenylation signal) was removed from the A150b-CMV-SB vector (Figure 2) with Nde I and Sal I. The vector was blunt-end ligated to the blunted Cla I fragment with the TK promoter. The structure of the resulting vector is illustrated in Figure 4. We are in the process of sequencing A1-50b clones that may contain the modified SB-transposase expression cassette. This modification of the A1-50b vector further reduced the size of the vector by 663 bp.

Once the sequence of this vector construct is confirmed, the A1-50b-CMV-SB (strong promoter, weak Kosak signal) and A1-50b-TK-SB (weak promoter, strong Kosak signal) vectors will be transfected into ROS 17/2.8 and SaOS-2 cells and RFP expression will be assessed by FACS analysis. It is anticipated that the longevity and level of expression will be increased in A1-50b-TK-SB cells compared to A1-50b-CMV-SB transfected cells. We will remove the SB cDNA coding region in the vectors to demonstrate the positive effect of SB Transposase on transfection efficiency and expression.

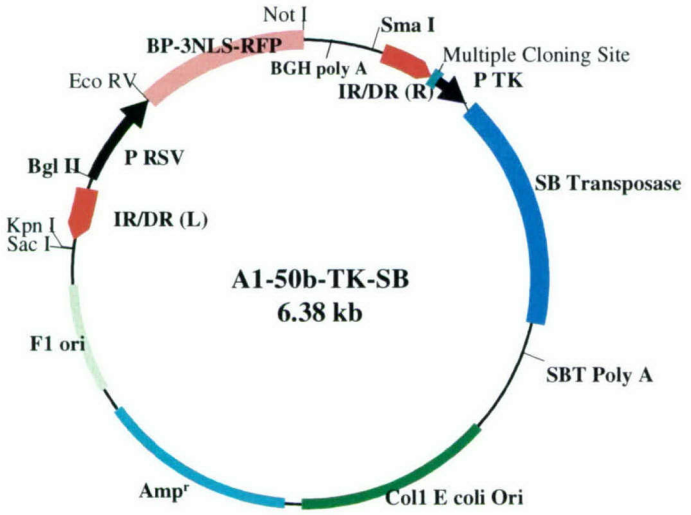

Figure 4. Structure of the A1-50b-TK-SB vector. The 6.38 kb modified pPC vector contains the BP3NLS-RFP expression cassette within the inverted repeats (IR/DRs). Weak constitutive expression of the SB Transposase is driven by the TK promoter. An enhancer can be placed in the multiple cloning site using the unique Nhe I site. A modified Kosak sequence was added to the SB Transposase cDNA to increase protein expression.

iv) Preparation of the rat type I alpha 1 procollagen promoter for RSV promoter replacement to provide osteoblast specific transgene expression. In the original grant, we proposed the preparation of a Sleeping Beauty-based plasmid vector that would support transgene expression only in osteoblasts even though the SB transposase cassette was expressed in all cell types and would lead to transgene integration. The application for this type of vector would be used in stem cells or marrow stromal cells which do not express the osteoblast phenotype and would not express the transgene until the cells mature into osteoblasts. *Ex vivo*

gene therapies with stem cells harboring transgenes driven by an osteoblast promoter would be activated only in cells that have migrated to the proper location and matured. This application would increase the safety of the plasmid vector for clinical applications.

We proposed to use the type I procollagen promoter to drive a transgene so that specific expression would occur in osteoblast lineage cells. The rat type I procollagen promoter in a CAT reporter vector was obtained from David Rowe (10) for this application. The promoter was placed in the $pGL3_{Basic}$ luciferase vector and tested for activity in osteoblasts. This promoter was actively expressed in rat ROS 17/2.8 cells (data not shown). The promoter can be removed from the $pGL3_{Basic}$ reporter vector to replace the RSV promoter in the A1-50b-CMV-SB or A150b-TK-SB vector (Figure 2 and 4) after the optimal SB Transposase cassette is identified and the optimum position of the SV40 DTS is determined.

Specific Objective 2:

To insert the Nuclear Entry Signal from the SV40 DNA virus (SV40 DTS) into different positions of an optimized plasmid vector that can express the sleeping beauty transposase (SBT) and a marker gene, Red Fluorescent Protein (RFP).

i) Preparation of the SV40 DTS fragment.The SV40 DTS (Figure 5) has been successfully subcloned into the $pGL3_{Basic}$ and the peGFP (Clontech) vectors for other studies. Large quantities of this fragment can be removed from the $pGL3_{Basic}$ vector with Sma I for blunt end ligation into the unique Sma I site of the A1-50b vector or with Bgl II for sticky end cloning into the unique Bgl II site in this vector. We have not been able to clone the SV40 DTS into the A1-50b vector in a forward orientation using blunt end ligation. We have cloned the SV40DTS into other vectors after numerous attempts and condition changes with either blunt-end ligation or sticky end ligation. Therefore, we know that the small fragment can be inserted into plasmid vector given enough time and we will continue to try to introduce this fragment in the forward orientation into the A1-50b vectors.

ATGCTTTGCATACTTCTGCCTGCTGGGGAGCCTGGGGACTTTCCACACCCTAACTGACACACA
TTCCACAGCTGGTTGGTACCTGCA

Figure 5. Structure of the SV40 nuclear entry sequence (SV40 DTS). The 87 bp SV40 early promoter sequence is indicated and has been released from several plasmid vectors constructed for other studies with Sma I for blunt end ligation or Bgl II for sticky end ligation into the A1-50b vectors.

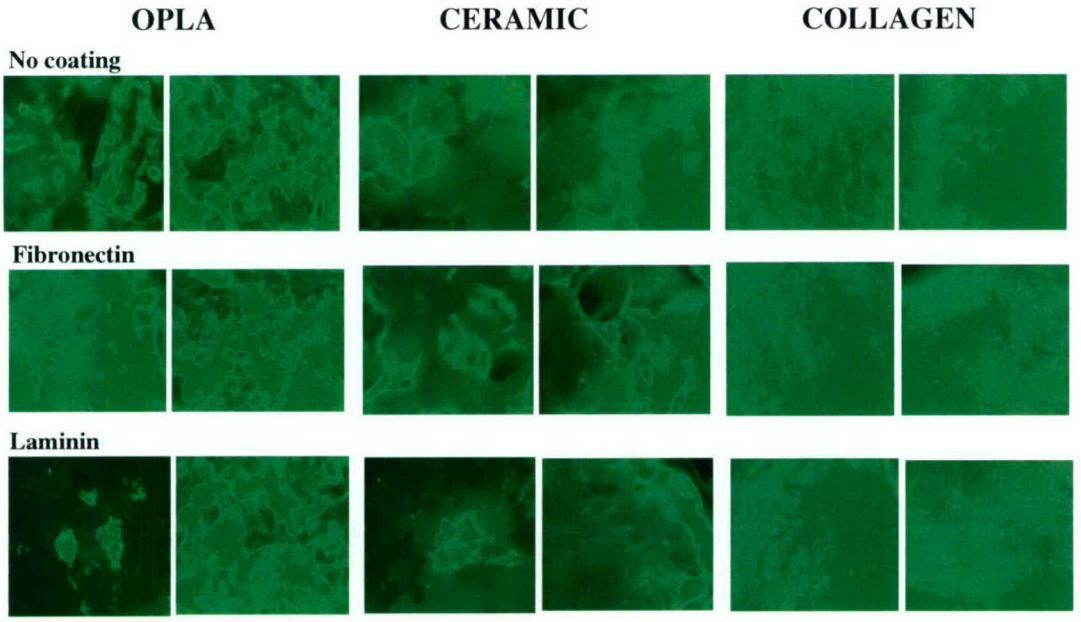

Figure 6. Cell viability and marker gene expression of rat MSCs on different support chips that could be used for implant studies. Rat marrow stromal cells (10^4) transduced with MLV-GFP virus were applied to three different solid supports (OPLA, Ceramic or Collagen) and were grown for three weeks in culture media (DMEM/10% CS) in 6 well plates with frequent media changes. GFP expression was viewed by epifluorescent microscopy. Patchy expression of GFP was noted especially on the Ceramic and OPLA chips in the first two weeks, while many more GFP expressing cells were noted on the collagen supports at all time points (data not shown). At week three, the collagen support contained the largest number of cells that expressed GFP compared to other supports. Cells grew and expressed the transgene with or without coating this support with fibronectin or laminin. One of two separate experiments is shown and the two photographs represent different areas on the same chip at three weeks.

Specific Objective 3:

To compare expression levels and longevity of marker genes *in vitro* in rat bone marrow stromal cells (MSCs), and osteoblasts transfected with the SBT/SV40DTS plasmid vectors or transduced with a MLV retroviral reporter gene vector.

i) **MSC culture and transduction**.We have prepared and cultured rat bone marrow stromal cells (MSCs) that express GFP after transduction with the MLV-GFP viral vector prepared by our Viral Vector Core facility. The cells stably express the GFP marker gene when cultured for several weeks as monolayers. When the plasmid vectors are constructed that contain both the SB transposase and the SV40 DTS, expression of marker genes from cells transduced with viral vector or transfected with plasmid will be compared by FACS analysis in cells grown as monolayer cultures for three weeks or more. We have cultured virally transduced MSCs expressing GFP for 3-4 weeks as monolayer cultures and found that GFP was expressed by 80% of the cells. We will use the BP3-NLS RFP transgene in both the viral and plasmid vectors to determine if cells carrying the SV40 DTS/SBT plasmid vector express transgene as long and as robustly as the viral vector. The MLV-BP3NLS-RFP viral vector is available in the Vector Core Facility for these experiments.

To determine if the virally transduced cells expressing GFP were viable and continue to express the transgene, MSCs were transduced with MLV-GFP. The cells were grown in

monolayers for several weeks and then were seeded onto several types of solid supports. The supports were made of collagen, OPLA or Ceramic (calcium phosphate). Some of the supports were coated with fibronectin or laminin protein used by others to enhance cell attachment and viability (11-14). The GFP-MSCs were placed on solid supports to assess cell viability and expression of the GFP marker gene in a system that can be used for *in vivo* studies. Cells were grown in culture on the supports for three weeks with media changes. GFP expressing cells on the supports were viewed weekly. Cells grew on the collagen supports more quickly than the other supports. At three weeks, all of the supports had GFP producing cells (Figure 6). However, the supports that were not coated did not sustain as many cells as the coated supports. This difference in cell number is indicated by the total amount of RNA isolated from one support chip (Table 1). The Fibronectin coated support chips appear to contain more cells than the other supports (Table 1 and Figure 6). From this work, any of the supports can be used for *in vivo* studies. If the all of the supports and coatings are not antigenic when placed under the skin for 28 days, than we will choose to use the fibronectin coated collagen support for year two studies.

Table 1. Isolation of total RNA from rat marrow stromal cell coated solid supports.

Sample/Support	**Amount of Total RNA (ng)/Chip**
OPLA	368
Ceramic	356
Collagen	383
OPLA/Fibronectin	455
Ceramic/Fibronectin	500
Collagen/Fibronectin	487
OPLA/Laminin	424
Ceramic/Laminin	427
Collagen/Laminin	459

ii) **RNA isolation and preparation of cDNA from rat MSCs on scaffolds**. RNA was isolated from one 3 mm^3 support chip using the "Absolutely RNA" kit from Stratagene. The amount of total RNA isolated from each chip is summarized in Table 1. Varying amounts of RNA were isolated from each type of support. More RNA was obtained from the fibronectin coated supports than from the uncoated or laminin coated supports. On the basis of cell growth, the ceramic or collagen coated chips support the best cell growth *in vitro*. The amount of RNA from one chip was adequate to make cDNA to analyze several mRNAs by Real-time PCR multiple times.

The cDNA was prepared with 15-20 ng of total RNA, 1 ul (5 uM) oligo dt 12-18 primer mix (IDT) and 1 ul of dNTP (10 mM) master mix. RNA was heated to 65 C for 5 minutes and at 4 C for 1 minute before adding 1 ul (200 units) of Superscript III (Invitrogen) reverse transcriptase, 4 ul 5 X first strand buffer mix (250 mM Tris HCl (pH 8.3 at RT), 375 mM KCl, 15 mM $MgCl_2$), 1 ul of 0.1 M DTT and 1 ul of RNAse Out, recombinant RNAse inhibitor (Invitrogen) to a 20 ul total reaction volume. After mixing, the solution was incubated at 50 C for 30 minutes and at 70 C for 15 minutes to inactivate the enzyme. After incubating the samples at 4 C for 2 minutes, 1 ul of RNAse H was added and incubation was continued for 20 min at 37 C. cDNA was made in a Minicycler from MJ Research. Samples were removed and stored at –20 C until use.

Table 2. Primer sets developed for Real Time PCR analysis of mRNA levels.

Gene	Accession #	Primer Sequence	Size of Product	Tm Amplification
cyclophilin	BC059141	gcatacaggtcctggcatct gctctcctgagctacagaag	281	56.4
Type I α2 procollagen 3333-3677	AF121217	gtgtcagcggaggaggctat gcacggctgtatgcattctt	344	56.4
Osteopontin 697-940	RATOSP	gaagaccagccatgagtcaag cttgtcctcatggctgtgtgaa	243	56.4

iii) **Real-Time PCR assay for osteoblast marker genes.** MSCs that are attached to a scaffold have previously been shown to undergo differentiation into mature osteoblasts that produce bone (15). To analyze bone formation from cells attached to the scaffolds that we will test *in vitro* and *in vivo*, the mRNA levels of a number of osteoblast marker genes will be analyzed. The osteoblast marker genes will be divided into categories that reflect several stages of differentiation. One gene expressed early in the differentiation process is type I procollagen (when preosteoblasts are in the proliferative stage, genes expressed at the onset of mineralization include ALP and SPARC/osteonectin, while genes expressed during the later mineralization stage include osteocalcin, and osteopontin). We will access the expression of these genes in solid supports *in vitro* and *in vivo*. Histological assessment of the solid supports for collagen production and ALP activity will confirm some of our mRNA analysis data. Preliminary analysis of expression of the type I procollagen, osteopontin and cyclophilin mRNAs have been conducted using *in vitro* cultures of cells on solid supports. Table 2 shows the primer sets that were used to assess the osteoblast phenotype of MSCs seeded on the solid supports visualized in Figure 6.

Table 3 provides the preliminary data from quantitative (q) RT-PCR analysis of RNA from support chips to develop and validate this method to measure osteoblast marker gene expression on chips after skin implant. Cycle thresholds of quadruplicate samples were determined from Real Time PCR products generated from cDNA (~1 ng) prepared from total RNA from cells on one of the support chips. Cyclophilin thresholds were determined and the cyclophilin C_T values were subtracted from C_Ts from either type I collagen or osteopontin to normalize for differences in cDNA starting material. Collagen and osteopontin mRNAs were expressed at high levels in the cells on all of the supports. In this preliminary study, cells from the collagen support coated with fibronectin make higher levels of osteopontin than the uncoated or laminin coated support. If osteopontin expression is more indicative of the osteoblasts in the mineralization, bone forming stage of differentiation and collagen more indicative of cells in a less mature proliferating phenotype, then this result suggests that the collagen support coated with fibronectin would be the best to use for the implant model to increase bone formation. When the *in vivo* experiments are initiated, bone formation in the solid supports will be studied more extensively by qRT-PCR and by histology (ALP activity staining and von Kossa staining).

Table 3. Expression of the osteoblast phenotype in MSCs attached to different supports.

Solid Support	ΔC_T Collagen	ΔC_T Osteopontin
Collagen	-2.28	2.14
Collagen coated with fibronectin	-2.56	3.13
Collagen coated with laminin	-4.04	1.99

C_T (cycle threshold) values for collagen and osteopontin were determined in quadruplicate and normalized to C_T values for cyclophilin also determined in quadruplicate. The normalized values are expressed as ΔC_Ts. Negative ΔC_T values indicate that expression of collagen mRNA was higher than cyclophilin mRNA expression.

These preliminary data demonstrate that adequate amounts of RNA can be obtained from cells on the implant supports to assay expression of a number of osteoblast marker genes. We will develop and test primers for alkaline phosphatase, osteocalcin and SPARC/osteonectin for the proposed *in vitro* and *in vivo* studies.

Specific Objective 4:

Prepare SBT/SV40DTS plasmid and MLV retroviral vectors to express human BMP-4, and test BMP-4 short term expression levels in transfected/ transduced rat MSC cultures.

i) **Preparation of a Retroviral BMP-2/4 vector**. The PY-BMP2/4 retroviral vector has been prepared so that virus can be produced when plasmid vectors are ready. The vector is illustrated in Figure 7.

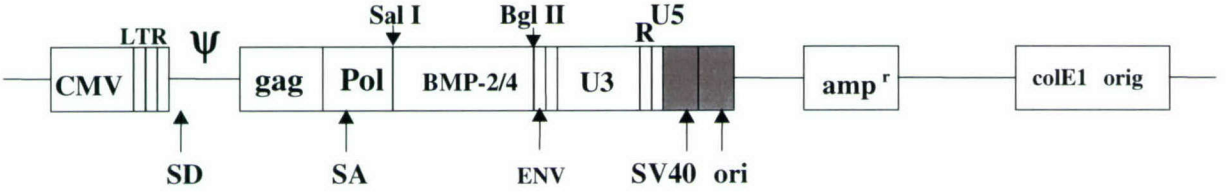

Figure 7. Structure of the pCLSA-MFG based BMP-2/4 retroviral vector. Virus was prepared in 293T cells with this vector as described in (1). The 1.3 kb cDNA contains the coding region for BMP-2/4. BMP-4 is secreted by cells transduced with this vector.

ii) **Preparation of the BMP-2/4 vector.** The A1-50b-CMV-SB-BMP2/4 vector has been prepared. The SV40 DTS must be introduced into this vector before the expression profiles of the viral and plasmid vectors can be compared. To prepare the 1.3 kb cDNA was removed from the pCLSA-MFG-BMP-2/4 vector with Sal I and Bgl II. The ends were filled in with Klenow. The A1-50b-CMV-SB vector was digested with Eco RV and Not I. The Not I ends were filled in with Klenow. The BMP-2/4 fragment was ligated into the A1-50b-CMV-SB vector in place of the BP3-NLS-RFP cDNA. The resulting vector is illustrated in Figure 8. The A1-50b-TK-SB vector with an SV40 DTS sequence will also be prepared.

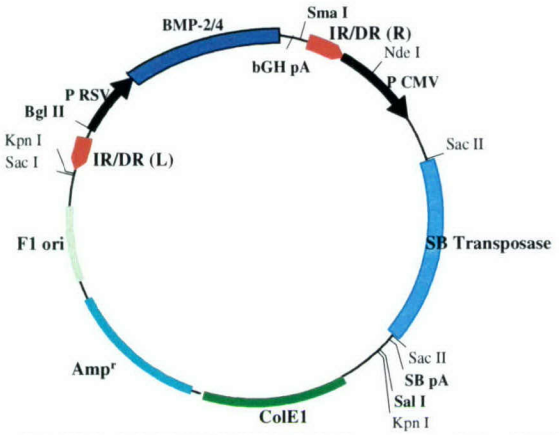

Figure 8. Structure of the A1-50b-CMV-SB-BMP-2/4 vector. The 1.3 kb BMP-2/4 cDNA was inserted in place of the 749 bp BP-3 NLS RFP cDNA in the A1-50b-CMV-SB vector in Figure 2. The 7.6 kb vector was sequenced to confirm the position of the BMP-2/4 protein coding region. The SV40 DTS will be inserted in the Sma I, Bgl II or Sal I site corresponding to the site.

Key Research Accomplishments:

- We have prepared the following enhanced plasmid vectors that express the sleeping beauty transgene and a marker gene or BMP-2/4:
  - A1-50b-CMV-SB-BP-3NLS-RFP
  - A1-50b-TK-SB-BP-3NLS-RFP
  - A1-50b-CMV-SB-BMP2/4

- We have shown that size reduction of the pPC vector results in an increase in transgene expression.

- We have determined the type of solid support that we will use in year two studies for the implant model. The collagen support coated with fibronectin supported cell growth and transgene expression better than ceramic or OPLA supports.

- We have shown that the MLV-GFP marker transgene in rat marrow stromal cells was expressed after viral transduction for at least three weeks on all of the solid supports tested.

- We have developed quantitative Real-time PCR assays for type I alpha 2 procollagen, osteopontin and cyclophilin to follow osteoblast maturation and bone formation in marrow stromal cells attached to solid supports. These assays will be used to access bone formation by cells harboring the BMP-2/4 transgene in viral or nonviral vectors on supports used in the implant model proposed in year two.

Reportable Outcomes

We have developed new plasmid vectors with higher transfection efficiencies that can be used for gene delivery and expression. Year two studies will demonstrate the utility of these

vectors compared to viral vectors for *in vivo* applications. These results will be presented at National meeting and will be published.

Conclusions

1) We have modified and reduced the size of the pPC plasmid vector to increase transfection efficiency and express the Sleeping beauty Transposase. These vectors also retain unique restriction sites for introduction of nuclear entry sequences.

2) It was recently reported that the level of SB Transposase expression in cells containing the Sleeping Beauty System is one of the most important aspects of using these vector systems. To address this, we have rebuilt the Sleeping Beauty Transposase expression cassette so that the promoter that drives its expression can be adapted for low levels of expression in all cell types or low levels of tissue specific expression with the use of tissue specific enhancers and the minimal Thymidine Kinase (TK) Promoter.

3) We have identified the best solid support and cells (marrow stromal cells) to use for the *in vivo* studies described in year two for the implant model.

References

1. Young JL, Benoit JN, Dean DA 2003 Effect of a DNA nuclear targeting sequence on gene transfer and expression of plasmids in the intact vasculature. Gene Ther 10:1465-70
2. Li S, MacLaughlin FC, Fewell JG, et al. 2001 Muscle-specific enhancement of gene expression by incorporation of SV40 enhancer in the expression plasmid. Gene Ther 8:494-7
3. Dean DA, Dean BS, Muller S, Smith LC 1999 Sequence requirements for plasmid nuclear import. Exp Cell Res 253:713-22
4. Vacik J, Dean BS, Zimmer WE, Dean DA 1999 Cell-specific nuclear import of plasmid DNA. Gene Ther 6:1006-14
5. Wilson GL, Dean BS, Wang G, Dean DA 1999 Nuclear import of plasmid DNA in digitonin-permeabilized cells requires both cytoplasmic factors and specific DNA sequences. J Biol Chem 274:22025-32
6. Dean DA, Byrd JN, Jr., Dean BS 1999 Nuclear targeting of plasmid DNA in human corneal cells. Curr Eye Res 19:66-75
7. Dean DA 1997 Import of plasmid DNA into the nucleus is sequence specific. Exp Cell Res 230:293-302
8. Ivics Z, Hackett PB, Plasterk RH, Izsvak Z 1997 Molecular reconstruction of Sleeping Beauty, a Tc1-like transposon from fish, and its transposition in human cells. Cell 91:501-10
9. Mikkelsen JG, Yant SR, Meuse L, Huang Z, Xu H, Kay MA 2003 Helper-Independent Sleeping Beauty transposon-transposase vectors for efficient nonviral gene delivery and persistent gene expression in vivo. Mol Ther 8:654-65
10. Dacic S, Kalajzic I, Visnjic D, Lichtler AC, Rowe DW 2001 Col1a1-driven transgenic markers of osteoblast lineage progression. J Bone Miner Res 16:1228-36
11. Ohgushi H, Dohi Y, Yoshikawa T, et al. 1996 Osteogenic differentiation of cultured marrow stromal stem cells on the surface of bioactive glass ceramics. J Biomed Mater Res 32:341-8

12. Ito Y, Tanaka N, Fujimoto Y, et al. 2004 Bone formation using novel interconnected porous calcium hydroxyapatite ceramic hybridized with cultured marrow stromal stem cells derived from Green rat. J Biomed Mater Res 69A:454-61
13. Knabe C, Ostapowicz W, Radlanski RJ, et al. 1998 In vitro investigation of novel calcium phosphates using osteogenic cultures. J Mater Sci Mater Med 9:337-45
14. Livingston T, Ducheyne P, Garino J 2002 In vivo evaluation of a bioactive scaffold for bone tissue engineering. J Biomed Mater Res 62:1-13
15. Lennon DP, Haynesworth SE, Young RG, Dennis JE, Caplan AI 1995 A chemically defined medium supports in vitro proliferation and maintains the osteochondral potential of rat marrow-derived mesenchymal stem cells. Exp Cell Res 219:211-22

C. SUPPORT SERVICE FACILITIES
Project 9: Administrative Support Service

Introduction

The research proposed in this application will be performed within the Musculoskeletal Disease Center (MDC), which is a large, multi-disciplinary research center consisting of more than 70 scientific and technical staff members, including 15 senior investigators with diverse expertise and research training. Of the 70 staff members, 43, including 13 senior investigators, are currently working on the Army projects. Strong administrative support is needed for organizing, coordinating, facilitating, and monitoring the research supported by the Army projects and is absolutely essential for the success of such a large, dynamic, and expanding research program. Consequently, the primary responsibility of this Administrative Support Service Facility is to support the administrative needs of the investigators supported by this Army grant. Moreover, synergistic interactions and collaborations between the investigators of the Army grant and other investigators of the MDC, as well as other investigators at local academic institutions and research organizations, such as Loma Linda University (LLU), Loma Linda Veterans Association for Research and Education (LLVARE), Loma Linda VA Medical Center, the University of California at Riverside, and City of Hope, would enhance the productivity of the Army projects. Accordingly, the secondary objective of this Administrative Support Service Facility is to provide and stimulate interdepartmental, interdisciplinary, and inter-institutional dialogue and to improve the existing interactions and productivity between various investigators of the local institutions and organizations in musculoskeletal research.

Body

Technical Objectives

Our Technical Objectives for this Project were as follows:

1. To set up organizational and oversight committees to promote, monitor, organize, and facilitate research work supported by the following Army grants: DAMD17-99-1-9571 ("Molecular Mechanisms Of Soft-Tissue Regeneration And Bone Formation In Mice: Implications In Fracture Repair And Wound Healing In Humans – Continuation Studies"); DAMD17-01-1-0744 ("Molecular Genetics Studies Of Bone Mechanical Strain And Of Pedigrees With Very High Bone Density"); Log # 02042008 ("Gene Therapy For Fracture Repair"); and this current proposal, "Molecular Genetic and Gene Therapy Studies of the Musculoskeletal System".
2. To assist Investigators supported by the aforementioned Army grant in all areas of research to administrative responsibilities that are necessary for successfully carrying out the research work.
3. To provide a stimulating and supportive environment for Investigators supported by the Army grant that is conducive to focusing on bench research work so that administrative responsibilities are reduced.
4. To serve as the necessary and essential Support Service in order to stimulate interdepartmental, interdisciplinary, and inter-institutional dialogue and enhance the

Project 10: Phenotype Support Services

Introduction

The phenotype support service facility is essential for efficient progress in all of the specific projects in this proposal in the molecular genetics division and also in the gene therapy division for a total of eight projects, ranging from clinical projects to projects involving molecular techniques. The assays to be performed in the phenotype support service facility include: 1) total bone density in rodents by pQCT; 2) total skeletal bone density in rodents by dual energy x-ray densitometry (PIXI); 3) bone strength analysis and performance of very precise femoral fracture using the Instron mechanical tester; 4) X-ray imaging by the Faxitron; 5) histological analysis, including quantitative morphology, immunocytochemistry, and fluorescence microscopy; 6) serum and urine chemical assays, including bone markers and IGF assays; and 7) statistical support. It would be difficult for the principal investigator of each of the separate projects to set-up the facilities to perform this large array of routine phenotypic measurements without considerable duplication of effort. Consequently, this phenotypic vector support facility will be highly efficient and cost effective for the proposed specific projects in this grant application. The emphasis in this support service facility will be to perform highly reliable, precise measurements of the phenotype requested. The director of this support facility will keep abreast of new technologies and transfer this information to those principal investigators potentially interested in the corresponding new technology. The director of this support facility will also provide training courses in the various phenotypic measurements made in this support service facility. It is essential for the investigators to have a fundamental understanding of the measurements being made so that they will be aware of the pitfalls and advantages of the application of there techniques. Study design and statistical support will also be provided when requested.

Body

Technical Objectives

The major technical objective for this phenotype support service facility will be to receive samples, perform the appropriate measurements on these samples, and then transfer all the data electronically to the corresponding investigator. Specific objectives include:

1. To assist investigators in the design of studies involving given phenotypes.
2. To perform measurements as requested by the investigators on the samples provided.
3. To follow the development of emerging technologies in the literature and at meetings and make recommendations to investigators regarding the possibility of adopting some of these new technologies in the phenotype support service facility.

Progress for Specific Objectives

Specific Objective 1:

Project 1: This project required the establishment of new protocols to carry out histological examination of regenerating mouse digit tips. Several embedding techniques

were tested to determine optimum methods of histology of mouse digits. Embedding in glycol methacrylate without demineralization allows good enzyme staining (alkaline phosphatase and acid phosphatase), which is useful for the identification of osteoblasts and osteoclasts at the site of regeneration. However, cracking of the mineralized bone occurs, leading to some loss of bone pieces during staining. Demineralization of specimens followed by embedding in paraffin gave better preservation of intact specimens. In addition, paraffin embedding allows better control over specimen orientation during embedding. Furthermore, paraffin sections are more suitable for immunostaining protocols to identify the presence of key molecules. It was also shown that penetration of the digits by the embedding medium was improved if the skin is at least partially removed before tissue processing. Paraffin embedding has been selected as the method of choice for routine processing of the samples. However, alternative methods of embedding will be used when special procedures are to be used.

Selection of the appropriate sampling site is always an important aspect of bone histology. The digits are composed of three phalanx, with the third phalanx being the digit tip that is covered by the nail. To keep the digits in a consistent orientation during embedding, the digits were left attached to the rest of the paw. The initial objective was to be able to see all three phalanx from each digit in order to compare the regeneration in the cut digit with uncut controls. Longitudinal sections through the middle of the phalanx potentially provided this view. One difficulty with obtaining a consistent sampling site was that the digits are normally slightly flexed. This was particularly true of phalanx 3, the main site of regeneration. Flexure was greater in the older animals than in the young ones. Maintaining pressure on the paws to orient the digits parallel to the bottom of the mold during embedding minimized the effect of flexure. However, it was still necessary to examine multiple section in order to see all phalanx and multiple digits. It also appeared that placing the upper or extensor surface of the paw down on the bottom of the mold gave the best orientation.

Several stains have been identified as informative for studying the regeneration process. The standard cell stain is an H&E. This works well for paraffin section to identify cell types and has proven useful in identification the regenerating epithelium and the blastema.

Project 4: Transgenic mice to assess gene function in mechanical testing and bone fracture. Transgenic mice with Leptin or Bax gene knockouts are being studied to determine the influence of these genes on mechanical testing and bone fracture. Evaluation of fracture healing is being done by pQCT densitometry and Faxitron X-ray analysis. Because fracture healing involves the addition of a cancellous bone bridge on the periosteal surface, the thresholding parameters in the pQCT analysis need to be adjusted. Parameters that work well with normal bone structure do not distinguish the new bone on the periosteal surface. Furthermore, lowering of the outer threshold value allows determination of the total hard and soft callus. These parameters have been established and are being used to assess the fracture healing in the transgenic mice.

Specific Objective 2:

Project 1: Samples of paws from several mouse strains and several time points have been obtained Paraffin sections are being prepared and studied with the various staining methods.

Project 4: Further confirmation of bone healing effects is being carried out by histomorphological evaluation. Fractured and control bones are demineralized in neutralized ethylendiaminetetraacetic acid. Samples are embedded in paraffin and cut longitudinally. Sections are stained for H&E, Mason's trichrome, Van Geisens, and Saffranin O.

Project 6: Bone samples are being processed for histological evaluation in the Phenotyping laboratory. This project involves the use of green fluorescent protein as a cell tag. Histological processing techniques tend to quench the fluorescence of the green fluorescent protein and increase the autofluorescence. Frozen sections are desirable because this technique requires less processing. A procedure for the preparation of frozen sections was established and initial samples have been examined. Bone is a difficult material to obtain good frozen sections from. Therefore, the frozen section methodology is still undergoing optimization.

Specific Objective 3:

Project 1: The study of the wound regeneration process will be facilitated by the establishment of additional histological methods based on literature and meeting presentations. Wounding or cutting the digit tip interrupts the basement membrane below the epithelium. The restoration of this basement membrane may act to regulate the extent of the regeneration. Several different immunhistochemical or cytochemical stains for basement membranes have been investigated. Laminum and type IV collagen are two compo nets of basement membranes that have been investigated immunohistologically. Two cytochemical stains based on the high carbohydrate content of the basement membrane, methenamine silver (GOYA) and the PAS stain, are under investigation. Collagen structure of the dermal tissues is being examined by Mason's Trichrome stain. The normal structure of the dermal layer includes a dense collagen layer just under the epidermal basement membrane and looser more randomly oriented fibers in the lower dermal layer. Restoration of this collagen organization is part of the regeneration process.

Development of New Technologies

1.General. MicroCT and microMRI are two relatively new techniques that have great potential for phenotyping bones. The resolution obtainable with these techniques has been steadily improving with technological advances. Both of these techniques have potential use for phenotyping in live animals as well as *in vitro* bone analysis. An advantage of these two techniques is that they are non-destructive. Dr. Obenause's Laboratory at Loma Linda University was visited to assess the usefulness of these instruments for the on going studies funded by the Department of Defense.

2.Summary of microCT. The microCT instrument at Loma Linda University is an ImTec Microcat II for *in vivo* scanning. Aluminum filters have been added to harden the beam and increase the discrimination for bone. From the pictures and monitor views it is evident that the resolution is in the neighborhood of 40 microns. The instrument can also be used for *in vitro* scanning. However, microCT instruments specifically designed for *in vitro* scanning can have better resolution on the order of 10-20 microns. Multiple bone samples could be scanned at the same time to reduce scanning time.

For *in vivo* scanning, the animals must be anesthetized so there is no movement during scanning. Dr. Obenause uses an isofluorane anesthetic system set up. This works very well for rats that can go 2-3 hours under anesthesia without any problems. Mice can also be anesthetized with this setup except that if the mice are sick there may be some mortality. The same anesthesia setup was used with MRI.

Dr. Obenause uses a proprietary software system ($3500) for analyzing the scans. The same software package is used for MRI, PET and microCT. Analysis could be done off site once scans were done. One difficulty is that there is no section specifically on bone analysis in the manual. Therefore, one needs to develop their own protocol for using the software. Other microCT systems such as the Scanco system have builtin software specifically designed for bone. The system is flexible in that if the threshold is set low during scanning, the software can adjust the threshold during analysis to extract structures of different density. While the analysis can separate structures of different densities, it does not provide readouts of the actual mineral density. The latest ScanCo microCt can give density values.

Test samples of mouse bone demonstrate that the ImTek instrument successfully scans mouse femurs and can generate trabecular bone parameters. Moreover, the literature and the ASBMR workshop on non-invasive methods indicate that trabecular parameters generated by microCT, even low resolution microCT, are highly correlated with histologically generated parameters. Thus, the instrument still should be able to examine and identify differences in trabecular structures. Further work with the instrument and analysis may be able to improve on the resolution. Although the resolution of the Imtek is not sufficient to give precise resolution of the woven bone that develops following fractures, this resolution is still better than that obtained with the current pQCT. Thus scanning with this instrument would have an advantage over our current methodology.

3.Summary of microMRI. Dr. Obenaus has two instruments with field strengths differing by five fold. They have a small coil designed for scanning rat brains that would work for bones. The scans are done in five different modes: "T", etc. The instruments have some versatility in that different modes of scanning can emphasize different structures. One of the modes is useful for blood flow and vascularity (*in vivo*) and might be useful for looking at the role of vascularity in bone fracture healing. The resolution is 40 microns so this would be a limitation (probably not good enough for digit tip studies). MRI is used at Loma Linda University for measuring volumes of different brain structures or tumors. Based on the views of the brain with micro MRI, it should be possible to identify

structures including bone. The instruments are setup to do primarily *in vivo* studies but *in vitro* scanning of bone specimens can be readily done.

The microMRI setup used the same anesthesia system and analysis system as the microCT. Further analysis of actual bone specimens are needed to fully evaluate the utility of this technique.

Project 11: Microarray and Informatics Support Services

Introduction

As a result of the sequencing of the human and mouse genomes there has been a tremendous increase in discovery of novel genes with unknown functions. It is important to next interpret and determine the function and genetic pathways of the large amounts of sequence information now available. One powerful method of determining unknown gene function and genetic pathways is by microarray expression profiling. Microarrays (also called DNA chips) are glass or plastic substrates on to which known sequences of DNA have been synthesized or spotted. Fluorescently labeled RNA from different biological samples are hybridized to their complementary sequences on the microarrays. The resulting fluorescent intensities are quantified and data analysis performed to determine expression levels of RNA transcripts. Thus, microarrays allow for the experimental analysis of many genes in a single experiment, and one can compare expression levels of genes over several timepoints and different biological or disease conditions. Comparing these expression levels gives clues to gene function and is a very powerful method of discovery. Project 11 of this grant had the goal to upgrade and improve the microarray and informatics support services in the Musculoskeletal Disease Center. Following are the technical objectives:

Body

Technical Objectives:

Following are the specific objectives during the second year of the grant period:

1) To provide technical service.
2) To provide education.
3) To update on recent advances.

To achieve the above technical objectives, the following Specific Objectives are proposed during years 1 and 2 of this proposal:

1) To provide technical service, microarray and informatics support service will:

i) Prepare cDNA probes for genes related to musculoskeletal tissues
ii) Spot cDNA probes on the slides
iii) Perform labeling of cDNA, hybridization and detection of labeled probes
iv) Develop the informative infrastructure to produce, analyze, interpret and house the information derived from microarray experiments
v) Mining of functional and expression data for genes spotted in the slides
vi) Identify SNPs for genes involved in the IGF regulatory system using various SNP databases
vii) Build maps of genetic loci for ENU mutant and QTL studies and identify overlapping BAC clones for functional testing

2) To provide education, microarray and informatics support service will:

i) Train investigators in the preparation of good quality RNA
ii) Train investigators in the use of appropriate statistical methods for data analysis

3) To update on recent advances, microarray and informatics support service will:

i) Improve spotting and labeling techniques by incorporating latest technology developments in these areas
ii) Incorporate new advances in data management and analysis

We have accomplished all of the above specific objectives. Our progress in each of the Specific Objectives is given below.

Progress on Technical Objectives

Specific Objective 1:

Our goal was to create a nearly complete representation of the genes in the mouse genome for spotting on to microarrays. For this purpose, we obtained a copy of a mouse clone library that consists of approximately 15,000 genes that was developed by researchers at the National Institute on Aging, a center of the National Institutes of Health. In the first year of this grant, we received a copy of this clone set and processed the clones for microarray spotting. The clone set has the following characteristics:

- Approximately 15,000 unique cDNA clones were obtained from expressed sequence tags (ESTs) from developing mouse embryos (E12.5).
- Up to 50% are derived from novel genes.
- The clones have approximately 1.5 kb average insert size.
- All the clones were sequenced from 5' and 3' termini to verify the clone's sequence and to insure that unique clones are represented in the library.

Processing of the clones involved first replicating the library by growing all 15,000 clone cultures and then purifying plasmid DNA from the clone cultures. The cloned inserts in the plasmid DNAs were then amplified by PCR and purified. The remainder of the plasmid DNAs were then archived at –20C. Following is the protocol used for processing the 15,000 clone cultures into plasmid DNA and then PCR products to make them suitable for microarray spotting:

Preparation of NIA 15K Clone Set

Growing the Plasmid Clones

Make stock 2XYT Medium (for 1L)

Tryptone	16g
Yeast Extract	10g
NaCl	5g
0.1 Sodium Citrate	17mL
1M KH_2PO_4	36mL
1M KH_2PO_4	13.2mL
80% Glycerol	55mL

Adjust the pH to 7.0 with HCl acid and sterilize media by autoclaving.

1. Take plasmids to be grown out of the –80 °C freezer and set on ice to thaw.

2. Preparing to grow the plasmids. Flame the caps and openings of the flasks used before and after transfer of medium. Add the following to the amount of 2XYT medium to be used:

1.0 $MgSO_4$	0.4uL per 1mL of 2XYT medium
2.0M $(NH_4)_2SO_4$	3.4uL per 1mL of 2XYT medium
100mg/mL Ampicillin	1.0uL per 1mL of 2XYT medium

3. Transfer 1.5mL per well of the 2XYT medium to a 96-deep well plate.
4. Add 1uL of the stock plasmid into each well using a 96-pin replicator. Dip the pins into the well, swirl gently to scrape up a few cells and insert into deep well plate with medium. Grow the plasmids with the 96-pin replicator as the lid.
5. Incubate at 37 °C, and shake at 120 rpms overnight. Make sure plate is secured on the base of the shaker. The lid should be loose to allow air flow.

Plasmid DNA Purification

For Plasmid DNA purification we use the Millipore Montage 96-well plate purification kit. Following is the protocol used to purify the 15,000 plasmid cultures:

1. Pellet the cells in the 96 well plate using a swinging bucket centrifuge. Spin at 1500xg for 10 minutes. For rotor GH-3.8, that is about 2000rpms for 10 minutes.
2. Discard the medium from the pellet by slowly inverting the plate. The solid cell mass will remain at the bottom of the plate. DON'T tap the plate-- this may dislodge the pellet. Leave the plate upside down on paper towels to drain the remainder of the medium (about 5 min).
3. Re-suspend the cells by adding 100uL of Solution 1 to each well. Re-suspend pellet by pipetting up and down. All cells must be suspended for best yields. If the samples cannot be taken to the next step immediately, keep at 4°C until ready to move on to the next step.
4. Lyse the cells by adding 100uL of Solution 2. Shake plate vigorously for 1 minute. Allow to sit at room temperature for 2 minutes, but not to exceed 5 minutes.
5. Neutralize the lysed cells by adding 100uL of Solution 3. Mix by shaking vigorously for 2 minute.
6. Place the Plasmid 96 well plate in the vacuum manifold. Place the Clearing plate on top of the manifold. The vacuum manifold needs to be connected to a flow through flask for waste solution to collect. The flow through should be disposed regularly. The waste in neutralized and can be dumped down the sink.
7. Transfer the full volume into the 96 well Clearing plate (300uL maximum volume). Vacuum at a maximum pressure of 8 inches of Hg until all the volume is has passed though the filter. Don't move the manifold during this time, it may cause cross contamination in the transfer from the clearing plate to the plasmid plate.
8. Discard the dry clearing plate. Move the plasmid plate to the top of the manifold.
9. Vacuum at a maximum pressure of 24 inches of Hg until the wells are dry.
10. Wash the plasmid DNA by adding 200uL of Solution 4. Vacuum until the wells are dry. Dab the bottom of the plate with a towel to remove excess wash.
11. Re-suspend the plasmids by adding 50uL of Solution 5. Shake the plate for 10 minutes on a plate shaker. Transfer the plasmid into a 96 well plate.
12. Use 2uL to run on an agarose gel to check the quality.

13. Store the stock plasmids at –20 °C.

PCR Amplification of Clone Inserts

PCR amplications are done using the following protocol:

PCR Primers: NIA15K-For 5'-CCAGTCACGACGTTGTAAAACGAC-3'
NIA15K-Rev 5'-GTGTGGAATTGTGAGCGGATAACAA-3'

1. Dilute an aliquot of the stock plasmids. Take 1ul of stock plasmid DNA into 99ul of DNA water in a 96 well plate.

2. PCR Reaction Master Mixes:

	100ul rxn	96 well plate
10X Qiagen PCR buffer	10ul	980ul
10mM dNTPs	2ul	196ul
10mM primer Forward	1ul	98ul
10mM primer Reverse	1ul	98ul
Sterile deionized water	84.8ul	8310.4ul
5U/uL HotStarTaq (5U/ul)	0.3ul	29.4 ul
		add 99 ul per well
1:100 plasmid DNA	1ul	1ul

3. PCR Cycling Parameters

Step 1	95°C for 14 minutes
Step 2	95°C for 1 minute
Step 3	56°C for 1 minute
Step 4	72°C for 1:30 minutes
Step 5	Go to Step 2 for 39 more times
Step 6	72°C for 10 minutes
Step 7	10°C hold

4. PCR success and quality is determined by running 4ul of the PCR product on a 1% agarose gel. Some samples that don't amplify with the diluted plasmid DNA will be seen. Re-amplification of failed PCRs should use 1ul of stock plasmid DNA to amplify and the above reaction mixes.

5. Store the PCR product at –20°C until ready for purification

Purification of PCR Products.

Purification of PCR products was done using Millipore Multiscreen kits. Following is the protocol:

1. Thaw the PCR products and transfer the full volume into the MultiScreen filtration plate and place the filter plate on the vacuum manifold. The filters have a maximum volume capacity of 300uL but for best results, no more than 200uL should be loaded.
2. Vacuum the plate at about 24psi until dry; it will take 5 to 10 minutes.
3. Remove dry plate from manifold and dab the bottom to absorb excess flow though.
4. To resuspend the DNA, add 40uL DNA water into each filter well. Shake the plate on a plate shaker for 10 to 15 minutes.
5. Collect the samples and transfer into a 96 well plates.
6. Store purified PCR plates at -20°C.

Using the above protocols, over 90% of the 15,000 NIA clones gave a single PCR amplification product. The purified PCR products were then re-arrayed into 384 well plates in

25% DMSO. Microarrays were created using these PCR products using a Genetix Q-Array2 robotic arrayer.

Creation of Microarrays Using the Genetix Q-Array2

Following amplification, the purified PCR products were re-arrayed into forty-four 384-well plates in 25% DMSO spotting buffer. For re-arraying 96-well plates to 384-well plates the Robbins Scientific Hydra-96 robotic liquid handler was used. Microarrays were then created using Corning UltraGaps II glass slides. The PCR products were spotted using a Genetix Q-Array2 robotic arrayer. The arrays are also spotted with Amersham Lucidea Universal Scorecard controls to insure correct gene expression values were obtained from each array. The Lucidea Universal ScoreCard is a set of 23 unique microarray controls that can be used with samples from most species and with any microarray platform. The controls are artificial genes that generate pre-determined signal intensities that do not change across samples or experiments. Thus the microarray analysis is not dependent on relative quantification. The controls generate a calibration curve for determining limits of detection, linear range, and data saturation, and they can be used as universal references for validating and normalizing microarray data. Controls are spotted in duplicate in the first and last PCR plates to insure proper data tracking. After extension optimization, the following parameters were used to create microarrays with 30,000 features (the 15,000 clones spotted in duplicate).

Head:	48-Pin Microarraying Head (65 micron split tungsten pins)		
Source:	Plate holder:	Stacker source plate holder	
Plate type:	Genetix plate 38X7022		
Plate number:	44		
Source order:	Column		
Slide Design:	3X1" Slide (48 pins/ 1 field)		
Arraying by:	Spotting position		
Array pattern:	Spot view, Estimated spot size:	65 microns	
Row count:	27 Row pitch:	160	
Column count:	27 Column pitch:	160	
Replicate type:	Cyclic		
Replicate count:	2		
Number of blot:	12		
Blot set / over spot:	6		
Blot pitch:	800		
Blot change:	Yes		
Max stamps per ink:	800		
Number of stamp per spot:	1		
Stamp time:	0		
Ink time: (ms)	1000		
Print adjustment:	0		
Wash:	Wash	Dry	Wait
Water:	5000		
Water:	5000		
Water:	5000		
80% EtOH:	5000	6000	2000

Export date: yes
File name: NIA 15K database
File format: GSI
Plate sequencing: See Data tracking NIA 15K
Barcodes: Manual
Spotting Position: From 1- 352 (Each Plate has 8 position)

Using the above parameters we have created to date over 100 microarray slides with over 30,000 features. Following spotting the slides were processed to fix the DNA to the slides and to denature the DNA to single stranded DNA. Below are the parameters developed to fix the slides:

1. Cross link the slides at 60 milliJoules using the Stratagene UV Crosslinker (600 setting). Place the slides on glass trays horizontally without overlapping.
2. Bake the slides for 3 hrs at 80°C in the hybridization oven. Place the slides on glass trays horizontally without overlapping.
3. Transfer slides to a slide histology rack. Allow one space between slides so they do not touch. Denature the DNA in 98°C water bath for 2 min.
4. Store the slides in a sealed slide holder in the dark at room temperature. The slides should be good for at least six months.

The microarray support laboratory has investigated new methods of RNA labeling and hybridization that require less amounts of initial total RNA. This is significant and important since in the past it has been difficult to obtain sufficient amounts of total RNA from limited amounts of cells that are obtained from bone and other tissues. The previous labeling methods used in the microarray laboratory required 2 to 10 micrograms of total RNA for each hybridization. In the past year, we have investigated new methods of RNA labeling and hybridization and have successfully reduced the amounts of initial RNA needed to 50 to 250 nanograms (a 40 to 200 fold reduction). The method that we have begun using is the Low RNA Input Fluorescent Linear Amplification Kit for cDNA Microarray Hybridization (Agilent). Following is the protocol:

cDNA Synthesis From total RNA

1. Add 200-400ng of total RNA in a volume of 9.3ul or less.
2. Add 1.0ul of Test Spikes (Amersham Lucidea controls) into the Experiment Sample or
3. Add 1.0ul of Reference Spikes into Control Sample.
4. Add 1.2ul of T7 Promoter Primer
5. Bring volume up to 11.5ul with nuclease-free water
6. Denature the primer and the template by incubating the reaction at 65°C in a heating block for 10 minutes.
7. Place the reactions on ice and incubate for 5 minutes
8. Prepare the cDNA Master Mix per reaction:

5X First Strand Buffer*	4.0ul (Pre-warm at 65°C, 3-4 min)
0.1 M DTT	2.0ul
10mM dNTP mix	1.0ul
RNaseOUT	0.5ul
MMLV RT	1.0ul
Total Volume	8.5ul

9. To each sample add 8.5ul cDNA Master Mix.
10. Incubate samples at 40°C for 2 hours, 65°C for 15 min, on ice 5 min.

cRNA Amplification

1. Prepare the Transcription Master Mix:

Nuclease-free water	12.1ul
4X Transcription Buffer	20.0ul
0.1 M DTT	6.0ul
NTP Mix	8.0ul
CTP	5.6ul
50% PEG	6.4ul(Pre-warm it at 40°C for 1min)
RNAseOUT	0.5ul
Inorganic Pyrophospatase	0.6ul
T7 RNA Polymerase*	0.8ul
Total Volume	60.0ul

2. Add 60.0ul of Transcription Master Mix.
3. Incubate samples at 40°C for 2 hours.

Purification of Amplified cRNA

1. Use the Qiagen's RNeasy mini spin columns.
2. 80ul cRNA sample
3. Add 20ul of DEPC water.
4. Add 350ul of Buffer RLT .
5. Add 250ul of ethanol (200 proof)
6. Transfer 700ul of mix to an RNeasy mini column in a 2mL collection tube. Centrifuge the sample at 13,000rpm for 30 seconds
7. Wash the column with 500ul of buffer RPE , Centrifuge the sample at 13,00rpm for 30 seconds.
8. Wash the column with 500ul of buffer RPE, Centrifuge the sample at 13,00rpm for 60 seconds.
9. Elute the cleaned cRNA sample. Add 35ul RNase-free water directly onto the RNeasy filter membrane. Wait 60 seconds before centrifuging for 30 seconds at 13,000 rpm. SAVE THE FLOW THROUGH and the collection tube. Store at -80°C until needed

Quantitating cRNA Products

1. Use 1.5ul on nuclease free water to blank the NanoDrop instrument. Then use 1.5ul of amplified cRNA for analysis. Calculate the concentration of cRNA by using the formula:
    a. 1 OD260 = (10) x 40ug/ml RNA

Fluorescent cDNA Synthesis from Amplified cRNA:

1. Add 500ng-2ug cRNA and bring the total volume to 13.25ul with nuclease free water.

2. Add 1ul of Random Hexamers.
3. Incubate the sample at 65°C for 10 minutes, on ice for 5 min.
4. Add 1.25ul of either Cyanine 3-dCTP or Cyanine 5-dCTP(500uM)
5. Prepare cDNA master mix:

5X FS Buffer	5.0ul
0.1M DTT	2.5ul
dNTP	1.0ul
MMLV RT	1.0ul
Total	9.5ul

6. Aliquot 9.5ul of cDNA master mix to each sample
7. Incubate cDNA synthesis reaction at 40°C for 60 min, 65°C for 10 min, on ice for 5 minutes.

Purifying Labeled cDNA:

1. Combine Cy3 and Cy5 cDNA reaction.
2. Add 5 volume of Buffer PB.
3. Apply the sample to the QIAquick Column and centrifuge at 13,000rpm for 30 sec.
4. Wash the column with 400ul of Buffer PE . Centrifuge the column at 13,000rpm at 30 seconds.
5. Wash the column with 400ul of Buffer PE. Centrifuge the column at 13,000rpm at 60 seconds.
6. Elute the sample, add 30ul of buffer EB, Wait 60 seconds before centrifuging for 30 seconds at 13,000 rpm.
7. Repeat the eluted step.
8. Dry the sample (Option).

Hybridization

1. Bring volume up to 250ul with sterile ddH20.
2. Denature at 98°C for 3 minutes.
3. Add 250ul 2X Hybridization buffer to the sample then mix it.
4. Add mix to the Hybridization Chamber.
5. Hybridize in oven at 60°C for 17 hours. Attach the chamber to the rotating rack securely.

Washing the Slides

1. Wash with Solution I (6X SSC, 0.005% Triton X-102) for 10 min. in dark.
2. Wash with Solution II (0.1X SSC, 0.005% Triton X-102) for 5 min. in dark.
3. Dry the slide with the nitrogen-filled air gun.
4. Slides are ready for scanning.

For scanning the laboratory uses a GSI Lumonics ScanArray 4000 scanner. This scanner is several years old but is still usable with our new microarrays. The arrays are scanned at a resolution of 10 microns which corresponds to ~15 pixels in diameter of each of the ~30,000

spots and a spacing of ~5 microns between the spots. The signal intensity of all microarray images is determined using Imagene 5.1 software. This software uses a patented image processing technology to provide quantification of microarray images of high density. Quality control measures include automated flagging of good, marginal and absent spots so that these can be filtered in the expression analysis.

Figure 1. Scanned Image of NIA15K Microarray. Shown below is a small region of a microarray manufactured and hybridized in the Microarray Laboratory in the Musculoskeletal Disease Center. Note that most spots are circular and well defined.

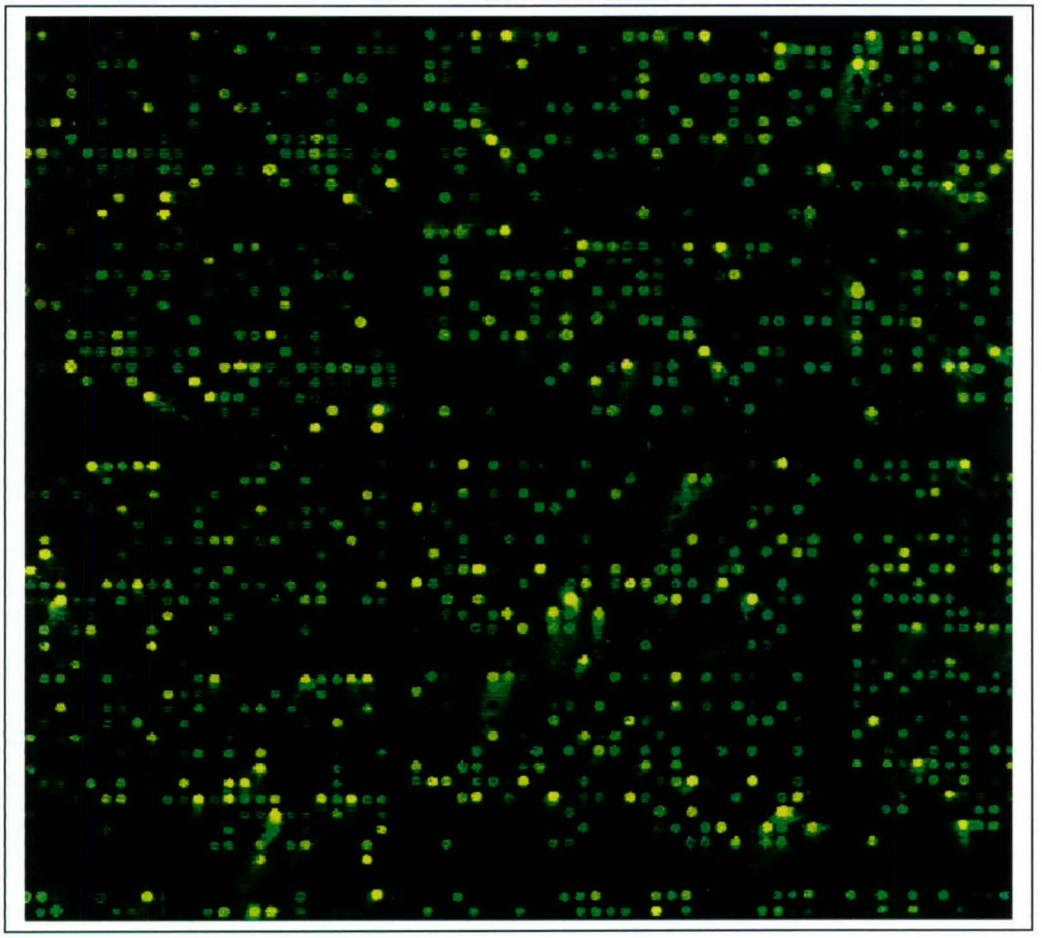

Specific Objective 2:

In the past year, we have investigated new methods of RNA isolation to improve the yields and quality of total RNA obtained from various tissues. Since the initial isolation of the total RNA is the most labor intensive step this has led to an increase in output in experimental data productivity. One method of RNA isolation has been found to increase the amounts of total RNA that we obtain from soft tissues. The method uses a polytron to quickly lyse cells rather than manually lysing cells with a mortar and pestle. The polytron processes tissue more quickly thus allowing for rapid RNA isolation and high quality RNA preparations. Following is the

protocol that we use for isolation of RNA from soft tissues and which we have trained investigators:

Total RNA Isolation Protocol with Polytron

1. Wash the Polytron probe with RNase away at half speed (15/30) for 1 minute. Rinse the probe with DEPC water twice at the same speed and time; use DEPC water at full speed 30 seconds, repeat twice. Use 100 percent ethanol at full speed to wash the probe 25 seconds, repeat twice. Air dry until use.
2. Prepare tissue homogenate in appropriate amount or lysis solution/beta-mecaptoethanaol mixture (20ul/mg).
3. Polytron the tissue in lysis solution for 20-40 seconds. Wash the probe with a small amount of lysis solution to insure that all cellular debris is removed from the probe.
4. Centrifuge up to 600ul of homogenate through the mini prefiltration column, for 3 minutes at 13000 rpm, collect the filtrate.
5. Add an equal volume of 70% ethanol to the filtrate, mixing very well, and place on ice at least 5 minutes.
6. Add up to 700ul ethanol/lysis mixture to the mini isolation column then centrifuge 30 seconds at 13000 rpm. Discard the flow through, and place the RNA-loaded column into the same collection tube.
7. Add 500ul wash solution to the mini isolation column, then centrifuge 30 seconds at 13000 rpm. Discard flow through, replace the mini isolation column in the collection tube.
8. Repeat step 5 one more time.
9. Spin the mini isolation column for 2 minutes at 13000rpm.
10. Elute the purified RNA by addition of 10-50ul of nuclease-free water, wait 1 minute, then centrifuge 1 minute at 13000rpm.

Using the above protocol we have obtained very high quality RNA from small amounts of tissue (50 milligrams and less). An example of RNA isolated from mouse DBA strain digit tips by the protocol is shown in Figure 2.

Figure 2. High Quality RNA Sample Isolated By Modified Protocol. RNA quality is determined by running the samples on the Agilent Bioanalyzer. The RNA sample in the upper panel indicates high quality RNA since the 28S ribosomal RNA peak (at ~47 seconds) is greater intensity than the 18S ribosomal RNA peak (at ~ 41 seconds). Quantification of the RNAs is calculated by comparing the fluorescent intensity of the marker peak that migrates at a time of approximately 23 seconds to the intensity of the ribosomal RNA bands.

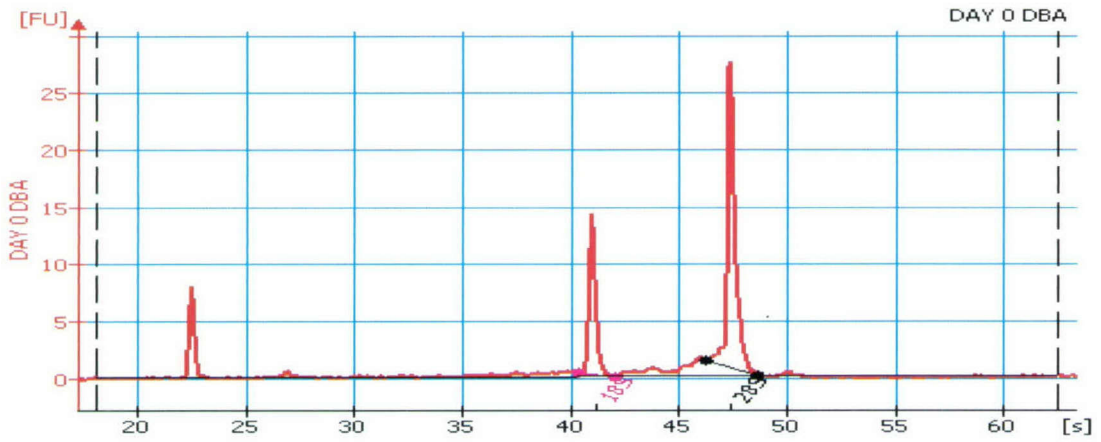

Informatics Support and Microarray Data Analysis

Microarray data is analyzed with GeneSpring software (Silicon Genetics, Redwood City, CA). The purpose of the analysis is to obtain a list of differentially expressed genes. These are the candidate genes that play an important role in a microarray study, for example in bone fracture in rat, one of our ongoing studies.

Before the formal analysis, we use the Scatter plot and the Condition tree features of GeneSpring software to evaluate the microarray chips to determine if they are suitable to be included in the analysis. The Scatter plot shows the data skewness between the Cy3 and Cy5 dyes (i.e. the treatment vs. control) for a particular chip. If there are too many genes that are highly expressed in one color, but not in the other, this might indicate that there are problems with the labeling process. Take the following image of scatter plot of Cy3 versus Cy5 intensities as an example. It can be seen that most genes are expressed nearly equally in both samples. This is usually the case in a well –designed expression experiment, since out of 15,000 genes most are not expected to show differential expression.

Figure 3. GeneSpring Analysis of Microarray Data. Shown below is a scatter plot of fluorescent intensities of 15000 genes from MRL mouse RNA. The normalized Cy3 (day 4) labeled cDNA is plotted versus the normalized Cy5 (day 0) labeled cDNA. The data is normalized to correct for differences in labeling or detection efficiencies between the fluorescent dyes used or for slightly unequal quantities of starting RNA. The center line of the three lines shown corresponds to a slope of one and samples that lie along this line show no differences in expression for that respective gene. Greater than 2-fold differences in expression are indicated by dots that fall outside the two outer lines.

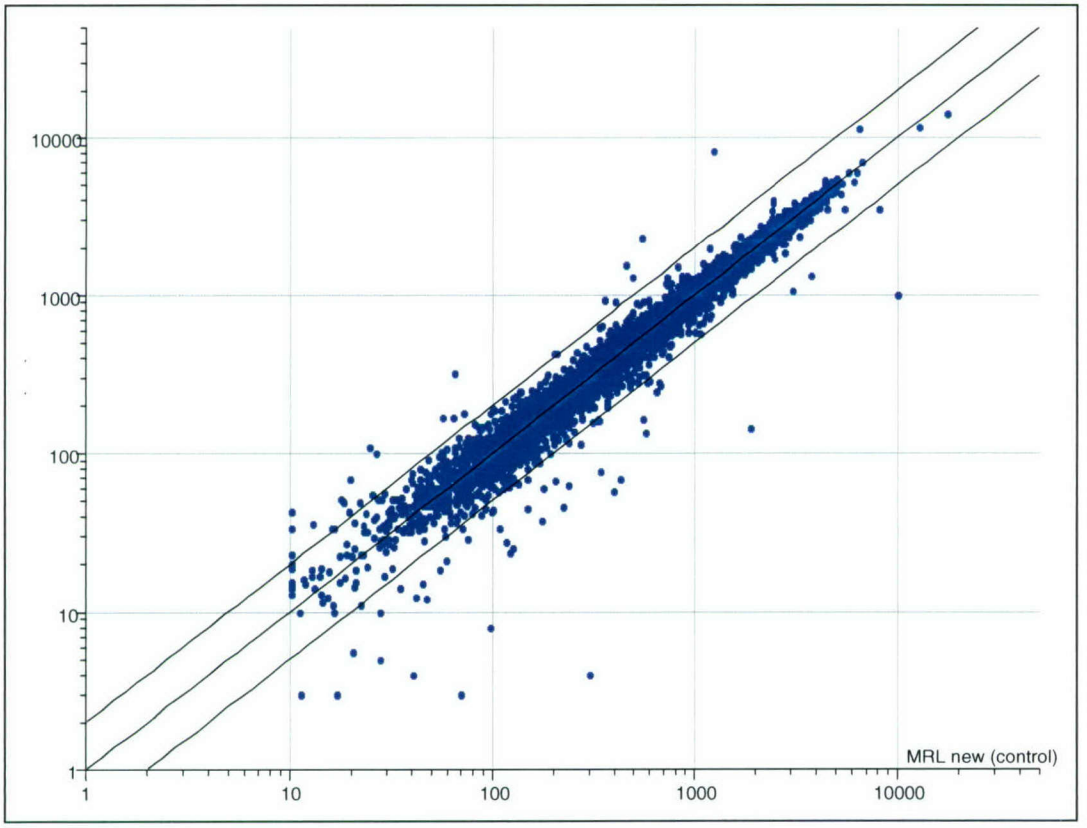

Another way to determine data quality is to examine the condition tree of the individual slides in a microarray experiment. For example in the following image of condition tree analysis, the expression pattern for RNA samples and control RNAs cluster together. The experiment is of digit tip RNA from two inbred strains of mice (MRL and DBA). The condition tree analysis shows that the DBA and MRL run samples are more different between each other than the replicate microarrays for that respective species. Also, the analysis shows that individual microarrays run of the respective specie's day 4 experimental RNA and day 0 control RNA are more like itself than another microarray. This indicates that for determination of differential expression of genes between the day 4 and day 0 RNA samples, the individual microarrays must first be normalized and expression ratios determined. Once these differential expression ratios are determined, the replicate microarrays can be combined for statistical analysis of significance.

Figure 4. GeneSpring Condition Tree Analysis of Microarray Data. RNA samples from MRL and DBA in-bred strains of mice cluster separately from each other. Since RNA from different strains should be more different from each other, this indicates that the microarray data is high quality.

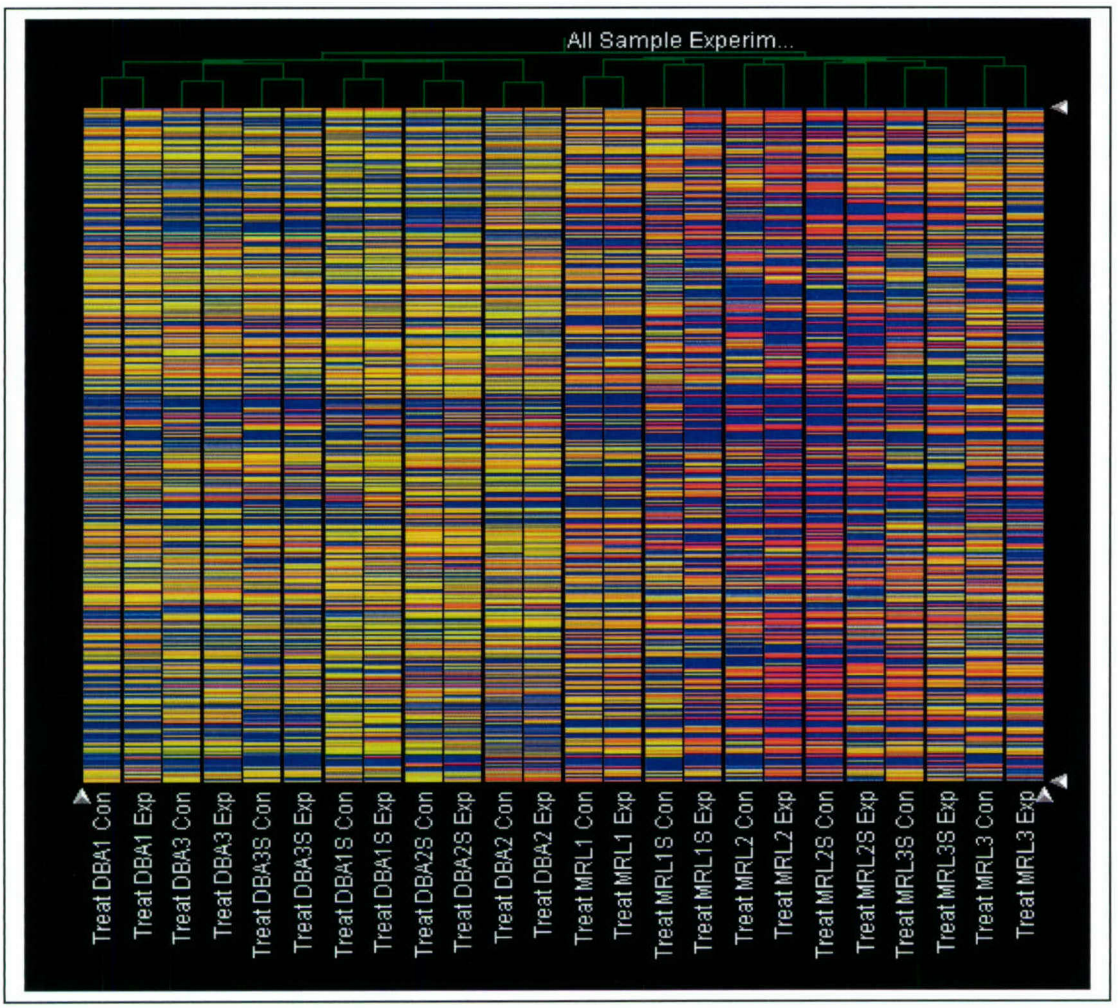

For two color (i.e. treatment vs. control) expression experiments, we do paired analysis and using the Per Spot and Per Chip: Intensity dependent (Lowess) normalization. We are using P of 0.05 and 0.01 as critical values to determine whether a gene is differentially expressed.

After we obtain the list of differentially expressed genes, we cluster these genes. We use the K-Mean clustering feature of the GeneSpring. This clustering will identify the major gene clusters or modules that are differentially expressed in the experiments (i.e. between experiment and control, or the time series). In this analysis, the transcription factors, regulatory elements, DNA biding motifs and signal proteins will be taken into the consideration. It is highly likely that a particular module of differentially expressed genes are under the same regulation of a common transcription factor, or they have the same set of DNA binding motifs. Understanding

the transcription regulation of the gene modules in a microarray study hold the key to understand the gene networks.

Master Gene Annotation of NIA15K Microarrays. For the in-house manufactured microarrays, we have also generate an annotated master gene table for use with GeneSpring software. This table is loaded into GeneSpring and investigator can display the annotation information for his/her list of differentially expressed genes.

In order to create this master gene table for our in-house microarray (NIA Mouse 15k Clone Set Data), information is downloaded from the NIA (National Institute of Aging) website (http://lgsun.grc.nia.nih.gov/download.html). A local database is then created using MySql software. A program is written in PHP computer language to create this table. This database is updated each time that the database in the NIA website is updated. The current annotation of the NIA15K microarrays is too large to include in this report. It is over 700 pages describing each gene's function and the molecular, functional and cellular location description. Approximately half of the 15,000 genes are unknown expressed sequence tags (ESTs) of unknown function, however.

Pathway Analysis Using Gene Ontology. Further understanding the role of the differentially expressed genes in the pathways is critical in microarray studies. For this purpose, we use Gene Ontology to classify genes, to identify the pathways involved in each microarrya study. Gene Ontologies are structured, controlled vocabularies that describe gene products in terms of their associated biological processes, cellular components and molecular functions in a species-independent manner. The current annotation of the NIA15K microarrays is too large to include in this report. It is over 700 pages describing each gene's function and gene ontology. Approximately half of the 15,000 genes are unknown expressed sequence tags (ESTs) of unknown function and ontology, however.

The whole Gene Ontology (GO) database was downloaded from the website of the Gene Ontology Consortium (http://www.godatabase.org/dev/database/archive/latest/) into a local MySql database. A program is written in PHP computer language to classify the differentially expressed genes into GO categories. The following table lists the GO classifications (ontology of biological process only) of an example set of differentially expressed genes. For each category, the GO accession number, full name, and the number of genes are shown. Below each category are the gene identification number, gene symbol, and the full name of the gene.

```
GO:0030198(extracellular matrix organization and biogenesis) (1)
1     DCN   Mouse Decorin (DCN)
GO:0006412(protein biosynthesis) (6)
3     Rpl7a Ribosomal Protein L7a(Rpl7a)
8     Erf1  Mouse ETS-Related Transcription Factor(Erf1)
27    Arbp  Mouse Acidic Ribosomal Phosphoprotein
28    Rps18 Mouse Ribosomal Protein S18(Rps18)
29    Rps9  Mouse Similar to Ribosomal Protein S9(Rps9)
35    Rps7a Mouse Ribosomal Protein L7a(Rps7a)
GO:0045103(intermediate filament-based process) (1)
4     Vim   Mouse Vimentin (Vim)
GO:0006259(DNA metabolism) (3)
```

```
7     NACA  Mouse Nascent Polypeptide
30    Naca  Mouse Nascent Polypeptide-Associated
31    Recql5      Mouse RecQ Protein-Like 5(Recql5)
GO:0006265(DNA topological change) (2)
7     NACA  Mouse Nascent Polypeptide
30    Naca  Mouse Nascent Polypeptide-Associated
GO:0006415(translational termination) (1)
8     Erf1  Mouse ETS-Related Transcription Factor(Erf1)
GO:0006444(nascent polypeptide association) (1)
8     Erf1  Mouse ETS-Related Transcription Factor(Erf1)
GO:0009873(ethylene mediated signaling pathway) (1)
8     Erf1  Mouse ETS-Related Transcription Factor(Erf1)
GO:0042829(defense response to pathogen) (1)
8     Erf1  Mouse ETS-Related Transcription Factor(Erf1)
GO:0006118(electron transport) (2)
9     Cox5a Mouse Cytochrome C oxidase (Cox)
34    cox5  Mouse Cytochrome C oxidase
GO:0009060(aerobic respiration) (1)
9     Cox5a Mouse Cytochrome C oxidase (Cox)
GO:0006355(regulation of transcription, DNA-dependent) (1)
14    EF1   Elongation Factor 1-Alpha 1 (EF1-alpha1)
GO:0007010(cytoskeleton organization and biogenesis) (1)
19    Krt1-14     Mouse Keratin Complex 1
GO:0008544(epidermal differentiation) (1)
19    Krt1-14     Mouse Keratin Complex 1
GO:0000902(cellular morphogenesis) (1)
19    Krt1-14     Mouse Keratin Complex 1
GO:0006122(mitochondrial electron transport, ubiquinol to cytochrome c) (1)
21    cytb  Cytochrome B (cytb)
GO:0008152(metabolism) (1)
25    Sptlc1      Mouse Serine Palmitoyltransferase(Sptlc)
GO:0009058(biosynthesis) (1)
25    Sptlc1      Mouse Serine Palmitoyltransferase(Sptlc)
GO:0006414(translational elongation) (1)
27    Arbp  Mouse Acidic Ribosomal Phosphoprotein
GO:0006413(translational initiation) (1)
28    Rps18 Mouse Ribosomal Protein S18(Rps18)
GO:0007046(ribosome biogenesis) (1)
28    Rps18 Mouse Ribosomal Protein S18(Rps18)
GO:0006281(DNA repair) (1)
31    Recql5      Mouse RecQ Protein-Like 5(Recql5)
GO:0006091(energy pathways) (1)
34    cox5  Mouse Cytochrome C oxidase
GO:0007391(dorsal closure) (1)
36    SAC1  mutations(SAC1 gene)
GO:0030384(phosphoinositide metabolism) (1)
36    SAC1  mutations(SAC1 gene)
GO:0016311(dephosphorylation) (1)
36    SAC1  mutations(SAC1 gene)
GO:0006378(mRNA polyadenylation) (1)
37    Pabpn1      Mouse Poly A Binding Protein
```

Investigators were trained in the use of Genespring for appropriate statistical methods for data analysis in a full day training session given by scientists from Silicon Genetics. Also, Dr.

Hongrun Yu, our bioinformatics scientist in the MDC, often consults with scientists and assists with their microarray data analysis.

Specific Objective 3:

The microarray laboratory and informatics support services have incorporated several of the latest technologies in cDNA microarray manufacture and analysis. The methods described previously are a result of learning of new methods and technologies from networking and scientific conferences attended by scientists in the MDC. Following is a list of conferences attended and talks given by scientists in the MDC. These conferences led to improvement and incorporations of state of the art technologies in the Microarray Laboratory and Informatics Support Services:

Latest Technologies and Development Conferences attended by Dr. Robert Chadwick:

- Basic Gene Mapping/Linkage Course, June 23-27, 2003, Rockefeller University, New York, New York
- 53rd Annual Meeting of The American Society of Human Genetics, November 4-8, 2003, Los Angeles, California.
- 7th International Meeting of the Microarray Gene Expression Data Society, September 8-10, 2004, Toronto, Ontario, Canada.

Latest Technologies and Development Talks given by Dr. Robert Chadwick:

- Update on genetics and new technologies, a report for the 53rd Annual Meeting of The American Society of Human Genetics, November 12, 2003, MDC staff meeting.
- Update on genetics and new technologies, a report for the 7th International Meeting of the Microarray Gene Expression Data Society, September 22, 2004, MDC staff meeting.

Data management and Analysis Conferences attended by Dr. Hongrun Yu:

- 6th Annual Conference on Computational Genomics, October 8-11, 2003, Hyatt Regency Cambridge Hotel, Cambridge, Massachusetts
- Computational Systems Bioinformatics Conference, August 16-19, 2004, Stanford University, Palo Alto, California.

Data management and Analysis Presentations given by Dr. Hongrun Yu:

- Update on mocroarray data analysis and linkage mapping analysis, a report for the 6th Annual Conference on Computational Genomics, October 22, 2003, MDC staff meeting.
- Gene ontology, May 26, 2004, MDC staff meeting.
- Genome browser and microarray data analysis, a report for the 2004 Computational Systems Bioinformatics Conference, August 25, 2004, MDC staff meeting.

Additional Progress

We have recently undertaken scientific collaborations with Dr. Kerby Oberg and Dr. Mike Lilly of Loma Linda University School of Medicine. Dr. Oberg is undertaking a microarray study utilizing Affymetrix technology and the MDC microarray laboratory will test the same RNA samples with our custom cDNA microarrays. Comparing the two technologies will likely lead to greater understanding of the best methods to process and analyze microarray

data. In a collaboration with Dr. Mike Lilly, we are undertaking investigations into isolating RNA from archival tissue specimens. Since these specimens will likely yield RNA that is of lower quality than flash frozen tissue samples, we hope to develop improved RNA isolation and labeling methods from degraded RNA. If the methods can be optimized to give consistent and reliable expression results from archival tissue, this will be of great use in proposed future clinical studies.

Key Research Accomplishments

- Increased the density of spotting on custom cDNA microarrays six fold (from 5,000 clones spotted singly to 15,000 clones spotted in duplicate).
- Decreased the amount of total RNA needed for a microarray hybridization eight fold (from 2 micrograms to 250 nanograms).
- Improved total RNA isolation methods from soft tissues to speed RNA isolations and improve RNA quality.
- Improved microarray analysis results by the use of Amersham Lucidea spotting and spike-in contols. These controls have known RNA concentrations and Cy3/Cy5 ratios and their use gives confidence that correct expression results are obtained.
- Trained multiple investigators in informatics and microarray data analysis.

Reportable Outcomes

None.

Conclusions

1) The technical objectives (1) To provide technical service; (2) To provide education; and (3) To update on recent advances have been achieved.

2) The microarray and informatics support services have increased throughput and improved microarray expression results in the Musculoskeletal Disease Center.

3) The improvements made to the microarray and informatics support services will expedite and advance research into gene discovery, function and genetic pathway analysis in the MDC.

References

Tanaka T.S. et al., Genome-wide expression profiling of mid-gestation placenta and embryo using a 15,000 mouse developmental cDNA microarray. Proc Natl Acad Sci U S A, 2000. 97(16), p. 9127-9132.

Project 12: Vector Support Service

Introduction

Several sub-projects in this proposal involve investigations of gene function and gene therapy, both of which require gene transfer technology. Accordingly, investigators working on these sub-projects of this Army grant need to use the gene transfer technology. Gene transfer technology uses vectors carrying the gene-of-interest and delivering it to the target cells. Development and design of appropriate vectors require technical expertise. It would be highly efficient and cost-effective to have a centralized Support Service facility within the Musculoskeletal Disease Center to serve these investigators by providing service in vector design and production, education and training, and technical advice in gene transfer technology. Accordingly, the Vector Support Service Facility serves as a dynamic resource for Investigators working on projects funded by the Army. As a result, the emphases of this Support Service focus on development and production of viral vectors, especially retroviral vectors that are based on Moloney murine leukemia virus (MLV) and human immunodeficiency virus (HIIV), and non-viral plasmid vectors for gene transfer and to provide training and assistance to investigators with respect to vector development and production.

Body

Technical Objectives

There were three specific objectives for this subproject:

1. To serve as a dynamic resource to construct and provide vectors for delivery and expression of appropriate genes for Investigators supported by the Army grant.
2. To serve as an educational resource, providing technical assistance and training to Investigators in the use of viral and non-viral vector gene delivery and gene expression.
3. To improve and expand vector systems available to Investigators as gene transfer technologies advance.

Progress on Specific Objectives

Specific Objective 1:

During the past twelve months, the vector support service produced numerous VSV-G pseudotyped MLV vectors and HIV-based vectors for various investigators working on projects supported by the Army. Specifically: 1) In collaboration with Dr. Rundle (sub-project 4), the facility generated various batches of concentrated VSV-G pseudotyped MLV vectors expressing different growth factor or control genes that have been used successfully in animal experiments. These growth factor or control genes included β–galactosidase (β-gal), enhances green fluorescent protein (EGFP), basic fibroblast growth factors (FGF-2) and its derivatives, bone morphogenetic protein-4 and its derivatives (BMP-4), growth hormone (GH), and inducible cyclooxygenase (Cox-2); 2) In collaboration with Dr. Gysin (sub-project 7), the facility produced three different batches of concentrated MLV-based vectors, expressing β–gal, BMP2/4, and Cox-2 genes, respectively. These viral vectors were used in Dr. Gysin's experiments testing potential synergistic interaction between BMP2/4 and Cox-2 in promoting bone formation in the critical sized calvarial bone defect model; 3) In collaboration with Dr. Strong (sub-project 8), the facility produced three different batches of concentrated VSV-G pseudotyped MLV vectors, expressing β–gal, LMP-HA, and IGFBP6 gene with or without

secretion signal, for animal experiments; 4) In support of sub-project 6 of this proposal, the facility generated a number of different batches of HIV-based vectors for use in the study of systemic gene therapy of musculoskeletal diseases. These HIV-based vectors included those expressing β-gal, EGFP, BMP2/4 and GH genes. To ensure the safety of these HIV-based vectors, each HIV-based vector was harvested and concentrated, tested for potential contamination of recombination competent retrovirus (RCR) within the preparation. None of these HIV-based vector preparations has shown RCR contamination in our assay system. The results have been submitted to the Biosafety committee and Animal Care and Use committee for review. The vectors were released to the investigators for the use in sub-project 6, only after both committees approved for the release of these batches of vectors.

Specific Objective 2:

With respect to providing education and tutorials to investigators, Dr. Chen (the director of the vector support facility) gave two lectures to staff at the J.L.Pettis VAMC, Musculoskeletal Diseases Center during the past 12 months. Both lectures were designed to educate and tutor Army project investigators in viral gene transfer technology. One lecture addressed the safety issues concerning the use of viral vectors in gene therapy, and the other lecture discussed the potential use of viral and plasmid vectors in research of musculoskeletal disease gene therapy. Dr. Chen also lectured the animal research facility personnel of J. L. Pettis VAMC in safe handling of animals treated with HIV-based and other viral vectors.

The Vector Support Service also provided essential technical assistance to various investigators. For example, the Service assisted Dr. Rundle (sub-project 4) in the design and development of several new HIV-based vectors for expression of therapeutic genes for the use of fracture repair in the rat tibial fracture model. In the past, ubiquitously expressed viral promoters (e.g., CMV or LTR) were used to drive expression of BMP2/4 in the viral vectors. While these promoters are powerful, they also lack tissue specificity. The lack of tissue specificity has been a potential safety risk with respect to BMP gene therapy, since BMPs are known to be converted muscles into bone. As a result, the use of ubiquitous promoters could represent a substantial safety risk of ectopic bone formation. A potential approach to minimize ectopic bone formation is to use an osteoblast specific promoter to drive the expression of the BMP gene. The use of an osteoblast-specific promoter should restrict the expression of the transgene in bone. HIV-based viral vectors are particularly suited for this application. Unlike vectors based on murine leukemia virus, HIV-based vectors are compatible with tissue-specific promoters and can also transduce non-dividing cells. HIV-based vectors have a much lower propensity for a strong immune response, which could lead to relatively long-term expression of the therapeutic gene. Consequently, The Vector Support Service assisted Dr. Rundle in the design and the production of several HIV-based viral vectors with different tissue-specific promoters in the pHIV-9 construct. The pHIV-9 construct is the third generation HIV-based vector with extra cPPT and wPRE sequences to ensure the high level of viral titer and gene expression. To evaluate these pHIV-9 vector constructs, we inserted 5 different promoters to drive a reporter gene, GFP. These promoters include: a strong viral promoter, cytomegalovirus immediate early promoter (CMV), a strong house-keeping promoter, human elongation factor 1-α (EF1–α), a 2.3 KB fragment of the promoter sequence from rat collagen 1α1 (Col2.3), a 310bp of promoter sequence from human α 1 type 1 procollagen (ColA2) and a 351bp of promoter sequence from

human Cbfa1 promoter (Cbfa1). The efficiency of these HIV-based vectors with tissue-specific promoter to drive expression of GFP was then determined and compared in osteoblastic (human SaSO-2 cells, rat ROS osteosarcoma cells, and mouse MC3T3-E1 cells) and non-osteoblastic cells (HT1080 human sarcoma fibroblastic cells, rat skin fibroblasts). We also included primary rat primary osteoblasts (RPO) in this study. The MLV-based vector was used as a control for comparison.

Each of cell types was plated in six-well plates and was transduced with 1-50 μl of each viral stock. Forty-eight hours after viral transduction, the GFP expression was evaluated by flow cytometry. The GFP positive cells were identified and the level of GFP expression were calculated from the software provide from the manufacture of the flow cytometer, B D Biosciences. The results were summarized in the **Table 1**.

Table 1. Mean GFP expression of HIV-based vectors in different types of cells. All the promoters are in HIV-based vector except for MLV-LTR. Cells lines were transduced with viral vectors and the level of GFP expression were determined by flow cytometry.

Promoters	HT1080	SaOS-2	RSF	ROS	RPO	MC3T3-E1
CMV	1173*	371	388	175	189	23
EF1-α	248	585	458	292	386	296
ColA2	24	51	46	ND	73	21
Col2.3	30	58	11	61	123	37
Cbfa1	37	92	18	52	117	37
MLV-LTR	255	216	504	149	619	61

*The level of GFP expression is expressed as arbitrate units. ND: Not detectable.

The viral promoters (CMV and MLV-LTR) and housekeeping promoter (EF1-α) were most potent in driving the expression of GFP gene in each test cell type, including osteoblasts. However, the viral promoters were more potent than EF1-α in non-osteoblastic cells. The EF1-α promoter in general appeared to be better than CMV and MLV-LTR in osteoblastic cells. As expected, the osteoblastic promoters were more effective in osteoblastic cells than non-osteoblastic cells. However, the potency of osteoblastic promoters was significantly lower than that of viral promoter or that of EF1-α. The differential preference of these test promoters in osteoblastic vs. non-osteoblastic cell types appeared to be species-independent. The lentiviral-based vector with the EF1-α promoter provides the optimal expression of the transgene in the bone cells. The relatively weak potency of the test osteoblastic promoter was somewhat surprising and disappointing. A much stronger osteoblastic-specific promoter is desirable for the use in gene therapy. Consequently, we are currently working with other investigators to identify more potent osteoblastic promoter sequences for testing.

Specific Objective 3:

a) Development of small interfering RNA retroviral vectors for studying of bone biology

Small interfering RNA (siRNA) has recently emerged as a new and powerful tool to knockdown the expression of endogenous genes. The high specificity and efficacy of siRNA to silence gene expression has opened up a new venue to study gene function *in vitro* and *in vivo*. The siRNA can be in the forms of oligonucleotides RNA or expressed as a hairpin RNA from plasmid or viral vectors. Within the past year, the Vector Support Service has developed a siRNA retroviral vector system that can be used by other investigators to suppress endogenous gene expression. Since the expression of siRNA requires a polIII promoter, we used the pSuppressor Retro vector (pSR) (from Imgenex Corporation) for siRNA vector development. With the pSR vector backbone, we have generated VSV-G pseudotyped MLV-based vectors in our viral facility. The viral titer was between $1X10^5$ to $1X10^6$ tfu/ml.

To test the efficacy of our siRNA vector system, we collaborated with Dr. Rundle to test the efficiency of our GFP siRNA vector in the suppression of GFP expression in cells transduced with our MLV-GFP vector. To prepare the GFP siRNA vector, we inserted a pair of synthesized DNA oligonucleotides corresponding to a unique sequence of the GFP gene into the pSR vector to generated pSR-GFP. The pSR-GFP vector contains a short hairpin sequence, which is specific to the GFP gene under the control of U6 promoter. To produce GFP expressing cells, we generated three HT1080 cell populations, each containing a single copy of the GFP gene using our MLV-based vector. Because the integration sites for MLV vectors are random, the use of three separate transduced cell population could minimize site-specific effects. We reasoned that the integration site would have a significant effect on the expression level of GFP. Accordingly, to ensure that the integration site of GFP in the transduced cells was different, we chose three different preparations with different GFP expression levels. After the establishment of each of the three HT1080 GFP cell lines, we transduced each line with the pSR-GFP retroviral vectors. Since the pSR-GFP vector also contains a neo gene, the siRNA-transduced cells could be selected by G418. After two weeks of selection, the G418 resistant colonies were pooled and the GFP expression level of each cell pool was analyzed by flow cytometry (**Table 2**).

Table 2. Mean GFP expression before and after siRNA transduction.

	GFP Level Before siRNA	GFP Level After siRNA	% Reduction of GFP Expression
HT1080 GFP-1*	**1392**	**58**	**96**
HT1080 GFP-2	**699**	**35**	**95**
HT1080 GFP-3	**95**	**12**	**91**
HT1080 Control	**4**	**ND**[#]	**ND**

*HT1080 GFP-1 to 3 represent three GFP transduced clones expressed different level of GFP.
[#]ND: Not done.

Table 2 clearly indicates that our GFP siRNA construct effectively suppressed GFP expression by >90%. The GFP siRNA construct was equally effective in each of the test cell pools of GFP transduced cells with varying degree of GFP expression. Consequently, we conclude that our siRNA construct was highly effective as well as integration-independent. We are now working with Dr. Rundle to design and prepare 6 concentrated, MLV-based FGF receptor siRNA targeting different domains of the FGF receptor to be used in his proposed

studies to test the role of FGF receptor in fracture healing. These studies are currently in progress.

b) Development of magnetic retroviral vectors for bone disease gene therapy.

Gene therapy for fracture repair requires accurate delivery of therapeutic genes to fracture sites. We recently showed that direct injection of an MLV-based vector expressing BMP4 to the rat femoral fracture callus enhanced bone formation. A major technical difficulty was associated with mis-injection of viral vector, resulting in extraperiosteal bone formation. We sought to develop a magnetic retroviral vector (MRV) targeting system for site-specific delivery of viral vector to fracture callus to improve the safety and efficiency of the therapy, because we believe that the magnetofection approach could allow the use of a magnet to direct target delivery of viral vector to fracture site. Moreover, magnetofection could significantly enhance viral transduction efficiency. To produce MRV, we collaborated with a research team in Taiwan, who fabricated magnetic nanoparticles of γ-Fe_2O_3 by a high-yield reduction-oxidation lyothermal method at high temperature under argon gas. Iron pentacarbonyl precursors were then reduced to form iron nanoparticles and oxidized by trimethylamine. High-resolution transmission electron microscopy (HRTEM) analysis revealed a narrow distribution of particle size of 4±0.8 nm. The resulting ferric nanoparticles were coated with polycationic, polyethyleneimine (PEI) by sonication. PEI is a cationic polymer capable of binding retroviral vectors. The average size of PEI-coated magnetic nanoparticles was 100-200 nm, determined by HRTEM (**Fig. 1**). Our Taiwanese collaborators provided us with the PEI-coated magnetic nanoparticles, we then synthesized the MRV complex by mixing the PEI-coated particles with various concentrations of our MLV vectors (**Fig. 2**).

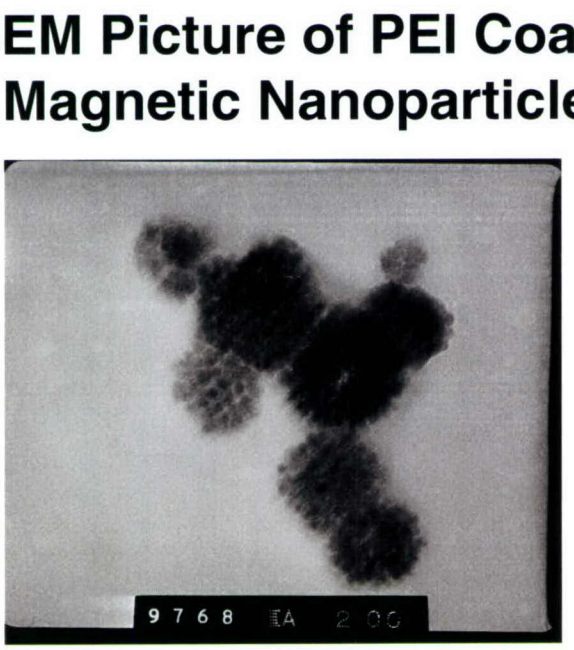

Figure 1. High-resolution transmission electron microscopic image of PEI Coated Magnetic nanoparticles.

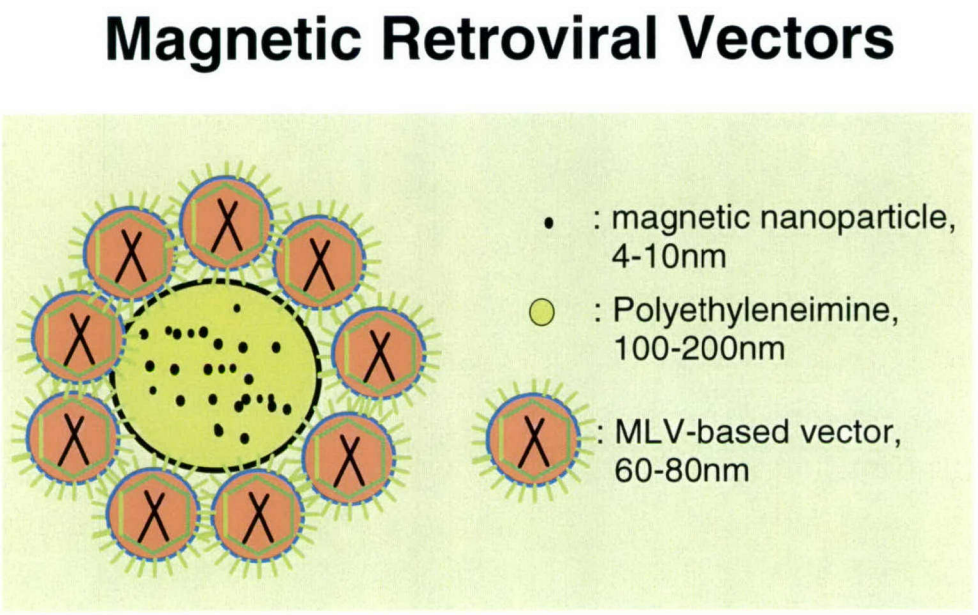

Figure 2. A schematic representation of magnetic retroviral vectors.

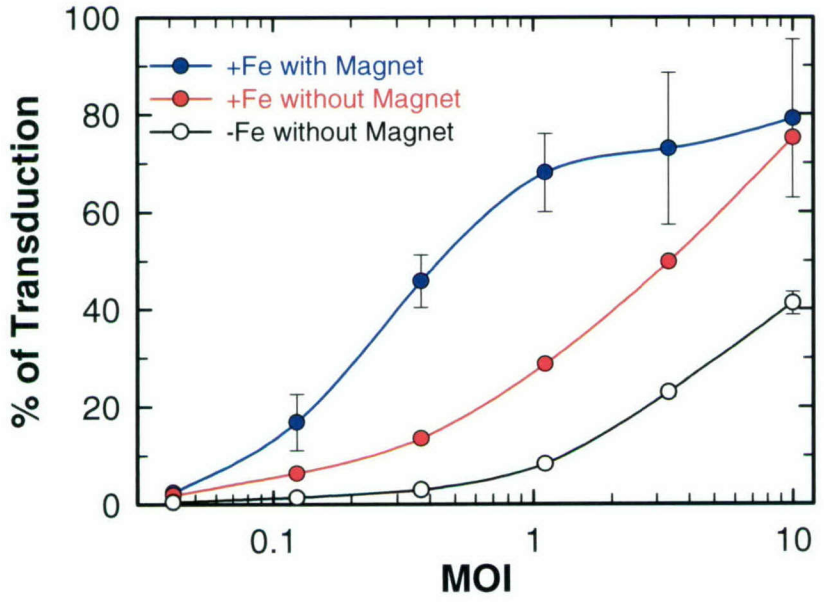

Figure 3: Magnetotransduction efficiency with respect to increasing multiplicity of infection (MOI). HT1080 cells (1.3 x 10^4 cells) in a 48-well plate were treated with various MOI of EGFP-MRV. A magnetic field was then applied for 20 min, and expression of GFP was measured by flow cytometry with the FACSCalibur. The transduction efficiency was assessed by measuring the percentage of transduced cells expressing GFP.

A. Regular β-gal viral vectors

B. β-gal MRVs with magnets

Figure 4: The MRV system enhanced targeted transduction in the femoral fracture model. The rat femur was stabilized with a pin, with a catheter then inserted. Sixteen hours after the insertion, the β-gal-MRV was injected into the marrow cavity through the catheter. A pair of magnets was placed outside of the injection site for 10 min (bottom femoral). Seven days after the delivery of the MRVs, the animal was sacrificed and the tissue from injection site was harvested for histological staining of β-gal. The top bone was injected with regular β-gal-MLV and without the magnet treatment.

We first evaluated the transduction efficiency of our MRV system expressing green fluorescent protein in HT-1080 cells. **Figure 3** shows that by applying a magnetic field created by a small magnet, the transduction efficiency of the MRV carrying the β-galactosidase (β-gal) was markedly increased by 3- to 5-fold ($p<0.001$) with an MOI between 0.1 to 1. This confirms the effectiveness of the MRV to transduce mammalian cells. To test the ability to target delivery of the MRV to fracture site, we collaborated with Dr. Rundle in assessing the effectiveness of the

MRV to produce targeted transduction at the fracture site in the rat femur model. In this experiment, we first inserted a metal rod in a rat femoral cavity, then using the rod as the guide to insert a catheter. The MRV (50μl of concentrated MLV-based vector and 50μl of magnetic nanoparticles mixed *in vitro*) was injected into the marrow space through the catheter. After the injection, two Nd-Fe-B permanent magnets were placed outside of the injection site for 15 min while the animals were under anesthesia. Seven days after injection, the animals were sacrificed and the femora were harvested. The femora were then spliced longitudinally and stained with x-gal overnight for β-gal activity. As shown in **Figure 4**, the femur with MRV has more x-gal staining than the control femur, particularly around the site where the magnets were placed.

At the present time, the fabrication procedure of magnetic nanoparticles has not been optimized by our Taiwanese collaborators. As a result, there have been significant variations in the quality of magnetic nanoparticle preparations. Accordingly, while some of the custom prepared magnetic nanoparticles yielded satisfactory results, a few others did not. On the other hand, magnetic nanoparticles have been used as magnetic resonance (MR) contrast agents and they can be obtained from commercial sources. Commercial magnetic nanoparticles are formulated specifically for *in vivo* applications and have been through rigorous quality control. Therefore, we tested whether these commercial magnetic nanoparticles would yield results that are more consistent. Thus far, we have tested two commercial magnetic nanoparticles, Resovist and FeridexIV. Both of these agents contain standard superparamagnetic iron oxide. The size of the iron oxide is between 4 to 10 nm. However, they are coated with different materials and formulated differently. The Resovist is coated with carboxydextran and the size is around 62nm after coating. The FeridexIV is coated with dextran and has sizes around 80-150nm. The Resovist is in the phase III trail in the Unites States, however, it is approved and commercially available from Europe and Asia. Resovist was obtained from our collaborator, Dr. Liu Hon-Man of the Department of Radiology at the National Taiwan University Medical Center. FeridexIV was purchased from a local commercial source. We compared the ability of these two commercial nanoparticles to form MRV complexes with our retroviral vector *in vitro*. Resovist, but not FeridexIV, was shown to be able to form active MRV complexes with our VSV-G pseudotyped MLV-based vector carrying β-galactosidase gene. Consequently, only Resovist was used in our subsequent testing.

The same rat femur model was then used to assess the enhancing effects of the Resovist-based MRV system on *in vivo* β-gal transduction of cells. Unlike the experiment shown in Fig. 4 above, we injected MRV directly into the femoral marrow cavity through the kneecap. After the injection, a pair of NdFeB-disk magnets (1.5 cm in diameter) was placed directly outside of the fracture site for 10 min. Seven days post-injection, the injected femora was dissected, cleaned, and stained with X-gal solution to examine the transduction efficiency. The pictures of X-gal stained femora are shown in **Figure 5**. There was markedly more β-gal activity staining in the MRV injected, magnet-treated femur than the control femur without the magnet treatment, particularly at the sites where the magnets were applied to. Histology of the MRV-injected, magnet-treated femur was also performed by the Phenotype Support Service. Briefly, the X-gal stained samples were demineralized and embedded in paraffin. Serial sections were prepared and stained with either Fast-red or Fast-red with Prussian blue. Fast-red stained the cell nuclei and Prussian blue stained iron particles. It was found that X-gal stains were co-localized with the Prussian blue stain, confirming that the transduced cells were found mostly in area populated

by the iron particles (i.e., MRV). As shown in **Figure 6**, The X-gal positive cells and the Prussian blue stained cells were close together. We believe this is the first demonstration that magnetic nanoparticles and viral vectors are physically linked *in vivo*. This demonstrates that certain MR contrast agents could be used to generate MRV. This successful preliminary evidence supports our belief that the MRV complexes could be useful for target delivery of viral vectors in gene therapy.

Figure 5: MRV complexes formed with Resovist enhanced viral vector transduction. Top panel shows the femur of the control animal, which was injected only with β-gal viral vector without magnetic nanoparticles. Bottom panel shows the MRV injected, magnet treated femur. Both femoral cavities received the same amount of viral vectors with equal volume of Resovist.

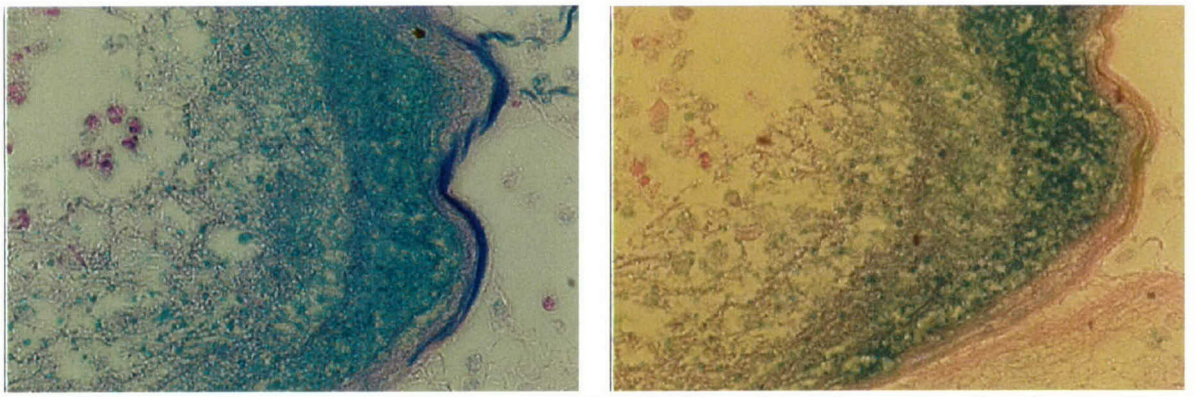

Figure 6: Histological staining of iron particles (Left) and β-gal countered stained with Fast Red (Right) in femur thin sections injected with the MRV and treated with the magnetic field. These two slides are serial sections.

In summary, these preliminary studies demonstrated that: 1) the magnetic nanoparticles are not cytotoxic; and 2) with the β-galactosidase reporter gene, the transduction of MRV was markedly enhanced in the direct injection in marrow cavity with the application of the magnetic field, particularly at the site where the magnets were applied. Therefore, the MRV system could be a very useful tool to deliver and enhanced the transduction efficiency of viral vectors at targeted sites.

c) Development of inducible retroviral vectors for bone disease gene therapy.

Bone disease gene therapy depends on the expression of growth factors, which can stimulate bone formation, at target sites at the appropriate time. The expression of the growth factor should be turned off when it is no longer necessary. Accordingly, the ubiquitous and unregulated expression of growth factor genes could be a major safety concern. For example, overexpression of BMP2/4 or FGF-2, two potent growth factors for bone formation, could cause serious side effects if their expression is unregulated. Consequently, the Vector Support Service has initiated work on the development of regulatable MLV-based vectors using ligand-inducible promoter. Our initial effort focused on the tetracycline-regulated systems. There are two general types of tetracycline-regulatable systems: 1) TET-ON system in which the expression of the transgene is enhanced by tetracycline or analogs; and 2) TET-OFF in which the transgene expression is inhibited by tetracyclines. Previously, our laboratory has developed a modified TET-OFF system in MLV-based vector. In this system, a ligand-binding domain of the estrogen receptor was fused to the carboxy terminus of tetracycline activated transcriptional activation (tTA) domain. This modified tetracycline-regulated system was referred to as tTAER. In the tTAER system, the toxicity of the VP16, transacting domain of the tTA, is modulated by the estrogen receptor ligand. The scheme of the tTARE is shown in **Figure 7**. To test the efficacy of the system, we inserted both the tTAER gene and the reporter gene (EGFP gene under the control of Tet-O promoter) into an MLV-based vector. We named this vector pAC-EGFP. **Figure 8** compares the molecular structure of pAC-EGFP with that of pY-EGF.

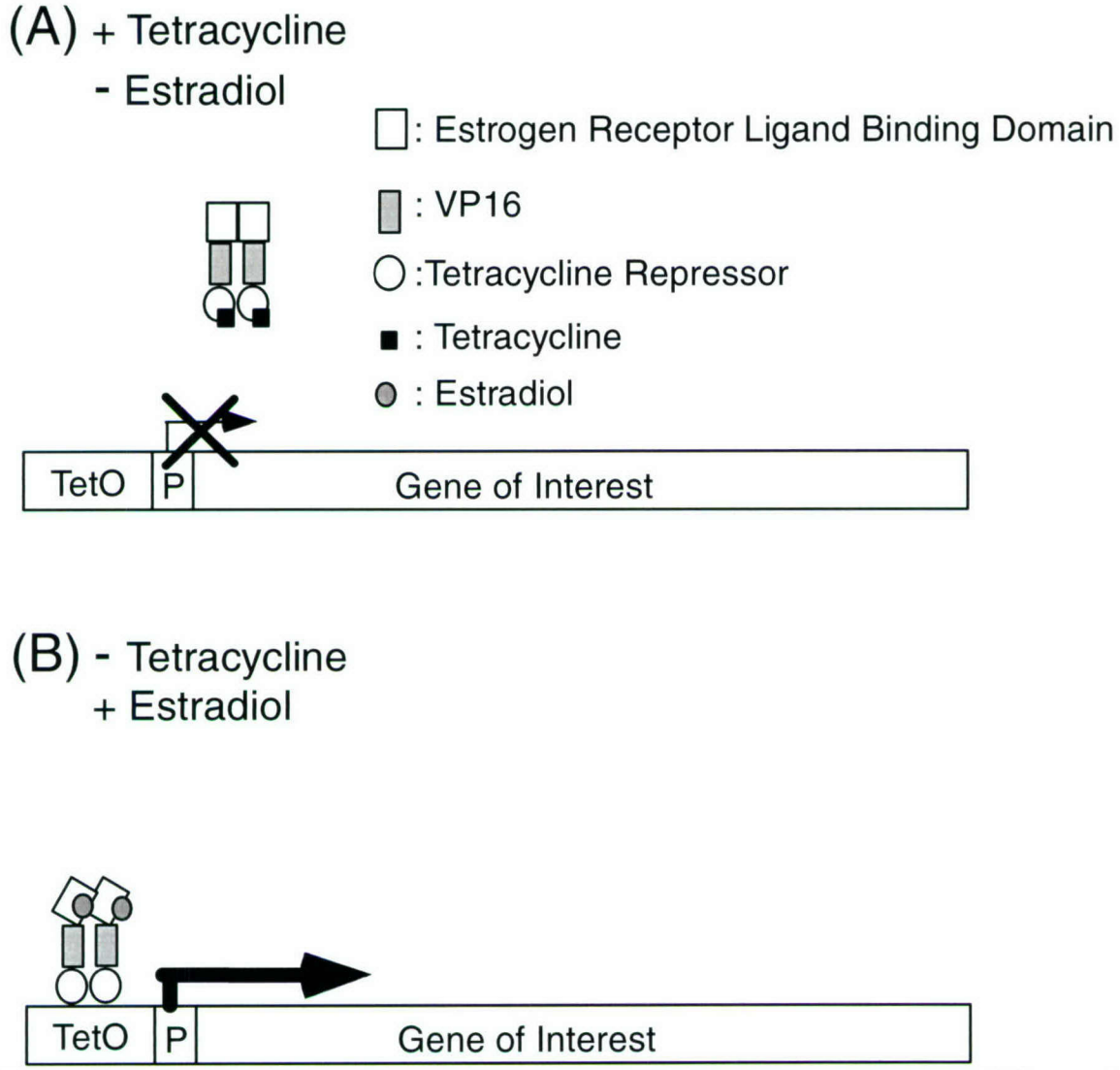

Figure 7: Schematic illustration of tTAER controlled gene expression. tTAER contains three major components. The tetracycline repressor binds to the TetO sites in the absence of the tetracycline. This component provides the promoter recognition and tetracycline control of gene expression. The second part of tTAER is VP16. VP16 is the transactivation domain of tTAER. It is originated from Herpes Simplex Virus, which can be cytotoxic when it is present in the nucleus. The third part of tTAER is the estrogen-binding domain of estrogen receptor. This component alleviates the toxic effect of VP16 and provides an additional control point of the gene expression. Under suppressive conditions, as illustrated in (A), the tetracycline prevents the binding of Tet repressor to the TetO promoter. Thus, the expression of the gene of interest will be turned off. In the absent of tetracycline and in the present of the estrogen receptor ligand, estradiol, the expression of the gene of interest will be turned on. Therefore, this system belongs to the TET-OFF system.

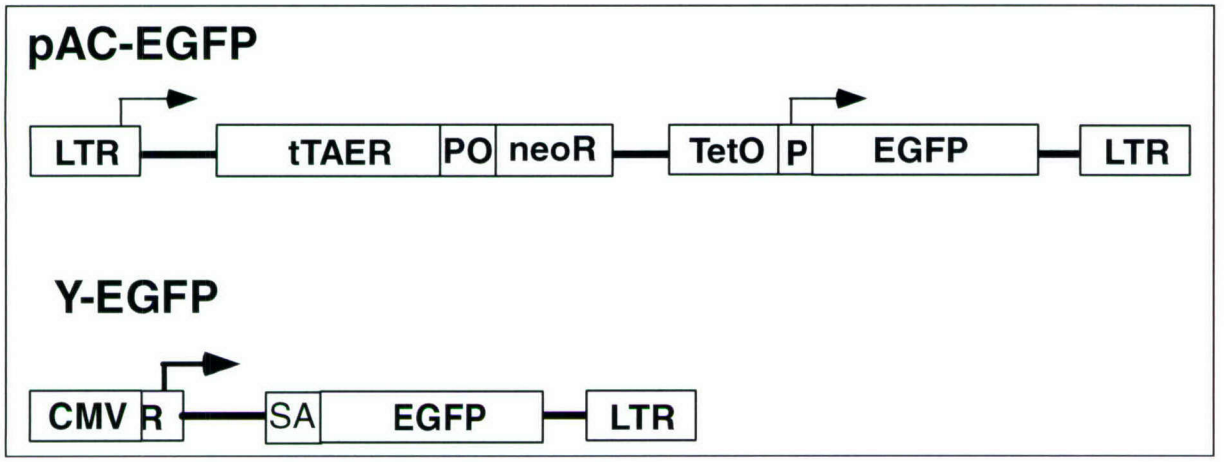

Figure 8: Schematic illustration of pAC-EGFP and pY-EGFP. The figure compares the structure of pAC-EGFP and pY-EGFP. The genomic RNA of pAC-EGFP is transcripted by 5' LTR and the genomic RNA of pY-EGFP is driven by CMV promoter. The expression of EGFP in pAC-EGFP is controlled by TetO promoter and can be modulated by tetracycline and estradiol. In the presence of tetracycline, the expression of EGFP will be turned off, however, in the present of estradiol, the EGFP expression will be turned on. On the other hand, the expression of EGFP in pY-EGFP is from the MLV-LTR promoter.

We prepared concentrated VSV-G pseudotypes MLV-based pAC-EGFP and tested its ability to drive expression of EGFP under different culturing conditions. The pY-EGFP (without the TET-OFF regulatory element) was included as a control for comparison. Accordingly, the expression EGFP of the pACEGFP vector was driven by the TetO promoter and the expression of EGFP of the pY-EGFP vector was driven by the unregulatable MLV-LTR promoter. Our results are summarized in **Table 3**. It was found the titer of pAC-EGFP is 4-7 fold lower than that of pY-EGFP. This significant decrease of viral titer could be attributed to the following reasons: 1) In order to accommodate the tTAER gene and Tet-O promoter, the insertion DNA in the MLV-based vector is 4 kB larger in pAC-EGFP than that in pY-EGFP. It has been shown that the extra inserts could interfere with the MLV packaging and subsequently result in a decrease of viral titer. 2) The pY-EGFP genomic RNA is generating from CMV promoter and the pAC-EGFP genomic RNA is from MLV-LTR promoter. It has been shown that the CMV promoter is stronger than MLV-LTR promoter in the packaging cells, 293T. The lower level of genomic MLV-vector RNA may also lead to a lower viral titer. Nonetheless, we have generated the vector with a titer of 3×10^6 tfu/ml, which should be sufficient for most gene therapy applications. Neither tetracycline nor β-estradiol had a significant effect on the mean intensity of EGFP in the pY-EGFP-transduced cells, whereas there was ~3-fold increase in the mean intensity under inducible conditions in pAC-EGFP-transduced cells, confirming the regulatable nature of the pAC vectors (**Table 3**).

To study the Tet-Regulated system in other cell types, we transduced various cell types, including 293T, rat marrow stromal cells (RMSC) and rat skin fibroblast (RSF), with the pACEGFP and pY-EGFP vectors. The EGFP expression level of each transduced cell type were determined and compared (**Table 4**). As expected, neither tetracycline nor β-estradiol had a significant effect on the mean intensity of EGFP in each of the pY-EGFP-transduced cell types.

In contrast, in each of the pAC-EGFP transduced cell types, there was up to a 10-fold increase under the inducible condition (-tetracycline and + β-estradiol). These findings confirm that we have developed a TET-OFF regulatable system for our MLV-based vectors. In the next funding period, we will insert growth factors genes into the pAC construct and test its ability to modulate the expression of growth factors and bone formation *in vitro* and *in vivo*.

Table 3: Viral titer and mean intensity of EGFP expression under different media. The medium containing β-estrodial is inducible for pAC-EGFP and medium with tetracycline is inhibitory. The viral titer and mean intensity are measure in the HT1080 cells.

	pY-EGFP		pAC-EGFP	
Types of Media	Viral Titer	Mean Intensity	Viral Titer	Mean Intensity
- Tetracycline, - β-estradiol	**1.90×10^7**	**349.2**	**3.84×10^6**	**65.9**
- Tetracycline, + β-estradiol	**2.05×10^7**	**382.3**	**2.86×10^6**	**218.0**
+Tetracycline, - β-estradiol	**1.88×10^7**	**394.5**	**2.82×10^6**	**69.1**
+Tetracycline, + β-estradiol	**1.47×10^7**	**420.8**	**3.60×10^6**	**96.4**

Table 4: Mean intensity of EGFP expression in different media and different cell types. The mean intensities of EGFP expression are measure in the three different types of cells.

	Mean Intensity of pY-EGFP			**Mean Intensity of pAC-EGFP**		
	293T	**RMSC**	**RSF**	**293T**	**RMSC**	**RSF**
- Tetracycline - β-estradiol	**84.1**	**830.6**	**2727.1**	**38.9**	**74.2**	**142.8**
- Tetracycline + β-estradiol	**73.2**	**756.4**	**3158.1**	**302.7**	**591.0**	**1023.6**
+Tetracycline - β-estradiol	**70.8**	**767.4**	**2886.1**	**39.5**	**67.9**	**118.0**
+Tetracycline + β-estradiol	**62.6**	**1032.5**	**3429.6**	**41.7**	**90.6**	**157.5**

Key Research Accomplishments

- Prepared MLV and HIV-based vectors for other sub-projects (sub-projects 4, 6. 7 and 8)
- Designed tissue specific HIV-based vectors for sub-project 4.
- Developed magnetic retroviral vectors for bone diseases gene therapy
- Developed siRNA retroviral vectors to study the function of genes in bone repair
- Developed inducible retroviral vectors for bone diseases gene therapy

Reportable Outcomes

Peer reviewed research papers:

1. Zhang, X., T. Linkhart, E. Wergedal, S.-T. Chen, H. Peng, M. Sheng, K. Lau and D. Baylink (2004) Local ex vivo gene therapy with bone marrow stromal cells expressing human BMP4 promotes endosteal bone formation in mice. J Gene Med. Jan;6(1):4-15.

2. Sivanandam A. S., S. Mohan, H. Kita, S. Kapur, S.-T. Chen., T. A. Linkhart, G. Bagi, D. Baylink and X. Qin (2004) Studies on regulation of IGF (insulin-like growth factor)-binding protein (IGFBP) 4 proteolysis by pregnancy-associated plasma protein-A (PAPP-A) in cells treated with phorbol ester. Biochem J. Apr 1;379:57-64.
3. Klamut H.J., S.-T. Chen, K.-H. W. Lau and D. Baylink. (2004) Progress toward skeletal gene therapy. Crit Rev Eukaryot Gene Expr. 14(1-2):89-136.
4. Kapur, S., S.-T. Chen, D. Baylink, and K.-H.W. Lau (2004) Extracellular signal-regulated kinase-1 and -2 are both essential for the shear stress-induced human osteoblast proliferation. Bone 35:525-534

Abstracts reported in conferences:

1. Sivanandam A. S., S. Mohan, H. Kita, S. Kapur, S.-T. Chen., T. A. Linkhart, G. Bagi, D. Baylink and X. Qin Identification of a novel mechanism by which activation of the PKC-suppresses the catalytic activity of the IGFBP-4 protease/pregnancy associated plasma protein-A. 25th Annual meeting of the American Society for Bone and Mineral Research, Minneapolis, USA, Sep. 19-23
2. S.-T. Chen, M.-F Tai, K.-M. Chi, M.-C Wen, C. H. Rundle, J. Wergedal, K. -H. W. Lau, and D. J. Baylink (2003) Development of Magnetic Retroviral Vectors for Site-Specific Targeting in Skeletal Gene Therapy, 25th Annual meeting of the American Society for Bone and Mineral Research, Minneapolis, USA, Sep. 19-23

Conclusions

1) In collaboration with investigators of other sub-projects of this Army grant, we have generated and provided with the investigators several different batches of MLV and HIV-based vectors for use in their approved projects.

2) We developed tissue specific HIV-based vector for delivering of growth factors to the bone repairing sites.

3) We developed siRNA retroviral vectors, which can specifically inhibit any target genes. This vector should be very useful for investigations into gene function during bone repair.

4) We developed a MRV system that provides efficient site-specific targeted delivery of viral vectors to specific bone sites. This MRV system should be useful in site-specific targeting and delivery of viral vectors for skeletal gene therapy.

5) We developed an inducible TET-OFF regulatory retroviral vector system. The gene expression of this vector can be modulated by tetracycline and β-estradiol. This vector system is essential for skeletal gene therapy and for studying the function of growth factor genes during bone repair.

APPENDICES

Abstracts Reported In Conferences:

1. Chadwick RB, Bu LM, Yu H, Hu Y, Sachdev R, Tan QW, Wergedal JE, Mohan S, and Baylink DJ. Digit Tip Regeneration and Global Gene Expression Profiling in the MRL Super-Healer Mouse. American Society for Bone and Mineral Research, Seattle, WA, October (2004)

2. Xing W, Baylink DJ, Kesavan C and Mohan S. Transfer of 128-kb BMP-2 Genomic Locus by HSV-Based Infectious BAC Stimulates Osteoblast Differentiation: A Platform for Functional Genomic Studies. American Society for Bone and Mineral Research, Seattle, WA, October (2004)

3. Xing W, Baylink DJ, Kesavan C, Yu H, Chadwick RC, Hu Y, Rajkumar R and Mohan S. Global Analysis of 22,000 Genes in the Bones Reveals Involvement of Several Novel Genes/ESTs and Pathways in Mediating the Anabolic Response of Mechanical Strain in Mice In Vivo, American Society for Bone and Mineral Research, Seattle, WA, October (2004)

Peer Reviewed Research Papers:

4. Xing W, Baylink D, Kesavan C and Mohan S. HSV-1 Amplicon-Mediated Transfer of 128-kb BMP-2 Genomic Locus Stimulates Osteoblast Differentiation in vitro. *Biochem Biophys Res Commun* 319(3): 781-6, (2004)

5. Klamut HJ, Chen S-T, Lau W K.-H., Baylink DJ. Progress Toward Skeletal gene Therapy. *Critical Rev in Eukaryotic Gene Exp*, 14 (1&2): 89-136 (2004)

Digit Tip Regeneration and Global Gene Expression Profiling in the MRL Super-Healer Mouse

Robert B. Chadwick, Liming Bu, Hongrun Yu, Yan Hu, Ralph Sachdev, Qianwei Tan, Jon E. Wergedal, Subburuman Mohan, and David J. Baylink.
Molecular Genetics Division, Musculoskeletal Disease Center, Loma Linda, CA.

Abstract: The MRL mouse is the only known strain of mouse that shows complete healing of an ear punch without scarring. Additionally, the MRL mouse can regenerate cardiac lesions. The present study sought to test the hypothesis that the MRL mouse also shows superior regeneration properties in the digit tip amputation model. The control mouse was the DBA mouse that exhibited only moderate healing in ear-punch experiments. Immediately after birth, right paw digit tips of neonatal mice were dissected, with the left front paws as uncut controls. The amount of tissue amputated was measured and consecutive x-ray images were captured of the left and right paws at 7, 14, 21 and 28 days post amputation. Additionally, at four days post dissection, total RNA from the MRL and DBA regenerating digit tips was isolated. Microarray expression profiling was undertaken of this RNA in comparison to RNA from control tissue collected at the time of surgery. At 14 days post amputation both mouse strains were found to regenerate, however the regeneration rate of the MRL digit tips was greater in comparison to the DBA strain ($p=0.016$). Over 500 genes out of 15,000 on the microarray were significantly differentially expressed ($p < 0.05$) in MRL and DBA mice at day four in comparison to control tissue at day zero. Of these, 170 genes were upregulated and 280 were downregulated in both mouse strains. About 50% of these genes represent ESTs and unknown genes. Pathway analysis reveals that genes in the BMP/TGF pathway are differentially expressed in both mouse strains (BMP-1, Actr2, Smad 4, TGFb1i4, Fstl3, Twsg1, TSC22), thus implicating the BMP/TGF signaling pathway in regulation of digit tip regeneration ($p < 0.05$). Multiple differences between MRL and DBA strains were found in transcription factors that are implicated in embryogenesis, including Mesp2 (involved in Notch signaling and somitogenesis, upregulated 2.8 fold), Net1 (highly expressed in neurons and involved in gastrulation, upregulated 1.7 fold), Bola-like transcription factor (upregulated 4.1 fold) and EST Mm. 270291 (DNA binding zinc-finger protein, upregulated 3.0 fold). We conclude that 1) MRL mice show greater regenerative capacity to heal digit tips compared to DBA mice; 2) The BMP/TGF signaling pathway is involved in digit tip regeneration; 3) Increased regenerative capacity of the MRL mouse may be due to strain specific increased expression of transcription factors that function in embryogenesis and development.

Introduction:

Experiments with amphibian limbs, first undertaken in the 18th century, demonstrate that limb regeneration in vertebrates is possible [1, 2]. It is also known that higher mammals have only marginal abilities to regenerate. One example of regeneration in mammals is the healing of ear holes in rabbits without scarring [3, 4]. Recently, we have also demonstrated that the MRL inbred strain of mouse shows greater regeneration and scarless healing of ear-hole punches as opposed to several other inbred strains of mice. [5-7]. It has also recently been shown that the MRL mouse is capable of cardiac muscle regeneration [8]. Thus, the MRL mouse is a unique model to study the genetic mechanisms that regulate wound healing and tissue regeneration.

However, to date, the MRL mouse has not been investigated extensively for its abilities to regenerate more complex biological structures such as digit tips. This study examined digit tip regeneration in inbred strains of mice in an attempt to identify good and poor digit tip regenerators. We also undertook global RNA expression profiling in those strains in order to identify the genes and genetic mechanisms responsible for wound healing and digit tip regeneration.

Materials and Methods:

Animals Four-week old MRL and DBA mice were obtained from The Jackson Laboratories (Bar Harbor, ME). The day that mouse pups were born surgery was conducted on the pup's digit tips. The right front 3rd and 4th digit tips were amputated, with the left side as uncut controls. The amputated tissues were collected into RNA later (Ambion), and the tissues from the pups of one litter were pooled. Both left (uncut) and right (cut) paws X-ray images were taken at 0, 7, 14, 21, and 28 days post surgery with a Faxitron. Also, at four days post surgery, mice were sacrificed and regenerating digit tips were collected by surgery and the tissue was pooled in RNA later and stored at –80C for later RNA extraction.

RNA Extraction Total RNA was isolated from dissected tissues at day 0 and day 4 day using the Agilent Total RNA Isolation Kit (Agilent Technologies). The total RNA concentration was determined by NanoDrop spectrophotometer and RNA quality was determined by 18S/28S ribosomal peak intensity on an Agilent Bioanalyzer. For microarray expression profiling and real-time PCR, RNA samples were used only if they showed little to no degradation.

Growth Rate Measurement Faxitron x-ray images were measured using the ruler feature of Photoshop (Adobe) (Figures 1, 2). Four growth amounts were determined. 1) the amount of dissected tissue; 2) the length of first phalanx of 3rd and 4th fingers of front two paws; 3) the length from the bottom of 2nd phlanx to the tissue edge; and 4) the length from the top of 2nd phalanx to the tissue edge. Measurements were made of both left uncut and right cut digits. The growth was determined for 7, 14, 21 and 28 days post surgery. In order to correct for strain specific size differences, right cut growth measurements were divided by the left uncut measurements to give a normalized ratio of the amount of regeneration for each strain.

Figure 1. Measurement of Amounts of Dissected Tissues in Newborn Mouse Pups. The digit tip dissections were carried out on the 3rd and 4th tips of the right paw. The left paw digit tips were not dissected and used as uncut controls to correct for inbred mouse strain size differences. Mice were x-rayed before and after digit tip dissection. Amounts of tissue dissected were calculated by subtracting the after dissection values from the before dissection values of the top of the second phalanx to the digit tip edge.

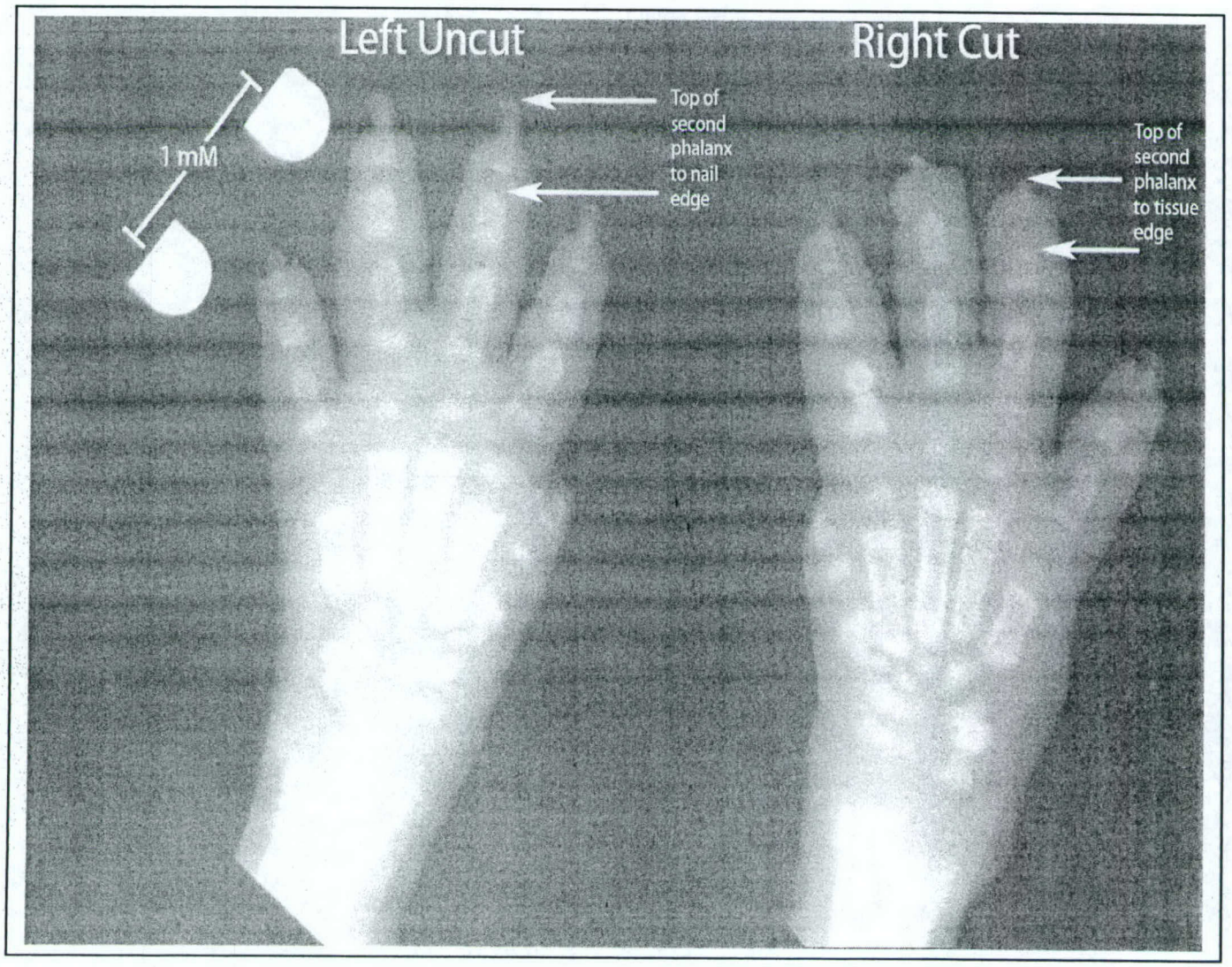

Figure 2. Measurement of Digit Tip Regrowth. Mice were x-rayed at days 7, 14, 21 and 28 post digit tip dissection. Growth was calculated as follows:

- The length of first phalanx of 3rd and 4th fingers of both front paws (C to D below);
- The length from the bottom of 2nd phlanx to the tissue edge (C to A below)
- The length from the top of 2nd phalanx to the tissue edge (B to A below).

In order to correct for strain specific size differences, right cut growth measurements were divided by the left uncut measurements to give a normalized ratio of the amount of regeneration for each strain.

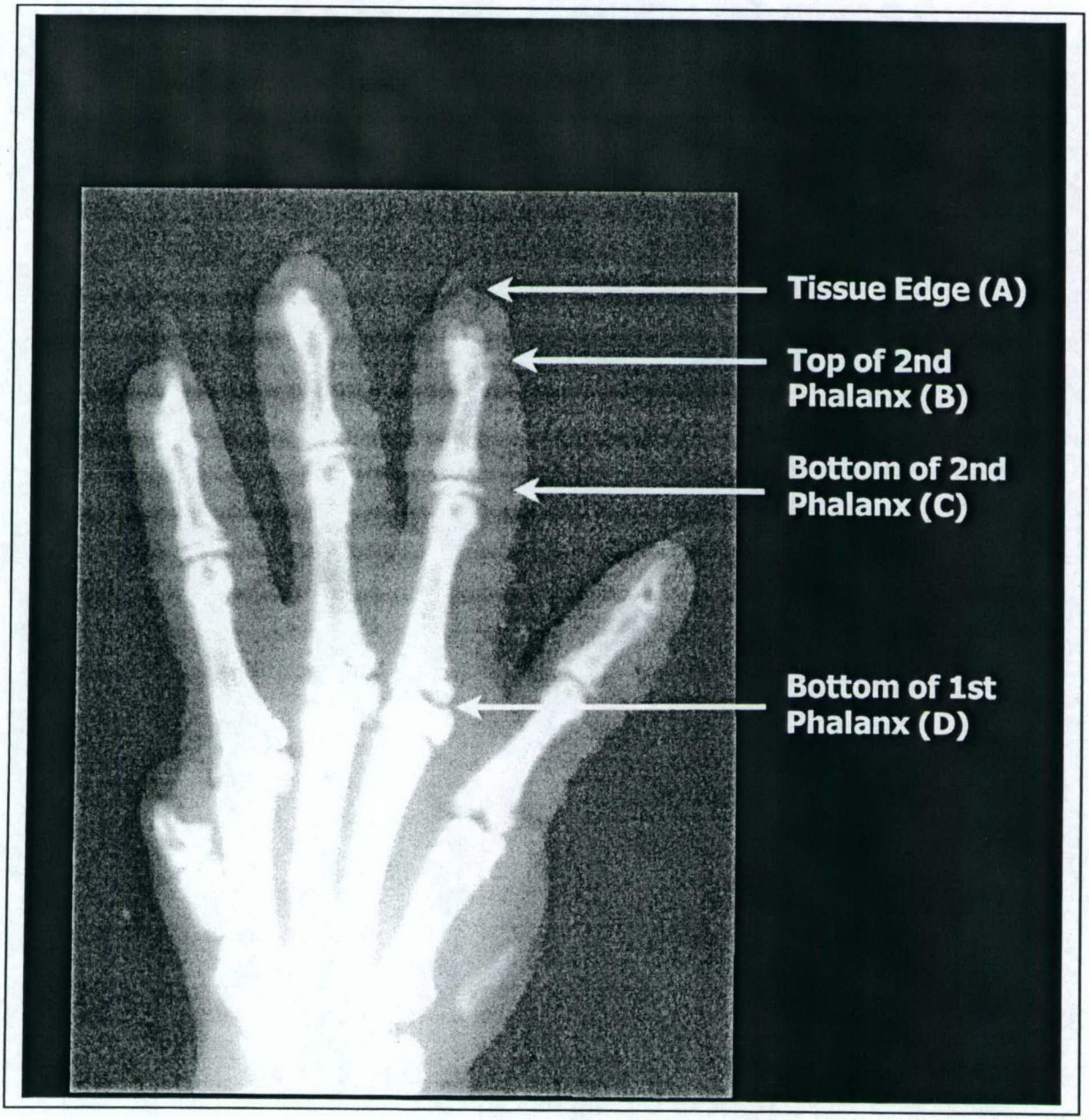

Microarray Expression Analysis: Custom cDNA slides were spotted in duplicate with ~15,000 cDNA clones obtained from the National Institute on Aging (NIA) [9]. A Q-Array2 robot (Genetix) was used for spotting. The arrays were also spotted with Amersham Lucidea Universal Scorecard controls to insure correct gene expression values were obtained from each array. A total of 250 ng of total RNA was used to synthesize double stranded cDNA using the Low RNA Input Fluorescent Linear Application Kit (Agilent). Cyanine-3-dCTP and cyanine-5-dCTP were used to label experimental samples (day 4) and control samples (day 0). Dye swaps were also conducted to eliminate potential dye bias effects. The slides were scanned using a GSI Lumonics ScanArray 4000 scanner. The signal intensity of all microarray images was determined using Imagene 5.6 software. Expression analysis of microarray experiments were performed with GeneSpring 6.1 (Silicon Genetics) using the raw intensity data generated by the ImaGene software. Local background-subtracted median signal intensities were used as intensity measures, and the data was normalized using per spot and per chip LOWESS normalization. The transcripts that passed with flag values present or marginal were targeted for further analyses. The transcripts were then further analyzed by utilizing a one-sample Student's t-test to test whether the mean normalized expression level for the gene is statistically different from 1.0. Genes greater than 1.7 fold up and downregulated at day 4 vs day 0 were determined for both the MRL and DBA strains.

Real Time PCR Reverse transcription of 200ng of total RNA (Day 4 and Day 0) was carried out in a final volume of 20ul using Invitrogen's reverse transcriptase kit according to the manufacturer's instructions. To prevent 3' bias of the real-time PCR reactions random decamers (Ambion) were used for priming rather than oligo-dT. Real-time PCR was done using the SYBR Green PCR Core Reagents Kit (Applied Biosystems). Cycling and signal detection was done using the ABI-7900HT Sequence Detection System. Gene expression levels were normalized to housekeeping gene Beta-Actin using the the $2^{-\Delta\Delta Ct}$ method. A subset of all RT-PCRs were sequenced to insure gene specificity for the reactions.

Results:

Figure 3. Normalization Ratio of Strain Size. In order to insure that regeneration results were not influenced by differences in strain size, the data was normalized by dividing right cut growth measurements by left uncut growth measurements.

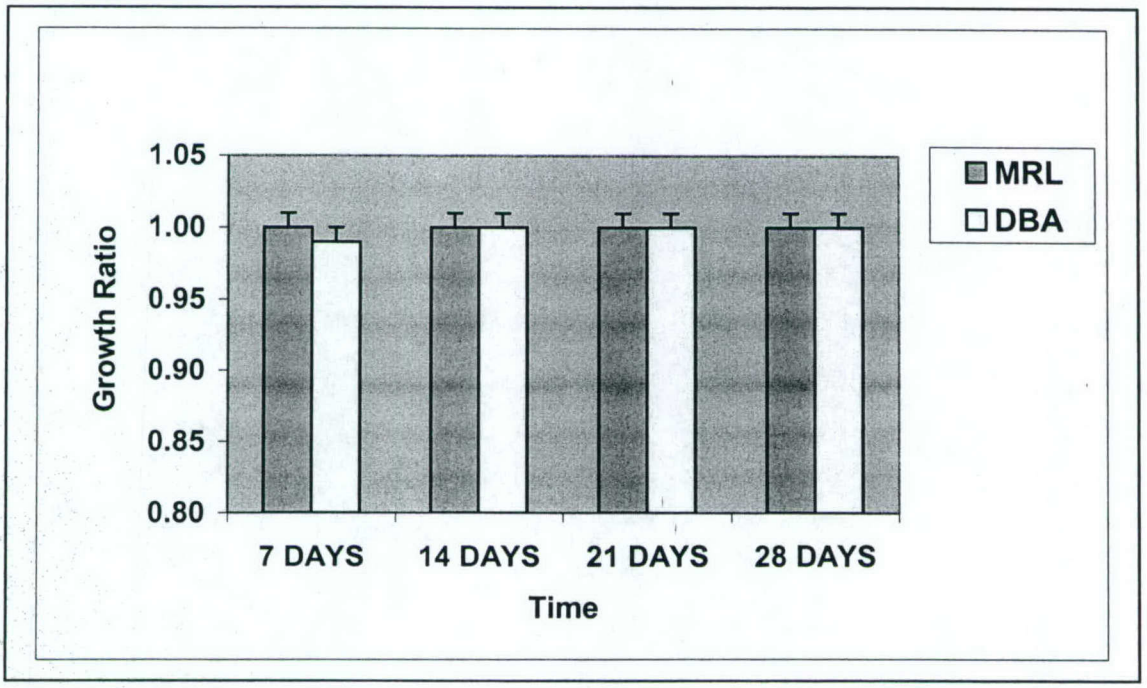

Interpretation: Division of first phalanx right measurements by left measurements gives expected ratios of ~1.00. Also, no significant difference between strains is seen in normalized data for the first phalange growth ratios. Since the first phalanges were not dissected, this demonstrates that normalizing for strain size by calculating a growth ratio is a valid method of correcting for strain size.

Figure 4. Normalized Growth Ratio Regeneration of MRL and DBA Digit Tips. Growth ratios from the bottom of 2nd phlanx to the tissue edge (C to A in Figure 2) are shown below.

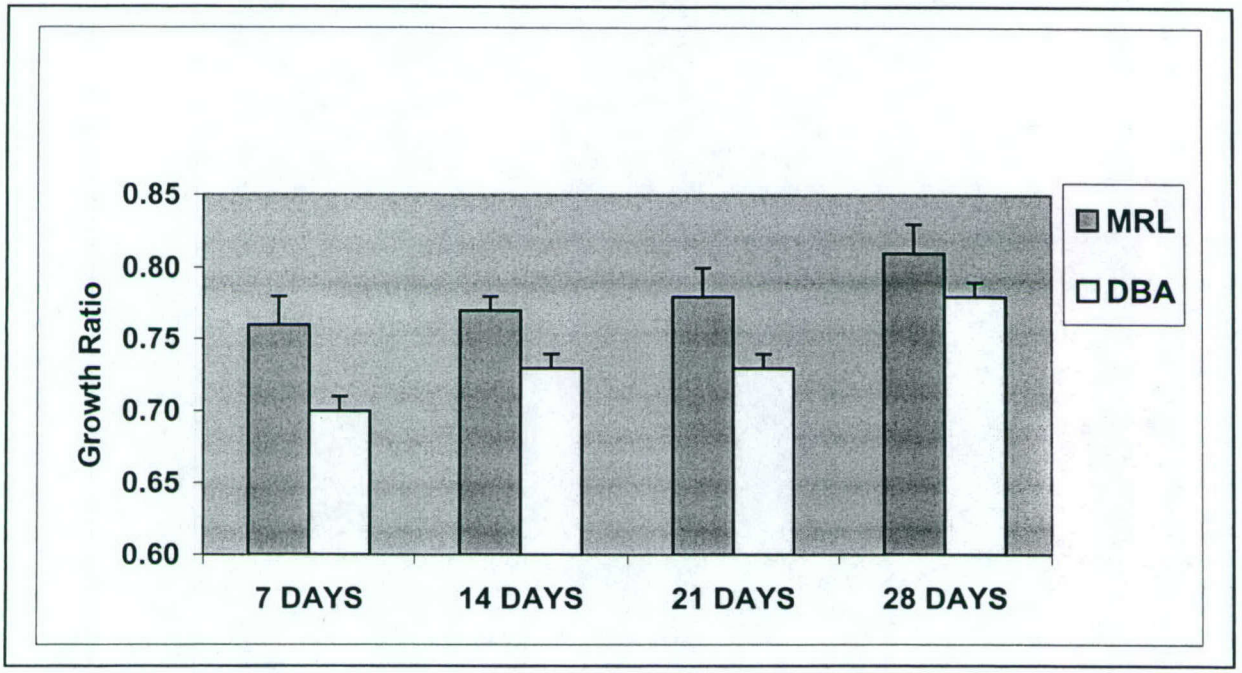

Interpretation: As expected, the regeneration ratios are below one, indicating growth of dissected digit tips is less than undissected digit tips. However, at 7, 14, and 21 days post dissection, MRL mice regenerate digit tips greater than DBA mice ($p < 0.05$). This is when pups are in their primary growth phase (days 0 to 21). The growth ratio does not equal one at 28 days since some of the mice did not completely regenerate digit tips within 28 days.

Table 1. Microarray Expression Results of Genes Differentially Expressed in Both MRL and DBA at Day 4 Post Digit Tip Dissection. Shown in Table 1 is a summary of genes with known functions that are differentially expressed in regenerating digits in both MRL and DBA strains at day 4 in comparison to control tissue at day 0.

Clone Name	Gene Name	Gene Ontology Function
H3031B07	**Twsg1**	**GO:0001503 ossification**
H3005D09	**Fstl3**	**GO:0030514 negative regulation of BMP signalling pathway**
H3098E10	Mor1	GO:0006099 tricarboxylic acid cycle
H3052A04	Mor2	GO:0006099 tricarboxylic acid cycle
H3138A12	4632428N09Rik	GO:0006118 electron transport
H3156A07	Nme6	GO:0006228 UTP biosynthesis
H3031E10	Ahcy	GO:0006306 DNA methylation
H3051D06	2700078H01Rik	GO:0006350 transcription
H3004A11	Tceb3	GO:0006350 transcription
H3097C06	**TGFB1I4 (TSC-22)**	**GO:0006355 regulation of transcription**
H3087E04	Cnot7	GO:0006355 regulation of transcription
H3016G05	Ewsh	GO:0006355 regulation of transcription
H3113H06	Fem1b	GO:0006355 regulation of transcription
H3123B05	Hdac2	GO:0006355 regulation of transcription
H3055B11	Nrf1	GO:0006355 regulation of transcription
H3058C01	Rora	GO:0006355 regulation of transcription
H3016H10	Sp1	GO:0006355 regulation of transcription
H3017H05	Wbp4	GO:0006355 regulation of transcription
H3089B10	Zfp398	GO:0006355 regulation of transcription
H3076G09	9430065L19Rik	GO:0006397 mRNA processing
H3107B08	Upf2	GO:0006397 mRNA processing
H3045D06	Psmd7	GO:0006413 translational initiation
H3023F07	Cct5	GO:0006457 protein folding
H3023D07	D630041K24Rik	GO:0006464 protein modification
H3066E06	C430014H23Rik	GO:0006468 protein amino acid phosphorylation
H3057F01	Csnk1e	GO:0006468 protein amino acid phosphorylation
H3063A08	Lgmn	GO:0006508 proteolysis and peptidolysis
H3048C09	Fbxl12	GO:0006511 ubiquitin-dependent protein catabolism
H3113D07	Psma3	GO:0006511 ubiquitin-dependent protein catabolism
H3013F01	Alad	GO:0006779 porphyrin biosynthesis
H3089A11	Abcf2	GO:0006810 transport
H3054H04	Kcnn4	GO:0006811 ion transport
H3109D12	2210017A09Rik	GO:0006813 potassium ion transport
H3030E02	Gabarapl2	GO:0006886 intracellular protein transport
H3040F06	Mpv17	GO:0006886 intracellular protein transport
H3028C06	Sec13r	GO:0006886 intracellular protein transport
H3076G10	Tomm22	GO:0006886 intracellular protein transport
H3085H07	Vps26	GO:0006886 intracellular protein transport
H3153D07	Ngfrap1	GO:0006917 induction of apoptosis
H3002C02	Actr2	GO:0006928 cell motility
H3006C11	Rps18	GO:0007046 ribosome biogenesis
H3125H12	Rps6	GO:0007046 ribosome biogenesis

H3147D06	Cdk4	GO:0007049 cell cycle
H3054A03	D5Ertd249e	GO:0007049 cell cycle
H3098A09	Epdm2-pending	GO:0007160 cell-matrix adhesion
H3066H10	Mapk8	GO:0007165 signal transduction
H3007D07	Pwp2h	GO:0007165 signal transduction
H3133D05	Rock1	GO:0007165 signal transduction
H3002D10	Madh4	GO:0007184 SMAD protein nuclear translocation
H3091D08	Gna14	GO:0007186 G-PCR protein signaling pathway
H3018D02	Gnai2	GO:0007186 G-PCR protein signaling pathway
H3001E05	Homer2	GO:0007186 G-PCR protein signaling pathway
H3154B03	Frap1	GO:0007281 germ-cell development
H3065C08	Ppp3cb	GO:0007507 heart development
H3040F05	Smyd1	GO:0007507 heart development
H3022F08	Tpm3	GO:0007517 muscle development
H3054D06	Ovgp1	GO:0008152 metabolism
H3082B04	Pfkfb3	GO:0008152 metabolism
H3048G06	Srm	GO:0008295 spermidine biosynthesis
H3069G01	9930118K05Rik	GO:0008654 phospholipid biosynthesis
H3115C03	**Bmp1**	**GO:0009887 organogenesis**
H3029F09	Atp6v1e1	GO:0015986 ATP synthesis coupled proton transport
H3002B06	Ehd1	GO:0016197 endosome transport
H3001H10	Tmsb10	GO:0030036 actin cytoskeleton organization and biogenesis
H3043B04	**Strap**	**GO:0030512 regulation of TGFB receptor signaling pathway**
H3020F08	Was	GO:0042110 T-cell activation
H3114B04	Rdx	GO:0045176 apical protein localization

Interpretation: Over 500 genes out of 15,000 were significantly differentially expressed ($p < 0.05$) in MRL and DBA mice at day four in comparison to control tissue at day zero. Of these, 170 genes were upregulated and 280 were downregulated in both mouse strains. About 50% of these genes represent ESTs and unknown genes. Pathway analysis of the known genes reveals that genes in the BMP/TGF pathway are differentially expressed in both mouse strains (BMP-1, Actr2, Smad 4, TGFb1i4, Fstl3, Twsg1, TSC22), thus implicating the BMP/TGF signaling pathway in regulation of digit tip regeneration.

Table 2. Genes Differentially Expressed in Only MRL Mice at Day 4 Post Digit Tip Dissection.

Clone ID	Gene ID	Expression Ratio	Description	Gene Ontology Biological Process
H3046D02B		6.3	UNKNOWN	
H3094C11	A630020C16Rik	5.5	UNKNOWN	ubiquitin-dependent protein catabolism(GO:0006511)
H3069B02	1810037G04Rik	4.1	EST similar to Bola-like transcription factor	
H3072F08		3.8	UNKNOWN	
H3001G12		3.4	UNKNOWN	
H3139B07	Hnrpu	3.2	Mus musculus heterogeneous nuclear ribonucleoprotein U (Hnrpu), mRNA	
H3139F02	Tcea1	3.2	UNKNOWN: Similar to Mouse transcription factor S-II, clone PSII-2	regulation of transcription, DNA-dependent(GO:0006355)
H3118G08A	G7e-pending	3.1	Mus musculus G7e protein (G7e-pending), mRNA	
H3139G05	EST Mm. 270291	3.0	UNKNOWN: Similar to Mus musculus similar to zinc finger protein 97 [Mus musculus] (LOC233168), mRNA	
H3043F11		2.9	UNKNOWN	
H3074G12	Mesp2	2.8	Mus musculus mesoderm posterior 2 (Mesp2), mRNA	gastrulation (GO:0048276)
H3133G07	Daf1	2.8	UNKNOWN	complement activation, classical pathway(GO:0006958)
H3076F01	Pdzk2	2.7	Mus musculus natrium-phosphate cotransporter IIa C-terminal-associated protein 2 (AF334612), mRNA	intracellular signaling cascade(GO:0007242)
H3138A06		2.6	UNKNOWN	
H3115F01	2610027O18Rik	2.6	Mus musculus RIKEN cDNA 2610027O18 gene (2610027O18Rik), mRNA	
H3137F08	G630041M05Rik	2.5	UNKNOWN: Similar to Homo sapiens chromosome 1 clone RP11-397P13, complete sequence	
H3072D07		2.2	UNKNOWN	
H3004A01	Gjb3	2.2	Mus musculus gap junction membrane channel protein beta 3 (Gjb3), mRNA	cell communication(GO:0007154);cell-cell signaling(GO:0007267)
H3138F07		2.2	UNKNOWN	
H3082B03	Mylk	2.2	Mus musculus myosin, light polypeptide kinase (Mylk), mRNA	cytoskeleton organization and biogenesis(GO:0007010)
H3155G11	1810024J12Rik	2.2	UNKNOWN: Similar to Mus musculus LOC244336 (LOC244336), mRNA	
H3098E07A	Calb1	2.2	Mus musculus calbindin-28K (Calb1), mRNA	
H3126F07		2.1	UNKNOWN	
H3024A05	Sparc	2.1	Mus musculus secreted acidic cysteine rich glycoprotein (Sparc), mRNA	
H3130D01	4933421G18Rik	2.1	UNKNOWN: Similar to Homo sapiens, Similar to IDN3 protein, clone IMAGE:5496103, mRNA	
H3028F04	Ctsl	2.0	Mus musculus cathepsin L (Ctsl), mRNA	proteolysis and peptidolysis(GO:0006508)
H3019H05		2.0	UNKNOWN	
H3029B05		2.0	Mus musculus brachyury (T), mRNA	regulation of transcription, DNA-dependent(GO:0006355);development(GO:0007275)
H3046F02A		2.0	UNKNOWN	
H3026H02	Nrd1	1.9	Mus musculus hypothetical protein MGC25477 (MGC25477), mRNA	proteolysis and peptidolysis(GO:0006508)
H3089C10	8430436C05Rik	1.9	Mus musculus 16 days embryo lung cDNA, RIKEN full-length enriched library, clone:8430436C05:unclassifiable transcript, full insert sequence	
H3077A05		1.9	UNKNOWN	
H3031F01	Uqcrc1	1.9	Mus musculus ubiquinol-cytochrome c reductase core protein 1 (Uqcrc1), mRNA	electron transport(GO:0006118);proteolysis and peptidolysis(GO:0006508)
H3048F06		1.9	UNKNOWN	
H3021A04		1.9	UNKNOWN	
H3078D11	shrm	1.9	Mus musculus, clone IMAGE:3484373, mRNA, partial cds	pattern specification(GO:0007389);intracellular signaling cascade(GO:0007242)
H3083B07		1.8	UNKNOWN	

Interpretation: The NIA15K library was created from developing mouse embryos and represents 15,264 unique genes (78% novel and 22% known). Many of these genes are expressed primarily in development and the clones are a unique source for studies of regeneration. Genes that are differentially expressed only in MRL include multiple transcription factors suggesting increased cellular replication in regenerating digit tips. Additional genes are implicated in gastrulation and pattern formation (Mesp2, Shrm). Also, genes differentially expressed are highly expressed in nerve cells (Fmn2, Net1). These genes are particularly intriguing since previous studies have shown that signals from nerves are required to induce formation of blastemas [10]. These results suggest that many genes and unknown ESTs are involved in digit regeneration.

Figure 5. Confirmation of MRL Microarray Results by Real-time PCR. Plotted below are the fold change values of RNA expression in MRL mice at day 4 in comparison to day 0 control RNA. Real-time PCR fold changes are normalized to beta-actin.

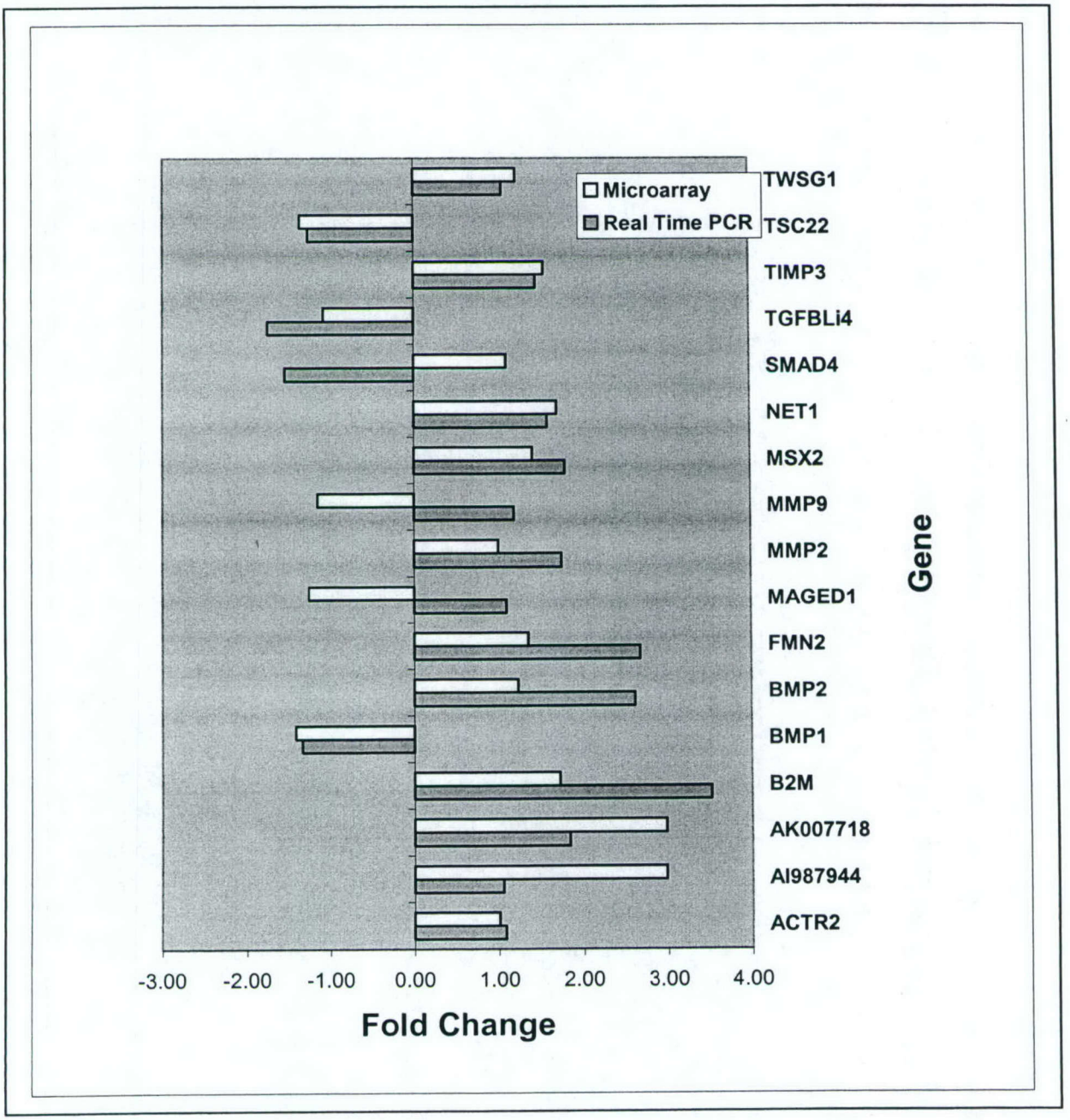

Interpretation: Most genes determined to be differentially expressed by microarray also show differential expression by real-time PCR. Differences in Smad4, MMP9 and Maged are likely due to cross hybridization of genes with high sequence similarity or polymorphic sequence mismatches in real-time PCR primers.

Figure 6. Confirmation of DBA Microarray Results by Real-time PCR. Plotted below are the fold change values of RNA expression of digit tips in DBA mice at day 4 in comparison to day 0 control RNA.

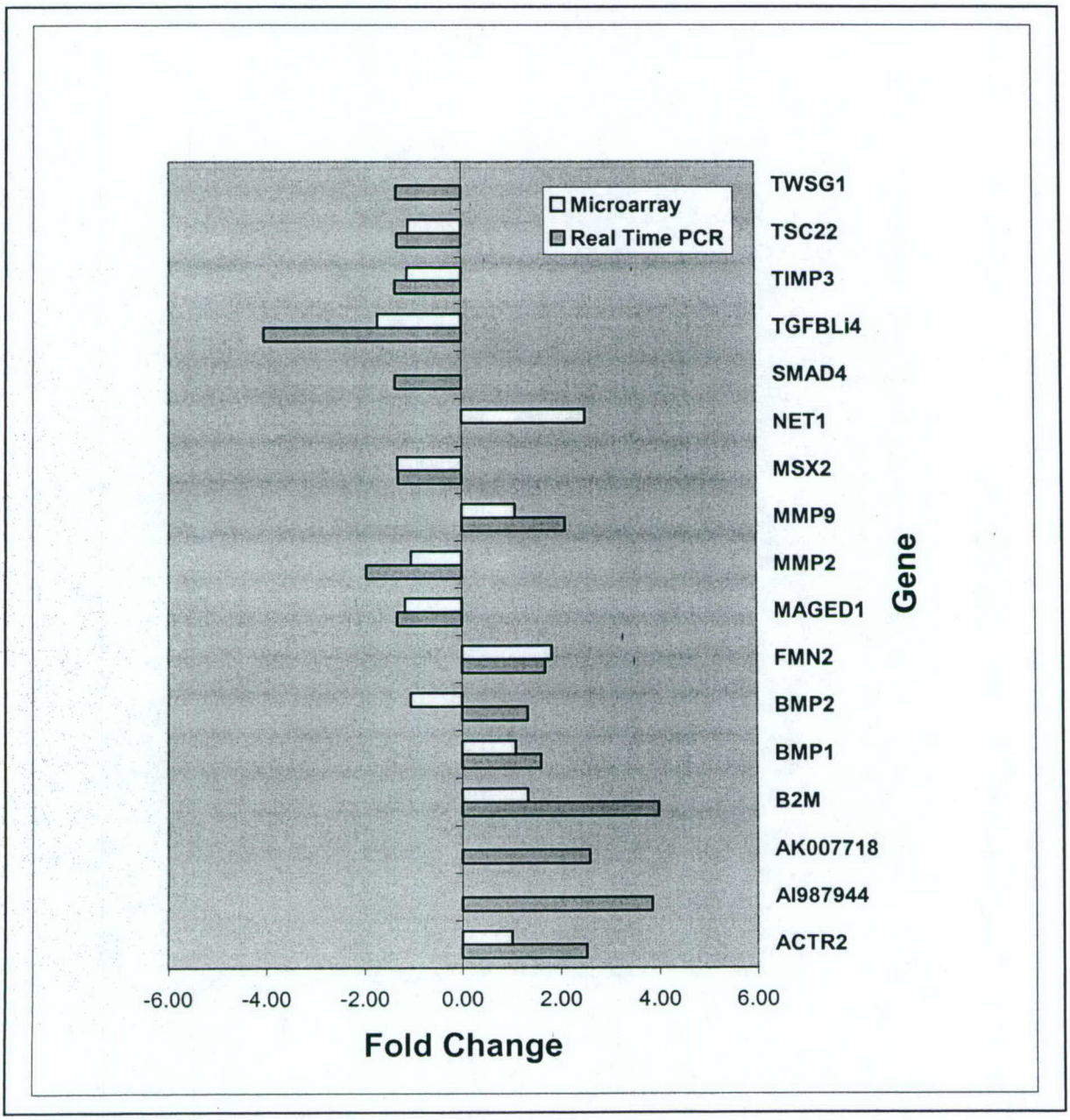

Interpretation: Most genes determined to be differentially expressed by microarray also show differential expression by real-time PCR. Differences in BMP2 are likely due to cross hybridization of genes with high sequence similarity or polymorphic sequence mismatches in real-time PCR primers.

Conclusions:

1) MRL mice show greater regenerative capacity to heal digit tips compared to DBA mice. This increased regeneration is seen primarily during the times of greatest growth in young mice (days 0 to 21).

2) Expression results suggest indicate that the BMP/TGF signaling pathway is likely involved in digit tip regeneration in both MRL and DBA in-bred strains of mice.

3) Increased regenerative capacity of the MRL mouse may be due to strain specific increased expression of transcription factors that function in embryogenesis, patterning and development.

Acknowledgements

This work was supported by Assistance Award No. DAMD17-03-2-0021. The U.S. Army Medical Research Acquisition Activity, 820 Chandler Street, Fort Detrick MD 21702-5014, is the awarding and administering acquisition office. The information contained in this publication does not necessarily reflect the position or the policy of the Government, and no official endorsement should be inferred. All work was performed in facilities provided by the Department of Veterans Affairs.

References

1. Muller, T.L., et al., Semin Cell Dev Biol, 1999. 10(4): p. 405-413.
2. Brockes, J.P., Science, 1997. 276(5309): p. 81-87.
4. Goss, R.J., et al., J Morphol, 1975. 146(4): p. 533-542.
5. Joseph, J., et al., Nature, 1966. 211(45): p. 193-194.
6. Li, X., et al., Heredity, 2001. 86(Pt 6): p. 668-674.
7. Clark, L.D, et al., Clin Immunol Immunopathol, 1998. 88(1): p. 35-45.
8. Leferovich, J.M., et al., Proc Natl Acad Sci U S A, 2001. 98(17): p. 9830-9835.
9. Tanaka T.S. et al., Proc Natl Acad Sci U S A, 2000. 97(16), p. 9127-9132.
10. Endo T. et al., Developmental Biology 2004. 270(1), p. 135-45.

Transfer of 128-kb BMP-2 Genomic Locus by HSV-Based Infectious BAC Stimulates Osteoblast Differentiation: A Platform for Functional Genomic Studies

Weirong Xing, David Baylink, Chandrasekhar Kesavan and Subburaman Mohan
Musculoskeletal Disease Center
JL Pettis Memorial Veterans Administration Medical Center, Loma Linda, CA 92357

ABSTRACT

In previous studies, we developed mouse genetic models and discovered genetic components of quantitative trait loci (QTL) on mouse chromosomes that contribute to phenotypes such as bone size, bone density and fracture healing. However, these regions contain dozens of genes in several overlapping bacterial artificial chromosomes (BACs) and are difficult to clone by physical cloning strategies. A feasible and efficient approach of identifying candidate genes is to transfer the genomic loci in BAC clones into mammalian cells for functional studies. In this study, we retrofitted a BAC construct into herpes simplex virus-1 (HSV-1) amplicon and packaged it into an infectious BAC (iBAC) to test gene function in a cell-based system, using a 128-kb clone containing the complete bone morphogenetic protein-2 (BMP-2) as a model. We transduced MC3T3-E1 cells with the iBAC bearing BMP-2 and examined transgene expression and function. Our results have demonstrated that an iBAC can efficiently deliver a BMP-2 genomic locus into preosteoblast cells and express functional BMP-2 protein, inducing a phenotype of cell differentiation, as indicated by an increase in alkaline phosphatase activity (ALP). Therefore, this experimental system provides a rapid, efficient cell-based model of high-throughput phenotypic screening to identify the BAC clones from physically mapped regions that are important for osteoblast differentiation. It also illustrates the potential of iBAC technology in functional testing of single nucleotide polymorphisms (SNP) located in the distal promoter or/and intron regions responsible for low bone density.

INTRODUCTION

Osteoporosis is a common disease characterized by an age-dependent decrease in bone mineral density (BMD) and a microarchitectural deterioration of bone tissue. Although multiple environmental, nutritional and hormonal factors influence the development of osteoporosis, it is clear that the major determinant for the disease is under genetic control. Recently, genome-wide linkage analyses have revealed that the genetic components of quantitative trait locus (QTL) on human chromosomes 1q, 2p, 4p, 11q, and 13q are attributed to BMD. In order to localize chromosomal regions and subsequently identify the genes responsible for skeletal diseases, we have developed mouse genetic models and discovered QTLs on mouse chromosomes that contribute to phenotypes such as bone size and bone density. However, these regions contain dozens of genes and are still difficult to clone by time-consuming, expensive positional cloning strategies. A feasible and efficient approach for identifying candidate genes is to transfer the genomic loci of overlapping bacterial artificial chromosomes (BACs) encompassing the QTL regions into bone cells *in vitro* for a high throughput functional screening.

The delivery of large genomic DNA inserts of BACs into mammalian cells via chemical methods and non-viral vectors, although possible, renders a poor efficiency of gene

transfer. However, the recent advances in the gene therapy field in infectious BAC (iBAC) technology using the herpes simplex virus type 1 (HSV-1) amplicon have made it possible to deliver a genomic locus as large as 150-kb with a high transduction efficiency in most mammalian cells, including dividing and non-dividing cells *in vitro* and *in vivo*. The improved delivery system of the HSV-1 amplicon allows long-term retention and high level of position-independent expression of BAC transgenes. In this study, we chose a BAC clone bearing the bone morphogenetic protein-2 (BMP-2) locus and assembled the genomic DNA as an infectious virion as a model to test the genomic DNA transfer and function.

MATERIALS AND METHODS:

1. Retrofitting HSV Amplicon into BMP-2 Genomic Locus

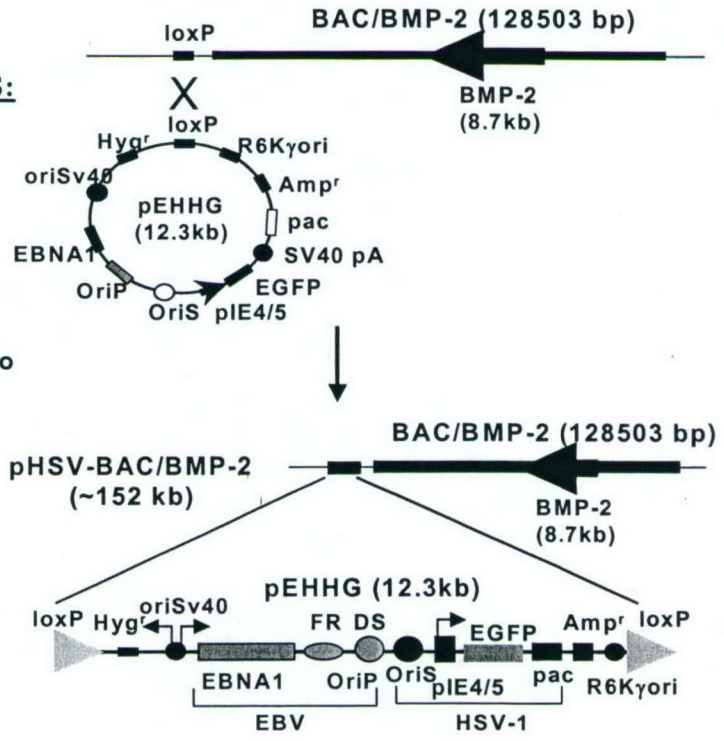

2. Make Helper Virus-free HSV-1 Amplicon

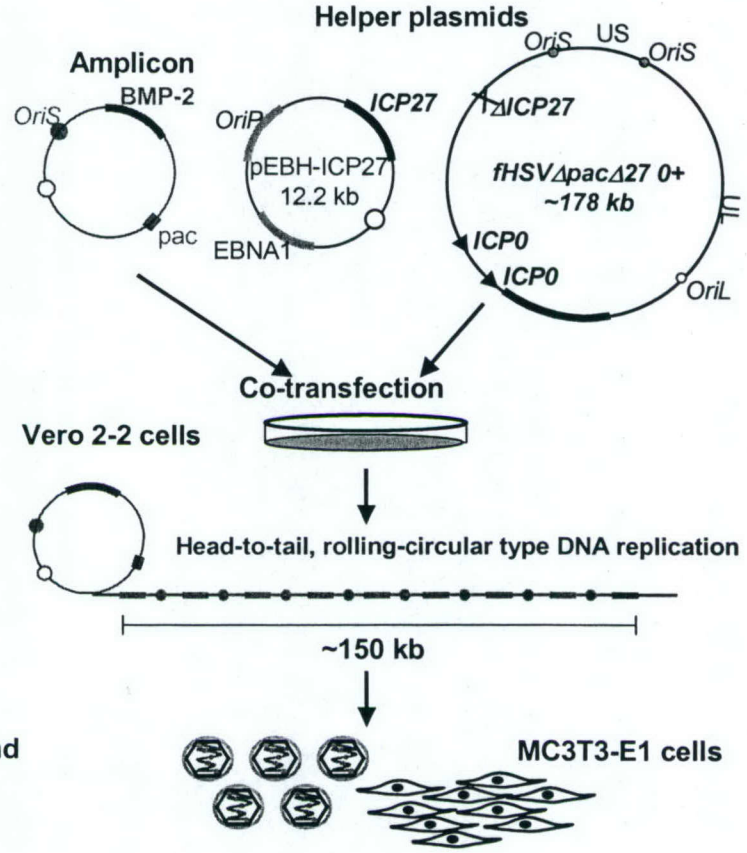

3. Infect Osteoblast Cells and Examine Phenotypes

RESULTS

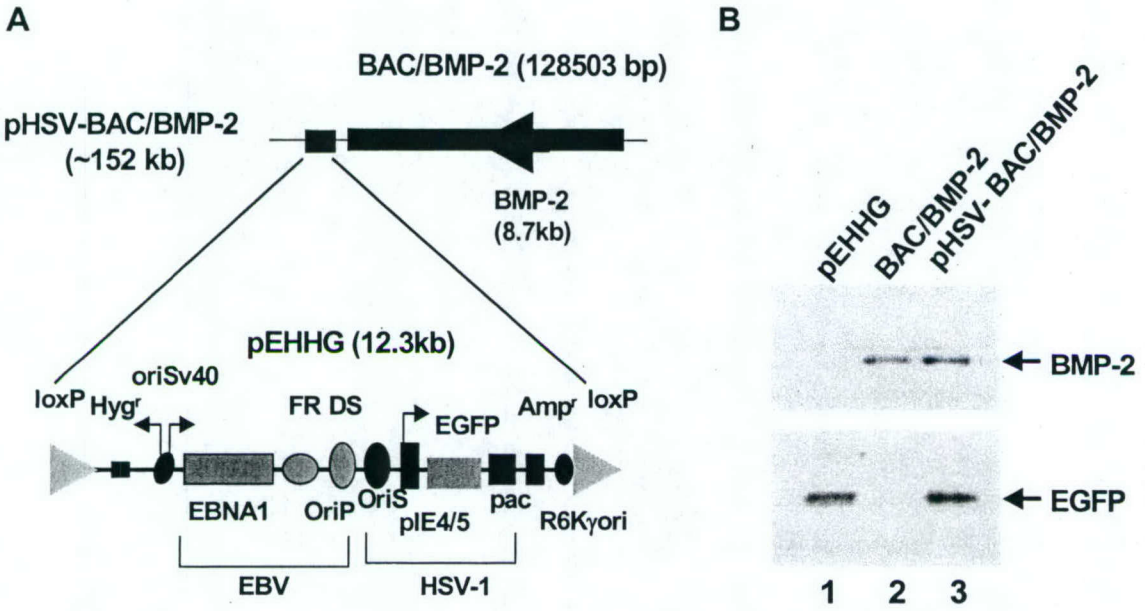

Figure 1. Schematic diagram of infectious HSV-1/BAC/BMP-2 construct. **A**: The retrofitted BAC contains both GFP reporter and BMP-2 genes **B**: Verification of pHSV-BAC/BMP-2 construct by polymerase chain reaction (PCR). Lane 1: pEHHG control; Lane 2: BAC/BMP-2 control; Lane 3: pHSV-BAC/BMP-2 containing both GFP and BMP-2 genes.

Interpretation: HSV amplicon was successfully retrofitted into BMP-2 genomic by homologous recombination in *E. Coli* to generate a BAC construct containing both BMP-2 intact gene and GFP reporter gene.

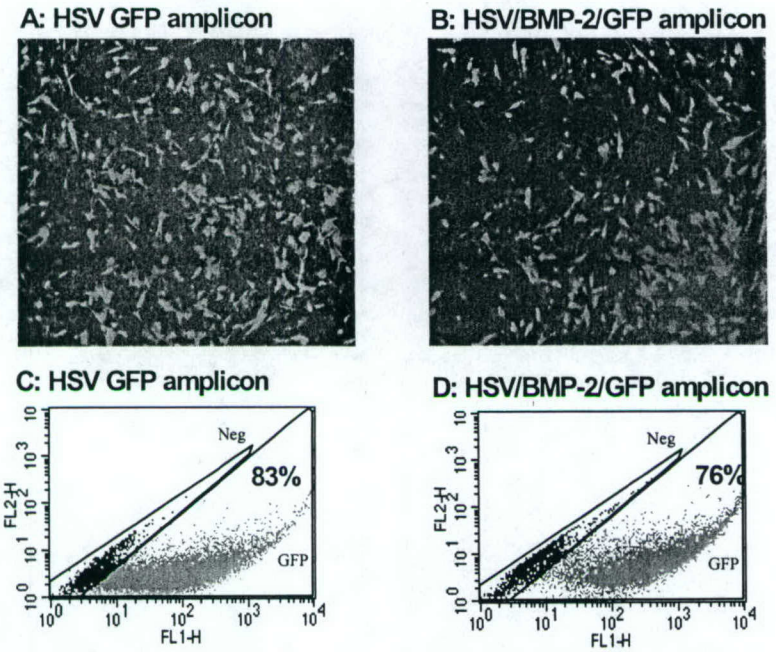

Figure 2. GFP reporter expression in MC3T3-E1 cells transduced with HSV-1 amplicon for 24 hours. **A**: cells transduced with infectious HSV-1 mock amplicon; **B**: cells transduced with infectious HSV-1 amplicon containing a BMP-2 locus; **C**: Flow cytometric analysis in cells infected with HSV-1 mock amplicon containing GFP only; **D**: Flow cytometric analysis in cells infected with HSV-1 amplicon containing GFP and a BMP-2 locus.

Interpretation: Infected MC3T3-E1 cells with HSV virion express GFP. The efficiency of transduction measured by flow cytometer was 83% and 76% in the cells transduced HSV mock virion and HSV virion containing BMP-2, respectively .

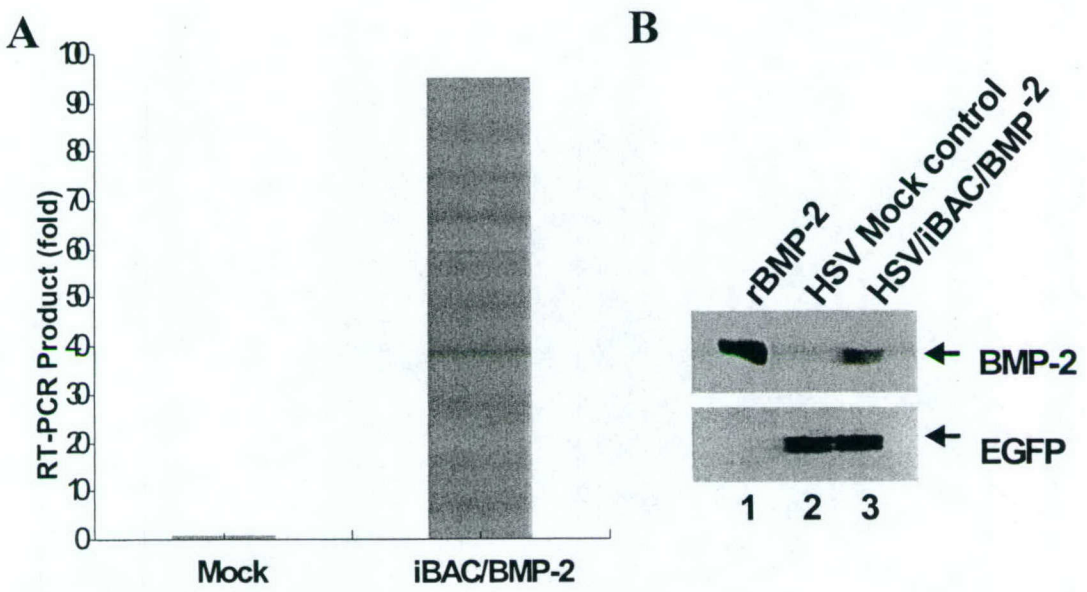

Figure 3. BMP-2 transgene expression in MC3T3-E1 cells. **A**: Real-time PCR data. **B**: Western blot analysis. Lane 1: positive control of recombinant BMP-2 (100 ng); Lane 2: the cells infected with HSV-1 mock amplicon containing GFP only; Lane 3: the cells infected with HSV-1 amplicon containing GFP and a BMP-2 locus.

Interpretation: The cells infected HSV amplicon containing BMP-2 genomic locus express more mRNA than the cells only containing GFP transgene alone (~ 99 fold induction). Western blot analysis detected full length BMP-2 protein.

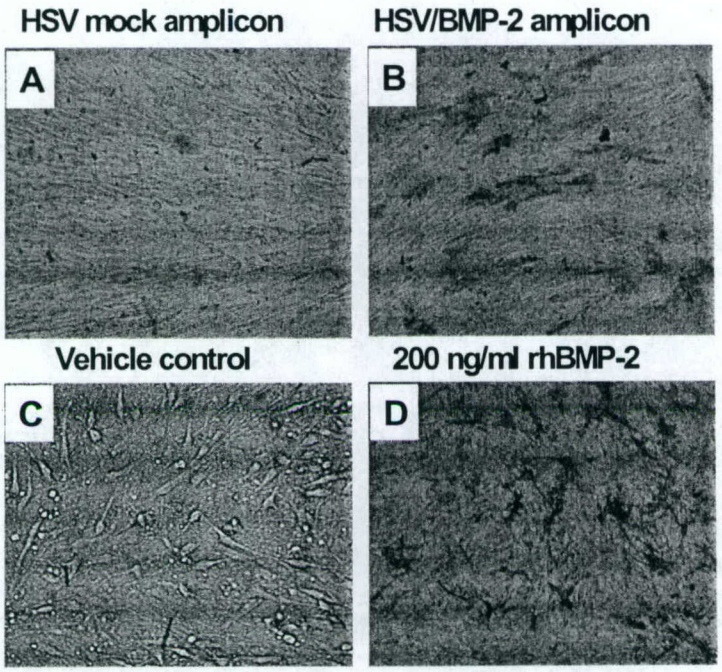

Figure 4: Alkaline phosphatase (ALP) staining of differentiated MC3T3-E1 cells (x 40 images). The cells are differentiated for 9 days and subjected for ALP staining. **A**: the cells infected with HSV-1 mock amplicon; **B**: the cells infected with HSV-1 amplicon containing a BMP-2 locus; **C**: The cells treated with vehicle; **D**: The cells treated with recombinant BMP-2 (200 ng/ml).

Interpretation: Approximately 20% of the osteoblast cells infected with HSV amplicon containing BMP-2 locus were differentiated and exhibited positive ALP-staining. No ALP-positive cells were seen in the control cells infected with HSV mock amplicon or the cells treated with vehicle alone. The cells treated with 200 ng recombinant BMP-2 also induced differentiation in approximately 20% of cells.

CONCLUSIONS

1.We have successfully transferred 128-kb BMP-2 genomic locus into osteoblast cells with high efficiency by utilizing HSV amplicon system.

2.The transgene was retained in osteoblast cells as minichromosomes for a long period of time.

3.The transgene-infected cells expressed functional protein, and induced cell differentiation.

4.The BAC gene transfer provides a rapid and efficient approach for functional testing of candidate genes within the QTL region *in vitro*

ACKNOWLEDGMENTS

This work was supported by Assistance Award No. DAMD17-03-2-0021. The U.S. Army Medical Research Acquisition Activity, 820 Chandler Street, Fort Detrick MD 21702-5014, is the awarding and administering acquisition office. The information contained in this publication does not necessarily reflect the position or the policy of the Government, and no official endorsement should be inferred. All work was performed in facilities provided by the Department of Veterans Affairs.

We are grateful to Dr. Yoshinaga Saeki (the Massachusetts General Hospital, Harvard Medical School, MA) for providing HSV-1 amplicon system and his technical assistance, and Dr. Rozanne Sandri-Goldin (the University of California, Irvine, CA) for her generous gift of a Vero 2-2 cell line.

Global Analysis of 22,000 Genes in the Bones Reveals Involvement of Several Novel Genes/ESTs and Pathways in Mediating the Anabolic Response of Mechanical Strain in Mice *In Vivo*

Weirong Xing, David Baylink, Chandrasekhar Kesavan, Hongrun Yu, Robert Chadwick, Yan Hu, Ravneesh Rajkumar and Subburaman MohanMusculoskeletal Disease CenterJL Pettis Memorial Veterans Administration Medical Center, Loma Linda, CA 92357

Abstract

In the present study, we evaluated differential gene expression on a global basis in the tibias of C57BL/6J mice after 4 days of four-point binding. The right tibias of the mice were loaded at 9N, 2Hz for 36 cycles per day and the left tibias were used as unloaded controls. RNA from the tibias harvested 24 hrs after last stimulation was subjected to oligo microarray. Of 20,280 genes, 346 were differentially expressed in the stimulated bones, of which, 110 genes were up- or down-regulated at least 2-fold. As expected, expression of bone-related genes such as pleiotrophin, osteoglycin and legumain increased and confirmed by real-time PCR, thus validating the microarray data. The functional categories of highly altered genes include cell growth, cell death, cell adhesion, proteolysis, immune and heat shock responses, cytoskeleton and microtubule-based movement, transcription factors, transport, receptor signaling molecules and others. Microarray analyses revealed several interesting and unique findings: 1) Of the known genes, 27 genes exhibit a direct biological network that are associated in bone remodeling and most of signaling molecules exhibit receptor activity for PDGF, VEGF, EGF, integrin, Ephrin B, C-C chemokine and endothelin. These findings suggest that multiple pathways are stimulated in mediating anabolic response to mechanical loading in the bone. In this regard, several growth factor genes (e.g. pleiotrophin, osteoclycin, nephroblastoma overexpressed gene) which have not been previously implicated in the mechanical loading pathway have been identified as mediators of mechanical stress; 2) Of the 131 significantly expressed genes, 45.3% genes are not characterized. Some of these genes contain functional domains such as LIM, cysteine-rich protein and leucine-rich repeats, which are characteristics of motifs associated with cell growth, thus suggesting that future studies on these unknown genes are essential for complete understanding of the molecular pathways for mechanical loading; 3) Pathway analysis revealed involvement of both well known (Integrin, EGF, Calcium channels) and less known (Eph B2 receptor kinase, adhesion G protein-coupled receptor, heparin-binding EGF-like) pathways in mediating the effects of loading in the bones. Conclusions: 1) This is the first study which examined the *in vivo* effect of mechanical loading on differentially expressed genes in the whole genome; 2) We have identified a number of novel genes and pathways that have not been previously implicated to play a role in mechanical loading.

IntroductionBone displays the ability to adapt to the mechanical forces applied to it to increase its density, shape and strength, and enable the bone to withstand reasonable loading during growth and daily physical activities. It is known that the bone anabolic response to mechanical loading varies generally in different individuals and in large part is genetically determined. Previous studies using *in vitro* model systems have discovered a number of stress-inducible genes and signaling pathways, including calcium-regulated PI3K-Akt and protein kinase C-dependent pathways, the extracellular signal-regulated kinases (ERK) pathway, prostaglandin synthesis and integrin pathway

that mediates the response to mechanical strain. However, these studies provided limited knowledge toward our understanding of mechanotransduction because most of these data were obtained from homogenous osteoblast cells *in vitro* that lack virtual communications of multiple cell types such as osteocytes and osteoblasts.

Recently, we have developed mouse genetic models (C57BL/6 and C3H/HeJ) and identified two inbred mouse strains that have an extreme difference in their anabolic response to mechanical loading. The C57BL/6 mice were more sensitive to mechanical stress than the C3H/HeJ mice. These and other studies have provided indispensable evidence that differential anabolic response to mechanical loading in different strains of mice is in large part determined genetically. There are several approaches that have been used to identify mechanosensetive genes, including quantitative trait loci (QTL), polymerase chain reaction (PCR) differential display and cDNA microarray. Among them, microarray has been proven to be a rapid and simple technique, allowing for the analysis of expressions of thousands of gene on the same chip using a small amount of RNA. In this study, we evaluated differential gene expression on a global basis in the tibias of C57BL/6J mice after 4 days of four-point bending. We hypothesized that mechanical activation of one or more sensitive signaling pathways leads to increased anabolic response in response to four-point bending in the highly responding C57BL/B6 mice.

Materials and Methods

Four-point bending: The right tibias of the mice (10-week old C57BL/6J females) were loaded at 9N, 2Hz for 36 cycles per day and the left tibias of the same mice were used as unloaded controls. Twenty-four hours after four days of stimulation, the corresponding tibias were removed and flushed with PBS to remove the bone marrow cells prior to RNA extraction. **Microarray hybridization:** An aliquot of 2 mg total RNA was reverse transcribed into cDNA. The product was used in an *in vitro* transcription reaction to generate cRNA. Two micrograms of fragmented cyanine 3-labeled cRNA of unloaded reference sample was mixed with an equal amount of cyanine 5-labeled cRNA of loaded experimental sample, and the mixture was hybridized to a 22K mouse development oligo microarray (Agilent Technologies) for 17 hours at 60°C with constant rotation at a slow pace. After hybridization, the slide was washed, dried and scanned using GSI Scanarray 4000. The images were analyzed using the ImaGene 5.6 software and data of the signals were outputted together with the Agilent probe name. **Normalization and analysis of microarray data:** Expression analysis of five replicates of microarray experiments was performed with GeneSpring 6.2 (Silicon Genetics). The data was normalized using per spot and per chip, intensity/dependent LOWESS normalization. The transcripts were then scaled to an expression level of 1.5-fold change, and the filtered genes (e.g. ^{3} 1.5-fold) were further analyzed by utilizing a one-sample Student's t-test with "Benjamini and Hochberg" Multiple Testing Correction. Differential expression was defined as those genes whose normalized average data had a difference of 1.5-fold or greater with P value < 0.01 after adjustment of Multiple Testing Correction.

Real time-PCR: Total RNA (2 mg) was reverse-transcribed into cDNA by oligo(dT)$_{12-18}$ into cDNA. The PCR contained 100 ng of template cDNA, 1x SYBR GREEN master mix (Qiagen) and 100 nM of specific forward and reverse primers in 25 ml volume of reaction. Primers for the housekeeping gene, b-2 microglobulin (B2M), were used to normalize the expression data of each of the genes.

Results

Table 1. Functional categories of differentially expressed genes

Functional categories	Up-regulated	Down-regulated
Cell adhesion	17	0
Cell cycle	7	5
Cell growth	26	2
Heat shock proteins	4	0
Apoptosis	4	0
Signaling molecules	35	
Growth hormone receptors and ligands	22	0
G-protein coupled receptor signaling	5	0
Ca++ dependent receptor signaling	1	0
Integrin receptor signaling	4	0
Tyrosine/Serine Threonine kinase signaling	8	0
Intracellular Signaling	11	0
STAT cascade	4	0
Developmental processes	23	0
Transcriptional regulation	17	2
Chaperoning pathways	18	1
Proteolysis and peptidolysis	10	0
Protein modification	9	1
Transport	29	4
Others	24	1
Unknown	131	26

A total of 346 genes/ESTs are characterized into 14 categories according to the simplified ontology. Some of mouse genes with multiple molecular functions fall into several categories, thus artificially increasing the number of genes beyond 189. A total of 157 genes/ESTs are yet to be characterized.

Interpretation: Mechanical loading stimulated the expression of genes related to biological processes such as signaling pathways, cell growth, development, cell adhesion, immune response, transcription regulation and proteolysis.

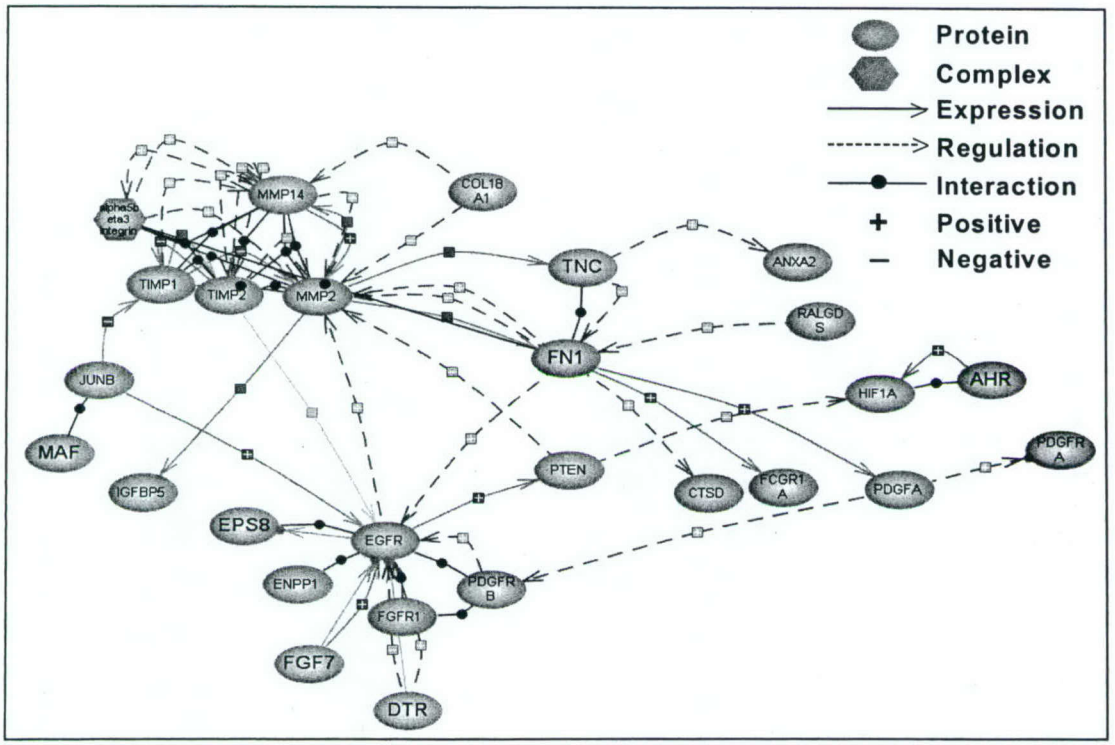

Figure 1. Direct biological association network of differentially expressed genes. Analysis of a direct biological association network of differentially expressed genes was performed using PathwayAssit 2.53 software (Stratagene, La Jolla, CA). Biologically linked proteins indicated by nodes are shown in the diagram. Other unlinked nodes have been deleted.

Interpretation: At least 27 out of 189 differentially expressed genes in loaded bones exhibit a direct biological association, providing a network that involved multiple signaling pathways: (i) stress-induced AP-1, JunB and Maf, (ii) epidermal growth factor (EGF) receptor signaling, including its ligand, heparin binding-like EGF (HB-EGF, pleiotrophin or DRT for the diphtheria toxin receptor), (iii) integrin signaling of fibronectin 1(FN1), (iv) platelet derived growth factor (PDGF) and PDGF receptor signaling, and (v) proteolysis pathway including a complex of tissue inhibitor of metalloproteinase 1/2 (TIMP1/2) and matrix metalloproteinase 2/14 (MMP2/14).

Table 2. Functional categories of selected genes differentially expressed in stressed bones

Gene	Access No	location	Description	Change
Cell Growth/Proliferation/Differentiation				
Ptn	D90225	6	pleiotrophin	4.3
Ogn	AK014259	13	osteoglycin	2.5
Nov	NM_010930	15	nephroblastoma overexpressed gene	2.1
Itm2a	NM_008409	X	integral membrane protein 2A (chondro-osteogenic differentiation)	2.8
Emp1	BC034257	6	epithelial membrane protein 1 (c-DNA from osteoblast cells)	2.6
Lepre1	NM_019783	4	leprecan 1	2.5
Tgfbi	XM_122567	13	transforming growth factor, beta induced, 68 kDa	2.3
Pdgfrl	NM_026840	13	platelet-derived growth factor receptor-like	2.2
Morf4l2	NM_019768	X	mortality factor 4 like 2	2.0
Csrp2	NM_007792	10 D1	cysteine and glycine-rich protein 2	4.1
Akr1b8	NM_008012	6	aldo-keto reductase family 1, member B8 (FGF regulated protein)	4.7
Ephb2	BM231330	4 D3	Eph receptor B2 (cDNA from osteoblast library)	2.5
Npdc1	NM_008721	2 A3	neural proliferation, differentiation and control gene 1	2.2
Cell Death				
Gas1	NM_008086	13	growth arrest specific 1	2.3
Bok	BC030069	1 D	Bcl-2-related ovarian killer protein	2.5
C1qtnf6	NM_028331	15 E1	C1q and tumor necrosis factor related protein 6	2.1
Cytokine and Immune Response				
Il13ra1	NM_133990	X	interleukin 13 receptor, alpha 1	2.4
Ccr5	XM_135269	9 F4	similar to C-C chemokine receptor 5, (rhodopsin family)	2.3
Ccl2	NM_011333	11	chemokine (C-C motif) ligand 2	2.4
Procr	NM_011171	2 H1	protein C receptor, endothelial	2.2
Igsf10	AK018323	3D	immunoglobulin superfamily, member 10	2.2
Receptor/Signal Transduction				
Semcap3	NM_018884	6	semaF cytoplasmic domain associated protein 3	2.0
Pdgfrb	NM_008809	18	platelet derived growth factor receptor, beta polypeptide	2.0
EPS8	BC030010	6	epidermal growth factor receptor pathway substrate 8	2.0
Arhe	NM_028810	2 C1.1	ras homolog gene family, member E	2.1
Gpr124	NM_054044	8	adhesion G protein-coupled receptor 124	2.0
Gprc5b	NM_022420	7	G protein-coupled receptor, family C, group 5, member B	2.2
Entpd2	NM_009849	2 A3	ectonucleoside triphosphate diphosphohydrolase 2	2.0
Stmn2	NM_025285	3	stathmin-like 2	2.1
Ppp1r14b	NM_008889	19	protein phosphatase 1, regulatory (inhibitor) subunit 14B	2.1
Dcamkl1	BE824672	3	double cortin and calcium/calmodulin-dependent protein kinase-like 1	3.8
Ania4	NM_021584	Y	activity and neurotransmitter-induced early gene, similar to CaM-Kinase	2.9
Ednrb	AE014177	14	endothelin receptor type B	2.9
Nek6	NM_021606	2	NIMA (never in mitosis gene a)-related expressed kinase 6	2.1
Calu	NM_007594	6	calumenin (Calmodulin and related proteins, cacium binding)	2.1
Rcn	NM_009037	2	reticulocalbin (Calmodulin and related proteins, cacium binding)	2.3
D7Ertd671e	XM_133470	7	DNA segment, Chr 7,Ca2+-binding protein	2.0
Fstl1	NM_008047	16	follistatin-like 1	3.1
Tax1bp3	NM_029564	11	Tax1 (human T-cell leukemia virus type I) binding protein 3 (PDZ domain)	2.0
Response to Heat				
Hspb1	NM_013560	5	heat shock protein 1 (27 kD)	2.2
Serpinh1	NM_009825	7 E1	serine (or cysteine) proteinase inhibitor, clade H, member 1 (Hsp47)	2.7

Table 2. Continue

Gene	Access No	Location	Description	Change
Cell Adhesion				
Col5a1	NM_015734	2	procollagen, type V, alpha 1	2.0
Col5a2	NM_000393	2q14-q32	collagen, type V, alpha 2	2.2
Col6a3	BC005491	1	procollagen, type VI, alpha 3	3.4
Col8a1	NM_007739	16 C1	procollagen, type VIII, alpha 1	2.6
Col14a1	XM_127997	15	procollagen, type XIV, alpha 1	2.4
Col18a1	BC008227	10	procollagen, type XVIII, alpha 1	3.4
Thbs2	L06421	17	thrombospondin 2	2.6
PCDH19	XM_033173	X	protocadherin 19	2.3
Lamb1-1	XM_126863	12	laminin B1 subunit 1	2.7
Nid1	NM_010917	13	nidogen 1	2.0
Nrp	AK011144	8	neuropilin (an alternate receptor for VEGF-A)	2.1
ESTs	NM_172399	6	ESTs (Fibronectin, type III domain)	2.1
Fn1	XM_129845	1	fibronectin 1	2.6
Matn2; Crtm2	NM_016762	15	Mus musculus matrilin 2 (Matn2), (skeletal development)	2.8
Loxl3	NM_013586	6	lysyl oxidase-like 3	2.1
Lox	NM_010728	18	lysyl oxidase (hydroxylysine residues in collagens)	3.2
Proteolysis				
Mest	NM_008590	6	mesoderm specific transcript	3.1
ESTs	NM_029614	7 D3	RIKEN cDNA 2310046G15 gene (serine-type endopeptidase activity)	2.3
Lgmn	NM_011175	12 E	legumain	3.2
ESTs	XM_136041	X	eukaryotic cysteine peptidase active site, Myb DNA binding motif	2.2
Mmp14	NM_008608	14	matrix metalloproteinase 14 (membrane-inserted)	2.0
Timp1	NM_011593	X	tissue inhibitor of metalloproteinase 1	2.5
Pcolce	NM_008788	5	procollagen C-proteinase enhancer protein	2.2
Serpinb6a	NM_009254	13	serine (or cysteine) proteinase inhibitor, clade B, member 6a	2.0
Sulf2	NM_028072	2	sulfatase 2 (heparin-degrading endosulfatases)	2.0
Sulf1	NM_172294	1	sulfatase 1 (heparin-degrading endosulfatases)	2.0
Cytoskeleton and Microtubule-Based Movement				
Tnnt2	NM_011619	1	troponin T2, cardiac	3.0
CALD1	BC015839	7q33	caldesmon 1	2.1
Myl4	M19436	11	myosin, light polypeptide 4, alkali;	3.2
ESTs	NM_023716	13	RIKEN cDNA 2410129E14 gene (tubulin, beta)	2.7
Tuba1	NM_011653	15	tubulin, alpha 1	2.4
Acta2	NM_007392	19	actin, alpha 2, smooth muscle, aorta	2.0
S100a10	NM_009112	3	S100 calcium binding protein A10 (calpactin)	2.0
ESTs	NM_026473	18 E1	RIKEN cDNA 2310057H16 gene (tubulin)	4.7
Transcription Factors/Cofactors				
Gsc	NM_010351	12	goosecoid	2.3
Tbx4	BM225983	11 C	T-box 4	2.3
Ankrd1	BC037138	19 C2	ankyrin repeat domain 1 (cardiac muscle)	2.3
Gli5	BC021517	16	GLI-Kruppel family member GLI5	
Maged1	NM_019791	X	melanoma antigen, family D, 1	2.3
Smarca1	NM_053123	X	SWI/SNF related, matrix associated, actin dependent regulator of chromatin	2.0
TFDP2	U18422	3q23	transcription factor Dp-2 (E2F dimerization partner 2)	-2.0
Mkrn1	NM_018810	6 B1	makorin, ring finger protein, 1	-2.2
Transport				
Kdelr3	NM_134090	15 E1	KDEL (Lys-Asp-Glu-Leu) endoplasmic reticulum protein retention receptor 3	2.3
Sec23a	AY082671	12	SEC23A (S. cerevisiae)	2.3
P4hb	XM_126743	11 80.0 cM	PDI, Thbp, ERp59; protein disulfide isomerase;	2.3

Table 2. Continue

Gene	Access No	location	Description	Change
Transport (continue)				
Slc39a1	BC005474	3	Solute carrier family 39 (zinc transporter), member 1	2.2
Slc35f5	NM_028787	1	solute carrier family 35, member F5	2.1
ESTs	NM_026211	13 B1	RIKEN cDNA 2400003B06 gene	2.1
Pr1	BC024613	1	protein distantly related to to the gamma subunit family (calcium channel)	2.0
Other				
Spats2	BC023432	15 F1	spermatogenesis associated, serine-rich 2	2.0
Ppfibp1	BC035209	6 G3	PTPRF interacting protein, binding protein 1	2.2
Fkbp9	NM_012056	6	FK506 binding protein 9	2.1
Scd2	NM_009128	19	stearoyl-Coenzyme A desaturase 2	2.6
ESTs	BG067354	10	expressed sequence AI480506	2.2
ESTs	XM_126864	12	RIKEN cDNA 2310075M15 gene (von Willebrand factor type C domain)	3.8
P37nb	XM_131917	5	Mus musculus 37 kDa leucine-rich repeat (LRR) protein	3.7
ESTs	XM_129689	1	RIKEN cDNA C130018M11 gene	3.4
Cav2	NM_016900	6	caveolin 2	2.0
Fer-1-like 3	XM_148914	19	RIKEN cDNA 2310051D19 gene, similar to myoferlin isoform b	2.6
Spon2	NM_133903	5	spondin 2, extracellular matrix protein	2.5
ESTs	NM_152261	12Q24.11	hypothetical protein MGC17943	2.4
Ecrg4	NM_024283	1 C1	esophageal cancer related gene 4 protein	2.2
ESTs	BG073351	9A	RIKEN cDNA 4833410J10 gene	2.2
ESTs	XM_134818	9	expressed sequence AL02422	2.0
Fkbp11	NM_024169	15	FK506 binding protein 11 (protein turnover, chaperones)	2.0
Ms4a6d	NM_026835	19	membrane-spanning 4-domains, subfamily A, member 6D (Ms4a6d)	2.0
Car1	BC011223	3	carbonic anhydrase 1	-2.1
Rex3	XM_129523	1	reduced expression 3	-2.0
Rhced	AF057524	4	Rhesus blood group CE and D	-2.0
EST	AK010906	6 B1	viral hemorrhagic septicemia virus(VHSV) induced gene 1	-2.2
EST	AJ341786	N	Homo sapiens genomic sequence surrounding NotI site	-2.3
ESTs	BM211961	5	ESTs, close to RBP-Jkappa, a key transcription factor in Notch signaling	-2.7
EST	NM_027464	14 B	ESTs	-2.0
ESTs	BG072471	3	ESTs	-2.0
ESTs	XM_177029	4	Mus musculus adult male tongue cDNA	-2.1
ESTs	BG071710	9A	ESTs	-2.1
EST	XM_126729	11	ESTs	-2.2

These genes were selected because their expressions were either up-regulated or down-regulated at least 2-fold and significantly different as compared to the control samples. GenBank accession numbers and chromosomal locations are also listed.

Interpretation: 1) Several growth factor genes (e.g. pleiotrophin, osteoclycin and nephroblastoma overexpressed gene) have been identified as mediators of mechanical stress; 2) Some genes/ESTs contain functional domains such as LIM, cysteine-rich protein and leucine-rich repeats, which may be associated with cell growth; 3) Mechanical loading induced expression of signaling molecules of both well known (Integrin, EGF, Calcium channels) and lesser known (Eph B2 receptor kinase, adhesion G protein-coupled receptor, heparin-binding EGF-like) genes.

Table 3. The osteogenic genes differentially expressed in mechanically stressed bones

Gene	Expression and function in bone remodeling	Reference
Ptn (DTR)	Induction of osteoprogenitor chemotaxis, proliferation, differentiation and bone formation	PMID: 12510805,
Ogn	Induction of cell proliferation, differentiation and adhesion, and bone formation	PMID: 2372374
Itm2a	Osteo-, chondrogenic differentiation and bone formation	PMID: 10893674
Nrp	Distraction osteogenesis, induced by mechanical stress	PMID: 15121017
Matn2	Expressed in epiphyseal cartilage of growing long bones, skeletal development	PMID: 9083061
Fn1	Promoting fluid shear stress induction of COX-2 and PGE2 release in MC3T3-E1 Osteoblasts	PMID: 15004000
Thbs2	Regulating the proliferation of osteoblast progenitors and endosteal bone formation	PMID: 10804014
Calu	Expressed in in the early stage of fracture healing	PMID: 15099630
Emp1	c-DNA from mouse osteoblast library	BM234011
Gsc	Expressed in osteoblast cells in early steps of chick calvarial development	PMID: 12710966
Tbx4	Playing a crucial role in lower limb development in chickens and mice, ossification	PMID: 15106123
Pdgfrl	Expressed in chicken limb buds	PMID: 8115382
Ephb2	Required for the normal morphogenesis of skeletal elements	PMID: 12919674
Cav2	Expressed in osteoblast cells and chondrocytes	PMID: 10461811
Stmn2	Expressed in chondrocytes and osteoblast cells	PMID: 8003023
Hspb1	Expressed in osteoblast cells, resisting to osteoblast apoptosis	PMID: 11056010
Serpinh1	Playing a major role during procollagen accumulation	PMID: 12842808
Serpinb6a	Metalloprotease inhibitors, cartilage remodeling	PMID: 9108368
Timp1	Expressed in osteoblasts and osteocytes, bone formation	PMID: 15052653
Car 1	Expressed in osteoclast cells, regulating osteoclast differentiation and bone resorption	PMID: 9665810
Mmp14	Expressed in an intermediate stage of chondrogenesis, bone resorption	PMID: 11917104
Pcolce	Binding to the procollagen cleavage site, facilitating the action of procollagen C-proteinases	PMID: 12105202
TFDP2	Dimerizing with E2F in FGF signaling, Inhibiting chondrocyte differentiation and bone formation	PMID: 12821644
Lgmn	Inhibiting osteoclast formation and bone resorption	PMID: 10488118
Ccr5	Expressed in osteoclast cells, regulating bone resorption	PMID: 12397598
Ccl2	Expressed in osteoclast cells, regulating bone resorption	PMID: 12397598
Lox	Expressed in osteoblast cells, hydroxylysine residues in bone collagen	PMID: 8626440
Sulf2	Expressed in osteoclast, arylsulfatase activity, bone resorption	PMID: 597752
Sulf1	Expressed in osteoclast, arylsulfatase activity, bone resorption	PMID: 597752

A list of genes selected on the basis of literature search for bone formation and resorption are shown with Pubmed identifications. Genes in bold were down-regulated.

Interpretation: Of the 110 genes, 29 are known to be involved in regulating bone formation and/or bone resorption. Some of them are stress-inducible and have been known to participate in mechanical stimulation induced bone regeneration. These findings provide validation to our microarray data.

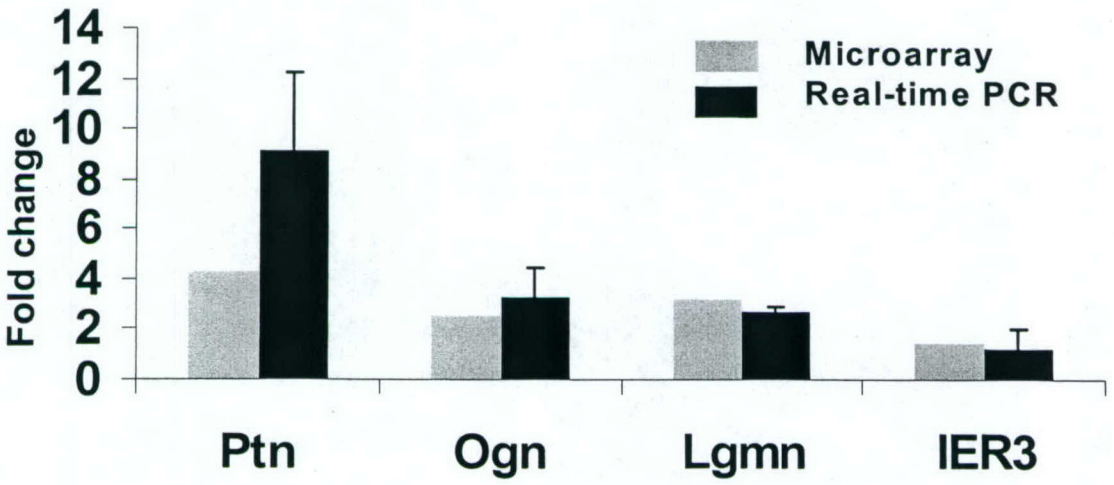

Figure 2. Comparison of fold changes in the expression of selected genes by microarray and real-time PCR. The results were normalized to the expression of β-2 microglobulin (B2M) in each of the samples, and expressed as fold change of the loaded sample over the expression level of the unloaded sample. The data shown are means ± S.D. from 5 replicates: Ptn, pleiotrophin; Ogn, osteoglycin; Lgmn, Legumain; IER3, Immediate early response gene 3.

Interpretation: In agreement with the data of microarray, real-time PCR confirmed the expression of selected genes in response to mechanical loading

Conclusions

1)This is the first study which examined the *in vivo* effect of mechanical loading on differentially expressed genes in the whole genome.

2)We have identified a number of novel genes and signal molecules involving receptor signal transduction pathways that have not been previously implicated to play a role in mechanical loading in the bones.

3)Over 45% of differentially expressed genes are not known or uncharacterized. Therefore, further studies on these genes are necessary to completely understand the mechanical signaling pathways.

Acknowledgment

This work was supported by Assistance Award No. DAMD17-01-1-0744. The U.S. Army Medical Research Acquisition Activity, 820 Chandler Street, Fort Detrick MD 21702-5014, is the awarding and administering acquisition office. The information contained in this publication does not necessarily reflect the position or the policy of the Government, and no official endorsement should be inferred. All work was performed in facilities provided by the Department of Veterans Affairs.

Available online at www.sciencedirect.com
SCIENCE DIRECT®
ELSEVIER
Biochemical and Biophysical Research Communications 319 (2004) 781–786
BBRC
www.elsevier.com/locate/ybbrc

HSV-1 amplicon-mediated transfer of 128-kb BMP-2 genomic locus stimulates osteoblast differentiation in vitro☆

Weirong Xing, David Baylink, Chandrasekhar Kesavan, and Subburaman Mohan*

Musculoskeletal Disease Center, JL Pettis Memorial Veterans Administration Medical Center, Loma Linda, CA 92357, USA

Received 5 May 2004
Available online 28 May 2004

Abstract

In previous studies, we developed mouse genetic models and discovered genetic components of quantitative trait loci on mouse chromosomes that contribute to phenotypes such as bone size, bone density, and fracture healing. However, these regions contain dozens of genes in several overlapping bacterial artificial chromosomes (BACs) and are difficult to clone by physical cloning strategies. A feasible and efficient approach of identifying candidate genes is to transfer the genomic loci in BAC clones into mammalian cells for functional studies. In this study, we retrofitted a BAC construct into herpes simplex virus-1 amplicon and packaged it into an infectious BAC (iBAC) to test gene function in a cell-based system, using a 128-kb clone containing the complete bone morphogenetic protein-2 (BMP-2) gene. We transduced MC3T3-E1 cells with the iBAC bearing BMP-2 gene and examined transgene expression and function. Our results have demonstrated that an iBAC can efficiently deliver a BMP-2 genomic locus into preosteoblast cells and express functional BMP-2 protein, inducing a phenotype of cell differentiation, as indicated by an increase in alkaline phosphatase activity. Therefore, this experimental system provides a rapid, efficient cell-based model of high-throughput phenotypic screening to identify the BAC clones from physically mapped regions that are important for osteoblast differentiation. It also illustrates the potential of iBAC technology in functional testing of single nucleotide polymorphisms located in the distal promoter or/and intron regions responsible for low bone density.

Keywords: Osteoblast; HSV-1 amplicon; BMP-2; BAC; Gene transfer; Osteogenesis

Osteoporosis is a common disease characterized by an age-dependent decrease in bone mineral density (BMD) and a microarchitectural deterioration of bone tissue with a consequent increase in the risk of developing fragility fractures of the hip, spine, and other skeletal sites [1]. Although multiple environmental, nutritional, and hormonal factors influence the development of osteoporosis, it is clear that the major determinant for the disease is genetic control of BMD, particularly the achievement of peak bone mass at maturity, bone size and structure, and the subsequent rate of bone turnover [2–5]. Recently, genome-wide linkage analyses have revealed that the genetic components of quantitative trait locus (QTL) on human chromosomes 1q, 2p, 4p, 11q, and 13q are attributed to BMD [6–8], while the loci on chromosomes 17q and 19p are responsible for bone size [9]. However, none of the QTLs reported have actually met criteria for genome-wide significance for linkage, and the results are inconsistent due to the great variation between study groups and populations, as well as the possible involvement of different pathways. To localize chromosomal regions and subsequently identify the genes responsible for skeletal diseases, we have developed mouse genetic models and discovered QTLs on mouse chromosomes that contribute to phenotypes such as bone size, bone density, and fracture healing [10–12]. Subsequent analyses of the

☆ *Abbreviations:* BAC, bacterial artificial chromosomes; iBAC, infectious BAC; PAC, P1 artificial chromosomes; HSV-1, herpes simplex virus-1; ALP, alkaline phosphatase; BMP-2, bone morphogenetic protein-2; QTL, quantitative trait loci; MOI, multiplicity of infection; FACS, fluorescence-activated cell sorter; GFP, green fluorescent protein; EBV, Epstein–Barr virus; PCR, polymerase chain reaction.

* Corresponding author. Fax: 1-909-796-1680.
E-mail address: Subburaman.Mohan@med.va.gov (S. Mohan).

0006-291X/$ - see front matter © 2004 Elsevier Inc. All rights reserved.
doi:10.1016/j.bbrc.2004.05.053

congenic mice further confirmed and narrowed the genes of interest to a 3–12.5 centimorgan (cM) region in mouse chromosome 1 [13,14]. However, these regions contain dozens of genes and are still difficult to clone by time-consuming, expensive position-cloning strategies. However, a feasible and efficient approach for identifying candidate genes is to transfer the genomic loci of overlapping bacterial artificial chromosomes (BACs) or P1 artificial chromosomes (PACs) encompassing the QTL regions into bone cells in vitro for a high-throughput functional screening.

The delivery of large genomic DNA inserts of BACs or PACs into mammalian cells via chemical methods and non-viral vectors, although possible, renders a poor efficiency of gene transfer and requires the drug-selection and identification of stably integrated transformants for functional testing [15–17]. However, the recent advances in infectious BAC (iBAC) technology using the herpes simplex virus type 1 (HSV-1) amplicon in the gene therapy field have made it possible to deliver a genomic locus as large as 150-kb with a high transduction efficiency in most mammalian cells, including dividing and non-dividing cells in vitro and in vivo [18–21]. The improved delivery system of the HSV-1 amplicon also contains an EBNA-1 episomal cassette from the Epstein–Barr virus, (EBV) allowing long-term retention and high level of position-independent expression of BAC transgenes as mini-chromosomes in the host cells [20,21]. Therefore, the iBAC offers a rapid and simple method of BAC DNA transfer for functional genomic studies. This system also allows us to test the functional significance of the large number of gene-associated single nucleotide polymorphisms (SNP) located in the regions of the distal promoter or/and introns that could contribute to low bone density [22,23]. In this study, we chose a BAC clone bearing the bone morphogenetic protein-2 (BMP-2) locus and assembled the genomic DNA as an infectious virion as a model to test the genomic DNA transfer and function. Our results indicated that the iBAC could efficiently deliver a BMP-2 genomic locus and express functional protein promoting osteoblast differentiation.

Materials and methods

Vector constructs. The DNA constructs of pCTP-T, pEBHICP27, pEHHG, and fHSVΔ-pac, Δ-27, 0+ were described in detail elsewhere [20,21], and kindly provided by Dr. Yoshinaga Saeki (Massachusetts General Hospital, Harvard Medical School, MA). A BAC clone, RP23-302H4, containing a complete BMP-2 locus was purchased from Invitrogen Life Technologies (Carlsbad, CA).

Cell culture. Vero 2-2 cells (kindly provided by Dr. Rozanne Sandri-Goldin, University of California, Irvine, CA) were routinely maintained in Dulbecco's modified minimal essential medium (Invitrogen) with 10% fetal bovine serum, 100 U/ml penicillin, 100 μg/ml streptomycin, and G486 (500 μg/ml). MC3T3-E1 cells (ATCC, Manassas, VA) were propagated in alpha minimum essential medium (Invitrogen) supplemented with 10% calf serum, 100 U/ml penicillin, and 100 μg/ml streptomycin. The cells were cultured in a humidified 37 °C incubator with 5% CO_2.

Retrofitting of BAC clone. The retrofitting of BAC clone into HSV-1/EBV amplicons was carried out by Cre-mediated recombination in bacterial cells as described previously [21]. Briefly, an aliquot of 35 μl electro-competent cells containing BAC/BMP-2 (RP23-302H4) was mixed with 10 ng each of pEHHG and pCTP-T plasmid DNA, and the mixture was transferred into 0.1-cm gap width electroporation cuvette (Bio-Rad, Hercules, CA). After 5 min incubation on ice, the cells were electroporated with 25 μF at 1800 V using a Gene Pulser (Bio-Rad), then transferred into a 15-ml conical tube containing 500 μl SOC with 20 μg chlortetracycline (Sigma, St. Louis, MO), and incubated at 30 °C with rigorous shaking for 1 h. An aliquot of 100 μl of the bacterial culture was transferred into a new 15-ml tube containing 20 μg/ml chlortetracycline, 100 μg/ml ampicillin, and 20 μg/ml chloramphenicol in 900 μl SOC, and incubated at 30 °C with shaking for another 3 h. Subsequently, 50–100 μl of the bacterial culture was plated on LB plates containing 100 μg/ml ampicillin and 20 μg/ml chloramphenicol, and incubated overnight at 43 °C. DNA of individual clones was purified and verified by polymerase chain reaction (PCR) using specific primers to BMP-2 (forward: 5′-CCTTCGGAAGACGTCCTCAG and reverse: 5′-TCACTCGATTTCCCTCCAGT) and GFP (forward: 5′-TGCCACCTACGGCAAGCTGA and reverse: 5′-CCATGTGATCG CGCTTCTCG) to confirm the correct retrofitted BAC clone.

Packaging HSV-1 amplicon into virion. HSV-1 amplicon was packaged into infectious virion as described previously [21]. Briefly, Vero 2-2 cells (10^6) were plated in a 60-mm dish. After 18 h, the cells were co-transfected with 2.0 μg pHSV-BAC/BMP-2 or pEHHG, 0.2 μg pEBHICP27, and 2 μg fHSVΔ-pac, Δ-27, 0+ using LipofectAMINE Plus (Invitrogen) for 4 h. The cells were scraped into the supernatant 60 h post-infection, frozen and thawed once, sonicated for 1 min, and centrifuged at 3500 r.p.m. for 15 min. The supernatant was then concentrated through a 25% sucrose by ultracentrifuging, and the amplicon pellet was resuspended in Hanks' buffered salt solution. The purified HSV-1 amplicon was titered in Vero 2-2 cells by counting the number of GFP positive cells after 24 h infection. Typically, the titration of HSV-1 amplicon stocks was around 5×10^6–10^7 GFP transducing units/ml.

HSV-1 virion infection, Western blot and FACS analyses. MC3T3-E1 cells were plated in a 6-well plate at a density of 10^5/well. After 24 h, the cells were infected at a multiplicity of infection (MOI) of 5 with HSV-1 amplicon. After 6 h infection, the medium was removed, and fresh medium was added to the cells. The cells were lysed in a lysis buffer containing 50 mM Tris, pH 8.0, 150 mM NaCl, 0.1% SDS, 1% Triton X-100, and 1× Protease Inhibitor cocktail (Sigma) 24 h after infection. An aliquot of 60 μg cellular protein was electrophoresed on a 15% SDS–polyacrylamide gel and transferred to nitrocellulose. The membrane was incubated at 4 °C overnight in a buffer containing 5% dried skim milk, 150 mM NaCl, 50 mM Tris–HCl (pH 8.0), and 0.05% Tween 20. Immunoblotting was performed in the same buffer containing 0.2 μg/ml antibody against BMP-2 or GFP (Santa Cruz, CA) at room temperature for 1 h. Specific proteins were detected using appropriate secondary antibodies and ECL + plus Western blotting detection system (Amersham–Pharmacia Biotech UK Limited, Buckinghamshire, England). The cells in a parallel well were trypsinized 24 h post-infection and analyzed by fluorescence-activated cell sorter (FACS) (BD Biosciences, San Lose, CA) to assess the transduction efficiency [24].

Cytochemical staining for alkaline phosphatase. The cytochemical staining for alkaline phosphatase (ALP) was performed according to the protocol described previously [25]. Nine days after HSV-1 amplicon infection, the MC3T3-E1 cells were washed with PBS and fixed in 0.05% glutaraldehyde at room temperature for 5 min. The cells were then incubated at 37 °C for 30 min in a staining buffer containing 50 mM Tris–HCl, pH 8.6, 100 mM NaCl, 5 mM KCl, 1 mM $CaCl_2$, 1 mM $MgCl_2$, 0.8 mg/ml naphthol AS-TR phosphate, and 0.6 mg/ml

fast red violet LB diazonium (Sigma) in dark, followed by observation without counterstain.

Results and discussion

We searched the GenBank database and identified a mouse BAC library clone containing a complete 8.7-kb BMP-2 genomic DNA locus driven by a 20.5-kb native promoter within a 128.5-kb insert. We chose this clone because it contains a single BMP-2 gene with most, if not all, of the regulatory elements in the promoter, introns, and 3′ non-coding regions that may regulate a physiological gene expression [26,27]. The length of the BAC clone is also within the size limits that the HSV-1 vector can efficiently package into an iBAC [21]. We used a Cre/loxP-based retrofitting method to convert the BAC/BMP-2 with the pEHHG, consisting of HSV-1 amplicon elements, enhanced green fluorescent protein (GFP), EBV episome retention cassette, R6K bacterial replication origin, and a *loxP* site to generate a 152-kb construct of pHSV-BAC/BMP-2 (Fig. 1A) [20,21]. Subsequently, a PCR with specific primers to BMP-2 and GFP was performed to confirm the presence of two genes within a single pHSV-BAC/BMP-2 construct (Fig. 1B). We then packaged the pHSV-BAC/BMP-2 into the iBAC [21] and infected MC3T3-E1 cells to test the transgenes' function (Fig. 2). Twenty-four hours after infection, the GFP reporter gene was expressed in most of MC3T3-E1 cells transduced with either an HSV-1 mock (Fig. 2C) or an HSV-BAC/BMP-2 amplicon (Fig. 2D). Flow cytometry analyses revealed that 84% of the osteoblast cells transduced with HSV-1 mock amplicon expressed GFP (Fig. 2E) and 77% of the cells infected with HSV-BAC/BMP-2 virion were GFP-positive (Fig. 2F). To compare the efficiencies of transduction and transfection, we also transfected MC3T3-E1 cells with pEHHG and pHSV-BAC/BMP-2 (Fig. 1A) using Lipofectamine-Plus. Only less than 5% of MC3T3-

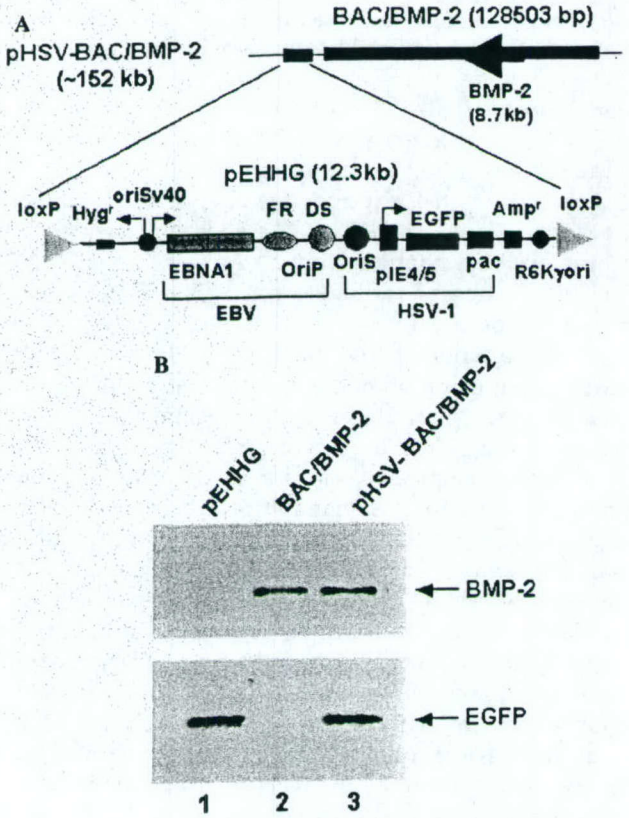

Fig. 1. Schematic diagram of infectious HSV-1/BAC/BMP-2 construct. (A) A detailed structure of retrofitted BAC clone. The retrofitting vector pEHHG containing the HSV-1 amplicon elements (*ori*$_s$ and *pac*) and GFP, the EBV episome retention cassette (*oriP*/*EBNA-1*/*hyg*^{r}), the R6K bacterial replication origin, and a *loxP* site is retrofitted into the BAC clone bearing a complete BMP-2 locus by homologous recombination. The retrofitted BAC contains both GFP reporter and BMP-2 genes. (B) Verification of pHSV-BAC/BMP-2 construct by polymerase chain reaction (PCR). Lane 1: pEHHG control; lane 2: BAC/BMP-2 control; and lane 3: pHSV-BAC/BMP-2 containing both GFP and BMP-2 genes.

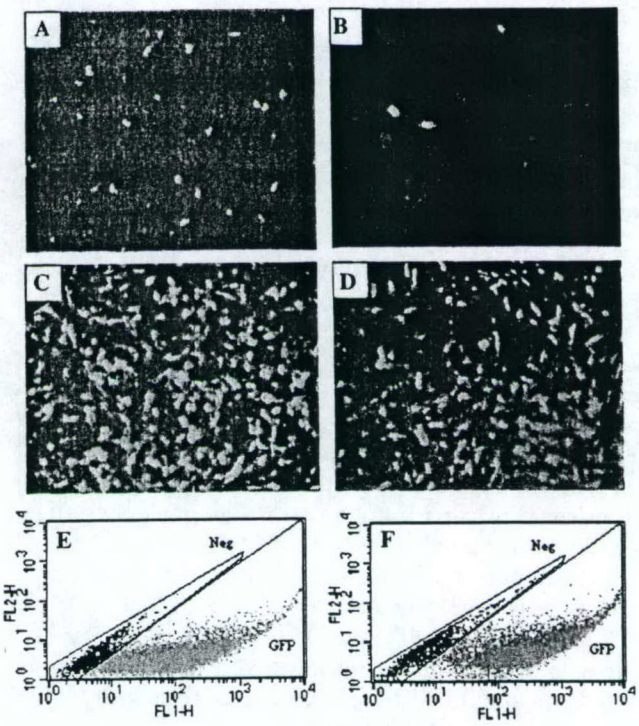

Fig. 2. GFP reporter expression in MC3T3-E1 cells transfected and transduced with HSV-1 amplicon for 24 h (40× images). (A) MC3T3-E1 cells transfected with pEHHG (4 μg) using optimized lipofectamine; (B) MC3T3-E1 cells transfected with pHSV-BAC/BMP-2 (4 μg) using optimized lipofectamine; (C) MC3T3-E1 cells transduced with infectious HSV-1 mock amplicon without BMP-2 genomic locus; (D) MC3T3-E1 cells transduced with infectious HSV-1 amplicon containing a BMP-2 genomic locus; (E) representative data of flow cytometric analysis in MC3T3-E1 cells infected with HSV-1 mock amplicon containing GFP but no BMP-2 genomic locus; and (F) representative data of flow cytometric analysis in MC3T3-E1 cells infected with HSV-1 amplicon containing GFP and a BMP-2 genomic locus.

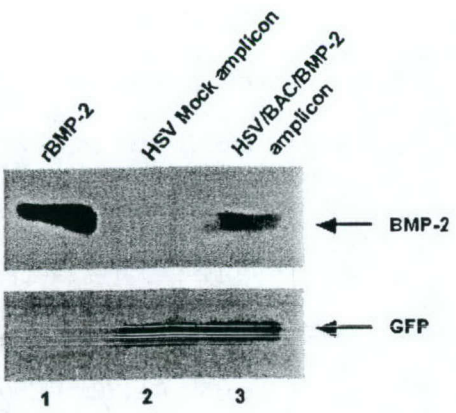

Fig. 3. Western immunoblot analyses of BMP-2 expressed in transduced MC3T3-E1 cells. MC3T3-E1 cells are infected with HSV-1 amplicon for 24 h and harvested for Western blot analysis. An aliquot (60 μg, 10^6 cells) of cellular lysate is separated on 15% SDS–PAGE, transferred to nitrocellulose membranes, and blotted using antibodies against BMP-2 and GFP, respectively. Lane 1: positive control of recombinant BMP-2 (100 ng); lane 2: the cells infected with HSV-1 mock amplicon containing GFP but no BMP-2 genomic locus; and lane 3: the cells infected with HSV-1 amplicon containing GFP and a BMP-2 genomic locus.

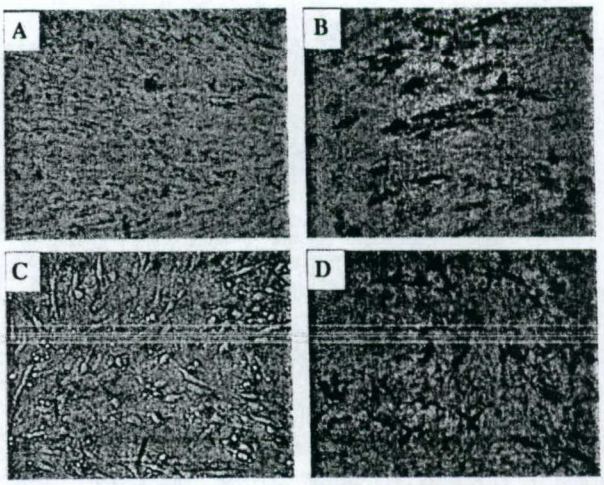

Fig. 4. Alkaline phosphatase (ALP) staining of differentiated MC3T3-E1 cells (40× images). MC3T3-E1 cells are differentiated for 9 days and subjected to ALP staining. (A) The cells infected with HSV-1 mock amplicon without a BMP-2 genomic locus; (B) the cells infected with HSV-1 amplicon containing a BMP-2 genomic locus; (C) negative control of MC3T3-E1 cells treated with vehicle; and (D) positive control of MC3T3-E1 cells treated with recombinant BMP-2 (200 ng/ml).

E1 cells transfected with pHSV-BAC/BMP-2 expressed GFP (Fig. 2A) whereas approximately 10% of the cells transfected with pEHHG turned green (Fig. 2A). Obviously, the efficiency of transduction of BAC-based amplicon was at least 15-fold higher than that of lipid-based transfection (Fig. 2).

The expression of the transgene was examined in cell extract by utilizing Western blot with specific antibodies against BMP-2 and GFP (Fig. 3). The amount of BMP-2 protein was estimated to be 10 ng/10^6 cells based on Western blot analysis (Fig. 3). However, we failed to detect BMP-2 expression in the same number of either native MC3T3-E1 cells or the cells transfected with pHSV-BAC/BMP-2 (Fig. 3 and data not shown). To assess osteoblast phenotype in the cells expressing BMP-2 transgene, we carried out an ALP staining 9 days after transduction (Fig. 4). Like the cells treated with 200 ng/ml recombinant human BMP-2, about 20% of the osteoblast cells were differentiated and exhibited positive ALP-staining (Figs. 4B and D). No ALP-positive cells were seen in the control cells infected with HSV-1 mock amplicon without BMP-2 genomic locus (Fig. 4A) or the cells treated with vehicle alone (Fig. 4C).

In this study, we have demonstrated that the HSV-1 amplicon can efficiently transfer a large piece of genomic locus (Fig. 2), and retain it as episomes in proliferating cells [18]. The GFP gene is consistently active and visible for at least 2 weeks, although the intensity becomes weaker as reported by other investigators [24]. The functional BMP-2 protein in the infected cells was detectable 24 h and even 72 h after infection (Fig. 3 and data not shown) and mediated cell differentiation (Fig. 4) [28]. However, accurate quantification of BMP-2 expression level was impossible because the secreted BMP-2 in the medium was not measured. Nevertheless, the transgene of BMP2 was active and promoted a phenotypic change of targeting cells (Fig. 3, lane 3 and Fig. 4), validating the application of iBAC technology.

In vivo testing of candidate genes in a BAC-based transgenic mouse is time-consuming and expensive, requiring the injection of BAC inserted into fertilized eggs and the examination of mouse phenotypes. Therefore, it would be more efficient to use in vitro cell models via the BAC clone approach to test candidate gene function before introducing in vivo transgenic studies. The studies provided in this manuscript demonstrate that retrofitting of the BAC clone and packaging of the HSV-1 amplicon into infectious virion can be accomplished within 1–2 weeks of work. By utilizing this approach, a candidate gene search in a QTL region is feasible once an appropriate cell model and end points for candidate gene function are determined. In this regard, our data demonstrate that MC3T3-E1 cells can be used as a model for high-throughput phenotypic screening to identify genes important for osteoblast cell differentiation. We have also used this system in C2C12 cells and proved that iBAC containing BMP-2 locus can induce premyoblast dedifferentiation and subsequently commit to osteoblast lineage (data not shown), providing another cell-based model for gene function of dedifferentiation. In addition, BAC or PAC can carry a genomic locus encompassing an intact gene(s) with all regulatory elements including enhancers, suppressors and locus control region that can direct physiological levels of tissue-specific expression for gene therapy. It can also be

manipulated to engineer a deletion, an insertion, and a site-specific mutation in *Escherichia coli* by homologous recombination to mimic natural polymorphisms to test the functional significance of SNPs located in the distal promoter or/and intron regions.

Acknowledgments

This work was supported by Assistance Award No. DAMD17-03-2-0021. The U.S. Army Medical Research Acquisition Activity, 820 Chandler Street, Fort Detrick MD 21702-5014, is the awarding and administering acquisition office. The information contained in this publication does not necessarily reflect the position or the policy of the Government, and no official endorsement should be inferred. All work was performed in facilities provided by the Department of Veterans Affairs. We are grateful to Dr. Yoshinaga Saeki (the Massachusetts General Hospital, Harvard Medical School, MA) for providing HSV-1 amplicon system and his technical assistance, and Dr. Rozanne Sandri-Goldin (the University of California, Irvine, CA) for her generous gift of a Vero 2-2 cell line. We also thank Dr. Shin-Tai Chen, Ms. Mahita Kadmiel, and Mr. Max Davis for their technical assistances of HSV-1 virion purification and FACS analyses (Musculoskeletal Disease Center, JL Pettis Memorial Veterans Medical Center, Loma Linda, CA).

References

[1] D.L. Glaser, F.S. Kaplan, Osteoporosis. Definition and clinical presentation, Spine 22 (1997) 12S–16S.

[2] C.W. Slemenda, J.C. Christian, T. Reed, T.K. Reister, C.J. Williams, C.C. Johnston Jr., Long-term bone loss in men: effects of genetic and environmental factors, Ann. Intern. Med. 117 (1992) 286–291.

[3] C.W. Slemenda, J.C. Christian, C.J. Williams, J.A. Norton, C.C. Johnston Jr., Genetic determinants of bone mass in adult women: a reevaluation of the twin model and the potential importance of gene interaction on heritability estimates, J. Bone Miner. Res. 6 (1991) 561–567.

[4] V. Nicolas, S. Mohan, Y. Honda, A. Prewett, R.D. Finkelman, D.J. Baylink, J.R. Farley, An age-related decrease in the concentration of insulin-like growth factor binding protein-5 in human cortical bone, Calcif. Tissue Int. 57 (1995) 206–212.

[5] D. Baylink, M. Stauffer, J. Wergedal, C. Rich, Formation, mineralization, and resorption of bone in vitamin D-deficient rats, J. Clin. Invest. 49 (1970) 1122–1134.

[6] M.J. Econs, D.L. Koller, S.L. Hui, T. Fishburn, P.M. Conneally, C.C. Johnston Jr., M. Peacock, T.M. Foroud, Confirmation of linkage to chromosome 1q for peak vertebral bone mineral density in premenopausal white women, Am. J. Hum. Genet. 74 (2004) 223–228.

[7] C.M. Kammerer, J.L. Schneider, S.A. Cole, J.E. Hixson, P.B. Samollow, J.R. O'Connell, R. Perez, T.D. Dyer, L. Almasy, J. Blangero, R.L. Bauer, B.D. Mitchell, Quantitative trait loci on chromosomes 2p, 4p, and 13q influence bone mineral density of the forearm and hip in Mexican Americans, J. Bone Miner. Res. 18 (2003) 2245–2252.

[8] F. Wynne, F.J. Drummond, M. Daly, M. Brown, F. Shanahan, M.G. Molloy, K.A. Quane, Suggestive linkage of 2p22-25 and 11q12-13 with low bone mineral density at the lumbar spine in the Irish population, Calcif. Tissue Int. 72 (2003) 651–658.

[9] H.W. Deng, H. Shen, F.H. Xu, H. Deng, T. Conway, Y.J. Liu, Y.Z. Liu, J.L. Li, Q.Y. Huang, K.M. Davies, R.R. Recker, Several genomic regions potentially containing QTLs for bone size variation were identified in a whole-genome linkage scan, Am. J. Med. Genet. 119A (2003) 121–131.

[10] G.L. Masinde, J. Wergedal, H. Davidson, S. Mohan, R. Li, X. Li, D.J. Baylink, Quantitative trait loci for periosteal circumference (PC): identification of single loci and epistatic effects in F2 MRL/SJL mice, Bone 32 (2003) 554–560.

[11] G.L. Masinde, X. Li, W. Gu, J. Wergedal, S. Mohan, D.J. Baylink, Quantitative trait loci for bone density in mice: the genes determining total skeletal density and femur density show little overlap in F2 mice, Calcif. Tissue Int. 71 (2002) 421–428.

[12] W.G. Beamer, C.J. Rosen, R.T. Bronson, W. Gu, L.R. Donahue, D.J. Baylink, C.C. Richardson, G.C. Crawford, J.E. Barker, Spontaneous fracture (sfx): a mouse genetic model of defective peripubertal bone formation, Bone 27 (2000) 619–626.

[13] K.L. Shultz, L.R. Donahue, M.L. Bouxsein, D.J. Baylink, C.J. Rosen, W.G. Beamer, Congenic strains of mice for verification and genetic decomposition of quantitative trait loci for femoral bone mineral density, J. Bone Miner. Res. 18 (2003) 175–185.

[14] W.K. Gu, X.M. Li, B. Edderkaoui, D.D. Strong, K.H. Lau, W.G. Beamer, L.R. Donahue, S. Mohan, D.J. Baylink, Construction of a BAC contig for a 3 cM biologically significant region of mouse chromosome 1, Genetica 114 (2002) 1–9.

[15] R.E. White, R. Wade-Martins, S.L. Hart, J. Frampton, B. Huey, A. Desai-Mehta, K.M. Cerosaletti, P. Concannon, M.R. James, Functional delivery of large genomic DNA to human cells with a peptide-lipid vector, J. Gene. Med. 5 (2003) 883–892.

[16] C. Magin-Lachmann, G. Kotzamanis, L. D'Aiuto, H. Cooke, C. Huxley, E. Wagner, In vitro and in vivo delivery of intact BAC DNA–comparison of different methods, J. Gene. Med. 6 (2004) 195–209.

[17] C. Magin-Lachmann, G. Kotzamanis, L. D'Aiuto, E. Wagner, C. Huxley, Retrofitting BACs with G418 resistance, luciferase, and oriP and EBNA-1-new vectors for in vitro and in vivo delivery, BMC Biotechnol. 3 (2003) 2.

[18] R. Wade-Martins, Y. Saeki, E. Antonio Chiocca, Infectious delivery of a 135-kb LDLR genomic locus leads to regulated complementation of low-density lipoprotein receptor deficiency in human cells, Mol. Ther. 7 (2003) 604–612.

[19] Y. Wang, C. Fraefel, F. Protasi, R.A. Moore, J.D. Fessenden, I.N. Pessah, A. DiFrancesco, X. Breakefield, P.D. Allen, HSV-1 amplicon vectors are a highly efficient gene delivery system for skeletal muscle myoblasts and myotubes, Am. J. Physiol. Cell Physiol. 278 (2000) C619–C626.

[20] R. Wade-Martins, E.R. Smith, E. Tyminski, E.A. Chiocca, Y. Saeki, An infectious transfer and expression system for genomic DNA loci in human and mouse cells, Nat. Biotechnol. 19 (2001) 1067–1070.

[21] Y. Saeki, X.O. Breakefield, E.A. Chiocca, Improved HSV-1 amplicon packaging system using ICP27-deleted, oversized HSV-1 BAC DNA, Methods Mol. Med. 76 (2003) 51–60.

[22] K. Ellnebo-Svedlund, L. Larsson, J. Jonasson, P. Magnusson, Rapid genotyping of the osteoporosis-associated polymorphic transcription factor Sp1 binding site in the COL1A1 gene by pyrosequencing, Mol. Biotechnol. 26 (2004) 87–90.

[23] S.L. Ferrari, D. Karasik, J. Liu, S. Karamohamed, A.G. Herbert, L.A. Cupples, D.P. Kiel, Interactions of interleukin-6 promoter polymorphisms with dietary and lifestyle factors and their association with bone mass in men and women from the Framingham Osteoporosis Study, J. Bone Miner. Res. 19 (2004) 552–559.

[24] R. Nunez, M. Ackermann, Y. Saeki, A. Chiocca, C. Fraefel, Flow cytometric assessment of transduction efficiency and cytotoxicity

of herpes simplex virus type 1-based amplicon vectors, Cytometry 44 (2001) 93–99.
[25] J.E. Wergedal, D.J. Baylink, Characterization of cells isolated and cultured from human bone, Proc. Soc. Exp. Biol. Med. 176 (1984) 60–69.
[26] K.L. Abrams, J. Xu, C. Nativelle-Serpentini, S. Dabirshahsahebi, M.B. Rogers, An evolutionary and molecular analysis of BMP2 expression, J. Biol. Chem. (2004).
[27] L.M. Helvering, R.L. Sharp, X. Ou, A.G. Geiser, Regulation of the promoters for the human bone morphogenetic protein 2 and 4 genes, Gene 256 (2000) 123–138.
[28] D. Noel, D. Gazit, C. Bouquet, F. Apparailly, C. Bony, P. Plence, V. Millet, G. Turgeman, M. Perricaudet, J. Sany, C. Jorgensen, Short-term BMP-2 expression is sufficient for in vivo osteochondral differentiation of mesenchymal stem cells, Stem Cells 22 (2004) 74–85.

Critical Reviews™ in Eukaryotic Gene Expression, 14(1&2):89–136 (2004)

Progress Toward Skeletal Gene Therapy

*Henry J. Klamut, Shin-Tai Chen, K.-H. William Lau, & David J. Baylink**

Departments of Medicine and Biochemistry, Loma Linda University and the Musculoskeletal Disease Center (151), Jerry L. Pettis Memorial Veterans Administration Medical Center, 11201 Benton Street, Loma Linda, CA 92357

*Author to whom all correspondence should be addressed: Tel.: (909) 422-3101; Fax: (909) 796-1680; email: David.Baylink@med.va.gov

ABSTRACT: Skeletal gene therapy is an attractive new approach to the treatment of bone disorders. Impressive advances in our knowledge of the molecular genetic basis of skeletal disorders and fracture healing have led to the development of novel therapeutics based on ectopic expression of one or more genes in patient cells that can influence repair or regenerative processes in bone. Although still a relatively immature field, proof-of-principle for enhanced bone formation through skeletal gene therapy has already been established. The challenge now is to more precisely define optimal cellular targets and therapeutic genes, and to develop safe and efficient ways to deliver therapeutic genes to target cells. In this review, we will highlight some of the exciting advances that have been made in skeletal gene therapy in recent years, with a focus on treatment of localized skeletal lesions. Strengths and weaknesses of current approaches will be discussed, as will strategies for improved safety and therapeutic outcome in the future. Skeletal gene therapy can have an enormous impact on patient care. The next 5 years will present us with unparalleled opportunities to develop more effective therapeutic strategies and overcome obstacles presented by current gene transfer technologies.

KEY WORDS: fracture healing, osteogenesis, viral vectors, gene therapy, growth factors, musculoskeletal disease, nonviral vectors

I. INTRODUCTION

Localized skeletal lesions (including all types of bone fractures [traumatic and nontraumatic], aseptic necrosis, and spinal fusion for intervertebral diseases) cause considerable human suffering and economic loss [1]. Almost 6 million fractures occur annually in the United States, and up to 10% are complicated by delayed or unsuccessful unions. Current treatments include autologous and allogenic bone grafts, electrical stimulation, and local growth factor therapy [2]. Although reasonably successful, these procedures are not optimal, and there remains a critical need to develop new therapeutic strategies that impact positively on fracture healing and bone repair in normal individuals and, in particular, on an aging population with a diminishing capacity for fracture healing.

We foresee in this era of molecular medicine future treatments for systemic and localized skeletal lesions that will involve small molecules,[1] protein therapy, tissue engineering, and gene therapy. The knowledge that growth factors play critical roles in bone repair and fracture healing has led to the notion that protein therapies can be developed to accelerate healing of complex nonunion fractures. Indeed, several studies have shown that recombinant growth factors, such as bone morphogenic proteins (BMPs), can accelerate healing of segmental defects in animal models [3–5]. With additional research to address current limitations, we anticipate that protein therapies will become an important clinical option for local and systemic skeletal disorders.

The goal of tissue engineering is to produce synthetic or biological materials that can either

[1] Although highly relevant to the treatment of skeletal disorders, the discussion of small molecule therapies falls beyond the scope of this review.

1045-4403/04/$5.00

replace injured or defective bone or enhance the healing process. These materials include polymers for orofacial and orthopedic implants and composites for use as bone graft substitutes. To assist in the healing process, these materials are being designed to provide sites for specialized cells to attach and synthesize new bone. Proteins such as growth factors and chemokines, and even plasmid DNA, are being incorporated into these matrices to accelerate the bone formation process. The successful application of tissue engineering to bone healing will be critical to the development of more effective therapeutics, particularly for localized skeletal disorders [6, 7].

Gene therapy represents a third, and in many ways more attractive, new approach to the treatment of skeletal defects. Skeletal gene therapy can be applied independently or in conjunction with tissue engineering [8, 9]. In general, the goal is to influence repair or regenerative processes in bone, either locally or systemically, that is compromised due to disease, aging, or skeletal defects beyond a critical size. Bone offers a number of advantages for gene therapy applications. It has a high regenerative capacity and contains a number of well-defined cellular targets that include progenitor stem cells, as well as highly specialized bone-forming cells (osteoblasts) and bone-ablating cells (osteoclasts). By delivering genes that promote healing directly to cells within the fracture site (*in vivo* gene therapy), or by genetically engineering bone marrow stromal cells, muscle stem cells, or other mesenchymal stem cell progenitors to produce osteogenic factors prior to implantation (*ex vivo* gene therapy), local or systemic growth factor production could be optimized for dose and duration to provide a robust and sustained osteoinductive stimulus (Fig. 1). A variety of candidate therapeutic genes are available based on advances made in recent years in our understanding of bone regeneration at the molecular level. Various target cells can be grown *in vitro*, providing noninvasive experimental models for studies of candidate therapeutic strategies. A number of well-established animal models are also available for preclinical testing. The challenge, as with all gene therapy approaches to date, is to identify optimal cell targets, to develop effective therapeutic genes, and to safely and efficiently deliver these genes to the patient. Several attempts have been made to compare the therapeutic potential of autografts, protein therapy, tissue engineering, and gene therapy, but because many of these modalities, and, in particular, gene therapy, have not yet been optimized, it is difficult to predict their true potential. What is clear, however, is that there exist considerable opportunities for gene therapy applications in the management of skeletal lesions. These range from the acceleration of local fracture healing to the prevention and reduction of age- or disease-associated deterioration of the skeleton.

In the first section of this review, we highlight some of the exciting advances that have been made in skeletal gene therapy in recent years, with a focus on treatment of localized skeletal lesions. Strengths and weaknesses of established animal models, cellular targets, therapeutic genes, and gene delivery systems are discussed. In the second section we explore the future of skeletal gene therapy, including novel cellular targets, therapeutic genes, and gene delivery systems, which might address some of the difficulties encountered in studies to date. Particular emphasis will be placed on the need to better understand the molecular basis of osteogenesis, to develop alternative gene delivery systems, and to develop bone-specific gene targeting strategies.

II. CURRENT SKELETAL GENE THERAPY

New knowledge of the molecular genetic basis of skeletal disorders and fracture healing has prompted the development of novel therapeutics based on the introduction and expression of osteogenic genes in patient cells. Gene therapy strategies for diseases, such as adenosine deaminase deficiency, Duchenne muscular dystrophy, and many types of cancer have been under development for at least a decade. However, the application of gene transfer technologies to the treatment of skeletal disorders is a concept that has emerged only in the last 5 years. Skeletal gene therapy is, therefore, a relatively immature field, and most studies to date have been exploratory in nature, examining the efficiency of gene delivery systems or the therapeutic potential of candidate osteogenic genes. In fact, many of the gene transfer vectors and candidate therapeutic genes available

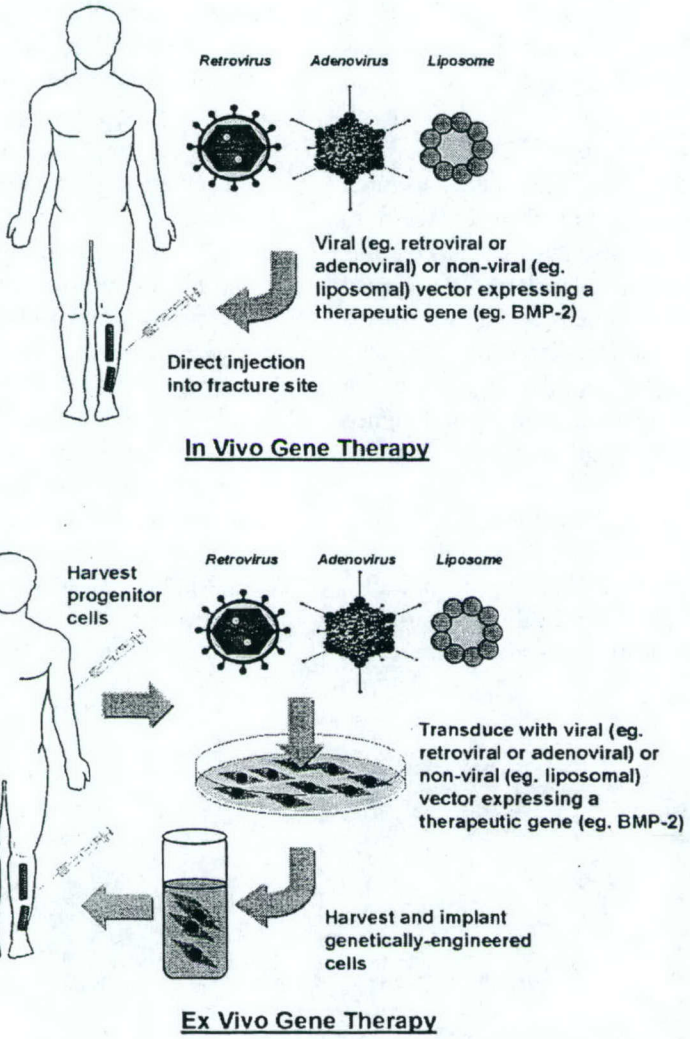

FIGURE 1. *In vivo* and *ex vivo* gene therapy strategies for local fracture healing. *In vivo* strategies involve direct injection of viral or nonviral vectors that carry the therapeutic gene into the fracture site to transduce osteoblasts or other cellular targets. *Ex vivo* strategies involve isolation, expansion, and transduction of patient cells (e.g., mesenchymal stem cells and other osteogenic precursors) in the laboratory. Genetically engineered cells that express the therapeutic gene are then transplanted back into the patient.

today have not been thoroughly evaluated in skeletal applications.

In this section, we present some of the animal models, cellular targets, genes, and vector systems that have been applied to this problem. In addition to providing strong evidence that gene therapy has great potential to dramatically improve the treatment of local and systemic disorders of the skeleton, these studies have also identified important areas that need further development. We conclude with a discussion of some of the unsettled issues that need to be resolved before these exciting advances can be successfully translated into routine clinical treatment of skeletal disorders.

A. Cellular Targets of Fracture Repair

Bone fracture healing involves a complex series of coordinated events that are initiated by complement activation, proteolytic degradation of the ECM, and the release of chemotactic signals that attract polymorphonuclear leukocytes (PMNs), lymphocytes, monocytes, and macrophages to the

wound environment (Fig. 2). A repair blastema develops within 5 days, consisting of collagen, cells such as fibroblasts and macrophages, and new blood vessels. Activated macrophages produce growth factors, such as fibroblast growth factor (FGF) and vascular endothelial growth factor (VEGF), which signal cell division and movement toward the fracture site. A cartilage-like structure (callus) containing various cellular and vascular elements is formed over the course of several weeks, and is then gradually replaced by normal lamellar bone. Although the entire process takes months to complete in humans, the fracture-healing cascade is designed to restore mechanical strength in the shortest time possible [10].

In complex nonunion fractures, the separation between bone ends exceeds a critical limit and union does not occur. Autologous and allogenic bone grafts promote healing of critical-sized defects by promoting the recruitment and differentiation of osteogenic precursors. This is accomplished through local increases in the concentrations of growth factors and cytokines. Skeletal gene therapy attempts to mimic and perhaps improve on the therapeutic effects of bone grafts by introducing genes encoding osteogenic growth factors directly to cells within the fracture site (Fig. 3). Although clinical situations do exist where it may be desirable to manipulate the bone resorptive capacity of osteoclasts, skeletal gene therapy strategies have, for the most part, been targeted primarily to osteoblasts, osteogenic progenitors, supporting cells within the fracture repair region, and, more recently, muscle stem cells. Osteoblasts arise from multipotent mesenchymal stem cells, which also produce bone marrow stromal cells, chondrocytes, adipocytes, and myoblasts (Fig. 4) [11, 12]. Osteoclasts, on the other hand, arise from monocytes/macrophages in the hematopoietic lineage [13]. Because of the large

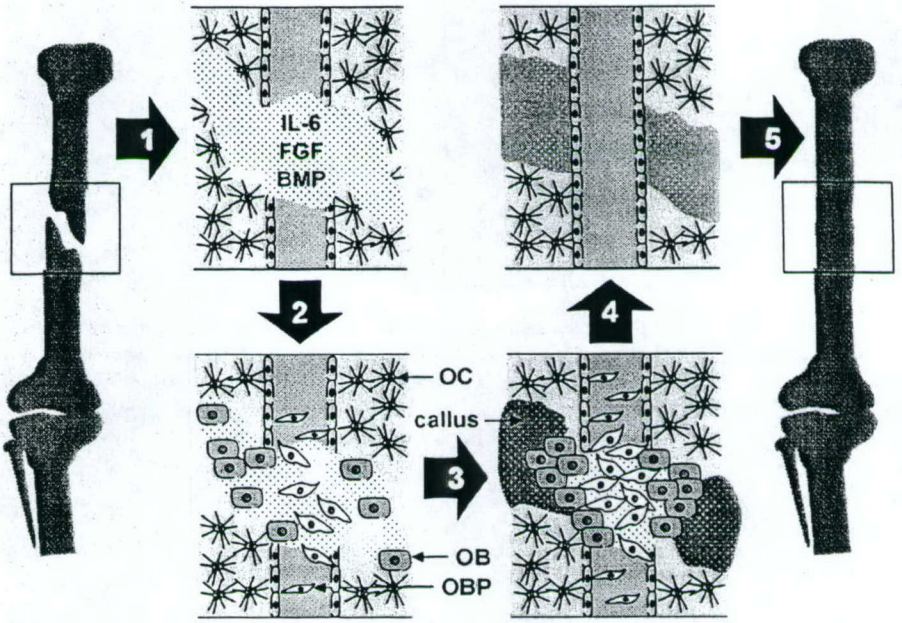

FIGURE 2. Simple fracture healing. **1.** Initiating events in fracture healing include the release of vasoactive mediators, growth factors, and other cytokines from injured tissues and platelets. **2.** Growth factors and cytokines recruit osteoblasts, mesenchymal osteoprogenitors, fibroblasts, and other cell types to the fracture site to initiate the healing process. **3.** During the healing process, osteogenic precursors continue to migrate to the fracture site where they proliferate and differentiate into cells (e.g., osteoblasts and chondrocytes) that form cartilage, bone, and fibrous tissue. The fracture hematoma is organized and a callus is formed between the bone ends, consisting of vascular elements, stromal products, various cell types, and a cartilage-like structure containing Type II collagen. **4.** Fracture healing is complete when there is repopulation of the medulary canal. **5.** Remodelling of woven bone arising from endochondrial ossification of the callus can continue for several months. OB: osteoblast; OC: osteocyte; OBP: osteoblast progenitor.

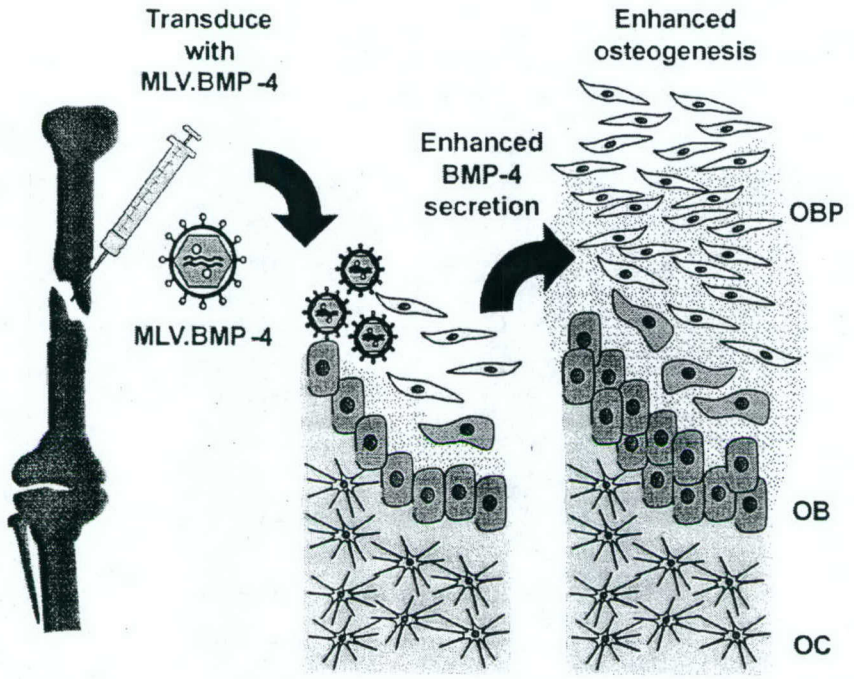

FIGURE 3. *In vivo* gene therapy for fracture healing. Direct injection of a vector carrying a therapeutic gene (e.g., a MLV-based retroviral vector expressing bone morphogenic protein 4 [MLV.BMP-4]) results in transduction of proliferating osteoblasts (OB) and osteogenic precursors (OBP), leading to increased secretion of BMP-4 within the fracture site. High local concentrations of BMP-4 enhance the recruitment and differentiation of osteogenic precursors, resulting in accelerated fracture healing. OC: osteocyte.

numbers of osteoblasts needed to repair a fracture site, and the fact that the average functional lifespan of an osteoblast (3 months) and osteoclast (2 weeks) is significantly shorter than the time it takes for fracture healing, these cell populations must be continuously replenished. The recruitment of osteoprogenitor cells to the fracture site, and their subsequent differentiation into osteoblasts, is in turn critically dependent on local concentrations of growth factors such as bone morphogenic proteins (BMPs), fibroblast growth factors (FGFs), transforming growth factor beta (TGF-β), platelet-derived growth factor (PDGF), and insulin-like growth factors (IGFs). All of these growth factors are produced by mature osteoblasts and supporting cells, such as macrophages and fibroblasts, within the fracture site. Ideally, skeletal gene therapy will provide sustained, controlled expression of one or more of these growth factors, leading to increased recruitment and differentiation of osteogenic precursors.

B. Animal Models of Fracture Repair

Although *in vitro* cell culture models can provide important information relating to the feasibility and efficacy of skeletal gene therapy strategies, they cannot provide a realistic assessment of clinical potential within the context of the myriad of secondary events within traumatized tissues that impact on the fracture healing process. Preclinical testing in animal models that reproduce human disorders and clinical situations will be crucial to successful implementation of skeletal gene therapy strategies. Fortunately, a variety of animal models representing human genetic disorders that affect the skeleton, as well as disorders arising from traumatic events, have already been established through studies of the molecular basis of bone development and repair, as well as in the development of novel therapeutics based on small molecules, bone grafts, protein factors, and tissue engineering. As shown in Table 1, those repre-

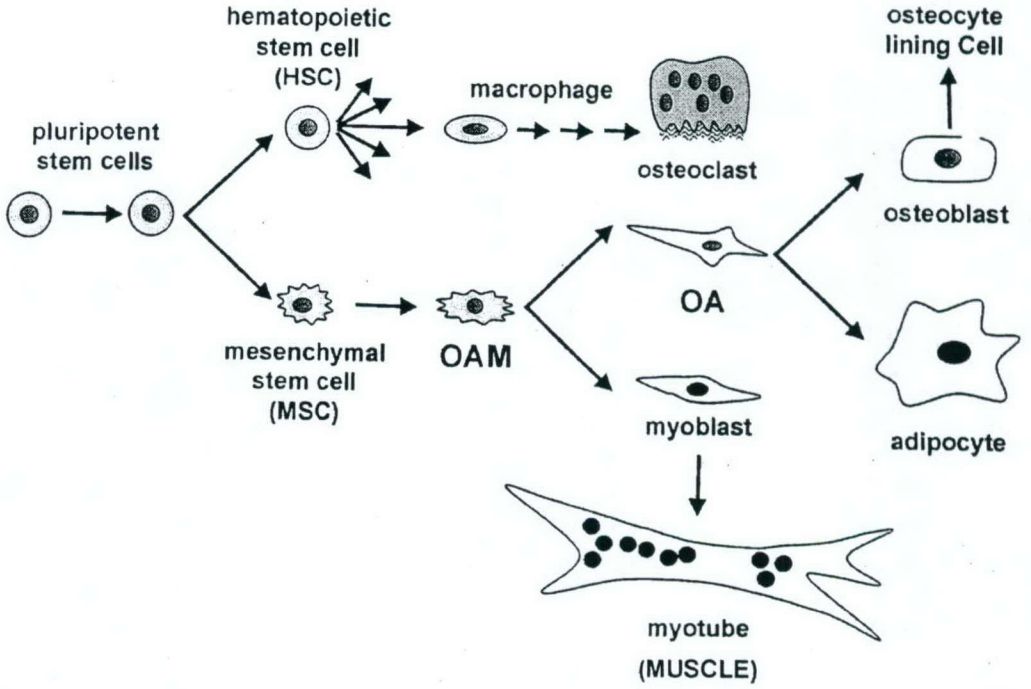

FIGURE 4. Schematic representation of osteoblast and osteoclast development from pluripotent stem cells. Osteoblasts arise from the mesenchymal stem cell (MSC) lineage. Preosteoblasts include progenitors with the potential to differentiate into osteoblasts and adipocytes (OA); or osteoblasts, adipocytes, and myoblasts (OAM). Osteoclasts are derived from the hematopoietic stem cell (HSC) lineage. Primary bone marrow stromal cell and muscle cell cultures are enriched for progenitors along the MSC lineage. Total bone marrow and muscle side population (SP) cells contain pluripotent stem cells capable of differentiating along both the HSC and MSC lineages.

senting traumatic events can be categorized as models of simple fractures, complex nonunion fractures (defect models, namely, calvarial and segmental defects), and spinal abnormalities (spinal fusion). The calvarial model is less technically demanding than the segmental defect model and involves membranous rather than endochondral bone formation. Although not a major focus of

TABLE 1
Animal Models for Skeletal Gene Therapy

Animal Model	Cellular Target	Therapeutic Strategy	References
Closed fractures	Osteoblasts and progentors fibroblasts and other supporting cell types	Primarily direct *in vivo* injection of viral vectors	26, 42, 285
Critical-sized defects • Calvarial defects • Segmental defects	Mesenchymal stem cells (osteogenic progenitors) from dura, bone marrow, or muscle; fibroblasts	Primarily *ex vivo* involving transplantation of genetically engineered cells	28, 29, 286
Spinal Fusion	Bone marrow cells; peripheral blood cells	*Ex vivo* and *in vivo*	287–289

this review, spinal fusion is an important component of the skeletal gene therapy field and many of the same principles apply to the design of gene therapy strategies for these defects. A variety of large and small animal models are available within each of these categories, but, for the most part, early preclinical testing has been done in rats and rabbits. The availability of established animal models of bone defects presents a major benefit to the emerging field of skeletal gene therapy. The impact of novel therapeutics can be evaluated at both the physiological and molecular levels, and this knowledge can be applied to the design and implementation of safer and more effective gene therapy strategies for skeletal disorders.

C. Therapeutic Genes

The successful development of gene therapy strategies for local or systemic disorders of the skeleton will depend on a variety of factors, but perhaps most critical of these is the availability of potent therapeutic genes that influence the rate of bone formation. The remarkable regenerative capacity of bone is dependent on the availability of a continuous supply of osteoblasts and osteoclasts from bone marrow progenitors. Osteoblast and osteoclast development, in turn, is controlled by a complex network of signaling events that respond to growth factors and cytokines, systemic hormones, cell–cell and cell–matrix interactions, and even mechanical stress [11, 12]. The complexity of this process is illustrated by the close coupling that exists between bone resorption and bone formation (Fig. 5). Growth factors, such as TGF-β and IGF-I, are released from osteoclasts and mineralized bone during the process of bone resorption. These growth factors then act in a paracrine manner to influence the recruitment, growth, and differentiation of osteogenic precursors needed to sustain bone formation. In this manner the amount of new bone formed by osteoblasts remains proportional to the bone resorptive activity of osteoclasts.

Gene therapy strategies designed to augment the rate of fracture healing take advantage of our understanding of the molecular basis of osteogenesis. The goal is to influence the bone-forming activity of osteoblasts.[2] This can be accomplished in one of two ways: by increasing extracellular concentrations of one or more osteogenic growth factors that recruit additional osteoblasts to the fracture site, or by altering the activity or survival of osteoblasts that are already present within the fracture site. All of the skeletal gene therapy strategies published to date have been based on the former strategy (Table 2). *In vivo* or *ex vivo* methods are used to introduce one or more growth factor genes to osteoblasts or supporting cells. Transduced cells then secrete growth factors into the local environment to accelerate fracture healing by promoting (1) the movement of existing bone-forming precursor cells to the site of the injury, (2) differentiation of bone precursor cells to the osteoblastic lineage, and (3) the growth of new blood vessels (angiogenesis). Although a variety of growth factors have been shown to stimulate local bone production in osseous sites (Table 3), many have not yet been tested in skeletal gene therapy applications.

The great majority of studies to date have taken advantage of the bone-forming properties of the BMP family of growth factors. BMPs are members of the transforming growth factor-beta (TGF-β) superfamily of growth factors, many of which have been shown to play critical roles in the development, regeneration, and repair of the skeleton [14]. For example, TGF-β1 influences various cell types directly involved in bone remodeling and fracture healing, including mesenchymal cells, chondrocytes, osteoblasts, and osteoclasts [15]. However, BMPs have the unique ability to initiate signaling events that promote the commitment of mesenchymal stem cells to the osteoblastic lineage [16] and to induce ectopic bone formation in vertebrates [17–19]. At least 17 different BMPs have

[2] One could also readily construct viral vectors carrying genes that inhibit bone destruction, but, for several reasons, current skeletal gene therapy has been focused primarily on strategies that stimulate bone formation. Up to this point, gene therapy has been applied only to the treatment of local lesions, and these generally require tissue enhancement. Also, in the case of systemic osteoporosis where the bone resorption rate exceeds the formation rate, adequate FDA-approved small molecule therapies that regulate bone resorption rates have been developed. However, there is a dearth of agents that can effectively stimulate bone regeneration.

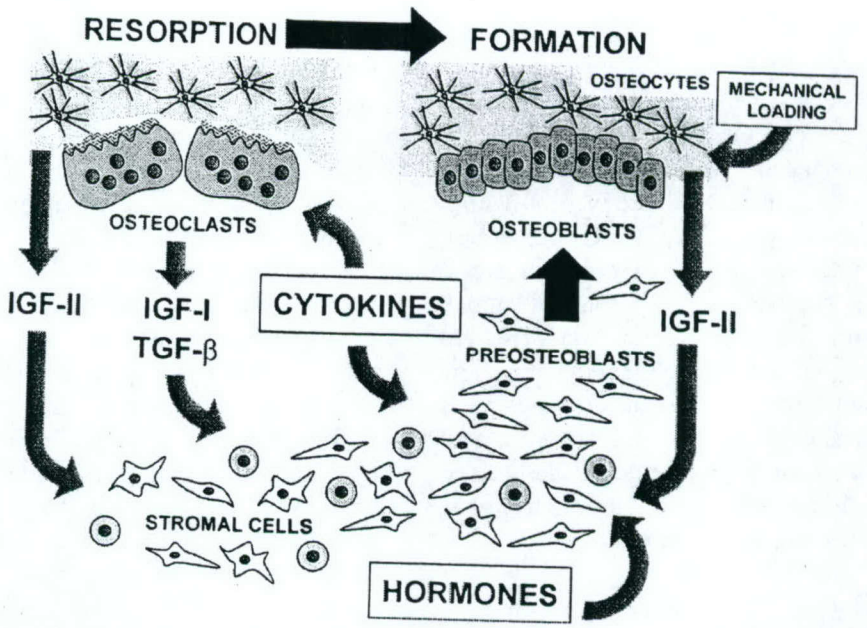

FIGURE 5. Coupling of bone resorption to bone formation. Several mechanisms have been implicated in the stimulation of bone formation by osteoblasts to levels that are proportional to the amount of bone that is being resorbed by osteoclasts (coupling): (1) Cytokines, such as IL-1, can stimulate the resorption phase and can also act as mitogens to stimulate the growth of stromal cells and preosteoblasts. (2) Growth factors, such as IGF-I and TGF-β, are released by osteoclasts during bone resorption. These can act in a paracrine manner to stimulate the growth, recruitment, and differentiation of stromal cells and preosteoblasts. (3) Bone resorption also results in the release of growth factors, such as IGF-II (the most abundant growth factor stored in human bone) from bone tissues, which also act in a delayed paracrine manner to increase the population of bone-forming cells. (4) Mechanical loading can also promote the release of growth factors, such as IGF-II from osteoblasts and, perhaps, osteocytes, which can further influence the rate of bone formation in the resorption cavity. (5) Hormones (e.g., GH and PTH) produced locally or systemically can also act to stimulate or inhibit osteogenesis. Close coupling between bone resorption and formation ensures that the volume of bone formed by osteoblasts is proportional to the volume of bone being resorbed by osteoclasts.

been identified since the initial observation by Urist [20] that demineralized bone matrix contains a factor that can induce ectopic bone formation when implanted into muscle tissue. So far only a handful of these BMP genes have been tested in skeletal gene therapy applications.

BMP-2, BMP-4, and BMP-7 (OP-1) are considered important candidate therapeutic genes, because these factors are localized to fracture repair sites, and, in the case of BMP-2 and -4, persist throughout the process of fracture healing [21]. In skeletal gene therapy applications, these BMPs have been shown to induce osteoblast differentiation *in vitro* [22, 23], heal critical-sized defects [3, 24], and induce spinal fusion [25] in a variety of animal models. For example, Baltzer et al. [26] have shown that direct injection of a recombinant adenovirus expressing human BMP-2 into muscle tissues surrounding an experimental femoral segmental defect significantly improved healing. More recently, Rundle et al. [27] demonstrated that direct injection of a retroviral vector expressing BMP-4 significantly accelerates callus formation in a rat femoral fracture model. In an *ex vivo* gene therapy approach, Gysin et al. [28] transduced bone stromal cells with a retroviral vector expressing BMP-4. Implantation of genetically engineered cells within a gelatin matrix resulted in enhanced bone formation and healing of critical-sized defects in calvariae of syngeneic rats. Similarly, Wright et al. [29] transduced isolated muscle-derived stem cells with a retroviral vector encoding BMP-4. Transplantation of BMP-4–expressing cells was shown to improve bone healing in critical-sized calvarial defects in immunocompetent mice.

TABLE 2
Skeletal Gene Therapy Strategies Applied to Animal Models of Fracture or Defect Healing[a]

Animal	Defect	Strategy	Cell Targets	Therapeutic Genes	Delivery System	References
Rat	Simple fracture	*In vivo*	Osteoblasts; fibroblasts	Marker genes: β-gal and GFP	Replication-defective adenovirus	42
Rabbit	Segmental defect	*In vivo*	Whole muscle	BMP-2 and TGF-β1	Replication-defective adenovirus	290
Rat	Calvarial defect	*In vivo*	Not specified	LIF	Plasmid	286
Rat	Simple fracture	*In vivo*	Not specified	BMP-4	MLV retrovirus	285
Rat	Calvarial defect	*Ex vivo*	Stromal cells	BMP-4	MLV retrovirus	28
Mouse	Calvarial defect	*Ex vivo*	Whole muscle	BMP-4	MLV retrovirus	29

[a] Spinal fusion models have not been included.

TABLE 3
Growth Factor Involvement in Fracture Repair

Growth Factor	Fracture Healing Function	References
Bone Morphogenetic Protein[a] (BMP-2, BMP-3, BMP-4, BMP-7)	• Activation of cortical osteoblasts	291
	• Differentiation of osteoprogenitor cells to osteoblasts	23, 292
	• Differentiation of mesenchymal cells to chondrocytes	291
Fibroblast Growth Factor[a] (FGF-1, FGF-2)	• Proliferation of mesenchymal cells, chondrocytes, and osteoblasts	293–295
	• Angiogenic	296
	• Remodeling	110
Transforming Growth Factor-β[a] (TGF-β1, TGF-β2)	• Pleiotropic, interactions with other growth factors	297, 298
	• Proliferation of osteoprogenitor cells, mesenchymal cells, and chondrocytes	15
	• Osteoblast differentiation	299
	• Extracellular matrix production	15
Platelet-Derived Growth Factor[a] (PDGF-AA, PDGF-AB, PDGF-BB)	• Chemotaxis of macrophages and mesenchymal cells	300
	• Proliferation of mesenchymal cells	298
Growth Hormone and Insulin-like Growth Factors (IGF-I, IGF-II)	• Not well characterized in endochondral bone repair	301
	• IGF-I might mediate growth hormone effects	118
	• Proliferation of cartilage and bone cells	118
	• Extracellular matrix production remodeling	302
Parathyroid Hormone (PTH) and Parathyroid Hormone-Related Peptide (PTHrP)	• Increased osteoclastic differentiation and activity	303
	• Increased bone synthesis	304
	• Osteoblast survival and differentiation	305

[a] Adapted from Reference 306.

Although the effects of BMP-4 on fracture healing have been impressive, Peng et al. [30] used an *ex vivo* approach to demonstrate that transplantation of a combination of muscle-derived stem cells expressing BMP-4 and vascular endothelial growth factor (VEGF) can have an even greater effect on bone healing. New blood vessel formation is essential for proper fracture healing [31], and VEGF plays a central role in the development and modulation of angiogenesis [32, 33]. This study demonstrated for the first time that skeletal gene therapy strategies employing combinations of different growth factors could produce synergistic gains in fracture healing. Although it is certain that BMPs will continue to play a very prominent role in the design of skeletal gene therapy strategies in the future, it is also likely that more effective combinatorial strategies will emerge as more is learned about the complex interactions between different growth factors in the fracture healing environment.

D. Gene Delivery Systems

As outlined earlier, skeletal gene therapy strategies can be developed in one of two ways. The therapeutic gene(s) can be delivered directly to target cells (immature and mature osteoblasts and supporting cells) within the fracture site (*in vivo* gene therapy), or to mesenchymal progenitor cells grown in culture prior to implantation into the fracture site (*ex vivo* gene therapy). In clinical situations that require accelerated fracture healing, acute bursts of growth factor expression may be sufficient to achieve therapeutic endpoints. In these situations, transient gene expression may be more desirable, because it provides an important safety advantage (i.e., it prevents excess accumulation of bone tissue at the treatment site), and both replicating (e.g., preosteoblasts) and quiescent (e.g., differentiated osteoblasts) cell types can be targeted. For long-term systemic expression, transduction of a relatively quiescent subpopulation of mesenchymal stem cells may be necessary, and sustained expression in osteogenic cells over an extended period of time may best be achieved by stable integration of the therapeutic gene into the target cell genome. Clearly, each of these clinical situations presents different challenges for gene delivery. A variety of viral (e.g., adenoviral and retroviral) and nonviral (e.g., liposomal) vector systems have been developed to meet these needs, but none offer optimal performance and many have not yet been tested in skeletal gene therapy applications. With the goal of providing proof-of-principle for a particular therapeutic strategy, the vast majority of skeletal gene therapy studies to date have employed adenoviral or retroviral vector systems. Important features of each of these vectors and their performance in skeletal gene therapy applications are summarized below.

1. Adenoviral Vectors

Because adenoviral vectors are relatively easy to manipulate, can be grown to high titers, and have the ability to efficiently infect both replicating and nonreplicating cells, they are currently the vector of choice for a wide range of gene therapy applications. Adenoviral vectors are particularly attractive in preclinical applications, where the primary goal is to establish proof-of-principle for a gene therapy strategy.

First-generation adenoviral vectors are based on human adenovirus type 5 (Ad5), which causes mild respiratory infections in humans, but is otherwise considered relatively harmless [34]. Genes within the E1 region of the 36-kb Ad5 genome are essential for viral replication. By replacing essential genes within E1 with a recombinant gene-of-interest, first-generation Ad5 vectors were made replication-defective and capable of carrying close to 5 kb of exogenous DNA. Additional deletions within the E3 region of the Ad5 genome expanded the cloning capacity of second-generation vectors to 8 kb [35]. First- and second-generation adenoviral vectors are capable of expressing high levels of recombinant protein following infection of target cells. However, because the adenovirus does not integrate into the host genome and does not replicate with its host cell, gene expression gradually declines as the cells divide and the episomal adenoviral genome is degraded. Initially this wasn't considered to be a significant limitation for gene therapy applications aimed at mature tissues containing differentiated, long-lived cells. However, in practice, gene

expression was also transient in this situation because background expression of adenoviral genes that remain within the recombinant vector elicits a strong cellular immune response against transduced cells. This represents the primary limitation of adenoviral vectors in skeletal and other gene therapy applications. The immune response not only abbreviates the lifespan of transduced cells but also diminishes the effectiveness of repeat administrations of the therapeutic vector.

To address this problem, helper-dependent (HDAdv; gutless) adenoviral vectors have been developed that retain the inverted terminal repeats (ITRs) and packaging signal (φ) needed for replication but otherwise contain no adenoviral genes [36, 37]. This modification not only significantly reduced the immunogenic properties of the vector; it also increased the cloning capacity to 36 kb—sufficient space to incorporate multiple genes or extended regulatory sequences. In the absence of background viral gene expression, transgene expression from HDAdv vectors, although still transient, is significantly prolonged *in vivo* [38, 39]. However, HDAdv vectors present some technical obstacles in that they are more difficult to engineer, grow to high titers, and purify away from helper virus.

Adenoviral vectors have been shown to transduce osteoblasts with high efficiency, both *in vitro* [40] and *in vivo* [41], and several groups have shown that adenovirus-mediated gene transfer can be effective in both *in vivo* and *ex vivo* skeletal gene therapy applications. As summarized in Table 4, the majority of these studies employed BMP-2 as a therapeutic gene under the control of a strong viral promoter (e.g., CMV). Often the endpoint was simply ectopic bone formation following either direct injection of the recombinant adenovirus or transplantation of progenitor cells transduced *ex vivo* into muscle tissues, providing proof-of-principle for the effectiveness of BMP-2 and adenoviral vectors in skeletal gene therapy applications. However, some studies have already looked at fracture healing in animal models with promising results. Mehrara et al. [41] observed good transduction of osteoblasts and osteoclasts, and significant changes in the epiphysial plate, following percutaneous injection of adenoviral vectors expressing lacZ and TGF-β1, respectively. More recently, Van Griensven et al. [42] reported strong staining of fibroblasts and osteoblasts within callus tissue following direct injection of a recombinant adenoviral vector expressing either a lacZ or green fluo-

TABLE 4
Adenovirus-Mediated Skeletal Gene Therapy

In vivo			*Ex vivo*		
Site	**Gene**	**References**	**Cell Type**	**Gene**	**References**
Ectopic (muscle)	BMP-3b BMP-4 and BMP-6 BMP-4 BMP-2 BMP-7 BMP-9	307–316	Bone marrow progenitors	BMP-2	45, 317–321
Bone	β-gal BMP-2 and BMP-9 TGF-β	41, 42, 44	C3H/10T1/2	BMP-2	260, 322
Cranial suture	FGF-1 (dominant negative)	323	Fibroblasts	BMP-7	46, 319
Knee	Oncostatin M	324			
Spine (lumbar musculature)	BMP-9	43	Muscle	BMP-2	319, 325

rescent protein (GFP) reporter gene. Helm et al. [43] observed that direct percutaneous injection of an adenoviral vector expressing BMP-9 into the lumbar paraspinal musculature promotes spinal fusion, with no evidence of local or systemic side effects, and Alden et al. [44] reported significant healing of critical-sized mandibular defects following direct injection of adenoviral vectors expressing either BMP-2 or -9.

Ex vivo strategies have also shown promising results in animal models. Howard et al. [45] observed bone formation following implantation of STRO-1 immunoselected human osteoprogenitors transduced with a BMP-2–expressing adenovirus in diffusion chambers implanted intraperitoneally in athymic nude mice, and Rutherford et al. [46] reported that gingival or dermal fibroblasts transduced with an adenoviral vector expressing BMP-7 exhibit (1) osteoblastic conversion in diffusion chambers, and (2) repair segmental defects in rat femurs.

To date, BMP delivery with adenoviral vectors has proven to be an effective way to stimulate bone induction *in vivo* [47]. The success of *ex vivo* strategies is, perhaps, most surprising, given the transient nature of adenovirus-mediated gene delivery. This would suggest that in these applications a short-term secretion of high levels of growth factors, such as BMP-2, within the fracture site is sufficient to elicit the desired therapeutic effect. Because adenoviral vectors transduce both replicating and nonreplicating cells with high efficiency and provide high levels of therapeutic gene expression, they may be ideally suited to skeletal gene therapy strategies designed to accelerate the fracture healing process.

2. Retroviral Vectors

Retroviral vectors were the first viral vectors to be used for gene therapy and they continue to be a popular choice, particularly in *ex vivo* applications. Most retroviral vectors in use today are based on the Moloney murine leukemia virus (MLV), and two important features distinguish them from adenoviral vectors. The first is their ability to integrate into the host cell genome, resulting in sustained long-term expression of the therapeutic gene. The second is the absence of background retroviral gene expression, which eliminates the problem of patient immune responses against transduced cells. Like adenoviral vectors, retroviral vectors can transduce proliferating cells very efficiently [10K] *in vitro* and *in vivo*; they have a large cloning capacity (8 kb), and large amounts of clinical grade vectors can be produced relatively easily. Properties that limit their use include a restricted host range, poor transduction of nondividing cells, and the danger that insertional events can promote tumorigenesis [48].

Host range restrictions have been addressed, for the most part, by substituting MLV envelope proteins with envelope proteins from other viruses that exhibit a wider tissue tropism (pseudotyping). Infection with retroviral vectors is dependent on specific interactions between a viral envelope glycoprotein and cellular receptors. These interactions define the host range and determine the efficiency of target cell infection. Although MLV-based vectors carrying an amphotropic envelope (Amp) transduce human cells with high efficiency, attempts to concentrate these vectors by centrifugation or other physical means generally result in significant losses of infectious virus. This problem can be overcome by replacing the envelope protein of MLV vectors with the spike G glycoprotein of the rhabdovirus vesicular stomatitis virus (VSV-G). VSV-G-pseudotyped MLV-based vectors have two important attributes: increased viral titers due to their ability to withstand shearing forces encountered during ultracentrifugation, and a broadened host-cell range [49]. The two major limitations of adenoviral vectors, namely, transient gene expression and the host immune response against viral proteins, can be avoided by the use of retroviral vectors. These properties, along with their ability to effectively transduce osteoblasts [50, 51], bone marrow stromal cells [52–54], and muscle-derived stem cells [55], have made retroviral vectors attractive candidate vector systems for skeletal gene therapy, particularly in *ex vivo* applications (Table 5). Mason et al. [56] examined the feasibility of retrovirus-mediated *ex vivo* transduction of primary rabbit periosteal mesenchymal stem cells and demonstrated long-term expression of a β-galactosidase marker gene following implantation of polymer scaffold grafts into femoral osteo-

TABLE 5
Retrovirus-Mediated Skeletal Gene Therapy

Strategy	Cell Target	Therapeutic Gene	References
Ex vivo	Bone marrow stromal MSC	BMP-7	326
	Bone marrow stromal MSC; skin fibroblasts	BMP-4	59
	Bone marrow stromal MSC	BMP-4	28
	Muscle MSC	BMP-4	29
	Muscle MSC	BMP-4 + VEGF	30
	Bone marrow stromal MSC	Telomerase	52
In vivo	Proliferating osteogenic progenitors and periosteal cells	BMP-4	285

chondral defects. In a follow-up study, Breitbart et al. [57] found that periosteal mesenchymal stem cells engineered to express BMP-7 using a retroviral vector can significantly enhance repair of critical-sized defects when seeded onto polyglycolic acid (PGA) matrices.

Difficulties achieving high levels of BMP-4 production from transduced cells [58] and in generating stable clones that produce high titres of a BMP-expressing retrovirus [56] were addressed by Peng et al. [59], who developed an MFG-like retroviral vector [60] that produces high levels of recombinant BMP-4 in bone marrow stromal cells, as well as in skin fibroblasts. BMP-4 secretion was substantially improved by swapping the propeptide domain of BMP-4 with the corresponding propeptide domain of BMP-2 [61] to create a chimeric BMP2/4 gene. Cells transduced *ex vivo* with this vector system were shown to induce ectopic bone formation when implanted subcutaneously in a syngeneic immune-competent rat model. Gysin et al. [28] subsequently observed complete healing of critical-sized calvarial defects following implantation of bone marrow stromal cells transduced with this retroviral BMP2/4 vector. Using a similar approach, Wright et al. [29] demonstrated that muscle-derived murine stem cells transduced *ex vivo* with a BMP2/4-expressing retrovirus induced ectopic bone formation and accelerated healing of calvarial defects in immunocompetent mice. As mentioned earlier, Peng et al. [30] observed synergistic effects on bone healing in a mouse calvarial model following coimplantation of muscle-derived stem cells transduced *ex vivo* with retroviral vectors expressing BMP2/4 and VEGF. Finally, in order to promote the healing of bone tissue, one needs to create new cells or extend the lifespan of existing cells. With respect to the latter possibility, Shi et al. [52] investigated the potential of human telomerase (hTERT) to extend the replicative lifespan of primary human bone marrow stromal stem cells. Retrovirus-mediated hTERT gene transfer was seen to not only extend replicative lifespan but also enhance the bone-forming capacity of stromal stem cells *in vivo*.

Because of the time needed to isolate, expand, and transduce target cells, *ex vivo* gene therapy may not be ideally suited to clinical situations (e.g., fractures) that require immediate attention. Acute therapeutic needs are more readily met by direct *in vivo* gene delivery. In general, the inability of MLV-based retroviral vectors to transduce quiescent, differentiated cells has precluded their use in these applications. However, during fracture repair, cells surrounding the fracture site (i.e., periosteal cells) are stimulated to proliferate. This not only provides a replicating cell population for MLV-based vectors, it also serves to effectively target the therapeutic gene specifically to replicating cells within the fracture site, thereby minimizing undesirable side effects, such as ectopic bone formation at distant sites. Rundle et al. [27] have recently presented evidence in support of this strategy. Direct injection of MLV-based retroviral vectors expressing either a marker gene or BMP2/4 resulted in high transduction efficiencies and substantial augmentation of bone formation at the site of vector administration. This study demonstrated for the first time that accelerated fracture healing can be achieved through direct *in vivo* administration of MLV-based retroviral vectors.

E. Pertinent Unsettled Issues

Studies to date have convincingly demonstrated that gene therapy holds enormous promise for the treatment of local and systemic disorders of the skeleton. However, this emerging field faces many challenges before these impressive advances can be translated to the clinic. For example, cellular targets, and, in particular, the nature of mesenchymal stem cells, remain poorly defined. The osteogenic properties and impressive therapeutic potential of the TGF-β, FGF, and IGF families of growth factors have been well established, but only a select few have been tested in skeletal gene therapy applications. Dosage and duration of treatment in different clinical situations have not been optimized, and, to complicate matters further, there is now evidence to suggest that a more robust regenerative response can be obtained by combined treatment with two or more growth factors. Adenoviral and retroviral vector systems, while effective for preclinical testing in animal models, present serious problems in clinical applications. These limitations have severely impeded progress in other therapeutic applications, and solutions to these problems must be found. Particularly important are the safety issues associated with the use of these viral vectors for gene delivery in patients, as well as the danger of ectopic bone formation and tumorigenesis associated with uncontrolled expression of growth factors. A variety of alternative vectors systems are available and impressive advances are being made in the development of new generations of adenoviral and retroviral vectors. In the next section, we highlight some of these important questions and discuss potential solutions to these problems.

III. THE FUTURE OF SKELETAL GENE THERAPY

The preceding section highlighted some of the major advances that have been made in recent years in our understanding of the cellular and molecular basis of fracture healing, and how this knowledge is being applied to the development of skeletal gene therapy. These exciting developments serve to reinforce our belief that gene therapy strategies can be successfully used to influence osteogenic processes that contribute to fracture healing. This would have an enormous impact on patient care in clinical situations where current therapeutic modalities are ineffective.

Having established proof-of-principle for bone formation, researchers can now focus their efforts on specific areas that need further development. Any successful gene therapy strategy will require a well-defined cellular target, an effective therapeutic gene, and a safe and efficient means to deliver the therapeutic gene to target cells. However, in each application, each of these design components will impact on one another differently. For example, if cell populations exist that can be readily isolated, genetically manipulated *ex vivo*, and efficiently transplanted back into the patient, considerations of vector design and cell-specific targeting may not be as crucial. Similarly, if the therapeutic gene has no adverse effects on surrounding tissues, gene targeting may not be a major requirement for clinical implementation. Nonetheless, achieving exclusive cell targeting (i.e., the ability to control the location, dose, and duration of therapeutic gene expression) would produce more predictable therapeutic outcomes and provide significant safety advantages. In skeletal gene therapy applications, a variety of options are available in each of these areas, but none have yet been thoroughly investigated and optimized. In this section, we explore some of these options and how they may impact on the design of skeletal gene therapy strategies in the future.

A. Cellular Targets: Taking Careful Aim at Osteogenic Progenitors

Because they secrete osteogenic growth factors and are responsible for bone formation, osteoblasts and their progenitors are obvious cellular targets for skeletal gene therapy. So far, however, skeletal gene therapies have not been designed to specifically target these cells. *In vivo* studies have been highly nonspecific, depending entirely on the innate tropism of adenoviral or retroviral vectors for different cell populations within the injection site. *Ex vivo* strategies offer an opportunity to be more selective of the cells being transduced, and the majority of studies to date have used bone marrow stromal cell cultures to increase the like-

lihood that osteogenic progenitors, and, ideally, mesenchymal stem cells, are transduced. However, stromal cell cultures contain a mixture of cell types and variable numbers of mesenchymal stem cells and osteogenic progenitors, and it is not known which cells are being preferentially transduced, or which provide the therapeutic benefits observed in experiments to date. To maximize the impact of skeletal gene therapy, it will be necessary to more precisely define the cell types that provide optimal therapeutic benefits. The difficulty at present is that relatively little is known about the nature of mesenchymal stem cells (MSCs) or the number of intermediary stages that MSCs pass through as they differentiate into osteoblasts, adipocytes, and myoblasts (Fig. 4). This is currently an area of intensive study, and significant advances in our understanding of these events can be anticipated in the near future. It will be important to apply this knowledge to the design of safer and more effective skeletal gene therapy strategies.

1. Osteogenic Progenitors That Home to Bone

A highly desirable property of target cell populations used for *ex vivo* skeletal gene therapy is the ability to home to bone marrow when injected back into the patient. In our experience, bone marrow stromal cells do not exhibit a strong propensity to localize to marrow when injected directly into the circulation of experimental animals. However, a multipotent mouse marrow stromal precursor cell line (D1) with osteogenic, chondrogenic, and adipogenic properties has been described that has the unique ability to home to marrow and participate in fracture callus formation when injected intravenously into syngeneic mice [62, 63]. Evidence that D1 cells can home to marrow raises the distinct possibility that stromal cell cultures do in fact contain a subpopulation of cells with this property. Using D1 cells as a model, it may be possible to identify cell surface markers specific for this subpopulation of osteogenic progenitors, allowing these cells to be isolated using established cell-sorting technologies. This would represent a major advance in the development of *ex vivo* skeletal gene therapy.

2. Osteogenic Progenitors From Other Tissues

As outlined in Figure 4, osteoblasts develop from pluripotent mesenchymal stem cells through a number of discrete stages that can be defined on the basis of the ability of progenitors to give rise to different determined cell populations. For example, at a discrete point in development, pluripotent progenitors give rise to myoblasts and an osteogenic precursor that retains the ability to differentiate into adipocytes. Bone marrow-derived MSCs, therefore, have the potential to regenerate muscle as well as bone. In recent years, a number of studies have identified reservoirs of pluripotent stem cells in tissues other than bone [64–66]. Muscle appears to contain at least two different stem cell pools. Side population (SP) cells represent a small population of stem cells that can be isolated from dissociated muscle by fluorescence-activated cell sorting on the basis of their ability to efflux the dye Hoeschst 33342. These cells have the ability to differentiate into both the mesenchymal and hematopoietic lineages [67, 68]. Multipotent cells have also been isolated from primary cultured skeletal muscle cells [69, 70], but these are distinct from SP cells [71]. Primary cultured myoblasts differentiate into osteoblasts and adipocytes, as well as myotubes, under appropriate culture conditions [72–75]. The existence of mesenchymal stem cell pools in muscle and other tissues, combined with evidence that ectopic BMP expression can induce these cells to differentiate along the osteogenic pathway, provides an alternative, and perhaps more abundant, source of MSC progenitors for skeletal gene therapy applications. In addition, clinical procedures involved in MSC isolation from muscle are less invasive and cause less discomfort to the patient. However, it remains to be determined if muscle-derived stem cells perform as well as marrow-derived cells in skeletal gene therapy applications, or if muscle contains a subpopulation of osteogenic progenitors with the ability to home to bone marrow.

Clearly, a precise definition of mesenchymal stem cell precursors in the osteoblastic lineage, the identification of cell-specific markers, and knowledge of receptor interactions that govern their tissue-homing characteristics would have a

tremendous impact on the future design of skeletal gene therapy strategies. As more is learned about the molecular basis of stem cell differentiation and osteoblast development, skeletal gene therapy strategies will be refined to specifically target osteogenic progenitors that maximize therapeutic benefit while minimizing undesirable side effects.

B. Candidate Therapeutic Genes: A Seemingly Endless Array of Possibilities

Fracture healing requires contributions from a variety of specialized cell types that respond to a complex assortment of growth factors and cytokines in a cooperative manner. In an effort to better understand the mechanisms that mediate fracture repair, we and others have characterized the expression of several growth factors and their receptors and have studied their physiological and morphological effects following local or systemic administration. These efforts have already produced an impressive repertoire of candidate genes for skeletal gene therapy applications. With the completion of the human genome project and the application of microarray technologies to the study of osteogenesis, many more can be expected in the near future. In this section, we highlight some of the growth factor families that will play major roles in the design of skeletal gene therapy strategies in the future.

1. Bone Morphogenic Proteins and Other TGF-β Family Members

Evidence that BMPs perform important osteogenic functions has led to the development of gene therapy strategies designed to increase local concentrations of BMPs in order to stimulate the recruitment and differentiation of osteogenic progenitors. The majority of studies to date have employed either BMP-2 or BMP-4. However, several additional BMP family members, as well as other members of the TGF-β superfamily that are known to have osteogenic activities, have not been extensively investigated. As shown in Table 6, at least 17 different BMPs have been identified. The existence of a large number of closely related BMPs suggests that each of these factors perform a highly specialized function. An understanding of how each BMP contributes to osteogenesis will undoubtedly lead to the development of more effective therapeutic strategies.

TGF-β superfamily members are classified into individual families based on sequence alignments of conserved cysteine residues in their C-terminal domains [76]. The BMPs represent one out of at least seven different families that include TGF-β, growth and differentiation factor (GDF), and inhibin-b/activin (ihbB). Members of families other than the BMPs also exhibit osteogenic properties. For example, activin, initially purified from demineralized bone matrix, was shown to stimulate ectopic bone formation, promote fracture healing, and increase bone mass and mechanical strength when administered systemically [77, 78]. Similarly, subcutaneous injection of placental bone morphogenic protein (PLAB) has been shown to induce cartilage formation and the early stages of endochondral bone formation [79]. PLAB, also known as placental TGF-β (PTGF-β) [80], prostate differentiation factor (PDF) [81], NSAID-activated gene (NAG-1) [82], and macrophage inhibitory cytokine-1 (MIC-1) [83] is interesting because it shares only 15 to 29% identity with other members of the TGF-β superfamily and may represent the first member of a new family of growth factors [83]. Consistent with its osteogenic properties, PLAB is most closely related to the BMPs. However, as evidenced by its diverse nomenclature, this growth factor participates in a broad range of cellular functions. For example, studies in our laboratory [80, 84], and in others [85], have shown that this gene is directly transactivated by the p53 tumor suppressor gene product and may be one of several downstream mediators of p53-dependent apoptosis in breast and prostate cancer cells. On the basis of its transcriptional activation in response to nonsteroidal anti-inflammatory drug (NSAID) treatment (NSAID-activated gene; NAG-1), PLAB has also been implicated in the apoptotic action of NSAIDs on colorectal cancer cells [82]. Evidence that p53 plays an important role in osteoblast differentiation [86], and that NSAIDs interfere with fracture healing [87, 88], raises the intriguing

TABLE 6
The Role of BMP Family Members in Bone Formation[a]

Name	Function	Model	References
BMP-2 (BMP-2A)	Cartilage and bone morphogenesis	Rodent, subcutaneous	327, 328
BMP-3 (OSTEOGENIN)	Bone formation	Rodent, subcutaneous	327, 328
BMP-3B (GDF-10)	Bone formation	NS	NS
BMP-4 (BMP-2B)	Cartilage and bone morphogenesis	Rodent, subcutaneous	327, 328
BMP-5	Bone morphogenesis	NS	NS
BMP-6 (Vgr-1)	Cartilage hypertrophy	Rodent, subcutaneous	329
BMP-7 (OP-1)	Bone differentiation	Rodent, subcutaneous	330
BMP-8 (OP-2)	Bone formation	NS	NS
BMP-8B (OP-3)	NS	NS	NS
BMP-9 (GDF-2)	NS	NS	NS
BMP-10	NS	NS	NS
BMP-11 (GDF-11)	NS	NS	NS
BMP-12 (GDF-7; CDMP-3)	Ligament and tendon development	NS	NS
BMP-13 (GDF-6; CDMP-2)	Cartilage development and hypertrophy	NS	NS
BMP-14 (GDF-5; CDMP-1; CDMP-2)	Mesenchymal condensation and chondrogenesis	Rodent, subcutaneous, intramuscular	331, 332
BMP-15 (CDMP-1)	NS	Rodent, subcutaneous	331
BMP-16	NS	NS	NS

Note: NS, not studied.
[a] Adapted from Ramoshebi LN et al., 2002 (www.expertreviews.org).

possibility that PLAB plays an important role in mediating osteoblast differentiation and apoptosis.

BMPs, activins, and other members of the TGF-β superfamily exert their osteogenic effects by binding to specific receptors on target cells. Receptor binding activates SMADs and other signaling molecules that together converge on the nucleus to influence the expression of genes that promote osteoblast differentiation and bone formation (Fig. 6). For example, BMPs have been shown to activate transcription of core-binding factor a1 (Cbfa1; also known as Runx2 and osteoblast specific factor 2 [Osf2]) [89], an osteoblast-specific transcription factor that, in turn, activates the expression of other osteoblast-specific genes, such as osteopontin, osteocalcin, bone sialoprotein, and type I collagen. Knockout mouse models have shown that osteoblast development and bone formation are disrupted in the absence of Cbfa1 [90]. The osterix (Osx) gene is also activated by BMPs, and, like Cbfa1, is absolutely required for bone formation [91]. BMP-4 also activates the homeobox-containing gene distal-less 5 (Dlx5). Like Cbfa1 and Osx, Dlx5 functions as a transcription factor to regulate the expression of osteoblast-specific genes, such as osteocalcin and

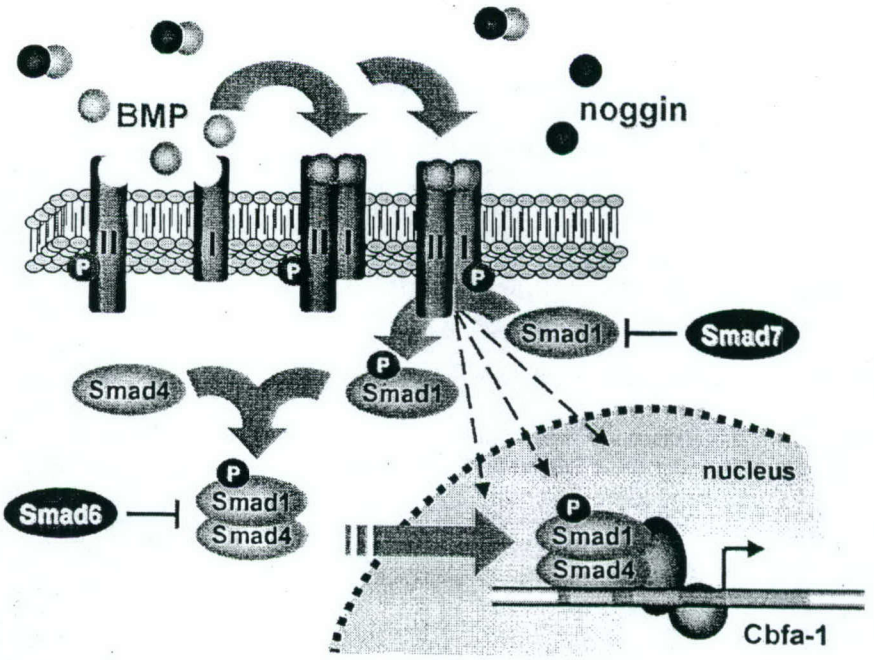

FIGURE 6. Schematic representation of BMP signaling events in osteogenic precursors. Levels of BMP binding to specific receptors on the surface of target cells are determined by the ratio of BMPs to BMP antagonists (e.g., noggin) present in the extracellular space. Receptor activation through phosphorylation events leads to Smad 1 (or 5) phosphorylation, binding with Smad 4 and translocation to the nucleus where interactions with other transcription factors results in activation of osteogenic genes like Cbfa1. Hatched lines represent SMAD-independent pathways that also converge on the nucleus and cooperate with SMAD signaling to influence gene expression. Repressor Smads like Smad 6 and Smad 7 can compete for receptor and Smad 4 binding.

alkaline phosphatase [92, 93]. Genes, such as Cbfa1, Osx, and Dlx5, function as osteogenic determination genes—master switches that commit progenitor cells to the osteoblast lineage. As more is learned about the signaling events and transcription factors that regulate these genes, new therapeutic strategies will be developed that take advantage of our ability to enhance the recruitment and proliferation of osteogenic precursors, as well as to promote differentiation of existing or transplanted cells into bone-forming osteoblasts [94].

To complicate matters further, a number of proteins have recently been identified that antagonize BMP action. Proteins, such as noggin, chordin, follistatin, and the DAN group of proteins, which include DAN, cereberus, caronte, and gremlin, function to bind and inactivate BMPs and other members of the TGF-β superfamily [95–98]. Relevant to current skeletal gene therapy strategies is the fact that noggin binds BMP-2 and BMP-4 with high affinity and specificity to inhibit both osteoblast and osteoclast formation [16, 99]. It is now recognized that the ratio of BMPs to BMP antagonists in the microenvironment is a major determinant of the rate of bone formation. The success of skeletal gene therapy will therefore depend not only on the levels of recombinant BMPs that are expressed from transduced cells, but also on the local concentrations of noggin and other BMP antagonists. Interestingly, fibroblast growth factor-2 (FGF-2) has been shown to suppress noggin expression, and, in a recent study, craniosynostosis arising from gain-of-function mutations in the fibroblast growth factor receptor (FGFR) has been linked to FGF-mediated suppression of noggin expression [100]. This would suggest that the combination of BMP-2 (to enhance osteogenesis) and FGF-2 (to suppress noggin) would be more effective in skeletal gene therapy applications than overexpression of BMP-2 alone. In the following section,

we highlight some of the other properties of the FGF family that make these growth factors strong candidate therapeutic genes for skeletal gene therapy applications.

2. Fibroblast Growth Factors (FGFs)

Fibroblast growth factor (FGF) genes have not yet been tested in skeletal gene therapy applications, but there is ample evidence that this family of growth factors has a very strong influence on the fracture healing process. The 23 members of the fibroblast growth factor (FGF) family promote mitogenic, chemotactic, and angiogenic activity in cells of mesodermal and neuroectodermal origin. Mutations in fibroblast growth factor receptor (FGFR) genes are associated with a number of human skeletal disorders [101], and a large body of evidence points to FGFs as critical regulators of bone development and regeneration.

FGFs appear to have distinct effects on immature and mature osteoblasts. They increase proliferation and inhibit differentiation of osteoblastic precursors, and at the same time promote apoptosis of differentiated osteoblasts [101–103]. These biological effects are mediated by FGF receptors (FGFRs), receptor tyrosine kinases that initiate intracellular signaling events by phosphorylating specific tyrosine residues on their cytoplasmic domains [101]. These phosphorylation events recruit other signaling molecules to activated receptors to propagate the signal through one or more transduction pathways [104]. Many details of FGFR-mediated signaling remain to be established. However, it appears that at least two independent pathways are activated. One is the traditional SH2-linked pathway that connects the FGFR directly to phospholipase C gamma (PLCγ) and Crk, and probably indirectly to Src. The other is linked to SNT-1/FRS2, which activates Ras/MAPK pathways important for growth factor–induced cell cycle progression [103]. It remains to be determined if these signaling pathways are responsible for the diverse effects of FGF on immature and mature osteoblasts.

Because FGF-2 (basic FGF, bFGF) is produced by osteoblasts [105], is stored in the bone matrix [106], and acts as a potent mitogen to bone cells *in vitro* [107, 108], this gene is a prime candidate for skeletal gene therapy. Systemic injections of recombinant FGF-2 protein have been shown to increase preosteoblast numbers, stimulate endosteal bone formation and fracture healing [109, 110], and increase bone mass in animal models [111]. In addition to these osteogenic properties, FGF-2 is also a potent modulator of angiogenesis (neovascularization), a multistep process in which new blood vessels grow from existing vessels. Angiogenesis is essential for proper fracture healing [31], and FGF-2 plays a prominent role in this process, in large part through activation of the potent angiogenic cytokine VEGF in endothelial cells [112] and osteoblasts [113]. Peng et al. [30] demonstrated that overexpression of VEGF alone has a minimal impact on fracture healing, but has synergistic effects when combined with BMP-4. Because it has both angiogenic and osteogenic properties, FGF-2 would be expected to have greater impact on BMP-mediated bone formation than VEGF. However, because FGF-2 is a potent regulator of cell proliferation, migration, adhesion, and differentiation, and influences processes such as wound healing and tumorigenesis, it will be important to maintain strict control over FGF-2 expression in any clinical skeletal gene therapy application.

3. Growth Hormone and Insulin-like Growth Factors

Like FGF, systemic administration of growth hormone (GH) can accelerate bone formation and fracture healing [114, 115]. The osteogenic effects of GH are mediated largely by insulin-like growth factors I and II (IGF-I and -II) [116]. IGF-I and -II are the most abundant growth factors stored in bone matrix [117] and IGF-I is expressed at high levels in the developing bone periosteum and growth plate, in the healing fracture callus, and in developing ectopic bone tissue induced by demineralized bone matrix [118, 119]. Systemic administration of recombinant IGF-I protein alone can increase growth in patients deficient in GH receptors [120], as well as accelerate healing in rat fracture models [121]. At the cellular level, IGFs have been shown to stimulate the proliferation and differentiation of osteoblast

precursors [117, 122–125] and to enhance bone matrix synthesis [126].

The biological actions of IGFs are mediated by the IGF-I receptor (IGF-IR), a transmembrane tyrosine kinase. A second IGF receptor, the IGF-II/cation-independent mannose-6-phosphate receptor, has no known signaling function but instead acts to preferentially bind, internalize, and degrade IGF-II [127]. Like the BMPs, IGF signaling is regulated at the ligand-binding level by several IGF-binding proteins (IGFBPs) that bind IGFs with higher affinities than their receptors [128, 129]. In serum, IGFBPs are thought to prolong the half-lives of circulating IGFs and to buffer hypoglycemic effects by preventing IGF binding to insulin receptors. Locally, IGFBPs may help to localize IGFs to specific microenvironments and to modulate their biological activities [130]. IGFBP-5 is an essential regulator of IGF activity in bone cells and is tightly regulated by IGFs and several other hormones and growth factors [124, 131]. In contrast to other IGFBPs that function to inhibit osteogenesis by sequestering IGFs away from IGF-IR, IGFBP-5 has the capacity to stimulate osteoblast growth through both IFG-dependent [132, 133] and IGF-independent [124, 134–136] mechanisms that are still relatively poorly defined. IGF-independent osteogenic effects may involve IGFBP-5 binding to specific receptors on the surface of osteoblasts and translocation to the nucleus where it can affect gene expression. Recently, nuclear-localized IGFBP-5 was found to interact with four and a half LIM protein 2 (FHL2), a member of the LIM domain-only family of transcription factors [137]. The IGFBP-5–FHL2 complex is thought to transactivate a subset of genes that promotes osteoblast growth. Interestingly, FHL2 gene expression can be transactivated by p53 [138]—further evidence that p53 is an important mediator of osteoblast development. It is also interesting that a second LIM protein, LIM mineralization protein-1 (LMP-1), also has osteoinductive properties. LMP-1 was shown to participate in the induction of bone nodule formation in fetal rat calvarial osteoblast cultures by BMP-6 [139].

In view of their osteogenic properties, GH, the IGFs, IGFBP-5, and LMP-1 all represent candidate therapeutic genes for skeletal gene therapy. Adenovirus-mediated gene transfer of LMP-1 has already been shown to promote spinal fusion in a rabbit model [140], but GH, the IGFs, and IGFBP-5 have not, as yet, been tested in skeletal gene therapy applications. The use of GH offers some advantages in that it is safe (not likely to produce hypoglycemia), its efficacy has been demonstrated in transgenic mouse models, and it increases not only IGF-I production but also other IGF system components that potentiate IGF action (e.g., IGFBP-5). However, GH also increases the production of inhibitory IGFBPs, such as IGFBP-4, which may neutralize some of its osteogenic effects. Also, since not all cells express GH receptors, the impact of local GH production may be limited, depending on the status of GH receptors on target cells. IGF-I receptors, on the other hand, are expressed in almost every cell type studied. IGF-I also increases the production of stimulatory IGFBPs (e.g., IGFBP-5) in certain cell types, but does not activate IGFBP-4—an important advantage over the use of GH. However, because high levels of circulating IGF-I can cause hypoglycemia and increase the risk of cancer, expression of this growth factor would have to be strictly controlled in clinical applications. These safety considerations, along with the fact that IGF-I functions as a downstream mediator of GH action, point to GH as the preferred candidate therapeutic gene for skeletal gene therapy applications.

4. Cyclooxygenase 2 (COX-2)

The negative effects of NSAIDs on fracture healing [87, 88] have been attributed primarily to their ability to inhibit the cyclooxygenases COX-1 and -2. These enzymes control the rate of synthesis of prostaglandins, which play important roles in bone metabolism and repair [141, 142]. For example, prostaglandin E2 (PGE2) promotes both bone formation and resorption, and induces the expression of core-binding factor α-1 (Cbfa1/Runx2) in bone marrow cell cultures [143]. COX-2 catalyzes the first committed step in the formation of PGE2 and other prostaglandins from arachidonic acid, and knockout mice lacking COX-2 exhibit decreased bone density [144] and a decreased capacity for both intramembranous

and endochondral bone formation during fracture repair [145]. These deficiencies appear to be related to decreased levels of Cbfa1 and osterix expression in COX-2 null mice. Prostaglandins, and by extension COX-2, therefore, appear to be key regulators of the expression of osteoblast determination genes, such as Cbfa1[89–91]. This raises the possibility that gene transfer and ectopic expression of recombinant COX-2 can produce a strong inductive signal for osteogenesis.

C. Toward the Osteogenic Transcriptome: Microarray Analysis of Osteoblast Differentiation

The above discussion of candidate therapeutic genes for skeletal gene therapy is illustrative of the complex network of molecular events that occur in response to changes in local concentrations of growth factors and cytokines that influence osteoblast maturation. In the adult skeleton, the balance of these events determines the size of the osteoblast population at any given time [146]. Our ability to design and implement safe and effective skeletal gene therapy strategies will depend to a great extent on our knowledge of gene function and regulation throughout the process of osteoblast maturation.

Until recently, studies of the molecular events associated with osteoblast differentiation typically focused on single genes, providing important information about their expression and function but little about their relationships with each other. Microarray technologies have changed this dramatically. By allowing for thousands of genes to be examined simultaneously, microarray analysis provides a totally new perspective on the coordinate transcriptional response to signaling events that promote cellular growth and differentiation. Relative expression profiles of known genes can be established over the course of osteoblast differentiation and maturation, and novel genes associated with this process can be easily identified. For example, Beck et al. [147] applied gene array technologies to an examination of the changes in gene expression with differentiation of MC3T3-E1 cells. By screening a panel of 588 well-characterized genes over several time points following the induction of MC3T3-E1 cell differentiation into osteoblasts, Beck et al. verified that genes such as TGF-β and BMP receptor 1A participate in this process, and showed for the first time that genes such as the antiproliferative factor Tob, DNA damage-associated proteins El24 and Gadd45, and transcription factors Nrf2 and SEF2 are involved in osteoblast maturation. In an independent study of MC3T3-El cell development, Raouf and Seth [148] utilized a high-density microarray gene chip to compare the expression of more than 8700 genes at the proliferative (day 3) and mineralization (day 34) stages of osteoblast maturation. A total of 252 genes were identified to be differentially expressed on days 3 and 34, a large proportion of which had not been previously associated with osteoblast development. Genes such as TACC3, Pr22 and EST317 (a mouse homologue of the human LB1.CTCL tumor antigen SE20/FLJ10749 gene) were expressed at high levels in proliferating preosteoblasts, and the expressed sequence tag EST350 was implicated in the regulation of osteoblast differentiation.

Hadjiargyrou et al. [149] used a suppressive subtractive hybridization (SSH) technique to examine genes associated with regeneration in a rat femur model of bone healing. A total of 588 known genes, 821 ESTs, and 116 novel genes were identified. These were then incorporated into custom cDNA microarrays and used to study temporal changes in expression during fracture healing. Cluster analysis revealed subsets of genes, both known and unknown, that exhibited distinct expression patterns over 21 days postfracture. Known genes represented families with functional involvement in a variety of cellular processes, including the cell cycle, cell adhesion and communication, and signaling and transcriptional regulation. In addition to expanding the catalogue of functional gene families involved in fracture healing, inferences could be made about the involvement of signal transduction pathways in the repair process. For example, elevated expression of genes such as Wnt-5A, frizzled, casein kinase II, β-catenin, and protein phosphatase 2A pointed to an important role for Wnt signaling in fracture healing [150]. More recently, Qin et al. [151] identified 125 known genes and 30 unknown ESTs that respond to parathyroid hormone (PTH) treatment of the UMR 106-01

osteoblastic cell line. PTH binds to its receptor PTH1R (parathyroid hormone 1 receptor) on osteoblasts to regulate bone remodeling and calcium homeostasis. Although prolonged exposure to PTH causes increased bone resorption, intermittent injections of PTH have anabolic effects. Because the molecular mechanisms regulating these processes are largely unknown, the majority of genes identified in this study represent novel mediators of PTH action.

These studies not only confirm the value of microarray technologies in elucidating the molecular mechanisms underlying fracture healing but also emphasize the complexity of the process. The precise definition of temporal expression patterns of known and novel genes throughout the fracture healing process, and their responsiveness to hormones, cytokines, growth factors, and pharmacological agents, certainly represents a formidable challenge. However, in addition to providing a rich supply of candidate therapeutic genes for skeletal gene therapy, this knowledge will be used to design safer and more effective gene delivery systems that incorporate transcriptional controls and targeting molecules specific for osteogenic cells.

D. Novel Gene Knockdown Strategies (siRNA) Applied to Skeletal Gene Therapy

For the most part, the design of skeletal gene therapy strategies will be based on the knowledge that elevated expression of one or more therapeutic genes in target cells will have a positive impact on bone formation. However, the discovery that double-stranded RNA can mediate selective gene silencing [152] provides new opportunities to develop therapeutic strategies that employ short interfering double-stranded RNA (siRNA) to target and destroy specific gene transcripts in mammalian cells [153]. siRNAs are 21–25 nucleotide dsRNAs that function to guide RNA-induced silencing protein complexes (RISC) to target mRNAs. This interaction is highly specific and leads to cleavage and inactivation of the target mRNA [153–155]. Examples of therapeutic applications of siRNA include protection of mammalian cells against infection with poliovirus and HIV [156, 157], and inhibition of tumor cell growth through inactivation of telomerase [158] or IGFR1 [159] transcripts.

At present, gene knockdown strategies have not been applied to skeletal disorders, but this approach may be useful in clinical situations that present with an imbalance between bone formation and bone resorption. For example, controlled inducible expression of siRNAs targeted to the receptor for activation of nuclear factor kappa B (RANK) in preosteoclasts, or to the RANK ligand in osteoblasts, could be used to adjust the relative rates of osteoclast formation and bone resorption [160]. In addition, because apoptosis of osteoblasts is a key pathogenic mechanism in osteoporosis arising from loss of sex steroids or glucocorticoid excess [161], regulated knockdown of important mediators of proapoptotic pathways, such as Bax and Bad [162, 163], could promote osteoblast survival and enhance bone formation. Finally, siRNA specifically targeted to BMP and IGF antagonists, such as noggin and IGFBP4, could significantly enhance osteogenesis in response to either endogenous or ectopic production of these growth factors.

E. Optimizing Skeletal Gene Therapy Through Protein Engineering

Difficulties with the synthesis, activity, stability, antigenicity, or toxicity of recombinant therapeutic proteins are often encountered in the development of gene therapy strategies. Protein engineering technologies have been applied to these problems, and, in many cases, this has led to significant improvements in therapeutic endpoints [164]. A good example in the skeletal gene therapy area is chimeric BMP2/4 [59]. Difficulties achieving therapeutic levels of BMP-4 secretion from genetically engineered cells were addressed by exchanging the propeptide domain of BMP-4 with the corresponding propeptide domain of BMP-2 [61].

Modifications that affect the stability or actions of osteogenic growth factors could have a powerful impact on therapeutic outcome. For example, site-directed mutagenesis of two cysteines at positions 70 and 88 to serine residues was shown to increase the stability of FGF-2

under acidic conditions without affecting its biological activity [165]. Facciano et al. [166] found that FGF-2 glycation reduces its chemotactic effects toward endothelial cells *in vitro* and its angiogenic activity *in vivo*, and Grieb et al. [167] showed that, in addition to receptor binding, the mitogenic effects of FGF-1 involve internalization and proteolytic processing. Modifications that affect these processes could be used to tailor FGF activities to meet specific therapeutic needs, and similar strategies could be used with other growth factors involved in bone formation and repair. For example, Sakai et al. [168] demonstrated that formation of IGFBP-1 multimers, which potentiates IGF-I action, is dependent on post-translational modification of IGFBP-1 by tissue transglutaminase. An IGFBP-I mutant, in which two glutamine residues at positions 66 and 67 are replaced by alanines, was resistant to multimer formation and had potent inhibitory effects on IGF-I activity. Clearly, site-directed mutagenesis can have a powerful impact on the actions of osteogenic growth factors.

The BMP2/4 construct is an example of an alternative strategy to site-directed mutagenesis that takes advantage of the modular nature of protein function. By bringing together functional domains from different proteins, novel genes can be constructed that produce fusion proteins with characteristics that optimize their therapeutic impact. For example, Yoneda et al. [169] produced a fusion protein that combines FGF-1 with the heparin sulfate proteoglycan (PG) core protein. The PG–FGF-1 fusion overrides the need for heparin or heparin sulfate to be present on or near the surface of target cells for FGF-1 to exert its biological activity. In addition to enhancing function, fusion proteins can be made that improve stability or biodistribution. For example, the herpes simplex virus protein VP22 has the ability to translocate between neighboring cells and accumulate in the nucleus [170]. This property can be exploited in therapeutic applications by producing VP22 fusion proteins that retain the activity of the therapeutic protein but have the added property of being transported to neighboring target cells that were not initially transduced with the therapeutic gene. For example, VP22 has been used successfully to enhance the proapoptotic actions of p53 in cancer gene therapy applications [170, 171]. In skeletal gene therapy strategies designed to increase the number of osteogenic progenitors through gene transfer of osteoblast determination genes, it will be important to maximize the number of cells that express the transgene. For this reason, it is likely that a VP22–Cbfa1 fusion protein would produce a much more robust therapeutic response than the wild-type Cbfa1 gene alone.

The chimeric BMP2/4 gene is illustrative of the enormous impact that protein engineering technologies can have on the success of skeletal gene therapy strategies. A number of modifications have already been made to candidate therapeutic genes, such as FGF-2, which can significantly improve their activity and biodistribution, and it is certain that protein engineering will play an increasingly important role in the design of skeletal gene therapy strategies in the future. The flood of new genetic information provided by microarray technologies and the human genome project, along with the development of siRNA and protein engineering technologies have provided us with an enormous supply of candidate therapeutic genes. It now appears that the major limitation preventing clinical implementation is the absence of an effective gene delivery system. However, as we outline in the next section, major advances are also being made in this area, making it highly likely that skeletal gene therapies will be a clinical reality in the very near future.

F. New Avenues for Therapeutic Gene Delivery to the Skeleton

As outlined above, a wide range of cellular targets and therapeutic genes are currently available for skeletal gene therapy applications, and many more can be anticipated in the near future. This enormous wealth of information will provide us with all of the raw materials necessary to implement gene therapy for skeletal disorders. Once it is determined what gene or combination of genes is most effective in a particular clinical situation, success will depend entirely on our ability to deliver therapeutic minigenes to patient cells and produce therapeutic proteins in a safe and effective manner. This can be achieved using either *ex vivo* or *in vivo* gene transfer strategies, both of

which currently present common and unique challenges for the delivery and expression of therapeutic genes.

Although more invasive and technically more complex, *ex vivo* gene therapy offers several important advantages to clinical implementation. Procedures for hematopoietic stem cell, muscle stem cell, and bone marrow stromal cell isolation have been established, demands for cell-specific targeting are not as great, and quality control testing (e.g., for gene transfer efficiencies or the presence of replication-competent virus) can be performed before genetically engineered cells are delivered to the patient. However, more precise methods of identifying and purifying early progenitor stem cells still need to be developed, and current vector systems cannot sustain long-term therapeutic gene expression in this population of cells. For example, because MLV-based retroviral vectors cannot transduce nonreplicating cells, it is unlikely that early progenitors, which represent a relatively small and quiescent subpopulation of hematopoietic or stromal cell cultures, will be effectively transduced. To compound this problem, retroviral vectors are highly susceptible to transcriptional silencing, particularly in early progenitor stem cells. This means that in early progenitors that are transduced, the therapeutic gene will only be expressed for a short period of time. Furthermore, random integration events pose the threat of insertional mutagenesis. Adenoviral vectors avoid some of these problems, but transient gene expression and problems with immunorejection of transduced cells limits their use in this application. Finally, even if early osteogenic progenitors could be safely and efficiently transduced, it remains to be established if these cells will home to marrow when transplanted back into the patient.

Many of the same challenges are faced by direct *in vivo* gene therapy applications, with the added danger that local or systemic dissemination of the vector may promote ectopic bone formation and tumorigenesis in nontarget cell populations. This places a greater premium on gene and vector targeting. The ideal gene delivery system for skeletal gene therapy would have the following characteristics: It would be nonimmunogenic and have sufficient cloning capacity to accommodate one or more therapeutic genes, as well as transcriptional controls and any other sequence elements needed to ensure safe and effective therapeutic gene expression (i.e., the ability to turn expression on and off). It would have the capacity to deliver the therapeutic gene(s) specifically to target cells following local or systemic administration to the patient; if administered systemically, it would endure in the circulation long enough to ensure effective transduction of target tissues and cells. It would provide for stable, long-term expression of the therapeutic gene, either through extrachromosomal replication or through targeted insertion into benign regions of the human genome. Finally, the therapeutic gene would be expressed in a controlled manner, reflecting endogenous gene expression patterns or responding to the host cell microenvironment (e.g., hypoxia), external stimuli (e.g., drugs, heat), or mechanical strain. Many of the gene delivery systems that are currently available possess one or more of these properties, but none can adequately address all of these needs. Two strategies can be used to develop better delivery systems for skeletal gene therapy. One is to explore alternative viral and nonviral vector platforms. The second is to build on our knowledge and experience with current adenoviral and retroviral platforms by continuing to engineer these systems to meet the demands of individual skeletal gene therapy applications.

1. Alternative Gene Delivery Systems: Viral Vectors

The most efficient gene delivery systems currently available for clinical applications are virus-based vectors. The potential of adenoviral and retroviral vectors for *in vivo* and *ex vivo* skeletal gene therapy has already been demonstrated. Related vector systems based on lentivirus and adenoassociated virus have received considerable attention in recent years, but these have not yet been tested in skeletal gene therapy applications.

a. Lentiviral Vectors

The two major limitations of adenoviral vectors for gene therapy applications, namely, transient

gene expression and the host immune response against viral proteins, can be avoided by the use of retroviral vectors [172, 173]. However, MLV-based retroviral vectors do not transduce quiescent cells with high efficiency, which in both *in vivo* (e.g., osteoblasts) and *ex vivo* (e.g., mesenchymal stem cells) skeletal gene therapy strategies represent important cellular targets. This limitation of MLV-based vectors originates from their most important strength, which is their ability to integrate into the host cell genome. Transduction of target cells by retroviral vectors involves binding of retroviral particles to specific receptors on the cell surface, entry into the cytoplasm, and reverse transcription of viral RNA into double-stranded DNA prior to integration into the host cell genome. All of these steps can be performed with equal efficiency in both replicating and nonreplicating cells. However, because MLV DNA cannot pass through the nuclear membrane, integration can only occur when the nuclear membrane breaks down just prior to cell division [173]. It is for this reason that MLV-based vectors preferentially transduce proliferating cell populations.

The retroviral DNA integration step is the major feature that distinguishes MLV vectors from lentiviral vectors. The nuclear membrane does not present a barrier to double-stranded lentiviral DNA, which can be transported into the nucleus in quiescent cells [174]. Lentiviral vectors can, therefore, effectively transduce both replicating and nonreplicating cells. This characteristic has been the major impetus for development of the lentiviral vector platform [175]. Most lentiviral vectors are based on Human Immunodeficiency Virus Type I (HIV), the etiologic agent of acquired immunodeficiency syndrome (AIDS). Accordingly, safety is the most important issue that must be addressed with the use of this gene delivery system. The major risk is contamination of viral stocks with replication-competent retrovirus (RCR) during vector production, and several strategies have been used to improve the biosafety of this vector platform (Fig. 7). One takes advantage of the complexity of the lentiviral genome by eliminating all viral genes that are not needed to generate an efficient vector. In third-generation lentiviral vectors, four accessory genes (*vif, vpr, vpu,* and *nef*) [176], along with the *tat* gene [177] required for viral replication and pathogenesis, are absent. Because these gene products are essential to lentiviral replication and pathogenesis, no RCR can be made that has the pathogenic features of the parental virus. A second strategy is to use nonoverlapping split-genome packaging constructs that require multiple recombination events with the transfer vector to generate RCR. The third-generation lentiviral vector system employs four independent plasmid constructs: two encoding essential packaging elements (*gag, pol,* and *rev*), one encoding the heterologous VSV-G envelope protein, and one corresponding to the transfer construct containing HIV cis-acting sequences (5′ and 3′ long terminal repeats [LTRs] plus the packaging signal [Ψ]) and therapeutic gene-of-interest [177]. Finally, by introducing a deletion in the U3 region of the 3′ LTR that abolishes its transcriptional activity, the lentiviral transfer construct becomes self-inactivating (SIN). During the process of reverse transcription and integration, SIN vectors lose the capacity to produce a full-length RNA copy of the recombinant viral genome. Loss of transcriptional activity from LTRs not only minimizes the risk of RCR formation, it also reduces transcriptional interference between the LTR and tissue-specific promoters that drive therapeutic gene expression. This also reduces the possibility that lentiviral LTRs will influence the expression of host cell genes positioned adjacent to the vector integration site. Because they carry a 400-nucleotide deletion of the U3 region in their 3′ LTR, third-generation lentiviral vectors have been effectively rendered self-inactivating [178].

On the basis of our experience, third generation lentiviral vectors offer four important advantages over the use of MLV-based retroviral vectors for skeletal gene therapy. First, they have the potential to efficiently transduce not only proliferating progenitors but also differentiated osteoblasts and quiescent mesenchymal stem cells. Second, because lentiviral LTRs are inherently less transcriptionally active than MLV LTRs, U3 deletions render them essentially silent, allowing for effective use of osteoblast-specific or inducible promoters to drive therapeutic gene expression. Promoter interference continues to be a significant problem with MLV-based vectors, even in those that carry self-inactivating mutations in

their LTRs. Third, MLV-based retroviral vectors are highly susceptible to transcriptional silencing, particularly in early progenitor stem cells [179]. This prevents long-term therapeutic gene expression. Although still relatively poorly understood, the major determinants for transcriptional silencing have been mapped to MLV LTR sequences [180, 181]. Third-generation lentiviral vector LTRs may not be as susceptible to transcriptional silencing as MLV LTRs. Finally, because their LTRs are transcriptionally silent, integration of third-generation lentiviral vectors poses a much lower risk of activation of neighboring cellular genes. Until recently, no adverse events associated with the integration of MLV-based vectors had been reported. However, in a clinical trial of gene therapy for X-linked severe combined immune deficiency (SCID), 2 out of 10 patients that had been successfully treated with genetically engineered bone marrow stem cells transduced *ex vivo* with retroviral vectors expressing the gamma C gene have developed leukemia, presumably due to trans-activation of the *LMO2* gene by MLV LTRs [182]. It remains to be determined if these events are specific to the MLV-based retroviral construct used in this study, or if retroviral integration is a more serious safety concern than had been anticipated based on previous studies.

In view of these advantages, we have begun to evaluate the potential of lentiviral vectors for skeletal gene therapy applications. As shown in Figure 7, normal human calvarial osteoblasts and rat marrow stromal cells are highly receptive to infection with recombinant lentivirus. Incubation with a lentiviral vector expressing a β-galactosidase reporter gene from the strong constitutively expressed cytomegalovirus (CMV) promoter at a multiplicity of infection (MOI) of 10 resulted in transduction efficiencies of 75 to 90%. On the basis of these preliminary results, lentiviral vectors appear to be attractive candidates for skeletal gene therapy applications. Although some concerns remain about their safety, their ability to transduce nondividing osteogenic cells, their compatibility with osteoblast-specific promoters, and their reduced propensity for gene silencing and trans-activation of host cell genes makes it almost certain that these vectors will play a prominent role in future skeletal gene therapy strategies.

b. Adeno-associated Viral Vectors

Recombinant adeno-associated viral (rAAV) vectors have emerged in recent years as an attractive alternative to the use of adenoviral and retroviral vectors for gene therapy. Like adenoviral vectors, rAAV can infect both replicating and nonreplicating cells, but has the advantage of being relatively nonimmunogenic. Efficient transduction of skeletal and cardiac muscle [183, 184], liver [185], lung [186], and brain [187] has been reported. Like retroviral vectors, rAAV has the potential to integrate into the host cell genome to provide stable long-term transduction of target cells, but offers the additional advantage of directing site-specific integration, while being refractory to transcriptional silencing. Transgene expression has been sustained for over a year following direct *in vivo* intramuscular delivery [188].

Adeno-associated virus (AAV) is a nonpathogenic human parvovirus that requires the presence of a helper virus, such as adenovirus, herpes virus, or vaccinia virus, for its replicative life cycle [189]. In the absence of helper virus, AAV integrates into the host genome and establishes a latent cycle. When a latently infected cell is superinfected with a helper virus, the integrated AAV genome rescues itself and undergoes a productive lytic cycle. The AAV genome consists of 4679 bases of single-stranded DNA [190] that encodes two proteins (Rep and Cap) that are not essential for the virus to function as a gene delivery system. The only viral DNA sequences needed for vector rescue, replication, packaging, and integration are the two ITRs at each end of the AAV genome [190]. Because rAAV doesn't carry any wild-type viral genes, it is considerably less immunogenic than adenoviral vectors [191].

The requirement for a helper virus to propagate rAAV, its relatively small cloning capacity (4.7 kb), a slow rise in transgene expression to steady state levels, and variations in transduction efficiencies among different cell types represent the major limitations of rAAV vectors for skeletal gene therapy applications. Many of the initial difficulties with achieving high titer, helper-free rAAV vector stocks have been addressed. Recent advances in vector production and purification have increased rAAV titers more than 10-fold [192], and current packaging methods eliminate any

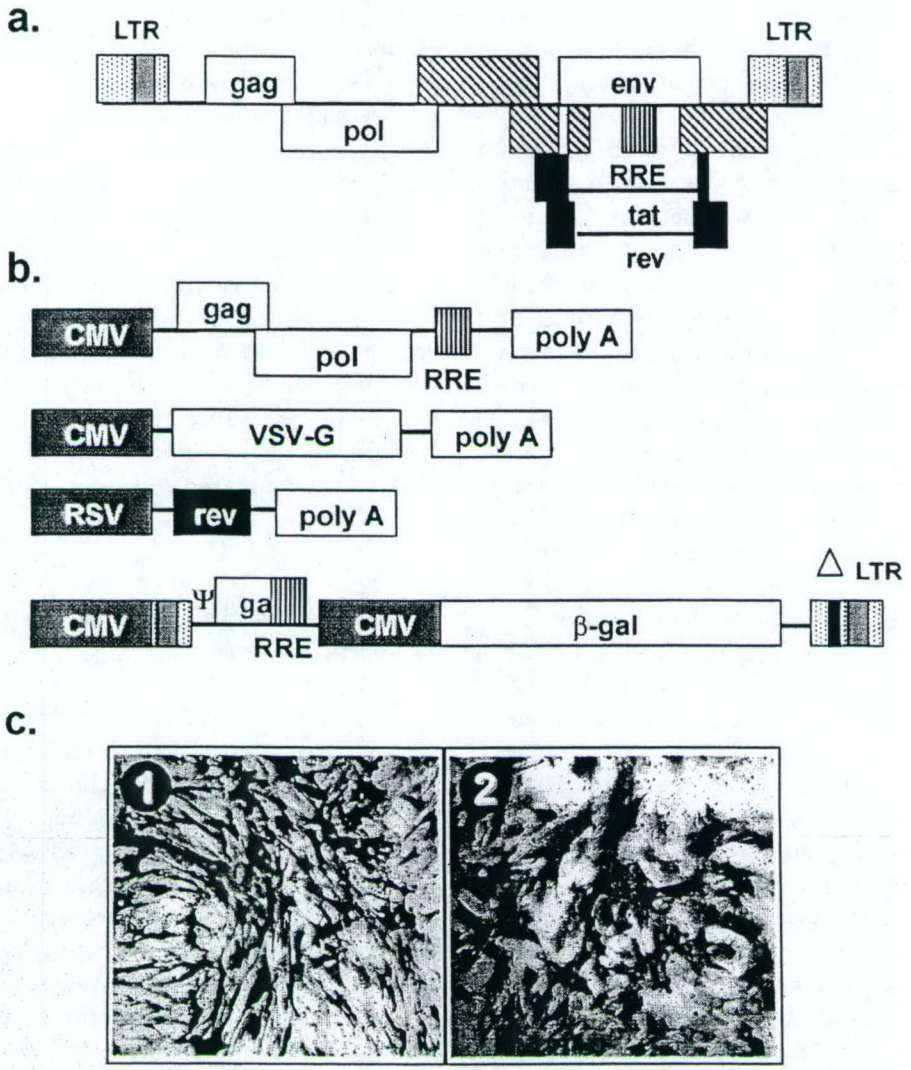

FIGURE 7. Schematic representation of third-generation lentiviral vector plasmids. (a) Striped boxes represent genes encoding accessory proteins (*vif, vpr, vpu,* and *nef*), and solid boxes represent genes encoding regulatory proteins (*tat* and *rev*). RRE denotes the position of the Rev-responsive element essential for transport of the HIV RNA genome. (b) Structures of expression plasmids that express *trans*-elements for HIV-based vector production. The CMV promoter is used to drive the expression of *gag and pol* genes as well as the RRE on one plasmid, and the heterologous VSV-G envelope gene on a second plasmid. The RSV promoter drives the expression of the *rev* gene on a third plasmid. The gene of interest, in this case a β-galactosidase reporter driven by a CMV promoter, is cloned into a fourth plasmid (transfer construct) that contains *cis*-elements needed for lentiviral vector production. The transfer construct does not contain any wild-type copies of the HIV LTR (self-inactivating). The 5′ LTR is chimeric, containing a CMV promoter replacing the U3 region to rescue transcriptional dependence on TAT. The 3′ LTR (ΔLTR) contains a deletion through the U3 region that renders it transcriptionally inactive. (c) Transduction of non-transformed human calvarial cells (panel 1) and nontransformed rat marrow stromal cells (panel 2) at a MOI of 10 produces high levels of β-galactosidase expression in the majority of cells.

possibility of wild-type adenovirus (helper virus) contamination of rAAV stocks. However, due to recombination between homologous regions in rAAV and AAV helper plasmids, rAAV stocks still tend to be contaminated with low levels of wtAAV [193].

The 4.7-kb cloning capacity of rAAV may not be a major limitation to skeletal gene therapy

applications designed to express growth factors, such as BMP2/4 (approximately 1.3 kb in size), driven by a strong CMV promoter (approximately 0.6 kb in size). However, this could become an issue in future strategies that incorporate multiple therapeutic genes or extended tissue-specific transcriptional control regions. One interesting approach to increasing the cloning capacity of rAAV vectors is through intermolecular recombination of two AAV episomes in the host cell nucleus. Yan et al. [194] demonstrated that co-administration of two independent AAV vectors carrying 5′ and 3′ portions of the erythropoietin gene can result in trans-splicing and the production of a functional protein product. Duan et al. [195] demonstrated that the efficiency of trans-splicing, although moderate, is greater than a distinct overlapping vector approach using homologous recombination.

The mechanism underlying the slow increase in therapeutic gene expression from rAAV vectors is not completely understood. For example, infusion of rAAV-expressing factor IX into the portal vein produced a slow increase in serum factor IX levels that reached steady state levels only after 5 weeks [196]. Because rAAV vectors have not been tested in skeletal gene therapy applications, it is not clear if expression of a therapeutic gene, such as BMP2/4, would occur with the same kinetics. This slow response could present problems in clinical situations such as complex fractures that require rapid treatment. However, this would not be an issue in clinical applications involving long-term systemic expression of an osteogenic growth factor.

Finally, it remains to be determined how well rAAV vectors transduce osteoblasts and other target cells for skeletal gene therapy. Evidence that rAAV can effectively transduce early progenitor hematopoietic cells [197, 198] raises the possibility that mesenchymal progenitors will also be amenable to rAAV infection. AAV utilizes the widely expressed heparin sulfate proteoglycan (HSPG) receptor [199] and possibly fibroblast growth factor-1 receptor (FGFR1) [200] and $\alpha_V\beta_5$ integrin [201] as co-receptors to infect cells. Evidence that HSPG plays an important role in the interaction of primitive hematopoietic cells with bone marrow stromal cells [202] and that cells in the osteoblast lineage synthesize HSPG [203] makes it likely that rAAV vectors can transduce osteogenic progenitors with high efficiency in *ex vivo* skeletal gene therapy applications.

Because they are nonpathogenic and relatively nonimmunogenic, transduce both dividing and nondividing cells, provide long-term transgene expression, and can be grown to high titers, rAAV vectors are gaining considerable attention as an alternative delivery system for gene therapy. It remains to be determined what advantages rAAV vectors will have over other gene delivery systems in skeletal gene therapy applications. However, on the basis of current knowledge it appears that this vector system can address some of the problems encountered with adenoviral and retroviral vectors.

2. Alternative Gene Delivery Systems: Nonviral Vectors

In many ways nonviral (synthetic) vector systems, such as liposomes, represent safer and more attractive delivery vehicles for clinical gene therapy applications [204]. Issues relating to viral cytotoxicity and immunogenicity are avoided, it is easier to construct, manipulate, and propagate the therapeutic minigene, and because they are synthetic, the vectors themselves are easier to modify in order to address specific needs or problems. Although for the most part, current nonviral vector systems do not perform as well as viral vectors for gene delivery to patient cells *in vivo*, they continue to be developed and some have reached clinical trials [205]. In view of their safety and ease of manipulation, nonviral vectors will receive serious consideration for skeletal gene therapy applications in the future.

At the most basic level, direct injection or electroporation of naked plasmid DNA has shown promise in a variety of *in vivo* applications, particularly for gene transfer to muscle, skin, and liver [206]. For example, intradermal injection of plasmid DNA can be an effective method for increasing local and systemic levels of cytokines [207], and high-volume tail vein injections of naked plasmid DNA can provide transient gene expression in the liver [208]. Direct injection of plasmid DNA to muscle or skin may represent a relatively safe and noninvasive procedure for in-

creasing circulating levels of osteogenic growth factors, such as GH or IGF-I.

In most *in vivo* applications, the primary limitation of direct plasmid injection has been poor vector uptake. A variety of cationic lipid and protein-based carriers are being developed to improve DNA bioavailability and transduction efficiencies. Cationic liposomes bind to plasmids and oligodeoxynucleotides to form complexes known as lipoplexes. Lipoplexes may represent the most promising alternative to the use of viral vectors for gene therapy. However, liposomal gene transfer efficiencies *in vivo* are still too low to be therapeutically effective in most clinical applications. Major efforts are underway to address problems, such as poor biodistribution and inefficient DNA transport to the nucleus [209, 210]. Recent examples of engineered liposomal complexes include TATp-liposomes containing the membrane-translocating HIV TAT peptide [211]; pH-dependent liposomes containing an amphipathic peptide designed to disrupt endosomes [212]; liposome:mu:DNA (LMD) complexes built around the adenoviral mu peptide [213]; pegylated immunoliposomes (PILs) targeted to brain tumor cells that incorporate monoclonal antibodies to either the insulin receptor [214] or the transferrin receptor [215]; and HVJ-liposomes (virosomes) containing hemagglutinating virus of Japan (HVJ; Sendai virus) envelope proteins [216]. Direct injection of lipoplexes designed to specifically transduce osteoblasts may prove to be a highly effective way to introduce osteogenic genes to fracture sites.

Protein-based carriers include the HIV TAT protein, which has the ability to translocate with high efficiency through plasma membranes. Systemic injection of a fusion protein consisting of HIV TAT coupled to a reporter gene (β-galactosidase) resulted in delivery to all major tissues including the brain [217]. More recently, TAT fusions with BclX(L), a well-characterized suppressor of apoptosis, were shown to have neuroprotective effects against ischemic brain injury following systemic injection in mouse models [218, 219]. TAT has been shown to enter primary osteoblast and osteoclasts with high efficiency [220], and TAT fusions carrying an inhibitor of NF-kappa B were shown to effectively enter macrophages to block osteoclastogenesis [221]. Although developed primarily as a way to deliver peptides and small proteins, HIV TAT protein can also carry large biomolecules into cells, raising the possibility that TAT can be used to deliver plasmid DNA with high efficiency *in vivo* [222].

3. Engineering New Generations of Adenoviral and Retroviral Vectors

A second approach that can be taken to improve the performance of gene delivery systems for skeletal gene therapy is to take advantage of our knowledge of adenoviral and MLV-based retroviral vectors to engineer new generations that address their current limitations. For example, helper-dependent adenoviral vectors provide significant improvements in immunogenicity and cloning capacity over first- and second-generation vectors. However, stable transfection and cell targeting remain important limitations. Envelope protein pseudotyping and lentiviral vector development have addressed important problems with host cell tropism and transduction of quiescent cells encountered with MLV-based retroviral vectors. However, transcriptional silencing, insertional mutagenesis, and cell-specific targeting are issues that still need to be addressed. Here we will touch on some of the important advances that are being made in adenoviral and retroviral vector design that have particular relevance to skeletal gene therapy applications.

a. Vector Targeting to the Skeleton

The ability to direct a gene delivery system specifically to a target cell population (vector targeting), or to control the location and duration of therapeutic gene expression (transcriptional targeting), would represent major advances in the safety and efficiency of skeletal gene therapy. Targeted vector delivery can be achieved in several ways. The simplest approach is through physical targeting—directing the delivery vehicle to a specific location through direct local injection. Physical targeting may be particularly effective for skeletal gene therapy, because mineralized bone provides a natural barrier to diffusion of vectors and therapeutic gene products. A second strategy is to take advantage of the inherent properties of the viral vector or target

cell population, such as the natural tropism of adenovirus for epithelial cells, or of MLV for dividing cells. Accordingly, Rundle et al. [27] have shown that direct injection of an MLV-based vector expressing BMP-4 in a rat fracture model can significantly improve healing. Their approach combines physical targeting with the natural propensity of the MLV retrovirus to transduce replicating cells within the fracture site.

Although strategies such as these can significantly improve the specificity of therapeutic gene delivery, they do not discriminate between different cell types. Cell-specific vector targeting can only be achieved by taking advantage of a distinctive feature of the target cell population, such as expression of a unique cell surface receptor. Cellular targets for skeletal gene therapy include a number of highly specialized cell types, such as mesenchymal stem cells, osteogenic precursors, mature osteoblasts, and even osteoclasts. Because they are highly specialized, these cells likely express one or more unique proteins that can be exploited in the design of targeted vectors. These "receptor-mediated" or "ligand-directed" strategies typically involve either direct engineering of viral capsid proteins to produce fusion proteins containing ligands for specific cell surface receptors (genetic approach), or the development of bridging molecules (e.g., bispecific antibodies) that specifically bind a target cell receptor at one end and the viral vector at the other end (nongenetic approach).

MLV-based retroviral vectors were the first viral vectors to be targeted in this manner [223], and, in recent years, substantial progress has been made toward overcoming key vector design issues (Fig. 8) [224]. For example, to overcome ligand interference with vector entry, a protease targeting strategy has been developed that takes advantage of the presence of a specific receptor on target cells as well as a specific protease in the microenvironment surrounding target cells. The target ligand is linked to the MLV envelope protein through a protease-sensitive linker. Upon attachment of the ligand to specific receptors on target cells, the linker is cleaved by the protease, exposing the envelope protein and allowing the virus to enter the cell using its native receptor (CAT-1)[225]. A second approach utilizes coat proteins from other enveloped viruses that are more amenable to manipulation without compromising viral entry. For example, Hatziioannou et al. [226] engineered influenza hemagglutinin (HA) glycoproteins from fowl plague virus (FPV) to display polypeptides, such as epidermal growth factor or an antimelanoma antigen single chain antibody, at their amino terminus. Incorporation of these FPV-HA chimeras into MLV retroviral particles resulted in specific binding and infection of cells expressing the targeted cell surface molecule. A variety of nongenetic strategies that utilize bispecific bridging molecules composed of a cell-specific ligand fused to the extracellular domain of a native retroviral receptor have also been developed [227]. For example, Snitkovsky et al. [228] demonstrated that fusion of the extracellular domain of the avian leukosis virus (ALV) receptor to either vascular endothelial growth factor (VEGF) or the EGF-like region of heregulin beta 2 results in specific binding to cells expressing VEGF and heregulin receptors, respectively. Although osteoblasts and osteoclasts have been shown to express distinct profiles of genes encoding cell surface proteins [147, 229, 230], to date these properties have not been exploited in vector targeting strategies.

Attempts have also been made to retarget adenoviral vectors using both genetic and nongenetic strategies, but none have been designed to target osteogenic cells. Adenoviral attachment and entry into cells involves binding of the knob domain of the adenoviral fiber protein to the coxsackievirus and adenovirus receptor (CAR) [231, 232]. A subsequent interaction between an RGD motif within the adenoviral penton base protein with $\alpha_V\beta_{3/5}$ integrins on the cell surface facilitates vector uptake through receptor-mediated endocytosis [233]. Several fusions have been produced between various cell-specific peptide ligands and adenoviral capsid proteins [234–236]. As well, a number of bispecific bridging molecules have been developed that recognize a cell-specific protein on one side and an adenoviral capsid protein on the other [237–240]. In a recent study, Kashentseva et al. [241] engineered a bispecific adapter protein consisting of the CAR knob binding domain fused to a single-chain antibody specific for the c-erbB-2/HER-2/neu oncoprotein. Incubation with cancer cells that overexpress c-erbB-2 resulted in a 17-fold enhancement of gene transfer efficiency. Van

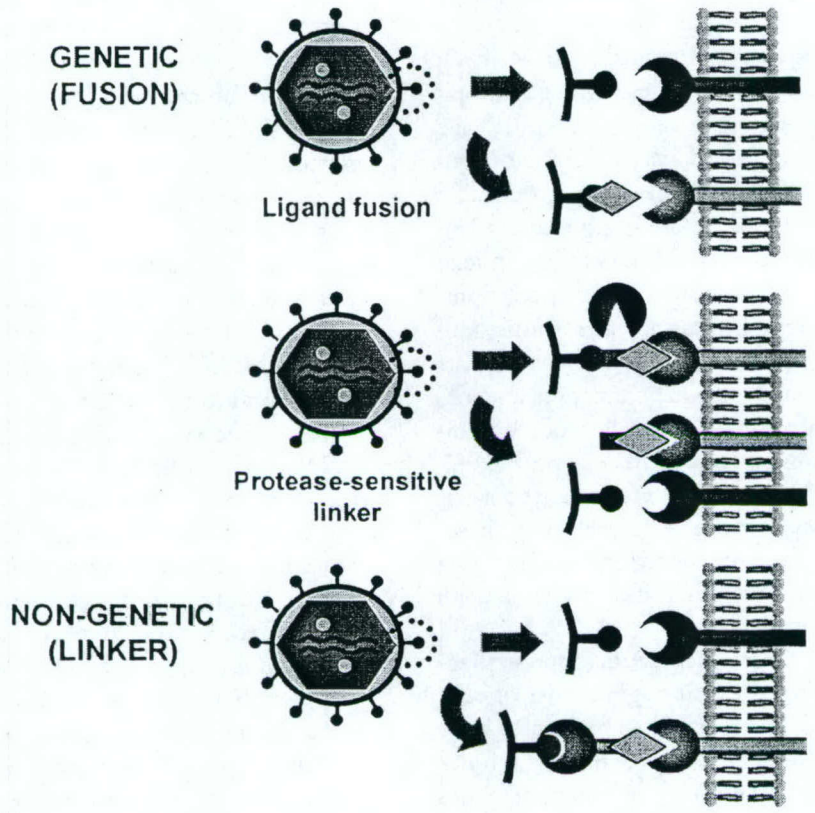

FIGURE 8. Vector-mediated targeting strategies applied to retroviral vectors. Genetic approaches involve engineering the gene encoding the endogenous envelope protein to express a fusion protein that displays an alternative receptor binding site. This ligand fusion approach has met with difficulties associated with viral uptake. The addition of a protease-sensitive linker directs MLV binding to an alternative receptor. Cleavage of the linker by a specific protease exposes the MLV env protein, which can then bind to its native receptor. Nongenetic approaches utilize bispecific bridging molecules that bind the retroviral env protein at one end and a cell-specific receptor at the other.

Beusechem et al. [242] have recently reported impressive improvements in brain tumor targeting using a bispecific single chain antibody directed toward the epidermal growth factor receptor (EGFR). These studies illustrate the current state of adenoviral vector targeting technologies. Although total specificity has not been achieved, the affinity of adenoviral vectors for target cells can be influenced to a significant degree. The development of adenoviral vectors targeted to osteogenic cells would certainly improve the safety and efficiency of skeletal gene therapy protocols.

There is no doubt that vector targeting strategies would be highly effective for skeletal gene therapy, particularly when combined with physical targeting in direct *in vivo* applications aimed at accelerating fracture healing. As more is learned about the profile of genes expressed in osteoblasts and their progenitors during bone development, additional cell-specific markers will certainly be identified that can be exploited in the design of retroviral and adenoviral vectors that are targeted specifically to cell types that provide optimal therapeutic gain.

b. Transcriptional Targeting to the Skeleton

In their initial phase of development, gene therapy strategies often employ strong viral promoters (e.g., CMV) that drive high levels of therapeutic gene

expression in target cells. However, these promoters rarely provide any degree of cell type specificity. In skeletal gene therapy, the goal is to positively influence the osteogenic process through ectopic expression of growth factors (e.g., BMP-2) and transcription factors (e.g., Cbfa1). Despite the fact that application of state-of-the-art approaches for gene therapy for the skeleton, using either adenoviral or retroviral vectors, currently results in relatively short-term expression, strict transcriptional control is necessary to maximize therapeutic benefit while ensuring patient safety. Because they are such strong inducers of bone formation and cell proliferation, uncontrolled expression of recombinant growth factors, such as BMP-2 and FGF-2, presents a significant risk of ectopic bone formation and tumor progression, respectively. It is, therefore, critical to develop regulatory systems that strictly limit where and when these potent growth factor genes are expressed.

One way to target therapeutic gene expression to osteogenic cells is through the use of cell-specific promoters. Studies of the molecular basis of osteoblast and osteoclast development and function have already identified a number of genes that are specifically expressed in these cell types. As outlined in Figure 9, genes, such as Cbfa1, osteocalcin, osteopontin, type I collagen, and alkaline phosphatase are expressed exclusively in osteoblasts [243–246], whereas osteoclasts are characterized by the expression of genes such as tartrate-resistant acid phosphatase (TRAP), NFATc1, ATP6i, and cathepsin K [247, 248]. The rate at which other bone cell-specific genes are identified will increase rapidly as microarray technologies are applied to studies of osteogenesis. Once identified as specific to the osteoblastic or osteoclastic lineage, transcriptional control elements (promoters and enhancers) that regulate gene expression can be identified and dissected for sequence elements that confer cell-specific expression [249, 250]. These promoter and enhancer elements can then be incorporated into the design of targeted minigenes for skeletal gene therapy.

Bone cell–specific promoters have not been broadly applied to skeletal gene therapy. Studies to date have predominantly employed the osteocalcin and collagen type I gene promoters to target gene expression to osteoblasts. For example, Abboud et al. [243] demonstrated that expression of soluble colony-stimulating factor-1 (sCSF-1) from the osteoblast-specific osteocalcin promoter can reverse the osteopetrotic phenotype of transgenic op/op mice, and Hou et al. [244, 245] and Lian et al. [244, 245] observed bone-specific expression of reporter genes under the control of the osteocalcin promoter in transplanted bone marrow cells. In an effort to overcome LTR-mediated retroviral vector silencing and transcriptional interference, Stover et al. [246] substituted the MLV retroviral LTR promoter with a collagen type I (Col1a1) gene promoter. The internal Col1a1 promoter functioned in an appropriate tissue-specific manner *in vitro* and, more importantly, *in vivo* following transduction of embryonic stem cells. These results suggest that this may be an effective strategy for increasing the durability and specificity of therapeutic gene expression from MLV-based retroviral vectors.

Two recent studies emphasize the importance of maintaining appropriate transcriptional control over therapeutic genes, particularly in strategies aimed at long-term correction of skeletal defects. The core-binding factor alpha 1 (Cbfa1) transcription factor is specific for osteoblasts and knockout mouse studies have shown that its expression is essential for bone formation. To study the role of this factor in the adult skeleton and in the regulation of bone turnover, Geoffroy et al. [251] produced transgenic mice overexpressing Cbfa1 from the rat collagen type I (Colla 1) promoter. Colla1 gene expression is an early marker of osteoblast commitment, and this promoter is known to direct transgene expression specifically to osteoblasts [252, 253]. Instead of seeing increased bone formation, transgenic animals developed severe osteopenia that increased progressively with age and presented with multiple fractures. On the basis of these results, it appears that inappropriate expression of Cbfa1 in osteoblasts enhances bone resorptive processes, possibly through increased RANKL expression and osteoclast function. Similarly, in a study of the effects of IGFBP-5 on bone remodeling, Devlin et al. [254] generated transgenic mice that express IGFBP-5 from the osteocalcin promoter. Despite the fact that IGFBP-5 was shown to stimulate bone cell growth *in vitro*, transgenic mice overexpressing IGFBP-5 exhibited a transient decrease in trabecular bone volume, impaired osteoblastic function, and osteopenia. These results

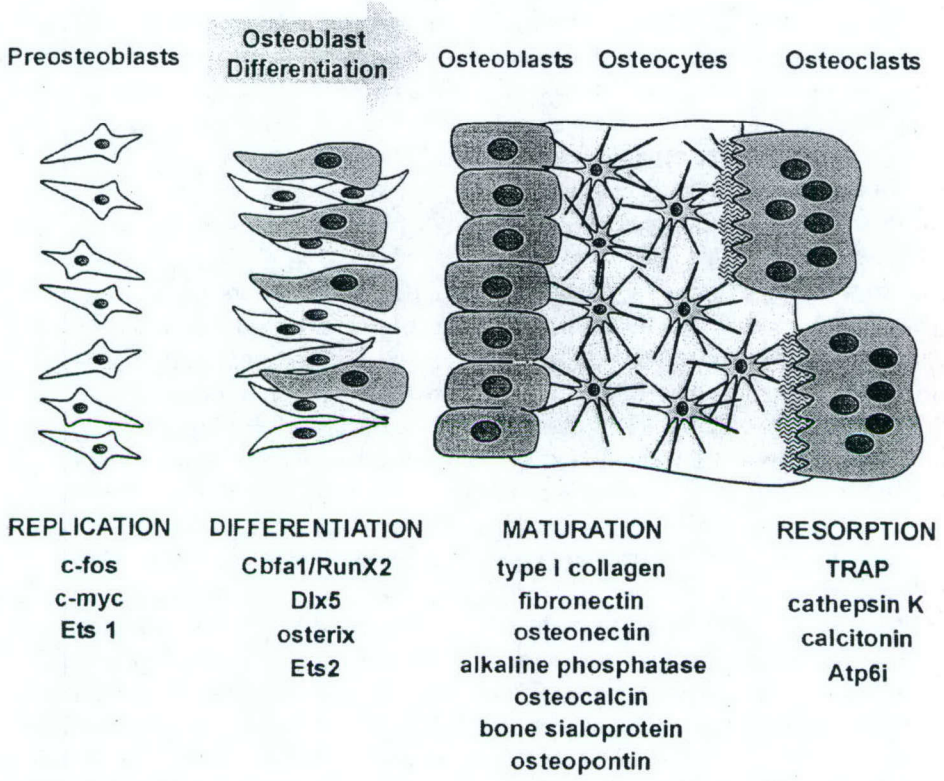

FIGURE 9. Genes associated with osteoblast and osteoclast differentiation. Osteoblast maturation can be divided into three stages, each characterized by the expression of a unique subset of transcription factors and bone-related genes. The first stage features active proliferation of preosteoblasts, with high levels of expression of cell cycle–related genes, such as c-*fos*, c-*myc*, and Etsl. As cells reach confluency, they enter a differentiation phase distinguished by the expression of (a) matrix-associated genes, such as type I collagen, fibronectin, and osteonectin; (b) osteoblast-specific genes, such as alkaline phosphatase and osteopontin; and (c) transcription factors, such as Ets2, CbfAl/Runx2, Dlx5, and osterix. The third stage represents the mature osteoblast and features the expression of genes involved in matrix maturation and mineralization. These include osteocalcin, bone sialoproteins, and osteopontin. Osteoclast-specific genes associated with the bone resorption process include TRAP, cathepsin K, calcitonin, and Atp6i.

suggest that the osteocalcin promoter, although osteoblast-specific, misregulates IBFBP-5 expression, producing detrimental rather than the expected beneficial effects on bone formation. On the basis of these studies, careful consideration should be given to the design of transcriptional control elements in skeletal gene therapy applications that require long-term expression of a therapeutic gene in osteoblasts or their precursors.

c. Inducible Promoters

A variety of transcriptional control elements have been identified that can be used to turn therapeutic gene expression on or off in response to drugs, hormones, or other external stimuli. In recent years the tetracycline (tet)-regulated system [255] has gained considerable attention as a way to control the expression of recombinant genes in functional studies and gene therapy applications [256, 257]. Genes under the control of the tet-regulated system can be turned on (tet-on) or off (tet-off) in response to the administration of tetracycline (Tc) or one of its derivatives (doxycycline; DOX). Regulation is dependent on constitutive expression in target cells of a chimeric tetracycline-dependent transcription factor (rTA or rtTA) consisting of a native or mutant tet repressor protein (tetR) fused to the activation

domain of the herpes simplex virus transactivator VP16. Binding of rTA or rtTA to the tetracycline operator (tetO) turns on transgene expression. In the tet-off system, Tc binding to rTA induces a conformational change that prevents it from binding to the tetO, turning off transgene expression. In the tet-on system, Tc promotes rtTA binding to tetO and turns on transgene expression.

Tet promoter systems have been used successfully in a variety of gene therapy applications [258, 259] and have recently been applied to skeletal gene therapy. Moutsatsos et al. [259] demonstrated that the Tet promoter system can provide effective regulation of BMP-2 expression in a model of regulated stem cell (C3H10T1/2)-mediated skeletal gene therapy. Following *in vivo* transplantation of genetically engineered C3H10T1/2 cells, doxycycline administration was shown to induce BMP-2 expression and increase osteogenic differentiation and bone formation [260]. This study provides a good example of the level of control over therapeutic gene expression that will be needed in skeletal gene therapy applications. In view of the detrimental effects of dysregulated Cbfa1 and IGFBP-5 on bone formation in transgenic mice, and the safety concerns associated with uncontrolled expression of BMPs and other osteogenic growth factors, skeletal gene therapy will require strict control over the dose, duration, and location of therapeutic gene expression. Current transcriptional control systems do not adequately address this need. Tissue-specific promoters may be effective for limiting expression to osteogenic cells but offer little control over dose and duration. Inducible promoters, such as the tet-on system, provide control over duration, and to some extent dose, but are not specific for osteogenic cells and must be combined with physical or vector targeting strategies. The tet system has other limitations as well. In the tet-off system, high levels of rTA expression can be toxic to target cells. In the tet-on system, residual affinity of rtTA for tetO produces high levels of background expression in the absence of Tc or Dox [261, 262]. Studies are underway to address these limitations [261, 263], and a variety of alternative transcriptional targeting systems are being developed that respond to specific changes in the microenvironment (e.g., hypoxia [264]) or to external stimuli, such as heat [265] or radiation [266, 267]. Combined with discoveries of new genes associated with osteogenesis, there is good reason to be highly optimistic that effective transcriptional targeting strategies will be available for skeletal gene therapy in the near future.

d. Hybrid Vector Systems

Adenoviral vectors have been used with good success to transduce both hematopoietic and mesenchymal stem cells [268–272]. However, because they do not provide for long-term stable integration of minigenes, their use in skeletal and other gene therapy applications is limited. One approach to this problem is to develop hybrid vector systems that take advantage of the large cloning capacity of adenoviral vectors to incorporate unrelated viral and nonviral vector elements that provide for long-term stable expression of transgenes. For example, Soifer et al. [273] have recently described a hybrid vector that incorporates a fully replication-competent ecotropic MLV-based retroviral genome into a helper-dependent adenoviral vector (HDAd [274]). By exploiting differences in the host range characteristics of the adenoviral and retroviral components of this vector, Soifer et al. [273] were able to demonstrate that the HDAd-MLV hybrid provides for highly efficient delivery and long-term integration of recombinant genes. Using a similar strategy, Kubo and Mitani [275] developed a hybrid HDAd-lentiviral vector. The large cloning capacity of HDAd allows for all of the sequence elements needed to produce an HIV-based lentiviral vector to be incorporated in a single lentivirus/adenovirus (LA) hybrid. The LA vector was shown to produce high titers of recombinant lentivirus following infection of human cell lines and to provide for stable integration of recombinant genes. In a third example of this strategy, Goncalves et al. [276] incorporated a replication-competent AAV genome into a recombinant adenoviral vector. This hybrid combines the site-directed integrative properties of AAV vectors with the wide cellular tropism of adenoviral vectors.

In addition to combinations with other viral vectors, adenoviral hybrids have also been produced with nonviral vector components. For ex-

ample, Yotnda et al. [277] recently reported that encapsulation of recombinant adenoviral vectors with bilammellar liposomes not only modifies their cell targeting characteristics but also effectively protects the adenoviral vector against neutralization by the humoral immune response following repeated administration. More relevant to the goal of achieving long-term therapeutic gene expression in bone marrow stem cells, Yant et al. [278–280] recently described an HDAd-based vector that incorporates the plasmid-based Sleeping Beauty transposon system for targeted stable integration of therapeutic genes (Fig. 10). The Sleeping Beauty (SB) transposon was reconstituted from an ancient transposon in fish through sequence alignment of nonfunctional remnants of members of the *Tcl*/mariner superfamily of transposons [279]. When a plasmid carrying the SB transposon is introduced into a cell that expresses the SB transposase, the transposon undergoes a "cut-and-paste" transposition through a DNA intermediate, inserting itself into a TA target dinucleotide within the host cell genome. The entire process is catalyzed by SB transposase binding to short direct-repeat (DR) sequences within the terminal inverted repeats (IRs) that flank the transposon [279]. Co-transfection or direct injection of plasmids carrying a gene-of-interest flanked by SB transposon IR/DR) sequences and an SB transposase expression cassette can result in stable integration and long term expression of reporter and therapeutic genes in human and mouse cells (including mouse embryonic stem cells)[278, 279, 281–283]. To avoid problems with multi-plasmid transfections, we recently successfully engineered a single-plasmid SB transposon-based gene transfer vector termed the "Prince Charming" (pPC) vector [284]. The pPC vector represents a significant improvement over previous two-plasmid systems and was shown to effectively generate stable long-term expression of a reporter gene in a human osteosarcoma cell line. The HDAd-based SB transposon vector system described by Yant et al. [280] effectively addresses a major limitation of HDAd vectors (transient gene expression) while maintaining many of its most attractive characteristics. This high capacity adeno-transposon vector was shown to facilitate transgene integration into host cell chromosomes and greatly improve the longevity of adenovirus-based gene expression in mouse models. If potential obstacles relating to transposition efficiency and epigenetic effects are successfully addressed, the adeno-transposon vector could represent a very significant development in gene transfer vector technologies, particularly in the area of *ex vivo* stem cell–based therapies.

IV. CONCLUSIONS AND PERSPECTIVES

Skeletal gene therapy is still an emerging and relatively immature field. According to the Journal of Gene Medicine Database (www.wiley.co.uk/genmed/clinical/), there are presently more than 500 clinical gene therapy trials in the United States alone, but only one—a phase 1 study of the safety of administration of naked plasmid DNA encoding parathyroid hormone to fractures—can be categorized as skeletal gene therapy. In this review we have attempted to summarize the state of skeletal gene therapy today and to highlight the impressive advances that have been made in recent years. We have also tried to identify areas that need further development and to present ways in which new knowledge in these areas can be used to improve safety and efficiency. In the next 5 years, we can anticipate a rapid increase in our understanding of genes and signaling pathways associated with osteoblast and osteoclast development. More effective therapeutic genes will be identified, and as more is learned about the way that different gene products cooperate with each other to promote osteogenesis, powerful therapeutic strategies utilizing two or more genes will emerge. Knowledge of osteogenic gene expression profiles will also be exploited in the design of more effective gene delivery systems employing both transductional and transcriptional targeting strategies. In fact, the success of skeletal gene therapy will ultimately depend on our ability to engineer vector systems that specifically transduce osteogenic cell targets. Impressive advances in this area can be anticipated over the next 5 years as new generations of adenoviral and MLV-based retroviral vectors, as well as lentiviral and adeno-associated viral vectors, are developed and applied to this problem. It is also likely that one or more nonviral vector systems will emerge as a strong alternative to these viral vector platforms.

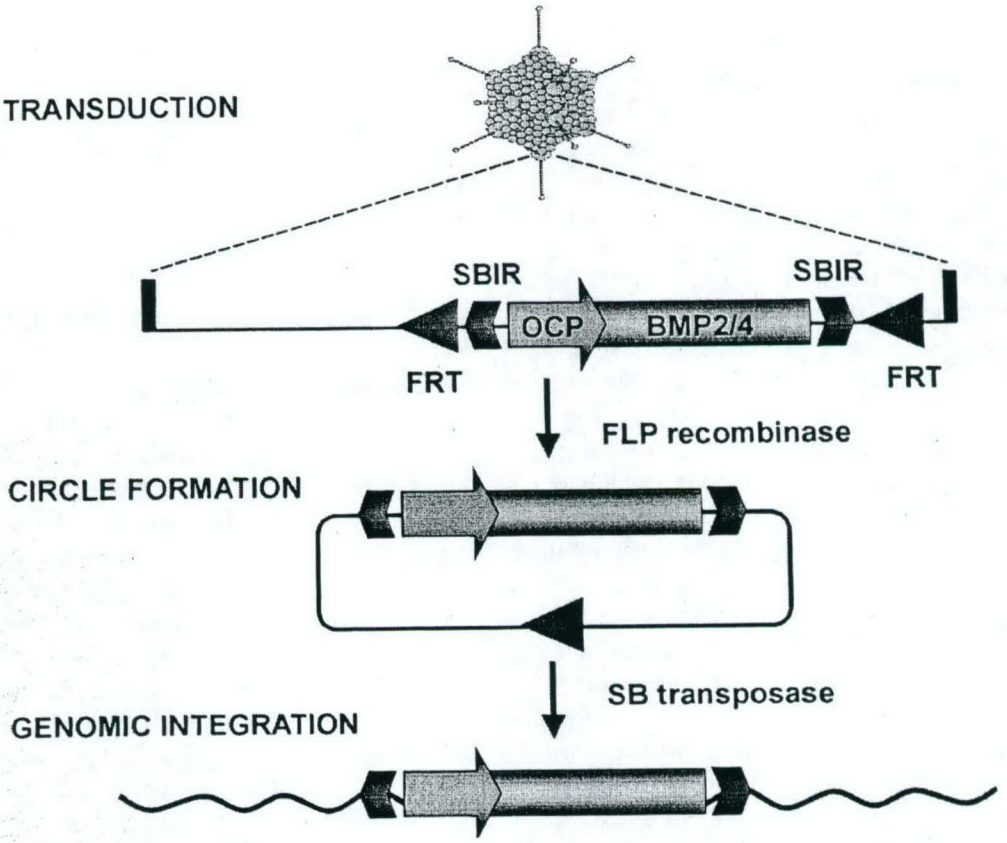

FIGURE 10. Schematic representation of a hybrid adenoviral vector incorporating the Sleeping Beauty (SB) transposon. Following infection of target cells (transduction), the linear adenoviral genome consisting of the therapeutic transgene (OCP: osteocalcin promoter; BMP2/4: the hybrid BMP2 leader/BMP4 coding region) surrounded by Sleeping Beauty inverted repeat sequences (SBIR), and again by a pair of FLP recombinase recognition target (FRT) sites. For reasons that aren't clear, the SB transposase does not efficiently act on linear DNA. FLP-mediated recombination results in excision of the transposon from the Ad genome and circularization, which then actively undergo DNA-mediated transposition resulting in stable insertion of the transposon into host cell chromosomes.

Because they offer long-term benefits and provide an extra margin of safety for the patient, a great deal of effort will be put into developing *ex vivo* strategies involving gene transfer to hematopoietic or mesenchymal stem cells derived from bone marrow or tissues, such as skeletal muscle. New opportunities will emerge to combine skeletal gene therapy with established therapeutic modalities or new treatments based on protein therapy or tissue engineering. In some cases, combined treatments will produce synergistic effects on the rate of bone formation. Finally, the impact of pharmaco-genomics on therapeutic design will increase substantially over the next 5 years, eventually leading to individualized treatments based on genetic predispositions and, perhaps more importantly, interventions that delay or even prevent skeletal disease processes.

The completion of the human genome project, the use of powerful microarray technologies to identify genes and proteins that participate in bone development and regeneration, and the continued development of gene transfer technologies will present unparalleled opportunities to develop novel gene therapies for skeletal disorders. Although a number of issues relating to therapeutic gene action, the nature of target cells, and the safety and efficiency of gene delivery systems still need to be addressed, there remains little doubt that gene therapy will play a prominent role in the

treatment of local and systemic skeletal disorders in the near future.

ACKNOWLEDGMENTS

This work was supported by a special appropriation to the Jerry L. Pettis Memorial VA Medical Center, Musculoskeletal Disease Center, and an Assistance Award from the United States Army (Award No. DAMD-17-03-2-0021). The United States Army Medical Research Acquisition Activity, 820 Chandler Street, Fort Detrick, MD 21702-5014, is the awarding and administering acquisition office. The information contained in this publication does not necessarily reflect the position or policy of the Government, and no official endorsement should be inferred. All work was performed in facilities provided by the Department of Veterans Affairs.

REFERENCES

1. Braithwaite RS, Col NF, Wong JB. Estimating hip fracture morbidity, mortality and costs. J Am Geriatr Soc 2003;51(3):364–70.
2. Muller ME, Thomas RJ. Treatment of non-union in fractures of long bones. Clin Orthop 1979;(138): 141–53.
3. Gerhart TN, Kirker-Head CA, Kriz MJ, Holtrop ME, Hennig GE, Hipp J, et al. Healing segmental femoral defects in sheep using recombinant human bone morphogenetic protein. Clin Orthop 1993;(293): 317–26.
4. Zegzula HD, Buck DC, Brekke J, Wozney JM, Hollinger JO. Bone formation with use of rhBMP-2 (recombinant human bone morphogenetic protein-2). J Bone Joint Surg Am 1997;79(12):1778–90.
5. Uludag H, Friess W, Williams D, Porter T, Timony G, D'Augusta D, et al. rhBMP-collagen sponges as osteoinductive devices: effects of *in vitro* sponge characteristics and protein pI on *in vivo* rhBMP pharmacokinetics. Ann N Y Acad Sci 1999;875:369–78.
6. Langer R, Vacanti JP. Tissue engineering. Science 1993;260(5110):920–6.
7. Caplan AI, Goldberg VM. Principles of tissue engineered regeneration of skeletal tissues. Clin Orthop 1999;(367 Suppl):S12–6.
8. Bonadio J. Tissue engineering via local gene delivery. J Mol Med 2000;78(6):303–11.
9. Wu D, Razzano P, Grande DA. Gene therapy and tissue engineering in repair of the musculoskeletal system. J Cell Biochem 2003;88(3):467–81.
10. Einhorn TA. Breakout session. 1: Definitions of fracture repair. Clin Orthop 1998;(355 Suppl):S353.
11. Manolagas SC. Birth and death of bone cells: basic regulatory mechanisms and implications for the pathogenesis and treatment of osteoporosis. Endocr Rev 2000;21(2):115–37.
12. Mohan S, Baylink DJ. In: Bilezikian JP, Raisz LG, Rodan GA, editors. Principles of Bone Biology. San Diego: Academic Press; 1996. p. 1111–1123.
13. Roodman GD. Advances in bone biology: the osteoclast. Endocr Rev 1996;17(4):308–32.
14. Hogan BL. Bone morphogenetic proteins in development. Curr Opin Genet Dev 1996;6(4):432–8.
15. Joyce ME, Roberts AB, Sporn MB, Bolander ME. Transforming growth factor-beta and the initiation of chondrogenesis and osteogenesis in the rat femur. J Cell Biol 1990;110(6):2195–207.
16. Abe E, Yamamoto M, Taguchi Y, Lecka-Czernik B, O'Brien CA, Economides AN, et al. Essential requirement of BMPs-2/4 for both osteoblast and osteoclast formation in murine bone marrow cultures from adult mice: antagonism by noggin. J Bone Miner Res 2000;15(4):663–73.
17. Kingsley DM. Genetic control of bone and joint formation. Novartis Found Symp 2001;232:213–22; discussion 222–34, 272–82.
18. Wozney JM, Rosen V. Bone morphogenetic protein and bone morphogenetic protein gene family in bone formation and repair. Clin Orthop 1998;(346):26–37.
19. Reddi AH. Bone morphogenetic proteins: from basic science to clinical applications. J Bone Joint Surg Am 2001;83-A Suppl 1(Pt 1):S1–6.
20. Urist MR. Bone: formation by autoinduction. Science 1965;150(698):893–9.
21. Onishi T, Ishidou Y, Nagamine T, Yone K, Imamura T, Kato M, et al. Distinct and overlapping patterns of localization of bone morphogenetic protein (BMP) family members and a BMP type II receptor during fracture healing in rats. Bone 1998;22(6):605–12.
22. Katagiri T, Yamaguchi A, Ikeda T, Yoshiki S, Wozney JM, Rosen V, et al. The non-osteogenic mouse pluripotent cell line, C3H10T1/2, is induced to differentiate into osteoblastic cells by recombinant human bone morphogenetic protein-2. Biochem Biophys Res Commun 1990;172(1):295–9.
23. Kawasaki K, Aihara M, Honmo J, Sakurai S, Fujimaki Y, Sakamoto K, et al. Effects of recombinant human bone morphogenetic protein-2 on differentiation of cells isolated from human bone, muscle, and skin. Bone 1998;23(3):223–31.
24. Cook SD, Wolfe MW, Salkeld SL, Rueger DC. Effect of recombinant human osteogenic protein-1 on healing of segmental defects in non-human primates. J Bone Joint Surg Am 1995;77(5):734–50.
25. Sandhu HS, Kanim LE, Kabo JM, Toth JM, Zeegan EN, Liu D, et al. Evaluation of rhBMP-2 with an OPLA carrier in a canine posterolateral (transverse process) spinal fusion model. Spine 1995;20(24): 2669–82.

26. Baltzer AW, Lattermann C, Whalen JD, Wooley P, Weiss K, Grimm M, et al. Genetic enhancement of fracture repair: healing of an experimental segmental defect by adenoviral transfer of the BMP-2 gene. Gene Ther 2000;7(9):734–9.
27. Rundle CH, Miyakoshi N, Kasukawa Y, Chen S-T, Sheng MH-C, Wergedal JE, Lau WK-H, Baylink, DJ. *In vivo* bone formation in fracture repair induced by direct retroviral-based gene therapy with BMP-4. Blood 2003;32:591–601.
28. Gysin R, Wergedal JE, Sheng MH, Kasukawa Y, Miyakoshi N, Chen ST, et al. *Ex vivo* gene therapy with stromal cells transduced with a retroviral vector containing the BMP4 gene completely heals critical size calvarial defect in rats. Gene Ther 2002; 9(15):991–9.
29. Wright V, Peng H, Usas A, Young B, Gearhart B, Cummins J, et al. BMP4-expressing muscle-derived stem cells differentiate into osteogenic lineage and improve bone healing in immunocompetent mice. Mol Ther 2002;6(2):169–78.
30. Peng H, Wright V, Usas A, Gearhart B, Shen HC, Cummins J, et al. Synergistic enhancement of bone formation and healing by stem cell-expressed VEGF and bone morphogenetic protein-4. J Clin Invest 2002;110(6):751–9.
31. Alini M, Marriott A, Chen T, Abe S, Poole AR. A novel angiogenic molecule produced at the time of chondrocyte hypertrophy during endochondral bone formation. Dev Biol 1996;176(1):124–32.
32. Leung DW, Cachianes G, Kuang WJ, Goeddel DV, Ferrara N. Vascular endothelial growth factor is a secreted angiogenic mitogen. Science 1989;246(4935): 1306–9.
33. Shalaby F, Rossant J, Yamaguchi TP, Gertsenstein M, Wu XF, Breitman ML, et al. Failure of blood-island formation and vasculogenesis in Flk-1-deficient mice. Nature 1995;376(6535):62–6.
34. Horwitz MS. Adenoviruses. In: Fields BN, Knipe DM, editors. Virology, 2nd ed. New York: Raven Press; 1990. p. 1723–1740.
35. Bett AJ, Haddara W, Prevec L, Graham FL. An efficient and flexible system for construction of adenovirus vectors with insertions or deletions in early regions 1 and 3. Proc Natl Acad Sci U S A 1994;91(19): 8802–6.
36. Mitani K, Graham FL, Caskey CT, Kochanek S. Rescue, propagation, and partial purification of a helper virus-dependent adenovirus vector. Proc Natl Acad Sci U S A 1995;92(9):3854–8.
37. Parks RJ. Improvements in adenoviral vector technology: overcoming barriers for gene therapy. Clin Genet 2000;58(1):1–11.
38. Morsy MA, Gu M, Motzel S, Zhao J, Lin J, Su Q, et al. An adenoviral vector deleted for all viral coding sequences results in enhanced safety and extended expression of a leptin transgene. Proc Natl Acad Sci U S A 1998;95(14):7866–71.
39. Morral N, O'Neal W, Rice K, Leland M, Kaplan J, Piedra PA, et al. Administration of helper-dependent adenoviral vectors and sequential delivery of different vector serotype for long-term liver-directed gene transfer in baboons. Proc Natl Acad Sci U S A 1999;96(22): 12816–21.
40. Baltzer AW, Whalen JD, Stefanovic-Racic M, Ziran B, Robbins PD, Evans CH. Adenoviral transduction of human osteoblastic cell cultures: a new perspective for gene therapy of bone diseases. Acta Orthop Scand 1999;70(5):419–24.
41. Mehrara BJ, Saadeh PB, Steinbrech DS, Dudziak M, Spector JA, Greenwald JA, et al. Adenovirus-mediated gene therapy of osteoblasts *in vitro* and *in vivo*. J Bone Miner Res 1999;14(8):1290–301.
42. van Griensven M, Lobenhoffer P, Barke A, Tschernig T, Lindenmaier W, Krettek C, et al. Adenoviral gene transfer in a rat fracture model. Lab Anim 2002;36(4): 455–61.
43. Helm GA, Alden TD, Beres EJ, Hudson SB, Das S, Engh JA, et al. Use of bone morphogenetic protein-9 gene therapy to induce spinal arthrodesis in the rodent. J Neurosurg 2000;92(2 Suppl):191–6.
44. Alden TD, Beres EJ, Laurent JS, Engh JA, Das S, London SD, et al. The use of bone morphogenetic protein gene therapy in craniofacial bone repair. J Craniofac Surg 2000;11(1):24–30.
45. Howard D, Partridge K, Yang X, Clarke NM, Okubo Y, Bessho K, et al. Immunoselection and adenoviral genetic modulation of human osteoprogenitors: *in vivo* bone formation on PLA scaffold. Biochem Biophys Res Commun 2002;299(2):208–15.
46. Rutherford RB, Moalli M, Franceschi RT, Wang D, Gu K, Krebsbach PH. Bone morphogenetic protein-transduced human fibroblasts convert to osteoblasts and form bone *in vivo*. Tissue Eng 2002;8(3): 441–52.
47. Alden TD, Varady P, Kallmes DF, Jane JA Jr, Helm GA. Bone morphogenetic protein gene therapy. Spine 2002;27(16 Suppl 1):S87–93.
48. Wu X, Li Y, Crise B, Burgess SM. Transcription start regions in the human genome are favored targets for MLV integration. Science 2003;300(5626):1749–51.
49. Burns JC, Friedmann T, Driever W, Burrascano M, Yee JK. Vesicular stomatitis virus G glycoprotein pseudotyped retroviral vectors: concentration to very high titer and efficient gene transfer into mammalian and nonmammalian cells. Proc Natl Acad Sci U S A 1993;90(17):8033–7.
50. Dodig M, Tadic T, Kronenberg MS, Dacic S, Liu YH, Maxson R, et al. Ectopic Msx2 overexpression inhibits and Msx2 antisense stimulates calvarial osteoblast differentiation. Dev Biol 1999;209(2):298–307.
51. Kalajzic I, Stover ML, Liu P, Kalajzic Z, Rowe DW, Lichtler AC. Use of VSV-G pseudotyped retroviral vectors to target murine osteoprogenitor cells. Virology 2001;284(1):37–45.
52. Shi S, Gronthos S, Chen S, Reddi A, Counter CM, Robey PG, et al. Bone formation by human postnatal bone marrow stromal stem cells is enhanced by

telomerase expression. Nat Biotechnol 2002;20(6): 587–91.
53. Oyama M, Tatlock A, Fukuta S, Kavalkovich K, Nishimura K, Johnstone B, et al. Retrovirally transduced bone marrow stromal cells isolated from a mouse model of human osteogenesis imperfecta (oim) persist in bone and retain the ability to form cartilage and bone after extended passaging. Gene Ther 1999;6(3): 321–9.
54. Oreffo RO, Virdi AS, Triffitt JT. Retroviral marking of human bone marrow fibroblasts: *in vitro* expansion and localization in calvarial sites after subcutaneous transplantation *in vivo*. J Cell Physiol 2001;186(2): 201–9.
55. Fiorellini JP, Buser D, Riley E, Howell TH. Effect on bone healing of bone morphogenetic protein placed in combination with endosseous implants: a pilot study in beagle dogs. Int J Periodontics Restorative Dent 2001;21(1):41–7.
56. Mason JM, Grande DA, Barcia M, Grant R, Pergolizzi RG, Breitbart AS. Expression of human bone morphogenic protein 7 in primary rabbit periosteal cells: potential utility in gene therapy for osteochondral repair. Gene Ther 1998;5(8):1098–104.
57. Breitbart AS, Grande DA, Mason JM, Barcia M, James T, Grant RT. Gene-enhanced tissue engineering: applications for bone healing using cultured periosteal cells transduced retrovirally with the BMP-7 gene. Ann Plast Surg 1999;42(5):488–95.
58. Engstrand T, Daluiski A, Bahamonde ME, Melhus H, Lyons KM. Transient production of bone morphogenetic protein 2 by allogeneic transplanted transduced cells induces bone formation. Hum Gene Ther 2000;11(1):205–11.
59. Peng H, Chen ST, Wergedal JE, Polo JM, Yee JK, Lau KH, et al. Development of an MFG-based retroviral vector system for secretion of high levels of functionally active human BMP4. Mol Ther 2001; 4(2):95–104.
60. Dranoff G, Jaffee E, Lazenby A, Golumbek P, Levitsky H, Brose K, et al. Vaccination with irradiated tumor cells engineered to secrete murine granulocyte-macrophage colony-stimulating factor stimulates potent, specific, and long-lasting anti-tumor immunity. Proc Natl Acad Sci U S A 1993;90(8):3539–43.
61. Hammonds RG Jr, Schwall R, Dudley A, Berkemeier L, Lai C, Lee J, et al. Bone-inducing activity of mature BMP-2b produced from a hybrid BMP-2a/2b precursor. Mol Endocrinol 1991;5(1):149–55.
62. Dahir GA, Cui Q, Anderson P, Simon C, Joyner C, Triffitt JT, et al. Pluripotential mesenchymal cells repopulate bone marrow and retain osteogenic properties. Clin Orthop 2000;(379 Suppl):S134–45.
63. Devine MJ, Mierisch CM, Jang E, Anderson PC, Balian G. Transplanted bone marrow cells localize to fracture callus in a mouse model. J Orthop Res 2002;20(6):1232–9.
64. Bjornson CR, Rietze RL, Reynolds BA, Magli MC, Vescovi AL. Turning brain into blood: a hematopoietic fate adopted by adult neural stem cells *in vivo*. Science 1999;283(5401):534–7.
65. Galli R, Borello U, Gritti A, Minasi MG, Bjornson C, Coletta M, et al. Skeletal myogenic potential of human and mouse neural stem cells. Nat Neurosci 2000;3(10):986–91.
66. McKay R. Stem cells in the central nervous system. Science 1997;276(5309):66–71.
67. Gussoni E, Soneoka Y, Strickland CD, Buzney EA, Khan MK, Flint AF, et al. Dystrophin expression in the mdx mouse restored by stem cell transplantation. Nature 1999;401(6751):390–4.
68. Jackson KA, Mi T, Goodell MA. Hematopoietic potential of stem cells isolated from murine skeletal muscle. Proc Natl Acad Sci U S A 1999;96(25): 14482–6.
69. Lee JY, Qu-Petersen Z, Cao B, Kimura S, Jankowski R, Cummins J, et al. Clonal isolation of muscle-derived cells capable of enhancing muscle regeneration and bone healing. J Cell Biol 2000;150(5): 1085–100.
70. Torrente Y, Tremblay JP, Pisati F, Belicchi M, Rossi B, Sironi M, et al. Intraarterial injection of muscle-derived CD34(+)Sca-1(+) stem cells restores dystrophin in mdx mice. J Cell Biol 2001;152(2):335–48.
71. Seale P, Rudnicki MA. A new look at the origin, function, and "stem-cell" status of muscle satellite cells. Dev Biol 2000;218(2):115–24.
72. Wada MR, Inagawa-Ogashiwa M, Shimizu S, Yasumoto S, Hashimoto N. Generation of different fates from multipotent muscle stem cells. Development 2002;129(12):2987–95.
73. Asakura A, Seale P, Girgis-Gabardo A, Rudnicki MA. Myogenic specification of side population cells in skeletal muscle. J Cell Biol 2002;159(1):123–34.
74. Katagiri T, Yamaguchi A, Komaki M, Abe E, Takahashi N, Ikeda T, et al. Bone morphogenetic protein-2 converts the differentiation pathway of C2C12 myoblasts into the osteoblast lineage. J Cell Biol 1994;127(6 Pt 1):1755–66.
75. Teboul L, Gaillard D, Staccini L, Inadera H, Amri EZ, Grimaldi PA. Thiazolidinediones and fatty acids convert myogenic cells into adipose-like cells. J Biol Chem 1995;270(47):28183–7.
76. Kingsley DM. The TGF-beta superfamily: new members, new receptors, and new genetic tests of function in different organisms. Genes Dev 1994;8(2):133–46.
77. Ogawa Y, Schmidt DK, Nathan RM, Armstrong RM, Miller KL, Sawamura SJ, et al. Bovine bone activin enhances bone morphogenetic protein-induced ectopic bone formation. J Biol Chem 1992;267(20): 14233–7.
78. Sakai R, Eto Y. Involvement of activin in the regulation of bone metabolism. Mol Cell Endocrinol 2001; 180(1–2):183–8.
79. Hromas R, Hufford M, Sutton J, Xu D, Li Y, Lu L. PLAB, a novel placental bone morphogenetic protein. Biochim Biophys Acta 1997;1354(1):40–4.
80. Li PX, Wong J, Ayed A, Ngo D, Brade AM,

Arrowsmith C, et al. Placental transforming growth factor-beta is a downstream mediator of the growth arrest and apoptotic response of tumor cells to DNA damage and p53 overexpression. J Biol Chem 2000; 275(26):20127–35.
81. Paralkar VM, Vail AL, Grasser WA, Brown TA, Xu H, Vukicevic S, et al. Cloning and characterization of a novel member of the transforming growth factor-beta/bone morphogenetic protein family. J Biol Chem 1998;273(22):13760–7.
82. Baek SJ, Kim KS, Nixon JB, Wilson LC, Eling TE. Cyclooxygenase inhibitors regulate the expression of a TGF-beta superfamily member that has proapoptotic and antitumorigenic activities. Mol Pharmacol 2001; 59(4):901–8.
83. Bootcov MR, Bauskin AR, Valenzuela SM, Moore AG, Bansal M, He XY, et al. MIC-1, a novel macrophage inhibitory cytokine, is a divergent member of the TGF-beta superfamily. Proc Natl Acad Sci U S A 1997;94(21):11514–9.
84. Wong J, Li PX, Klamut HJ. A novel p53 transcriptional repressor element (p53 TRE) and the asymmetrical contribution of two p53 binding sites modulate the response of the PTGF-beta promoter to p53. J Biol Chem 2002;277(29):26699–707.
85. Tan M, Wang Y, Guan K, Sun Y. PTGF-beta, a type beta transforming growth factor (TGF-beta) superfamily member, is a p53 target gene that inhibits tumor cell growth via TGF-beta signaling pathway. Proc Natl Acad Sci U S A 2000;97(1):109–14.
86. Chandar N, Donehower L, Lanciloti N. Reduction in p53 gene dosage diminishes differentiation capacity of osteoblasts. Anticancer Res 2000;20(4): 2553–9.
87. Altman RD, Latta LL, Keer R, Renfree K, Hornicek FJ, Banovac K. Effect of nonsteroidal antiinflammatory drugs on fracture healing: a laboratory study in rats. J Orthop Trauma 1995;9(5):392–400.
88. Giannoudis PV, MacDonald DA, Matthews SJ, Smith RM, Furlong AJ, De Boer P. Nonunion of the femoral diaphysis. The influence of reaming and nonsteroidal anti-inflammatory drugs. J Bone Joint Surg Br 2000;82(5):655–8.
89. Ducy P, Zhang R, Geoffroy V, Ridall AL, Karsenty G. Osf2/Cbfa1: a transcriptional activator of osteoblast differentiation. Cell 1997;89(5):747–54.
90. Komori T, Yagi H, Nomura S, Yamaguchi A, Sasaki K, Deguchi K, et al. Targeted disruption of Cbfa1 results in a complete lack of bone formation owing to maturational arrest of osteoblasts. Cell 1997;89(5): 755–64.
91. Nakashima K, Zhou X, Kunkel G, Zhang Z, Deng JM, Behringer RR, et al. The novel zinc finger-containing transcription factor osterix is required for osteoblast differentiation and bone formation. Cell 2002;108(1):17–29.
92. Ryoo HM, Hoffmann HM, Beumer T, Frenkel B, Towler DA, Stein GS, et al. Stage-specific expression of Dlx-5 during osteoblast differentiation: involvement in regulation of osteocalcin gene expression. Mol Endocrinol 1997;11(11):1681–94.
93. Miyama K, Yamada G, Yamamoto TS, Takagi C, Miyado K, Sakai M, et al. A BMP-inducible gene, dlx5, regulates osteoblast differentiation and mesoderm induction. Dev Biol 1999;208(1):123–33.
94. Nishimura R, Hata K, Harris SE, Ikeda F, Yoneda T. Core-binding factor alpha 1 (Cbfa1) induces osteoblastic differentiation of C2C12 cells without interactions with Smad1 and Smad5. Bone 2002;31(2):303–12.
95. Pearce JJ, Penny G, Rossant J. A mouse cerberus/Dan-related gene family. Dev Biol 1999;209(1):98–110.
96. Piccolo S, Sasai Y, Lu B, De Robertis EM. Dorsoventral patterning in *Xenopus*: inhibition of ventral signals by direct binding of chordin to BMP-4. Cell 1996;86(4):589–98.
97. Holley SA, Neul JL, Attisano L, Wrana JL, Sasai Y, O'Connor MB, et al. The Xenopus dorsalizing factor noggin ventralizes *Drosophila* embryos by preventing DPP from activating its receptor. Cell 1996; 86(4):607–17.
98. Bouwmeester T, Kim S, Sasai Y, Lu B, De Robertis EM. Cerberus is a head-inducing secreted factor expressed in the anterior endoderm of Spemann's organizer. Nature 1996;382(6592):595–601.
99. Zimmerman LB, De Jesus-Escobar JM, Harland RM. The Spemann organizer signal noggin binds and inactivates bone morphogenetic protein 4. Cell 1996; 86(4):599–606.
100. Warren SM, Brunet LJ, Harland RM, Economides AN, Longaker MT. The BMP antagonist noggin regulates cranial suture fusion. Nature 2003;422(6932): 625–9.
101. Muenke M, Schell U. Fibroblast-growth-factor receptor mutations in human skeletal disorders. Trends Genet 1995;11(8):308–13.
102. Mansukhani A, Bellosta P, Sahni M, Basilico C. Signaling by fibroblast growth factors (FGF) and fibroblast growth factor receptor 2 (FGFR2)-activating mutations blocks mineralization and induces apoptosis in osteoblasts. J Cell Biol 2000;149(6):1297–308.
103. Powers CJ, McLeskey SW, Wellstein A. Fibroblast growth factors, their receptors and signaling. Endocr Relat Cancer 2000;7(3):165–97.
104. Pawson T. Protein modules and signalling networks. Nature 1995;373(6515):573–80.
105. Globus RK, Plouet J, Gospodarowicz D. Cultured bovine bone cells synthesize basic fibroblast growth factor and store it in their extracellular matrix. Endocrinology 1989;124(3):1539–47.
106. Hauschka PV, Mavrakos AE, Iafrati MD, Doleman SE, Klagsbrun M. Growth factors in bone matrix. Isolation of multiple types by affinity chromatography on heparin-Sepharose. J Biol Chem 1986;261(27): 12665–74.
107. Globus RK, Patterson-Buckendahl P, Gospodarowicz D. Regulation of bovine bone cell proliferation by fibroblast growth factor and transforming growth factor beta. Endocrinology 1988;123(1):98–105.

108. Rodan SB, Wesolowski G, Thomas KA, Yoon K, Rodan GA. Effects of acidic and basic fibroblast growth factors on osteoblastic cells. Connect Tissue Res 1989;20(1–4):283–8.
109. Kawaguchi H, Kurokawa T, Hanada K, Hiyama Y, Tamura M, Ogata E, et al. Stimulation of fracture repair by recombinant human basic fibroblast growth factor in normal and streptozotocin-diabetic rats. Endocrinology 1994;135(2):774–81.
110. Nakamura T, Hara Y, Tagawa M, Tamura M, Yuge T, Fukuda H, et al. Recombinant human basic fibroblast growth factor accelerates fracture healing by enhancing callus remodeling in experimental dog tibial fracture. J Bone Miner Res 1998; 13(6):942–9.
111. Nakamura K, Kurokawa T, Kato T, Okazaki H, Mamada K, Hanada K, et al. Local application of basic fibroblast growth factor into the bone increases bone mass at the applied site in rabbits. Arch Orthop Trauma Surg 1996;115(6):344–6.
112. Seghezzi G, Patel S, Ren CJ, Gualandris A, Pintucci G, Robbins ES, et al. Fibroblast growth factor-2 (FGF-2) induces vascular endothelial growth factor (VEGF) expression in the endothelial cells of forming capillaries: an autocrine mechanism contributing to angiogenesis. J Cell Biol 1998;141(7):1659–73.
113. Saadeh PB, Mehrara BJ, Steinbrech DS, Spector JA, Greenwald JA, Chin GS, et al. Mechanisms of fibroblast growth factor-2 modulation of vascular endothelial growth factor expression by osteoblastic cells. Endocrinology 2000;141(6):2075–83.
114. Andreassen TT, Jorgensen PH, Flyvbjerg A, Orskov H, Oxlund H. Growth hormone stimulates bone formation and strength of cortical bone in aged rats. J Bone Miner Res 1995;10(7):1057–67.
115. Raschke M, Kolbeck S, Bail H, Schmidmaier G, Flyvbjerg A, Lindner T, et al. Homologous growth hormone accelerates healing of segmental bone defects. Bone 2001;29(4):368–73.
116. Green H, Morikawa M, Nixon T. A dual effector theory of growth-hormone action. Differentiation 1985;29(3):195–8.
117. Mohan S, Baylink DJ. Bone growth factors. Clin Orthop 1991;(263):30–48.
118. Andrew JG, Hoyland J, Freemont AJ, Marsh D. Insulinlike growth factor gene expression in human fracture callus. Calcif Tissue Int 1993;53(2):97–102.
119. Prisell PT, Edwall D, Lindblad JB, Levinovitz A, Norstedt G. Expression of insulin-like growth factors during bone induction in rat. Calcif Tissue Int 1993; 53(3):201–5.
120. Wilton P. Treatment with recombinant human insulin-like growth factor I of children with growth hormone receptor deficiency (Laron syndrome). Kabi Pharmacia Study Group on Insulin-like Growth Factor I Treatment in Growth Hormone Insensitivity Syndromes. Acta Paediatr Suppl 1992;383:137–42.
121. Isgaard J, Nilsson A, Lindahl A, Jansson JO, Isaksson OG. Effects of local administration of GH and IGF-I on longitudinal bone growth in rats. Am J Physiol 1986;250(4 Pt 1):E367–72.
122. Canalis E, Pash J, Varghese S. Skeletal growth factors. Crit Rev Eukaryot Gene Expr 1993;3(3):155–66.
123. Dequeker J, Mohan S, Finkelman RD, Aerssens J, Baylink DJ. Generalized osteoarthritis associated with increased insulin-like growth factor types I and II and transforming growth factor beta in cortical bone from the iliac crest. Possible mechanism of increased bone density and protection against osteoporosis. Arthritis Rheum 1993;36(12):1702–8.
124. Mohan S, Nakao Y, Honda Y, Landale E, Leser U, Dony C, et al. Studies on the mechanisms by which insulin-like growth factor (IGF) binding protein-4 (IGFBP-4) and IGFBP-5 modulate IGF actions in bone cells. J Biol Chem 1995;270(35):20424–31.
125. Mundy GR. Factors which stimulate bone growth *in vivo*. Growth Regul 1993;3(2):124–8.
126. Hock JM, Centrella M, Canalis E. Insulin-like growth factor I has independent effects on bone matrix formation and cell replication. Endocrinology 1988; 122(1):254–60.
127. LeRoith D. Insulin-like growth factor receptors and binding proteins. Baillieres Clin Endocrinol Metab 1996;10(1):49–73.
128. Hwa V, Oh Y, Rosenfeld RG. The insulin-like growth factor-binding protein (IGFBP) superfamily. Endocr Rev 1999;20(6):761–87.
129. Collett-Solberg PF, Cohen P. Genetics, chemistry, and function of the IGF/IGFBP system. Endocrine 2000;12(2):121–36.
130. Mohan S, Baylink DJ. IGF-binding proteins are multifunctional and act via IGF-dependent and -independent mechanisms. J Endocrinol 2002;175(1):19–31.
131. Mohan S, Baylink DJ, Pettis JL. Insulin-like growth factor (IGF)-binding proteins in serum—do they have additional roles besides modulating the endocrine IGF actions? J Clin Endocrinol Metab 1996; 81(11):3817–20.
132. Mohan S, Farley JR, Baylink DJ. Age-related changes in IGFBP-4 and IGFBP-5 levels in human serum and bone: implications for bone loss with aging. Prog Growth Factor Res 1995;6(2–4):465–73.
133. Bautista CM, Baylink DJ, Mohan S. Isolation of a novel insulin-like growth factor (IGF) binding protein from human bone: a potential candidate for fixing IGF-II in human bone. Biochem Biophys Res Commun 1991;176(2):756–63.
134. Andress DL, Birnbaum RS. Human osteoblast-derived insulin-like growth factor (IGF) binding protein-5 stimulates osteoblast mitogenesis and potentiates IGF action. J Biol Chem 1992;267(31):22467–72.
135. Richman C, Baylink DJ, Lang K, Dony C, Mohan S. Recombinant human insulin-like growth factor-binding protein-5 stimulates bone formation parameters *in vitro* and *in vivo*. Endocrinology 1999;140(10): 4699–705.
136. Miyakoshi N, Richman C, Kasukawa Y, Linkhart TA, Baylink DJ, Mohan S. Evidence that IGF-bind-

ing protein-5 functions as a growth factor. J Clin Invest 2001;107(1):73–81.
137. Amaar YG, Thompson GR, Linkhart TA, Chen ST, Baylink DJ, Mohan S. Insulin-like growth factor-binding protein 5 (IGFBP-5) interacts with a four and a half LIM protein 2 (FHL2). J Biol Chem 2002;277(14):12053–60.
138. Scholl FA, McLoughlin P, Ehler E, de Giovanni C, Schafer BW. DRAL is a p53-responsive gene whose four and a half LIM domain protein product induces apoptosis. J Cell Biol 2000;151(3):495–506.
139. Liu Y, Hair GA, Boden SD, Viggeswarapu M, Titus L. Overexpressed LIM mineralization proteins do not require LIM domains to induce bone. J Bone Miner Res 2002;17(3):406–14.
140. Kim HS, Viggeswarapu M, Boden SD, Liu Y, Hair GA, Louis-Ugbo J, et al. Overcoming the immune response to permit *ex vivo* gene therapy for spine fusion with human type 5 adenoviral delivery of the LIM mineralization protein-1 cDNA. Spine 2003;28(3):219–26.
141. Suponitzky I, Weinreb M. Differential effects of systemic prostaglandin E2 on bone mass in rat long bones and calvariae. J Endocrinol 1998;156(1):51–7.
142. Raisz LG. Physiologic and pathologic roles of prostaglandins and other eicosanoids in bone metabolism. J Nutr 1995;125(7 Suppl):2024S–2027S.
143. Yoshida K, Oida H, Kobayashi T, Maruyama T, Tanaka M, Katayama T, et al. Stimulation of bone formation and prevention of bone loss by prostaglandin E EP4 receptor activation. Proc Natl Acad Sci U S A 2002;99(7):4580–5.
144. Okada Y, Lorenzo JA, Freeman AM, Tomita M, Morham SG, Raisz LG, et al. Prostaglandin G/H synthase-2 is required for maximal formation of osteoclast-like cells in culture. J Clin Invest 2000;105(6): 823–32.
145. Zhang X, Schwarz EM, Young DA, Puzas JE, Rosier RN, O'Keefe RJ. Cyclooxygenase-2 regulates mesenchymal cell differentiation into the osteoblast lineage and is critically involved in bone repair. J Clin Invest 2002;109(11):1405–15.
146. Hock JM, Krishnan V, Onyia JE, Bidwell JP, Milas J, Stanislaus D. Osteoblast apoptosis and bone turnover. J Bone Miner Res 2001;16(6):975–84.
147. Beck GR Jr, Zerler B, Moran E. Gene array analysis of osteoblast differentiation. Cell Growth Differ 2001; 12(2):61–83.
148. Raouf A, Seth A. Discovery of osteoblast-associated genes using cDNA microarrays. Bone 2002;30(3): 463–71.
149. Hadjiargyrou M, Lombardo F, Zhao S, Ahrens W, Joo J, Ahn H, et al. Transcriptional profiling of bone regeneration. Insight into the molecular complexity of wound repair. J Biol Chem 2002;277(33):30177–82.
150. Huelsken J, Birchmeier W. New aspects of Wnt signaling pathways in higher vertebrates. Curr Opin Genet Dev 2001;11(5):547–53.
151. Qin L, Qiu P, Wang L, Li X, Swarthout JT, Soteropoulos P, et al. Gene expression profiles and transcription factors involved in PTH signaling in osteoblasts revealed by microarray and bioinformatics. J Biol Chem 2003;278(22):19723–31.
152. Fire A, Xu S, Montgomery MK, Kostas SA, Driver SE, Mello CC. Potent and specific genetic interference by double-stranded RNA in *Caenorhabditis elegans*. Nature 1998;391(6669):806–11.
153. Elbashir SM, Harborth J, Lendeckel W, Yalcin A, Weber K, Tuschl T. Duplexes of 21-nucleotide RNAs mediate RNA interference in cultured mammalian cells. Nature 2001;411(6836):494–8.
154. Hammond SM, Bernstein E, Beach D, Hannon GJ. An RNA-directed nuclease mediates post-transcriptional gene silencing in *Drosophila* cells. Nature 2000; 404(6775):293–6.
155. Agami R. RNAi and related mechanisms and their potential use for therapy. Curr Opin Chem Biol 2002; 6(6):829–34.
156. Gitlin L, Karelsky S, Andino R. Short interfering RNA confers intracellular antiviral immunity in human cells. Nature 2002;418(6896):430–4.
157. Qin XF, An DS, Chen IS, Baltimore D. Inhibiting HIV-1 infection in human T cells by lentiviral-mediated delivery of small interfering RNA against CCR5. Proc Natl Acad Sci U S A 2003;100(1):183–8.
158. Kosciolek BA, Kalantidis K, Tabler M, Rowley PT. Inhibition of telomerase activity in human cancer Cells by RNA interference. Mol Cancer Ther 2003;2(3): 209–216.
159. Bohula EA, Salisbury AJ, Sohail M, Playford MP, Riedemann J, Southern EM, et al. The efficacy of small interfering RNAs targeted to the type 1 IGF receptor is influenced by secondary structure in the IGF1R transcript. J Biol Chem 2003;278(18): 15991–7.
160. Khosla S. Minireview: the OPG/RANKL/RANK system. Endocrinology 2001;142(12):5050–5.
161. Manolagas SC, Kousteni S, Jilka RL. Sex steroids and bone. Recent Prog Horm Res 2002;57:385–409.
162. Verborgt O, Tatton NA, Majeska RJ, Schaffler MB. Spatial distribution of Bax and Bcl-2 in osteocytes after bone fatigue: complementary roles in bone remodeling regulation? J Bone Miner Res 2002;17(5): 907–14.
163. Chao DT, Korsmeyer SJ. BCL-2 family: regulators of cell death. Annu Rev Immunol 1998;16:395–419.
164. Anthony-Cahill SJ, Magliery TJ. Expanding the natural repertoire of protein structure and function. Curr Pharm Biotechnol 2002;3(4):299–315.
165. Seno M, Sasada R, Iwane M, Sudo K, Kurokawa T, Ito K, et al. Stabilizing basic fibroblast growth factor using protein engineering. Biochem Biophys Res Commun 1988;151(2):701–8.
166. Facchiano F, Lentini A, Fogliano V, Mancarella S, Rossi C, Facchiano A, et al. Sugar-induced modification of fibroblast growth factor 2 reduces its angiogenic activity *in vivo*. Am J Pathol 2002;161(2): 531–41.

167. Grieb TA, Burgess WH. The mitogenic activity of fibroblast growth factor-1 correlates with its internalization and limited proteolytic processing. J Cell Physiol 2000;184(2):171–82.
168. Sakai K, Busby WH Jr, Clarke JB, Clemmons DR. Tissue transglutaminase facilitates the polymerization of insulin-like growth factor-binding protein-1 (IGFBP-1) and leads to loss of IGFBP-1's ability to inhibit insulin-like growth factor-I-stimulated protein synthesis. J Biol Chem 2001;276(12):8740–5.
169. Yoneda A, Asada M, Oda Y, Suzuki M, Imamura T. Engineering of an FGF-proteoglycan fusion protein with heparin-independent, mitogenic activity. Nat Biotechnol 2000;18(6):641–4.
170. Elliott G, O'Hare P. Intercellular trafficking and protein delivery by a herpesvirus structural protein. Cell 1997;88(2):223–33.
171. Phelan A, Elliott G, O'Hare P. Intercellular delivery of functional p53 by the herpesvirus protein VP22. Nat Biotechnol 1998;16(5):440–3.
172. Anderson WF. Prospects for human gene therapy. Science 1984;226(4673):401–9.
173. Varmus H. Retroviruses. Science 1988;240(4858): 1427–35.
174. Lewis P, Hensel M, Emerman M. Human immunodeficiency virus infection of cells arrested in the cell cycle. EMBO J 1992;11(8):3053–8.
175. Naldini L, Blomer U, Gallay P, Ory D, Mulligan R, Gage FH, et al. *In vivo* gene delivery and stable transduction of nondividing cells by a lentiviral vector. Science 1996;272(5259):263–7.
176. Zufferey R, Nagy D, Mandel RJ, Naldini L, Trono D. Multiply attenuated lentiviral vector achieves efficient gene delivery *in vivo*. Nat Biotechnol 1997;15(9): 871–5.
177. Dull T, Zufferey R, Kelly M, Mandel RJ, Nguyen M, Trono D, et al. A third-generation lentivirus vector with a conditional packaging system. J Virol 1998; 72(11):8463–71.
178. Zufferey R, Dull T, Mandel RJ, Bukovsky A, Quiroz D, Naldini L, et al. Self-inactivating lentivirus vector for safe and efficient *in vivo* gene delivery. J Virol 1998;72(12):9873–80.
179. Pannell D, Ellis J. Silencing of gene expression: implications for design of retrovirus vectors. Rev Med Virol 2001;11(4):205–17.
180. Challita PM, Kohn DB. Lack of expression from a retroviral vector after transduction of murine hematopoietic stem cells is associated with methylation *in vivo*. Proc Natl Acad Sci U S A 1994;91(7): 2567–71.
181. Halene S, Wang L, Cooper RM, Bockstoce DC, Robbins PB, Kohn DB. Improved expression in hematopoietic and lymphoid cells in mice after transplantation of bone marrow transduced with a modified retroviral vector. Blood 1999;94(10):3349–57.
182. Hacein-Bey-Abina S, von Kalle C, Schmidt M, Le Deist F, Wulffraat N, McIntyre E, et al. A serious adverse event after successful gene therapy for X-linked severe combined immunodeficiency. N Engl J Med 2003;348(3):255–6.
183. Fisher KJ, Jooss K, Alston J, Yang Y, Haecker SE, High K, et al. Recombinant adeno-associated virus for muscle directed gene therapy. Nat Med 1997;3(3): 306–12.
184. Su H, Lu R, Kan YW. Adeno-associated viral vector-mediated vascular endothelial growth factor gene transfer induces neovascular formation in ischemic heart. Proc Natl Acad Sci U S A 2000;97(25):13801–6.
185. Grimm D, Zhou S, Nakai H, Thomas CE, Storm TA, Fuess S, et al. Pre-clinical *in vivo* evaluation of pseudotyped adeno-associated virus (AAV) vectors for liver gene therapy. Blood 2003;102(7):2412–9.
186. Halbert CL, Allen JM, Miller AD. Efficient mouse airway transduction following recombination between AAV vectors carrying parts of a larger gene. Nat Biotechnol 2002;20(7):697–701.
187. During MJ, Samulski RJ, Elsworth JD, Kaplitt MG, Leone P, Xiao X, et al. *In vivo* expression of therapeutic human genes for dopamine production in the caudates of MPTP-treated monkeys using an AAV vector. Gene Ther 1998;5(6):820–7.
188. Monahan PE, Samulski RJ, Tazelaar J, Xiao X, Nichols TC, Bellinger DA, et al. Direct intramuscular injection with recombinant AAV vectors results in sustained expression in a dog model of hemophilia. Gene Ther 1998;5(1):40–9.
189. Hoggan MD, Blacklow NR, Rowe WP. Studies of small DNA viruses found in various adenovirus preparations: physical, biological, and immunological characteristics. Proc Natl Acad Sci U S A 1966;55(6):1467–74.
190. Srivastava A, Lusby EW, Berns KI. Nucleotide sequence and organization of the adeno-associated virus 2 genome. J Virol 1983;45(2):555–64.
191. Jooss K, Yang Y, Fisher KJ, Wilson JM. Transduction of dendritic cells by DNA viral vectors directs the immune response to transgene products in muscle fibers. J Virol 1998;72(5):4212–23.
192. Clark KR. Recent advances in recombinant adeno-associated virus vector production. Kidney Int 2002;61 Suppl 1:9–15.
193. Ponnazhagan S, Curiel DT, Shaw DR, Alvarez RD, Siegal GP. Adeno-associated virus for cancer gene therapy. Cancer Res 2001;61(17):6313–21.
194. Yan Z, Zhang Y, Duan D, Engelhardt JF. Trans-splicing vectors expand the utility of adeno-associated virus for gene therapy. Proc Natl Acad Sci U S A 2000;97(12):6716–21.
195. Duan D, Yue Y, Engelhardt JF. Expanding AAV packaging capacity with trans-splicing or overlapping vectors: a quantitative comparison. Mol Ther 2001; 4(4):383–91.
196. Miao CH, Snyder RO, Schowalter DB, Patijn GA, Donahue B, Winther B, et al. The kinetics of rAAV integration in the liver. Nat Genet 1998;19(1):13–5.
197. Ponnazhagan S, Mukherjee P, Wang XS, Qing K, Kube DM, Mah C, et al. Adeno-associated virus type 2-mediated transduction in primary human bone

marrow-derived CD34+ hematopoietic progenitor cells: donor variation and correlation of transgene expression with cellular differentiation. J Virol 1997; 71(11):8262–7.
198. Schimmenti S, Boesen J, Claassen EA, Valerio D, Einerhand MP. Long-term genetic modification of rhesus monkey hematopoietic cells following transplantation of adenoassociated virus vector-transduced CD34+ cells. Hum Gene Ther 1998;9(18):2727–34.
199. Summerford C, Samulski RJ. Membrane-associated heparan sulfate proteoglycan is a receptor for adeno-associated virus type 2 virions. J Virol 1998;72(2): 1438–45.
200. Qing K, Mah C, Hansen J, Zhou S, Dwarki V, Srivastava A. Human fibroblast growth factor receptor 1 is a co-receptor for infection by adeno-associated virus 2. Nat Med 1999;5(1):71–7.
201. Summerford C, Bartlett JS, Samulski RJ. AlphaVbeta5 integrin: a co-receptor for adeno-associated virus type 2 infection. Nat Med 1999;5(1):78–82.
202. Drzeniek Z, Stocker G, Siebertz B, Just U, Schroeder T, Ostertag W, et al. Heparan sulfate proteoglycan expression is induced during early erythroid differentiation of multipotent hematopoietic stem cells. Blood 1999;93(9):2884–97.
203. Newman P, Bonello F, Wierzbicki AS, Lumb P, Savidge GF, Shearer MJ. The uptake of lipoprotein-borne phylloquinone (vitamin K1) by osteoblasts and osteoblast-like cells: role of heparan sulfate proteoglycans and apolipoprotein E. J Bone Miner Res 2002;17(3):426–33.
204. Lollo CP, Banaszczyk MG, Chiou HC. Obstacles and advances in non-viral gene delivery. Curr Opin Mol Ther 2000;2(2):136–42.
205. Nishikawa M, Huang L. Nonviral vectors in the new millennium: delivery barriers in gene transfer. Hum Gene Ther 2001;12(8):861–70.
206. Herweijer H, Wolff JA. Progress and prospects: naked DNA gene transfer and therapy. Gene Ther 2003; 10(6):453–8.
207. Sawamura D, Akiyama M, Shimizu H. Direct injection of naked DNA and cytokine transgene expression: implications for keratinocyte gene therapy. Clin Exp Dermatol 2002;27(6):480–4.
208. Rossmanith W, Chabicovsky M, Herkner K, Schulte-Hermann R. Cellular gene dose and kinetics of gene expression in mouse livers transfected by high-volume tail-vein injection of naked DNA. DNA Cell Biol 2002;21(11):847–53.
209. Maurer N, Fenske DB, Cullis PR. Developments in liposomal drug delivery systems. Expert Opin Biol Ther 2001;1(6):923–47.
210. Smyth Templeton N. Liposomal delivery of nucleic acids *in vivo*. DNA Cell Biol 2002;21(12):857–67.
211. Torchilin VP, Levchenko TS, Rammohan R, Volodina N, Papahadjopoulos-Sternberg B, D'Souza GG. Cell transfection *in vitro* and *in vivo* with nontoxic TAT peptide-liposome-DNA complexes. Proc Natl Acad Sci U S A 2003;100(4):1972–7.
212. Turk MJ, Reddy JA, Chmielewski JA, Low PS. Characterization of a novel pH-sensitive peptide that enhances drug release from folate-targeted liposomes at endosomal pHs. Biochim Biophys Acta 2002;1559(1): 56–68.
213. Tagawa T, Manvell M, Brown N, Keller M, Perouzel E, Murray KD, et al. Characterisation of LMD virus-like nanoparticles self-assembled from cationic liposomes, adenovirus core peptide mu and plasmid DNA. Gene Ther 2002;9(9):564–76.
214. Zhang Y, Jeong Lee H, Boado RJ, Pardridge WM. Receptor-mediated delivery of an antisense gene to human brain cancer cells. J Gene Med 2002;4(2):183–94.
215. Shi N, Zhang Y, Zhu C, Boado RJ, Pardridge WM. Brain-specific expression of an exogenous gene after i.v. administration. Proc Natl Acad Sci U S A 2001; 98(22):12754–9.
216. Kim HS, Park YS. Gene transfection by quantitatively reconstituted Sendai envelope proteins into liposomes. Cancer Gene Ther 2002;9(2):173–7.
217. Schwarze SR, Ho A, Vocero-Akbani A, Dowdy SF. *In vivo* protein transduction: delivery of a biologically active protein into the mouse. Science 1999;285(5433): 1569–72.
218. Kilic E, Dietz GP, Hermann DM, Bahr M. Intravenous TAT-Bcl-Xl is protective after middle cerebral artery occlusion in mice. Ann Neurol 2002;52(5): 617–22.
219. Cao G, Pei W, Ge H, Liang Q, Luo Y, Sharp FR, et al. *In vivo* delivery of a Bcl-xL fusion protein containing the TAT protein transduction domain protects against ischemic brain injury and neuronal apoptosis. J Neurosci 2002;22(13):5423–31.
220. Dolgilevich S, Zaidi N, Song J, Abe E, Moonga BS, Sun L. Transduction of TAT fusion proteins into osteoclasts and osteoblasts. Biochem Biophys Res Commun 2002;299(3):505–9.
221. Abu-Amer Y, Dowdy SF, Ross FP, Clohisy JC, Teitelbaum SL. TAT fusion proteins containing tyrosine 42-deleted IkappaBalpha arrest osteoclastogenesis. J Biol Chem 2001;276(32):30499–503.
222. Snyder EL, Dowdy SF. Protein/peptide transduction domains: potential to deliver large DNA molecules into cells. Curr Opin Mol Ther 2001;3(2):147–52.
223. Dingli D, Russell SJ. Genetic targeting of retroviral vectors. In: Curiel DT, Douglas JT, editors. Vector targeting for therapeutic gene delivery. Hoboken (NJ): Wiley-Liss; 2002. p. 267–291.
224. Wickham TJ. Ligand-directed targeting of genes to the site of disease. Nat Med 2003;9(1):135–9.
225. Peng KW, Morling FJ, Cosset FL, Murphy G, Russell SJ. A gene delivery system activatable by disease-associated matrix metalloproteinases. Hum Gene Ther 1997;8(6):729–38.
226. Hatziioannou T, Delahaye E, Martin F, Russell SJ, Cosset FL. Retroviral display of functional binding domains fused to the amino terminus of influenza hemagglutinin. Hum Gene Ther 1999;10(9):1533–44.
227. Boerger AL, Snitkovsky S, Young JA. Retroviral vec-

tors preloaded with a viral receptor-ligand bridge protein are targeted to specific cell types. Proc Natl Acad Sci U S A 1999;96(17):9867–72.
228. Snitkovsky S, Niederman TM, Mulligan RC, Young JA. Targeting avian leukosis virus subgroup A vectors by using a TVA-VEGF bridge protein. J Virol 2001; 75(3):1571–5.
229. Dallas DJ, Genever PG, Patton AJ, Millichip MI, McKie N, Skerry TM. Localization of ADAM10 and Notch receptors in bone. Bone 1999;25(1):9–15.
230. Kim N, Takami M, Rho J, Josien R, Choi Y. A novel member of the leukocyte receptor complex regulates osteoclast differentiation. J Exp Med 2002;195(2): 201–9.
231. Tomko RP, Xu R, Philipson L. HCAR and MCAR: the human and mouse cellular receptors for subgroup C adenoviruses and group B coxsackieviruses. Proc Natl Acad Sci U S A 1997;94(7):3352–6.
232. Bergelson JM, Cunningham JA, Droguett G, Kurt-Jones EA, Krithivas A, Hong JS, et al. Isolation of a common receptor for Coxsackie B viruses and adenoviruses 2 and 5. Science 1997;275(5304):1320–3.
233. Wickham TJ, Mathias P, Cheresh DA, Nemerow GR. Integrins alpha v beta 3 and alpha v beta 5 promote adenovirus internalization but not virus attachment. Cell 1993;73(2):309–19.
234. Wickham TJ, Tzeng E, Shears LL II, Roelvink PW, Li Y, Lee GM, et al. Increased *in vitro* and *in vivo* gene transfer by adenovirus vectors containing chimeric fiber proteins. J Virol 1997;71(11):8221–9.
235. Einfeld DA, Brough DE, Roelvink PW, Kovesdi I, Wickham TJ. Construction of a pseudoreceptor that mediates transduction by adenoviruses expressing a ligand in fiber or penton base. J Virol 1999;73(11): 9130–6.
236. Dmitriev I, Kashentseva E, Rogers BE, Krasnykh V, Curiel DT. Ectodomain of coxsackievirus and adenovirus receptor genetically fused to epidermal growth factor mediates adenovirus targeting to epidermal growth factor receptor-positive cells. J Virol 2000; 74(15):6875–84.
237. Douglas JT, Rogers BE, Rosenfeld ME, Michael SI, Feng M, Curiel DT. Targeted gene delivery by tropism-modified adenoviral vectors. Nat Biotechnol 1996;14(11):1574–8.
238. Haisma HJ, Grill J, Curiel DT, Hoogeland S, van Beusechem VW, Pinedo HM, et al. Targeting of adenoviral vectors through a bispecific single-chain antibody. Cancer Gene Ther 2000;7(6):901–4.
239. Hong SS, Galaup A, Peytavi R, Chazal N, Boulanger P. Enhancement of adenovirus-mediated gene delivery by use of an oligopeptide with dual binding specificity. Hum Gene Ther 1999;10(16):2577–86.
240. Wickham TJ, Segal DM, Roelvink PW, Carrion ME, Lizonova A, Lee GM, et al. Targeted adenovirus gene transfer to endothelial and smooth muscle cells by using bispecific antibodies. J Virol 1996;70(10):6831–8.
241. Kashentseva EA, Seki T, Curiel DT, Dmitriev IP. Adenovirus targeting to c-erbB-2 oncoprotein by single-chain antibody fused to trimeric form of adenovirus receptor ectodomain. Cancer Res 2002;62(2): 609–16.
242. van Beusechem VW, Grill J, Mastenbroek DC, Wickham TJ, Roelvink PW, Haisma HJ, et al. Efficient and selective gene transfer into primary human brain tumors by using single-chain antibody-targeted adenoviral vectors with native tropism abolished. J Virol 2002;76(6):2753–62.
243. Abboud SL, Woodruff K, Liu C, Shen V, Ghosh-Choudhury N. Rescue of the osteopetrotic defect in op/op mice by osteoblast-specific targeting of soluble colony-stimulating factor-1. Endocrinology 2002; 143(5):1942–9.
244. Hou Z, Nguyen Q, Frenkel B, Nilsson SK, Milne M, van Wijnen AJ, et al. Osteoblast-specific gene expression after transplantation of marrow cells: implications for skeletal gene therapy. Proc Natl Acad Sci U S A 1999;96(13):7294–9.
245. Lian JB, Stein GS, Stein JL, van Wijnen AJ. Marrow transplantation and targeted gene therapy to the skeleton. Clin Orthop 2000;(379 Suppl):S146–55.
246. Stover ML, Wang CK, McKinstry MB, Kalajzic I, Gronowicz G, Clark SH, et al. Bone-directed expression of Col1a1 promoter-driven self-inactivating retroviral vector in bone marrow cells and transgenic mice. Mol Ther 2001;3(4):543–50.
247. Li YP, Chen W. Characterization of mouse cathepsin K gene, the gene promoter, and the gene expression. J Bone Miner Res 1999;14(4):487–99.
248. Deng W, Stashenko P, Chen W, Liang Y, Shimizu K, Li YP. Characterization of mouse Atp6i gene, the gene promoter, and the gene expression. J Bone Miner Res 2001;16(6):1136–46.
249. Sierra J, Villagra A, Paredes R, Cruzat F, Gutierrez S, Javed A, et al. Regulation of the bone-specific osteocalcin gene by p300 requires Runx2/Cbfa1 and the vitamin D3 receptor but not p300 intrinsic histone acetyltransferase activity. Mol Cell Biol 2003; 23(9):3339–51.
250. Stein GS, Lian JB, Stein JL, van Wijnen AJ, Montecino M, Pratap J, et al. Intranuclear organization of RUNX transcriptional regulatory machinery in biological control of skeletogenesis and cancer. Blood Cells Mol Dis 2003;30(2):170–6.
251. Geoffroy V, Kneissel M, Fournier B, Boyde A, Matthias P. High bone resorption in adult aging transgenic mice overexpressing cbfa1/runx2 in cells of the osteoblastic lineage. Mol Cell Biol 2002;22(17): 6222–33.
252. Bedalov A, Salvatori R, Dodig M, Kronenberg MS, Kapural B, Bogdanovic Z, et al. Regulation of COL1A1 expression in type I collagen producing tissues: identification of a 49 base pair region which is required for transgene expression in bone of transgenic mice. J Bone Miner Res 1995;10(10):1443–51.
253. Rossert J, Eberspaecher H, de Crombrugghe B. Separate cis-acting DNA elements of the mouse pro-alpha 1(I) collagen promoter direct expression of reporter

genes to different type I collagen-producing cells in transgenic mice. J Cell Biol 1995;129(5):1421–32.
254. Devlin RD, Du Z, Buccilli V, Jorgetti V, Canalis E. Transgenic mice overexpressing insulin-like growth factor binding protein-5 display transiently decreased osteoblastic function and osteopenia. Endocrinology 2002;143(10):3955–62.
255. Gossen M, Freundlieb S, Bender G, Muller G, Hillen W, Bujard H. Transcriptional activation by tetracyclines in mammalian cells. Science 1995;268(5218):-1766–9.
256. Fishman GI, Kaplan ML, Buttrick PM. Tetracycline-regulated cardiac gene expression *in vivo*. J Clin Invest 1994;93(4):1864–8.
257. Kistner A, Gossen M, Zimmermann F, Jerecic J, Ullmer C, Lubbert H, et al. Doxycycline-mediated quantitative and tissue-specific control of gene expression in transgenic mice. Proc Natl Acad Sci U S A 1996;93(20):10933–8.
258. Harding TC, Geddes BJ, Murphy D, Knight D, Uney JB. Switching transgene expression in the brain using an adenoviral tetracycline-regulatable system. Nat Biotechnol 1998;16(6):553–5.
259. Bohl D, Salvetti A, Moullier P, Heard JM. Control of erythropoietin delivery by doxycycline in mice after intramuscular injection of adeno-associated vector. Blood 1998;92(5):1512–7.
260. Moutsatsos IK, Turgeman G, Zhou S, Kurkalli BG, Pelled G, Tzur L, et al. Exogenously regulated stem cell-mediated gene therapy for bone regeneration. Mol Ther 2001;3(4):449–61.
261. Urlinger S, Baron U, Thellmann M, Hasan MT, Bujard H, Hillen W. Exploring the sequence space for tetracycline-dependent transcriptional activators: novel mutations yield expanded range and sensitivity. Proc Natl Acad Sci U S A 2000;97(14):7963–8.
262. Kenny PA, Enver T, Ashworth A. Retroviral vectors for establishing tetracycline-regulated gene expression in an otherwise recalcitrant cell line. BMC Mol Biol 2002;3(1):13.
263. Kamper MR, Gohla G, Schluter G. A novel positive tetracycline-dependent transactivator (rtTA) variant with reduced background activity and enhanced activation potential. FEBS Lett 2002;517(1–3):115–20.
264. Binley K, Askham Z, Martin L, Spearman H, Day D, Kingsman S, et al. Hypoxia-mediated tumour targeting. Gene Ther 2003;10(7):540–9.
265. Brade AM, Ngo D, Szmitko P, Li PX, Liu FF, Klamut HJ. Heat-directed gene targeting of adenoviral vectors to tumor cells. Cancer Gene Ther 2000; 7(12):1566–74.
266. Scott SD, Joiner MC, Marples B. Optimizing radiation-responsive gene promoters for radiogenetic cancer therapy. Gene Ther 2002;9(20):1396–402.
267. Weichselbaum RR, Kufe DW, Hellman S, Rasmussen HS, King CR, Fischer PH, et al. Radiation-induced tumour necrosis factor-alpha expression: clinical application of transcriptional and physical targeting of gene therapy. Lancet Oncol 2002;3(11):665–71.
268. Bradfute SB, Goodell MA. Adenoviral transduction of mouse hematopoietic stem cells. Mol Ther 2003;7(3):334–40.
269. Fan X, Brun A, Segren S, Jacobsen SE, Karlsson S. Efficient adenoviral vector transduction of human hematopoietic SCID-repopulating and long-term culture-initiating cells. Hum Gene Ther 2000;11(9): 1313–27.
270. Knaan-Shanzer S, Van Der Velde I, Havenga MJ, Lemckert AA, De Vries AA, Valerio D. Highly efficient targeted transduction of undifferentiated human hematopoietic cells by adenoviral vectors displaying fiber knobs of subgroup B. Hum Gene Ther 2001; 12(16):1989–2005.
271. Tsuda H, Wada T, Ito Y, Uchida H, Dehari H, Nakamura K, et al. Efficient BMP2 gene transfer and bone formation of mesenchymal stem cells by a fiber-mutant adenoviral vector. Mol Ther 2003;7(3): 354–65.
272. Conget PA, Minguell JJ. Adenoviral-mediated gene transfer into *ex vivo* expanded human bone marrow mesenchymal progenitor cells. Exp Hematol 2000; 28(4):382–90.
273. Soifer H, Higo C, Logg CR, Jih LJ, Shichinohe T, Harboe-Schmidt E, et al. A novel, helper-dependent, adenovirus-retrovirus hybrid vector: stable transduction by a two-stage mechanism. Mol Ther 2002;5(5 Pt 1):599–608.
274. Parks RJ, Chen L, Anton M, Sankar U, Rudnicki MA, Graham FL. A helper-dependent adenovirus vector system: removal of helper virus by Cre-mediated excision of the viral packaging signal. Proc Natl Acad Sci U S A 1996;93(24):13565–70.
275. Kubo S, Mitani K. A new hybrid system capable of efficient lentiviral vector production and stable gene transfer mediated by a single helper-dependent adenoviral vector. J Virol 2003;77(5):2964–71.
276. Goncalves MA, van der Velde I, Janssen JM, Maassen BT, Heemskerk EH, Opstelten DJ, et al. Efficient generation and amplification of high-capacity adeno-associated virus/adenovirus hybrid vectors. J Virol 2002;76(21):10734–44.
277. Yotnda P, Chen DH, Chiu W, Piedra PA, Davis A, Templeton NS, et al. Bilamellar cationic liposomes protect adenovectors from preexisting humoral immune responses. Mol Ther 2002;5(3):233–41.
278. Yant SR, Meuse L, Chiu W, Ivics Z, Izsvak Z, Kay MA. Somatic integration and long-term transgene expression in normal and haemophilic mice using a DNA transposon system. Nat Genet 2000;25(1):35–41.
279. Ivics Z, Hackett PB, Plasterk RH, Izsvak Z. Molecular reconstruction of Sleeping Beauty, a Tc1-like transposon from fish, and its transposition in human cells. Cell 1997;91(4):501–10.
280. Yant SR, Ehrhardt A, Mikkelsen JG, Meuse L, Pham T, Kay MA. Transposition from a gutless adeno-transposon vector stabilizes transgene expression *in vivo*. Nat Biotechnol 2002;20(10):999–1005.
281. Luo G, Ivics Z, Izsvak Z, Bradley A. Chromosomal

transposition of a Tc1/mariner-like element in mouse embryonic stem cells. Proc Natl Acad Sci U S A 1998;95(18):10769–73.
282. Horie K, Kuroiwa A, Ikawa M, Okabe M, Kondoh G, Matsuda Y, et al. Efficient chromosomal transposition of a Tc1/mariner-like transposon Sleeping Beauty in mice. Proc Natl Acad Sci U S A 2001;98(16): 9191–6.
283. Nakai H, Yant SR, Storm TA, Fuess S, Meuse L, Kay MA. Extrachromosomal recombinant adeno-associated virus vector genomes are primarily responsible for stable liver transduction *in vivo*. J Virol 2001;75(15):6969–76.
284. Harris JW, Strong DD, Amoui M, Baylink DJ, Lau KH. Construction of a Tc1-like transposon Sleeping Beauty-based gene transfer plasmid vector for generation of stable transgenic mammalian cell clones. Anal Biochem 2002;310(1):15–26.
285. Rundle CH, Miyakoshi N, Kasukawa Y, Chen ST, Sheng MH, Wergedal JE, et al. *In vivo* bone formation in fracture repair induced by direct retroviral-based gene therapy with bone morphogenetic protein-4. Bone 2003;32(6):591–601.
286. Dazai S, Akita S, Hirano A, Rashid MA, Naito S, Akino K, et al. Leukemia inhibitory factor enhances bone formation in calvarial bone defect. J Craniofac Surg 2000;11(6):513–20.
287. Sandhu HS, Khan SN, Suh DY, Boden SD. Demineralized bone matrix, bone morphogenetic proteins, and animal models of spine fusion: an overview. Eur Spine J 2001;10 Suppl 2:S122–31.
288. Chen Y. Orthopedic applications of gene therapy. J Orthop Sci 2001;6(2):199–207.
289. Li H, Zou X, Bunger C. Gene therapy and spinal disorders. Int Orthop 2001;25(1):1–4.
290. Baltzer AW, Lattermann C, Whalen JD, Ghivizzani S, Wooley P, Krauspe R, et al. Potential role of direct adenoviral gene transfer in enhancing fracture repair. Clin Orthop 2000(379 Suppl):S120–5.
291. Bostrom MP, Camacho NP. Potential role of bone morphogenetic proteins in fracture healing. Clin Orthop 1998;(355 Suppl):S274–82.
292. Vukicevic S, Luyten FP, Reddi AH. Stimulation of the expression of osteogenic and chondrogenic phenotypes *in vitro* by osteogenin. Proc Natl Acad Sci U S A 1989;86(22):8793–7.
293. Canalis E, Centrella M, McCarthy T. Effects of basic fibroblast growth factor on bone formation *in vitro*. J Clin Invest 1988;81(5):1572–7.
294. Jingushi S, Heydemann A, Kana SK, Macey LR, Bolander ME. Acidic fibroblast growth factor (aFGF) injection stimulates cartilage enlargement and inhibits cartilage gene expression in rat fracture healing. J Orthop Res 1990;8(3):364–71.
295. Rodan SB, Wesolowski G, Thomas K, Rodan GA. Growth stimulation of rat calvaria osteoblastic cells by acidic fibroblast growth factor. Endocrinology 1987; 121(6):1917–23.
296. Baron J, Klein KO, Yanovski JA, Novosad JA, Bacher JD, Bolander ME, et al. Induction of growth plate cartilage ossification by basic fibroblast growth factor. Endocrinology 1994;135(6):2790–3.
297. Andrew JG, Hoyland JA, Freemont AJ, Marsh DR. Platelet-derived growth factor expression in normally healing human fractures. Bone 1995;16(4):455–60.
298. Bostrom MP, Asnis P. Transforming growth factor beta in fracture repair. Clin Orthop 1998;(355 Suppl): S124–31.
299. Wergedal JE, Matsuyama T, Strong DD. Differentiation of normal human bone cells by transforming growth factor-beta and 1,25(OH)2 vitamin D3. Metabolism 1992;41(1):42–8.
300. Nash TJ, Howlett CR, Martin C, Steele J, Johnson KA, Hicklin DJ. Effect of platelet-derived growth factor on tibial osteotomies in rabbits. Bone 1994; 15(2):203–8.
301. Northmore-Ball MD, Wood MR, Meggitt BF. A biomechanical study of the effects of growth hormone in experimental fracture healing. J Bone Joint Surg Br 1980;62(3):391–6.
302. Lazowski DA, Fraher LJ, Hodsman A, Steer B, Modrowski D, Han VK. Regional variation of insulin-like growth factor-I gene expression in mature rat bone and cartilage. Bone 1994;15(5):563–76.
303. Karaplis AC. PTHrP: novel roles in skeletal biology. Curr Pharm Des 2001;7(8):655–70.
304. Lanske B, Karaplis AC, Lee K, Luz A, Vortkamp A, Pirro A, et al. PTH/PTHrP receptor in early development and Indian hedgehog-regulated bone growth. Science 1996;273(5275):663–6.
305. Jilka RL, Weinstein RS, Bellido T, Roberson P, Parfitt AM, Manolagas SC. Increased bone formation by prevention of osteoblast apoptosis with parathyroid hormone. J Clin Invest 1999;104(4):439–46.
306. Barnes GL, Kostenuik PJ, Gerstenfeld LC, Einhorn TA. Growth factor regulation of fracture repair. J Bone Miner Res 1999;14(11):1805–15.
307. Kaihara S, Bessho K, Okubo Y, Sonobe J, Komatsu Y, Miura M, et al. Over expression of bone morphogenetic protein-3b (BMP-3b) using an adenoviral vector promote the osteoblastic differentiation in C2C12 cells and augment the bone formation induced by bone morphogenetic protein-2 (BMP-2) in rats. Life Sci 2003;72(15):1683–93.
308. Jane JA Jr, Dunford BA, Kron A, Pittman DD, Sasaki T, Li JZ, et al. Ectopic osteogenesis using adenoviral bone morphogenetic protein (BMP)-4 and BMP-6 gene transfer. Mol Ther 2002;6(4):464–70.
309. Chen Y, Cheung KM, Kung HF, Leong JC, Lu WW, Luk KD. *In vivo* new bone formation by direct transfer of adenoviral-mediated bone morphogenetic protein-4 gene. Biochem Biophys Res Commun 2002; 298(1):121–7.
310. Musgrave DS, Pruchnic R, Bosch P, Ziran BH, Whalen J, Huard J. Human skeletal muscle cells in *ex vivo* gene therapy to deliver bone morphogenetic protein-2. J Bone Joint Surg Br 2002;84(1):120–7.
311. Varady P, Li JZ, Alden TD, Kallmes DF, Williams

MB, Helm GA. CT and radionuclide study of BMP-2 gene therapy-induced bone formation. Acad Radiol 2002;9(6):632–7.
312. Okubo Y, Bessho K, Fujimura K, Iizuka T, Miyatake SI. *In vitro* and *in vivo* studies of a bone morphogenetic protein-2 expressing adenoviral vector. J Bone Joint Surg Am 2001;83-A Suppl 1(Pt 2):S99–104.
313. Alden TD, Pittman DD, Hankins GR, Beres EJ, Engh JA, Das S, et al. *In vivo* endochondral bone formation using a bone morphogenetic protein 2 adenoviral vector. Hum Gene Ther 1999;10(13):2245–53.
314. Musgrave DS, Bosch P, Ghivizzani S, Robbins PD, Evans CH, Huard J. Adenovirus-mediated direct gene therapy with bone morphogenetic protein-2 produces bone. Bone 1999;24(6):541–7.
315. Varady P, Li JZ, Cunningham M, Beres EJ, Das S, Engh J, et al. Morphologic analysis of BMP-9 gene therapy-induced osteogenesis. Hum Gene Ther 2001; 12(6):697–710.
316. Franceschi RT, Wang D, Krebsbach PH, Rutherford RB. Gene therapy for bone formation: *in vitro* and *in vivo* osteogenic activity of an adenovirus expressing BMP7. J Cell Biochem 2000;78(3):476–86.
317. Abe N, Lee YP, Sato M, Zhang X, Wu J, Mitani K, et al. Enhancement of bone repair with a helper-dependent adenoviral transfer of bone morphogenetic protein-2. Biochem Biophys Res Commun 2002; 297(3):523–7.
318. Partridge K, Yang X, Clarke NM, Okubo Y, Bessho K, Sebald W, et al. Adenoviral BMP-2 gene transfer in mesenchymal stem cells: *in vitro* and *in vivo* bone formation on biodegradable polymer scaffolds. Biochem Biophys Res Commun 2002;292(1):144–52.
319. Musgrave DS, Bosch P, Lee JY, Pelinkovic D, Ghivizzani SC, Whalen J, et al. *Ex vivo* gene therapy to produce bone using different cell types. Clin Orthop 2000;(378):290–305.
320. Lieberman JR, Daluiski A, Stevenson S, Wu L, McAllister P, Lee YP, et al. The effect of regional gene therapy with bone morphogenetic protein-2-producing bone-marrow cells on the repair of segmental femoral defects in rats. J Bone Joint Surg Am 1999;81(7):905–17.
321. Lieberman JR, Le LQ, Wu L, Finerman GA, Berk A, Witte ON, et al. Regional gene therapy with a BMP-2-producing murine stromal cell line induces heterotopic and orthotopic bone formation in rodents. J Orthop Res 1998;16(3):330–9.
322. Lou J, Xu F, Merkel K, Manske P. Gene therapy: adenovirus-mediated human bone morphogenetic protein-2 gene transfer induces mesenchymal progenitor cell proliferation and differentiation *in vitro* and bone formation *in vivo*. J Orthop Res 1999;17(1):43–50.
323. Greenwald JA, Mehrara BJ, Spector JA, Warren SM, Fagenholz PJ, Smith LE, et al. *In vivo* modulation of FGF biological activity alters cranial suture fate. Am J Pathol 2001;158(2):441–52.
324. de Hooge AS, van de Loo FA, Bennink MB, de Jong DS, Arntz OJ, Lubberts E, et al. Adenoviral transfer of murine oncostatin M elicits periosteal bone apposition in knee joints of mice, despite synovial inflammation and up-regulated expression of interleukin-6 and receptor activator of nuclear factor-kappa B ligand. Am J Pathol 2002;160(5):1733–43.
325. Bosch P, Musgrave DS, Lee JY, Cummins J, Shuler T, Ghivizzani TC, et al. Osteoprogenitor cells within skeletal muscle. J Orthop Res 2000;18(6):933–44.
326. Breitbart AS, Grande DA, Mason JM, Barcia M, James T, Grant RT. Gene-enhanced tissue engineering: applications for bone healing using cultured periosteal cells transduced retrovirally with the BMP-7 gene. Ann Plast Surg 1999;42(5):488–95.
327. Wozney JM, Rosen V, Celeste AJ, Mitsock LM, Whitters MJ, Kriz RW, et al. Novel regulators of bone formation: molecular clones and activities. Science 1988;242(4885):1528–34.
328. Wang EA, Rosen V, Cordes P, Hewick RM, Kriz MJ, Luxenberg DP, et al. Purification and characterization of other distinct bone-inducing factors. Proc Natl Acad Sci U S A 1988;85(24):9484–8.
329. Gitelman SE, Kobrin MS, Ye JQ, Lopez AR, Lee A, Derynck R. Recombinant Vgr-1/BMP-6-expressing tumors induce fibrosis and endochondral bone formation *in vivo*. J Cell Biol 1994;126(6):1595–609.
330. Sampath TK, Maliakal JC, Hauschka PV, Jones WK, Sasak H, Tucker RF, et al. Recombinant human osteogenic protein-1 (hOP-1) induces new bone formation *in vivo* with a specific activity comparable with natural bovine osteogenic protein and stimulates osteoblast proliferation and differentiation *in vitro*. J Biol Chem 1992;267(28):20352–62.
331. Erlacher L, McCartney J, Piek E, ten Dijke P, Yanagishita M, Oppermann H, et al. Cartilage-derived morphogenetic proteins and osteogenic protein-1 differentially regulate osteogenesis. J Bone Miner Res 1998;13(3):383–92.
332. Hotten GC, Matsumoto T, Kimura M, Bechtold RF, Kron R, Ohara T, et al. Recombinant human growth/differentiation factor 5 stimulates mesenchyme aggregation and chondrogenesis responsible for the skeletal development of limbs. Growth Factors 1996;13(1–2): 65–74.